Indole Prenyltransferases: Mechanistic Studies and Inhibitor Design

by

Niusha Mahmoodi

B.Sc., K. N. Toosi University of Technology, Iran, 2004

M.Sc., Tehran University, Iran, 2007

A THESIS SUMBITTED IN PARTIAL FULFILLMENT OF

THE REQUIREMENTS FOR THE DEGREE OF

DOCTOR OF PHILOSOPHY

in

The Faculty of Graduate and Postdoctoral Studies

(Chemistry)

The University of British Columbia

(Vancouver)

December, 2015

Abstract

The cyclic dipeptide *N*-prenyltransferase (CdpNPT) catalyzes the reverse C-3 prenylation of a variety of cyclic dipeptides and benzodiazepinediones. A previous study misassigned the structure of the product of this reaction. In this work, the true product of the CdpNPT-catalyzed reaction between cyclo-L-Trp-L-Trp and dimethylallyl diphosphate (DMAPP) is identified as a C-3 reverse prenylated species. Furthermore, the non-enzymatic Cope/aza-Cope rearrangement of the CdpNPT product was examined under acidic conditions. Our results indicated that only the aza-Cope rearrangement onto the N-1 position of the indole ring can occur and no Cope rearrangement onto the C-4 position was observed. These results suggest that in the absence of an enzyme active site, the aza-Cope rearrangement is preferred over the Cope rearrangement.

Brevianamide F prenyltransferase (FtmPT1) catalyzes the C-2 normal prenylation of brevianamide F (cyclo-L-Trp-L-Pro). A mechanism involving a direct C-2 attack was proposed for this reaction. However, the structural analysis of FtmPT1, as well as studies of alternate substrates and mutant enzymes suggested that a different mechanism involving an initial C-3 reverse prenylation followed by a rearrangement may be operative. In this work, we investigated the reactivity of FtmPT1 with tryptophan and cyclo-L-Trp-L-Trp, as well as two alternate substrates: 5-hydroxybrevianamide F and 2-methylbrevianamide F. The isolated products were reverse prenylated at C-3 and normal prenylated at N-1, C-2, C-3, or C-4. The formation of these products can be rationalized through mechanisms involving either an initial C-3 normal or C-3 reverse prenylation as the first step of catalysis.

4-Dimethylallyltryptophan synthase is an aromatic prenyltransferase that catalyzes an electrophilic aromatic substitution reaction between DMAPP and L-tryptophan. The reaction is believed to proceed via the dissociation of DMAPP to form a dimethylallyl cation/phosphate ion

pair. An inhibitor containing a guanidinium moiety appended to a phosphorylated phosphonate was designed in order to mimic the transition state for the dissociation of DMAPP into an allylic carbocation and pyrophosphate. This compound was found to serve as a potent competitive inhibitor (submicromolar K_i value) of the enzyme 4-DMATS.

Preface

A version of Chapter 2 has been published and some figures are reproduced with permission from: Mahmoodi, N.; Tanner, M. E. *ChemBioChem: A European Journal of Biochemstry* **2013**, *14*, 2029-2037 (© Wiley-VCH Verlag). All the studies reported in this publication and the rest of Chapter 2 were performed by the author of this thesis under the supervision of Professor Martin Tanner.

The third chapter of this thesis is original unpublished work. All the synthetic experiments and kinetic studies were completed by the author of this thesis under the supervision of Professor Martin Tanner.

Table of Contents

List of Tables

List of Figures

List of Abbreviations and Symbols

δ	chemical shift (ppm)
ε	molar absorptivity
ε_{360}	extinction coefficient at 360 nm
Å	angstrom, 0.1 nm
[E]	enzyme concentration
[S]	substrate concentration
[I]	inhibitor concentration
ABBA	a unique protein fold found in certain aromatic prenyltransferases, such as 4-DMATS, CdpNPT, and FtmPT1
BOC	*tert*-butyloxycarbonyl
Bn	benzyl
BP	bisphosphonate
BSA	bovine serum albumin
Cbz	benzyloxycarbonyl
CDI	*N,N'*-carbonyldiimidazole
cdpNPT	gene of cyclic dipeptide *N*-prenyltransferase from *Aspergillus fumigatus*
COSY	correlation spectroscopy
cpaD	gene of cyclo-acetoacetyl-L-tryptophan dimethylallyltransferase from *Aspergillus oryzae*
D	deuterium (^{2}H)
Da	Dalton
DCC	*N,N'*-dicyclohexylcarbodiimide
DCM	dichloromethane
DEAE	diethylaminoethanol
DIPEA	*N,N*-diisopropylethylamine
DMAPP	dimethylallyl diphosphate
4-DMAT	4-dimethylallyltryptophan
4-DMATS	4-dimethylallyltryptophan synthase
dmaW	gene of dimethylallyltryptophan synthase from *Claviceps* sp.

DMF	dimethylformamide
DMSO	dimethyl sulfoxide
DNA	deoxyribonucleic acid
DTT	dithiothreitol
k_H/k_D	deuterium kinetic isotope effect (on k_{cat}/K_M)
E. coli	*Escherichia coli*
EDTA	ethylenediaminetetraacetate, disodium salt
ESI-MS	electrospray ionization mass spectrometry
Et_3N	triethylamine
Et_2O	diethyl ether
EtOAc	ethyl acetate
fgaPT2	gene of dimethylallyltryptophan synthase from *Aspergillus fumigatus*
Fmoc	fluorenylmethyloxycarbonyl
FPP	farnesyl diphosphate
ftmPT1	gene of brevianamide F prenyltransferase from *Aspergillus fumigatus*
GPP	geranyl diphosphate
GGPP	geranylgeranyl diphosphate
IC_{50}	half maximal inhibitory concentration
HCl	hydrochloric acid
HMBC	heteronuclear multiple bond coherence
HOBt	1-hydroxybenzotriazole
HPLC	high pressure liquid chromatography
HSQC	heteronuclear single quantum coherence
*i*PrOH	isopropyl alcohol
IPP	isopentenyl diphosphate
IPTG	isopropyl 1-thio-β-D-galactopyranoside
J	coupling constant (NMR); subscripts indicate coupling partners
k_{cat}	catalytic rate constant
k_{cat}/K_M	specificity constant; second-order rate constant
k_H, k_D	rate of reaction involving protiated and deuterated substrates

K_i	inhibition constant
kDa	kilodalton
KIE	kinetic isotope effect
K_M	Michaelis constant
LB	Luria-Bertani medium
m/z	mass to charge ratio (mass spectrometry)
M	molar
Me	methyl
MeOH	methanol
MESG	2-amino-6-mercapto-7-methylpurine ribonucleoside
$MgSO_4$	magnesium sulfate
MHz	megahertz
MW	molecular weight
NaH	sodium hydride
$NaHCO_3$	sodium bicarbonate
NaCl	sodium chloride
Na_2CO_3	sodium carbonate
$NaHSO_4$	sodium bisulfate
NaOH	sodium hydroxide
NEt_3	triethylamine
$NiSO_4$	nickel sulfate
NMR	nuclear magnetic resonance
NOESY	nuclear overhauser effect spectroscopy
NphB	bacterial aromatic prenyltransferase isolated from *Streptomyces* sp.
OD_{600}	optical dispersion at 600 nm
PIX	positional isotope exchange
PLP	pyridoxal-5-phosphate
P_i	inorganic phosphate
PMSF	phenylmethanesulfonylfluoride
PNP	purine nucleoside phosphorylase

PP_i	pyrophosphate
ppm	parts per million
PT	prenyltransferase
RT	room temperature
SDS-PAGE	sodium dodecylsulfate polyacrylamide gel electrophoresis
TB	Terrific Broth
TCA	trichloroacetic acid
TEAB	triethylammonium bicarbonate
TEAP	*bis*-triethylammonium phosphate
TFA	trifluoroacetic acid
THF	tetrahydrofuran
TLC	thin layer chromatography
TMS	trimethylsilyl
Tris	tris(hydroxymethyl)aminomethane
UV	ultraviolet
UV-Vis	ultraviolet-visible
v	initial reaction velocity (rate)
WT	wild type

Common Amino Acid Abbreviations

A	Ala	alanine
C	Cys	cysteine
D	Asp	aspartate
E	Glu	glutamate
F	Phe	phenylalanine
G	Gly	glycine
H	His	histidine
I	Ile	isoleucine
K	Lys	lysine
L	Leu	leucine

M	Met	methionine
N	Asn	asparagine
P	Pro	proline
Q	Gln	glutamine
R	Arg	arginine
S	Ser	serine
T	Thr	threonine
V	Val	valine
W	Trp	tryptophan
Y	Tyr	tyrosine

Nucleotide Base Abbreviations

A	adenine
C	cytosine
G	guanine
T	thymine
U	uracil

Acknowledgements

I would like to thank my supervisor, Professor Martin Tanner, for his continuous enthusiasm and support. My experience in the lab would have been certainly very different without his guidance and understanding throughout the challenges I encountered while doing my PhD. I would like to thank past and present members of the Tanner lab for being there from the very first day to support me both in lab and life. In particular, I would like to send my gratitude to Louis Luk for taking the time to teach me the basics of biology and Feng Liu for being that one very helpful person in the lab. I woud also like to acknowledge Qi Qian for assistance in making Figure 2.44. I owe my good memories to the time I spent with my dear friend Jennifer Griffith and my life coach Timin Hadi. This adventure would not have been the same without you two. I would also like to thank the exceptionally helpful staff in the Department of Chemistry at UBC for their ongoing assistance. Specifically, I would like to thank the staff members in the Biological Services Laboratory, NMR and mass spectrometry facilities, including Dr. Elena Polishchuk, Jesse Chen, and Dr. Maria Ezhova. Your aid with problem solving was invaluable in the difficult times.

Finally, I would like to thank my family and friends for their contagious positive attitude and support. Mom, Dad, and Nika, thank you for your cheerful words when I was feeling down. Your unconditional love is the most precious thing I have ever had. My friends Montse, Emmanuel, and Jannu, this journey would not have been the same without chilli mangos, aciduladitos, and valentina. Cannot thank you enough. And Philip, life is simply better when you are around. Thanks for existing.

Dedicated to

People I love

Chapter 1: The Prenyltransferase Family of Enzymes

1.1 Terpenes and Terpenoids: A Brief History and Classification

Most people are familiar with terpenes whether they know it or not. These compounds are primarily derived from plants and give many of our food items their pleasant aromas and tastes. [1] Many members of the terpene family are used as food flavoring, spices, and as fragrances. In nature, terpenes are particularly important molecules in plants, animals, fungi, bacteria, and insects. Many plants produce volatile terpenes to attract beneficial insects for pollination. Others use bitter-tasting isoprenoids/alkaloids or poisonous terpenes in order to protect themselves from being eaten by animals. Last, but not least, terpenes play an important role as signalling compounds and growth regulators (phytohormones) in plants. [2] Many insects are capable of metabolizing the terpenes they have received with their food into growth hormones and pheromones. Pheromones are signalling compounds that insects and other organisms produce to communicate with other members of their group. This is needed to mark food resources and their location, as well as to attract sexual partners for mating. As pheromones are harmless to the environment, they may replace conventional insecticides when used to trap harmful and damaging insects such as bark beetles. [2]

Simple, linear terpenes are less widely distributed in nature but upon undergoing oxidation, cyclization, and rearrangement modifications, an infinite array of structurally diverse natural products are generated. These highly functionalized terpenes are generally referred to as terpenoids, and they possess biological properties ranging from anticancer and antimalaria activities to tumor promotion and ion-channel binding. [2] Although a terpenoid is a more complex version of a terpene, organic chemists increasingly use these two terms interchangeably. Tens of

thousands of terpenoids have been identified to date and each one of them has been derived from branched five-carbon isoprene substrates. [3,4,5,6] Depending on the number of isoprene subunits present in the molecule, one can distinguish between hemi- (C_5), mono- (C_{10}), sesqui- (C_{15}), di- (C_{20}), sester- (C_{25}), and tri-terpenoids (C_{30}).

Monoterpenes are best known as the main components of essential oils and floral scents. [7] Citronellol is a natural acyclic monoterpenoid found in citronella oils (Figure 1.1). In addition to its inhibitory properties against *Mycobacterium tuberculosis*, citronellol has long been used in perfumes and insect repellents. [8,9] Perillyl alcohol, a cyclic monoterpenoid, exhibits chemopreventive activity against liver cancer in rats. [10] The two monoterpene esters pyrethrin I and II are important insecticidal components isolated from pyrethrum flowers. They are used for treatment of skin parasites such as head lice and act by blocking sodium channels. [11] Sesquiterpenoids are generally less volatile than monoterpenoids. Among all sesquiterpenoids, the sesquiterpene lactones isolated from marine and terrestrial organisms are well recognized for their biological activities. [12] The anti-inflammatory properties of some medicinal plants have been attributed to the presence of sesquiterpene lactones. Artemisinin is perhaps the most prominent member of the sesquiterpene lactone family. It possesses antimalarial properties and is used world-wide to treat both drug resistant, and cerebral, malaria. [13] Parthenolide is another example of a sesquiterpene lactone. It occurs naturally in the plant feverfew and has been used for over 200 years to treat fever, headache, and stomach aches. It is commonly used today to treat arthritis, migranes, asthma, and psoriasis. [14] Bisabolol oxide A is a plant sesquiterpenoid that is commonly used in herbal medicine for the treatment of skin inflammation, and as an antibacterial and antifungal agent. [15] Illudins are a family of toxic sesquiterpenes produced by some mushrooms. Illudins S and M are highly cytotoxic and have been found to exhibit

antitumor activities. [16] Avarol, a sesquiterpene hydroquinone, is a marine sesquiterpenoid that has been shown to exhibit anti-HIV, anticancer, and antibacterial activities. [17,18] Interestingly, many marine sesquiterpenoids also show activity against tuberculosis. Puupehenone, which is a cyanosesquiterpene, is an example of an inhibitor of the growth of *M. tuberculosis.* [19]

The diterpenes represent a large class of terpenoids with a wide range of biological activities. Phytol is one of the simplest and most important acyclic diterpenes. (*E*)-Phytol is the side chain found in vitamin K1 and chlorophyll and it also exhibits significant activity against tuberculosis bacteria. [9] Among the cyclic diterpenes, taxines isolated from the common yew, have attracted much attention due to their anticancer activity. [20] Paclitaxel (Taxol®) is possibly the most well known example of a cyclic diterpenoid. This diterpenoid is currently used to treat lung, ovarian, and breast cancer. Eleutherobine, a glycosylated diterpenoid, is isolated from marine soft corals and possesses anticancer properties. [21] Erogorgiaene is another example of a diterpenoid with antituberculosis activity (Figure 1.1). [22]

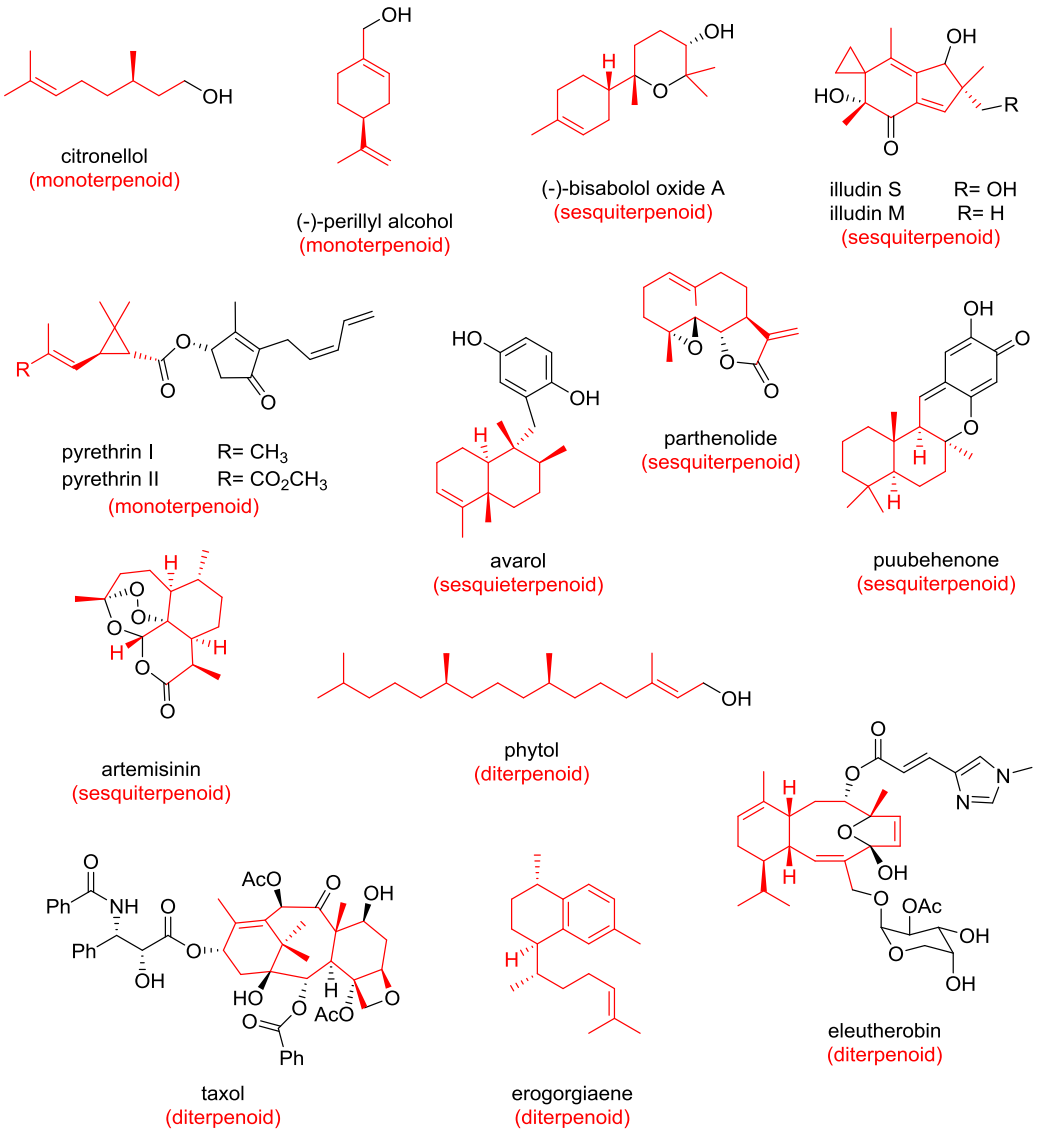

Figure 1.1 Examples of mono-, sesqui- and di-terpenoids found in nature. (Red chemical bonds denote the terpene-derived carbons)

1.2 Biosynthesis of Terpenoids: Terpene Cyclases

What makes terpenes/terpenoids so unique is the spectacular strategy nature employs to produce them. A terpene cyclase, also known as a terpene synthase, is an enzyme that converts simple linear prenyl diphosphates into chiral carbocyclic skeletons of high diversity and value. All the isoprenoid substrates used by the terpene cyclases are synthesized from the simple five-

carbon building blocks dimethylallyl diphosphate (DMAPP) and isopentenyl diphosphate (IPP). From these two precursors, a group of enzymes known as prenyltransferases catalyze the synthesis of linear prenyl diphosphates, which serve as the substrates for the synthesis of various terpenoids. In the prenyltransferase reactions, IPP is added successively to DMAPP in a head-to-tail manner to generate geranyl diphosphate (GPP, 10 carbons), farnesyl diphosphate (FPP, 15 carbons), geranylgeranyl diphosphate (GPP, 20 carbons), and geranylfarnesyl diphosphate (GFP, 25 carbons) (Figure 1.2). [23,24] GPP and FPP serve as precursors to monoterpenes and sesquiterpenes, respectively, while GGPP serves as the precursor to diterpenes.

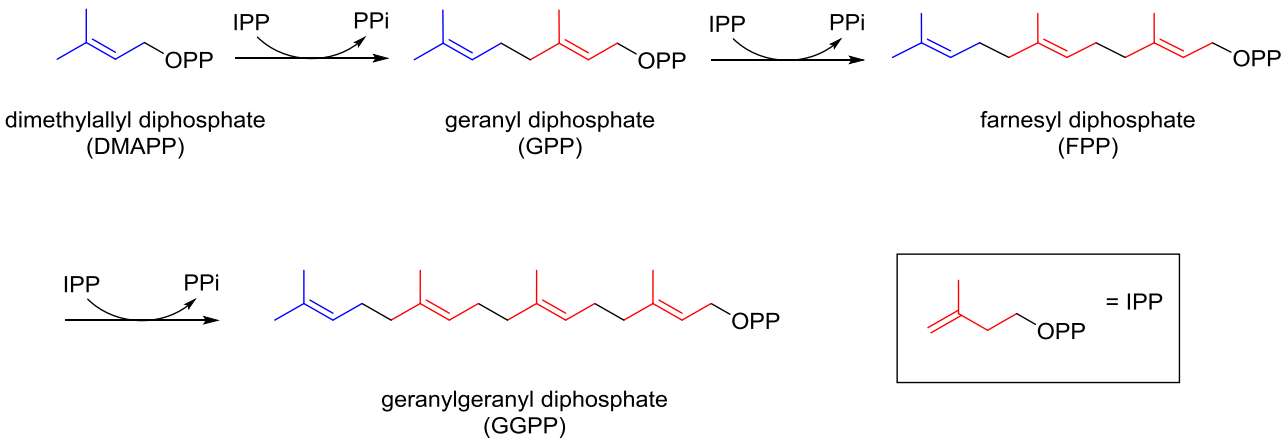

Figure 1.2 Structures of the substrates of terpene cyclases. (Blue color denotes the carbon atoms originated from DMAPP and red color denotes the carbon atoms originated from IPP)

Terpene cyclases catalyze unique multistep cyclization cascades to generate the thousands of natural terpenoid compounds found in different organisms. Each enzyme binds the allylic diphosphate substrate and initiates catalysis through dissociation of the diphosphate group (PP_i) (Figure 1.3). The resultant reactive allylic carbocation is protected in the active site from being prematurely quenched by water or other nucleophiles. These highly reactive carbocationic

intermediates are directed to undergo dramatic structural rearrangements to give a variety of products. An example is the conversion of GPP to myrcene, 4*S*-limonene, and 4*S*-β-phellandrene catalyzed by monoterpene synthases from grand fir (Figure 1.3). The cyclase controls the precise rearrangements and cyclizations to generate a specific terpene. The chemical and structural diversity of terpenoids results primarily from variations in the number of isoprene units, cyclization reactions, and rearrangements. [25] Based on the number of five-carbon isoprene units present in the structure of their products, terpene cyclases are classified as monoterpene- (C_{10}), sesquiterpene- (C_{15}), and diterpene cyclases (C_{20}).

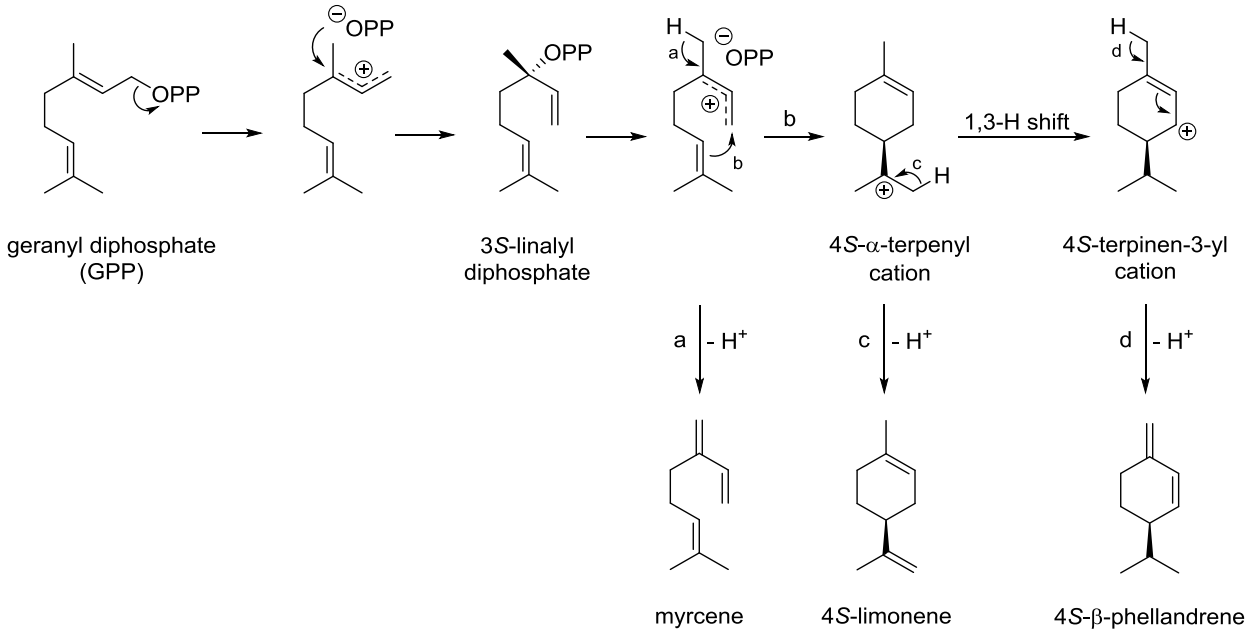

Figure 1.3 Mechanism for the conversion of geranyl diphosphate to myrcene, limonene, and β-phellandrene by monoterpene synthases from grand fir. Formation of the monocyclic and bicyclic products requires preliminary isomerisation of geranyl diphosphate to linalyl diphosphate. The acyclic product, myrcene, could be formed from either geranyl diphosphate or linalyl diphosphate. [26]

Monoterpene cyclases catalyze the simplest terpene cyclization reactions. These enzymes use geranyl diphosphate (GPP) which is the shortest isoprenoid substrate available to terpene

cyclases. The volatile monoterpenes and their derivatives are responsible for the pleasing fragrances and flavors of aromatic plants. [27] Limonene, for example, is an unsaturated monocyclic terpene synthesized by limonene synthase (Figure 1.4). Its (*R*)-(+)-enantiomer is the main component of mandarin peel oil from *Citrus reticulata.* (-)-Menthol is synthesized from (-)-limonene upon hydroxylation at C3 and a series of four redox transformations (one oxidative and three reductive) and an isomerization step (Figure 1.4). [28] Menthol is the major component of peppermint oil and has mildly anesthetic, antiseptic, antipruritic, carminative, and cooling properties. [29]

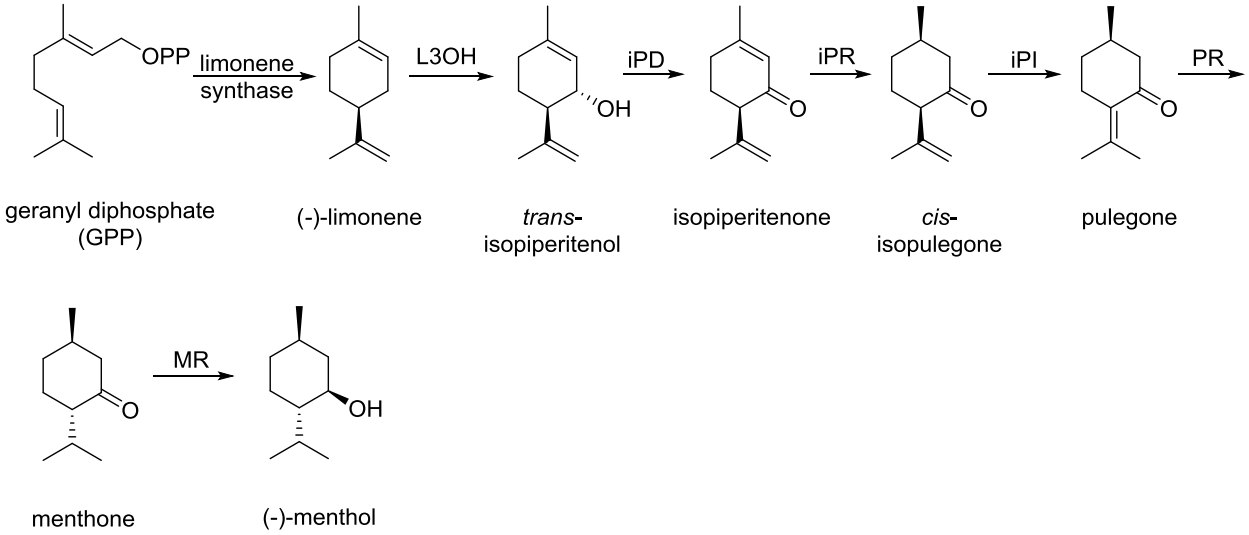

Figure 1.4 Biosynthesis of (-)-menthol from (-)-limonene. The enzymatic steps are catalyzed by (-)-limonene-3-hydroxylase (L3OH), (-)-*trans*-isopiperitenol dehydrogenase (iPD), (-)-isopiperitenone reductase (iPR), (+)-*cis*-isopulegone isomerase (iPl), (+)-pulegone reductase (PR), and (-)-menthone reductase (MR).

Sesquiterpene cyclases catalyze the cyclization of farnesyl diphosphate to generate a variety of cyclic terpenes (Figure 1.5). Trichodiene synthase, for example, catalyzes the first committed step in the biosynthesis of nearly 300 trichothecene mycotoxins such as T-2 toxin and vomitoxin, which are common contaminants of grain-based agricultural products. [30, 31] Amorpha-

4,11-diene synthase is another example of a sesquiterpene synthase that catalyzes the first committed step in the biosynthesis of the antimalarial drug artemisinin. [32] Cyclization of the 20-carbon geranylgeranyl diphosphate is catalyzed by diterpene cyclases. Paclitaxel (Taxol) is isolated from the bark of the pacific yew (*Taxus brevifolia*) and exhibits antitumor activities. [33] Taxadiene synthase is the enzyme that catalyzes the first committed step in the paclitaxel biosynthesis through cyclization of geranylgeranyl diphosphate to form taxadiene (Figure 1.5).

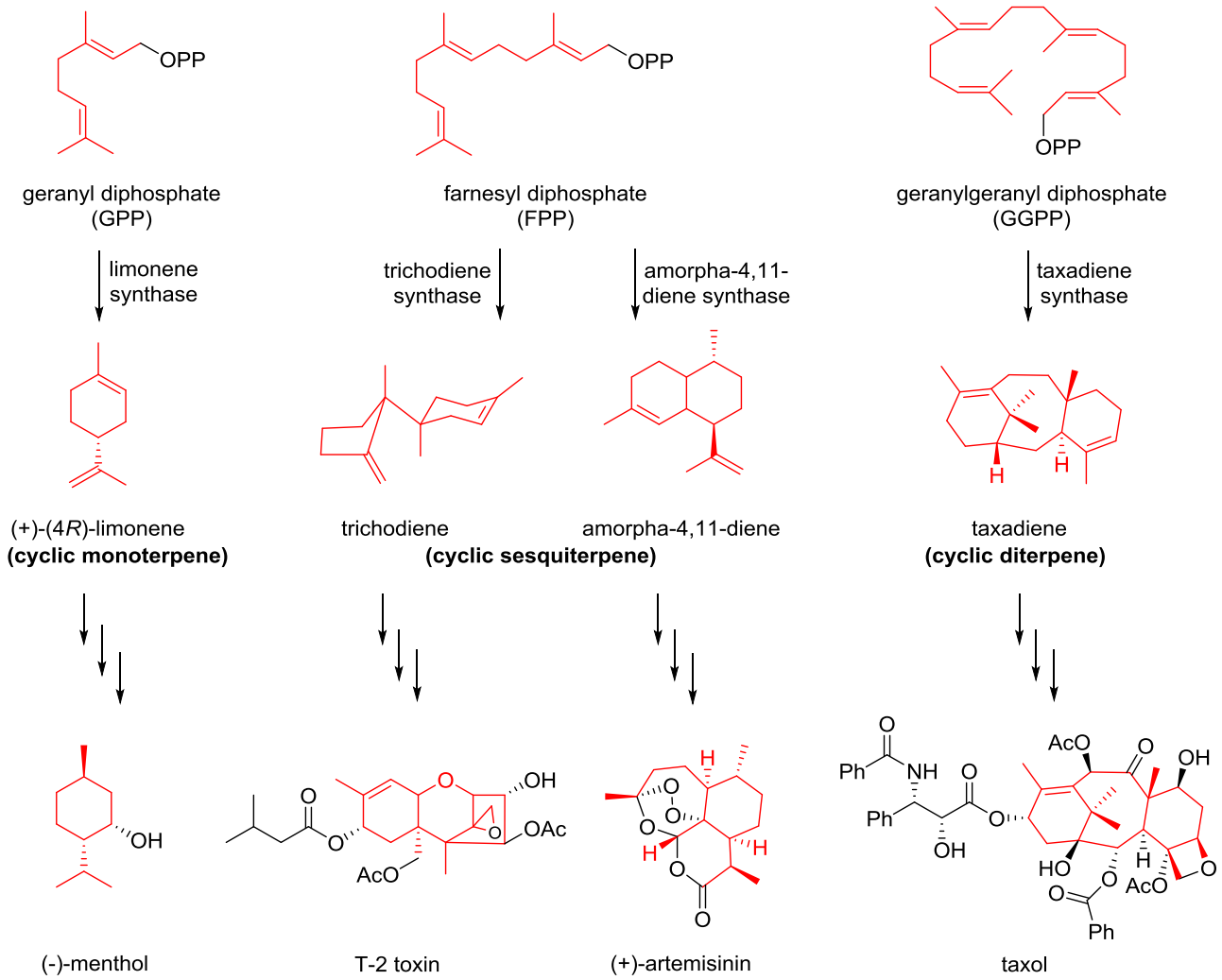

Figure 1.5 Examples of cyclization reactions catalyzed by terpene cyclases. (Bonds colored in red denote the terpenoid derived atoms)

1.3 Meroterpenoids

With more than 23,000 known compounds, terpenoids are the largest class of natural products. What makes terpenoids even more appealing to researchers is that they can be linked to other molecules to create a variety of structurally diverse molecules. In 1968, Cornforth introduced the term meroterpenoid to describe natural products in which the terpenoid moieties are mixed with molecules of different biosynthetic origins. [34] The Greek prefix mero- means 'part, partial, or fragment' and, thus, several secondary metabolites that contain a terpenoid moiety can be described under this definition. Although meroterpenoids are diverse in structure, they can be classified into two major groups based on their biosynthetic origins: polyketide terpenoids and non-polyketide terpenoids. [35] The main representative of the non-polyketide class of terpenoids is terpenoid alkaloids, where a nitrogen-containing moiety is introduced into the structure. Due to their broad range of biological activities and interesting chemistry, intensive research has been conducted on alkaloids, as well as terpenoid alkaloids.

1.3.1 Alkaloids

Alkaloids have been known to humans since the beginning of world civilization. They were used in shamanism, in traditional herbal medicine for curing various diseases, and as weapons during tribal wars and hunting. [36,37] The first alkaloid to be identified was morphine which was isolated from the opium poppy, *Papaver somniferum*, by Sertüner in 1806 (Figure 1.6). Interestingly, the structure of morphine was first elucidated a century later in 1952 due to the stereochemical complexity of the molecule. [38,39,40] Thanks to their potent biological activity, as many as 12,000 known alkaloids have been exploited as pharmaceuticals, stimulants, narcotics, and poisons. [39] A few examples of plant-derived alkaloids currently in clinical use

include the analgesics morphine and codeine, the anticancer agents vinblastine and taxol, the muscle relaxant tubocurarine, the antiarrythmic ajmaline, and the antibiotic sanguinarine. Other alkaloids that play an important role in human life include caffeine, nicotine, cocaine, and the synthetic *O,O*-acetylated morphine derivative heroin (Figure 1.6). [39,40]

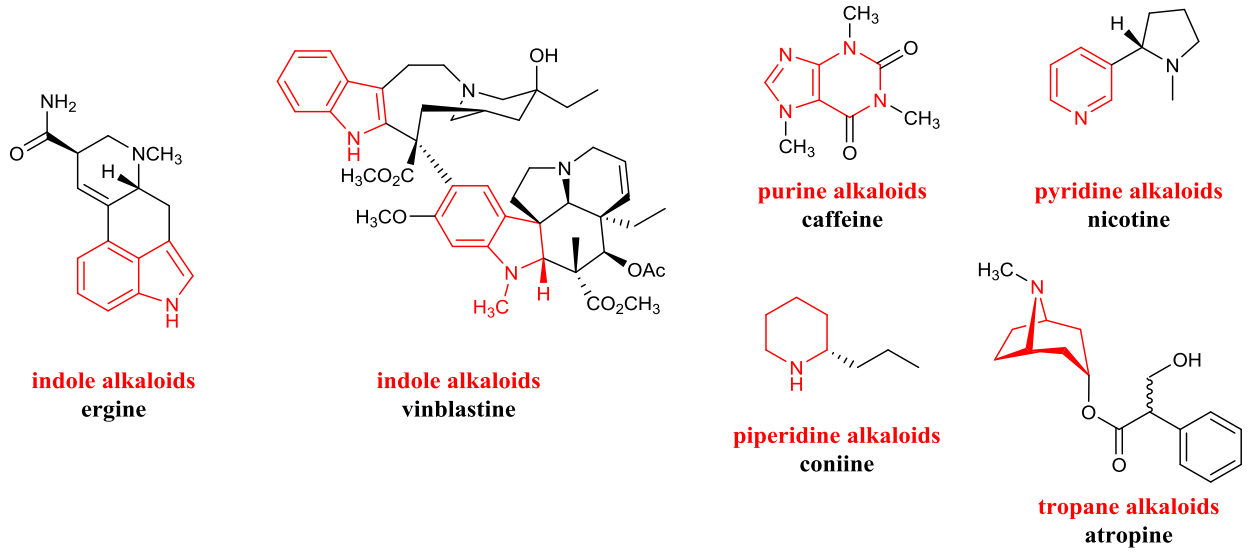

Figure 1.6 Examples of alkaloids. (Bonds colored in red show the chemical moiety to which the alkaloid is sub-classified)

Alkaloids comprise a large family of nitrogen-containing secondary metabolites. The term originally implied molecules of plant origin that possessed high physiological activity, but the definition has gradually been broadened to include the majority of nitrogen-containing

natural products.[38] Since the structure of alkaloids can be so varied, sorting them into different classes can be useful for ease of classification. One can group alkaloids based on the location of nitrogen(s) within the structure. Each group can then be further branched into several subcategories on the basis of the chemical functionalities present in the molecules and the organisms from which they were isolated.[41] The class of heterocyclic alkaloids is an example of this classification. These natural products possess nitrogen atom(s) inside a cyclic carbon ring. Depending on the type of ring moiety featured in the molecule, these alkaloids are further subcategorized as follows: the indole alkaloids such as ergine and vinblastine, the pyridine alkaloids such as nicotine, the purine alkaloids such as caffeine, the piperidine alkaloids such as coniine, the quinoline/isoquinoline alkaloids such as quinine, tubocurarine, morphine and codeine, and finally the tropane alkaloids such as cocaine and atropine (Figure 1.6).

1.3.2 Terpenoid Alkaloids: Monoterpenoid Indole Alkaloids

Terpenoid alkaloids can be described as aminated terpenes or even azaterpenes.[42] In contrast to other classes of alkaloids, which are derived from amino acid precursors, the nitrogen in many terpenoid alkaloids comes from methylamine, ethylamine and β-aminoethanol. The exception is the indole terpenoid alkaloid class where the nitrogen atom is introduced through tryptophan. Biosynthesis of these molecules begins in the same manner as terpenoids. Upon the introduction of nitrogen atom(s) in one of the forms listed above, the compound can no longer be considered a terpenoid and will be classified as a terpenoid alkaloid.[42] Over 20,000 alkaloids and 55,000 terpenes have been isolated to date but only a few thousand molecules qualify as terpenoid alkaloids.[43,44] They can be further subdivided into mono-, sesqui-, di- and tri-terpenoid alkaloid sub-groups based on the number of isoprene units present in the terpenoid structure.

Most members of the monoterpenoid alkaloid family possess an indole moiety as a part of their alkaloid constituent. A rare example of a monoterpenoid alkaloid with a non-indole structure is α-skytanthine. [45] Dendrobine and pumiliotoxins A and B are examples of sesquiterpenoid alkaloids with the former demonstrating analgesic and anti-fever activities while the two latter are among the toxins present in the skin of poison dart frogs (Figure 1.7). Methyllycaconitine is a diterpenoid alkaloid found in larkspurs. It is toxic to animals and causes the majority of cattle deaths in western North America. [46] Other diterpenoid alkaloids including hetisine have been used as insect repellents. [47] Cortistatin A is a triterpenoid alkaloid, also known as steroidal alkaloid, with potential anti-angiogenic properties that can treat cancer and blindness (Figure 1.7). [48,49,50]

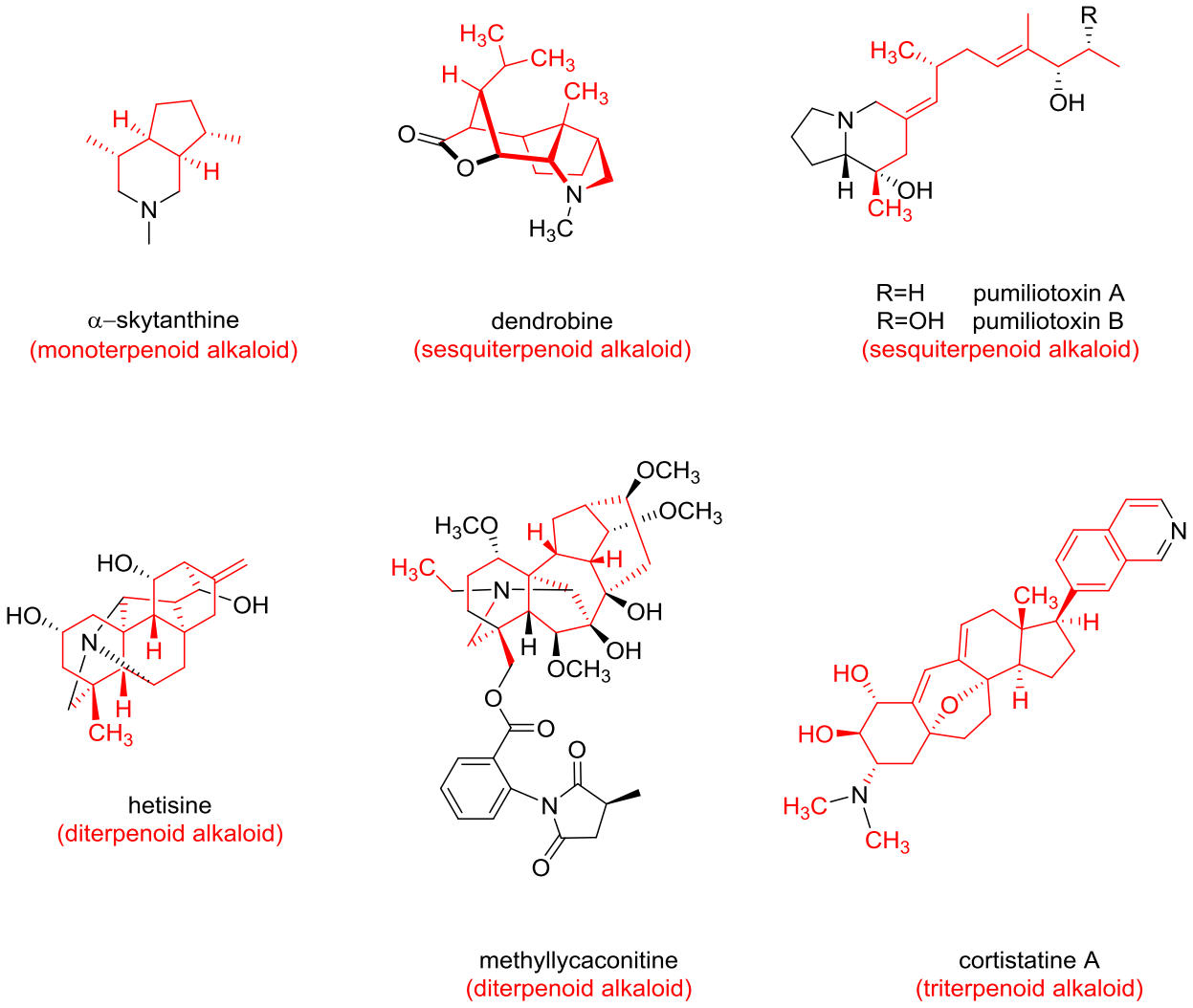

Figure 1.7 Structures of various terpenoid alkaloids. (Bonds colored in red denote the terpenoid skeleton)

The most extensively studied sub-group in the family of terpenoid alkaloids consists of the monoterpenoid indole alkaloids (MIAs). Approximately 2000 structurally and pharmaceutically diverse monoterpenoid indole alkaloids have been identified to date. Some of the MIAs widely used in medicine include vinblastine for the treatment of cancer and ajmaline for antiarrythmic heart disorders. [38,39,40] All terpene indole alkaloids are derived from the amino acid tryptophan and the monoterpenoid secologanin (Figure 1.8). [40] Initially, tryptophan

decarboxylase converts tryptophan to tryptamine. Strictosidine synthase catalyzes a Pictet-Spengler type condensation reaction of tryptamine and secologanin to generate strictosidine, which can undergo further modifications to generate ajmaline and vinblastine. [51,52]

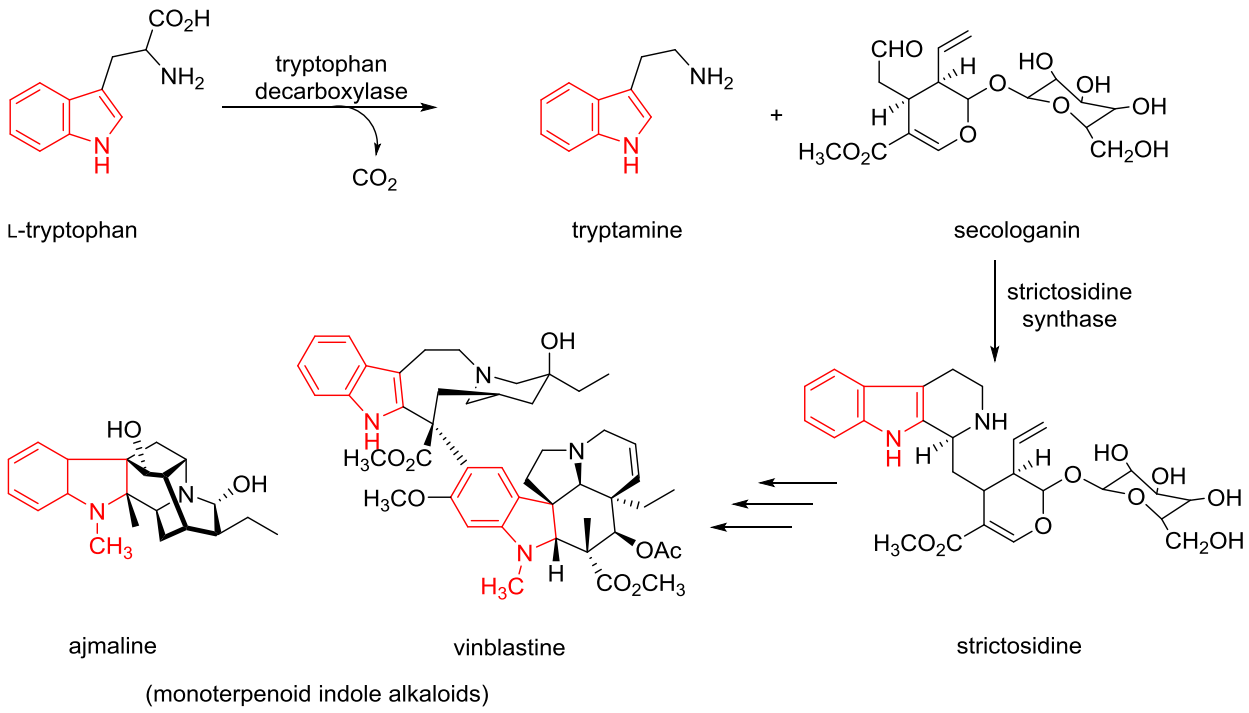

Figure 1.8 The first steps in the biosynthesis of monoterpenoid alkaloids vinblastine and ajmaline. (Bonds shown in red represent the indole moiety)

Secologanin is an iridoid terpene, and the biosynthetic pathway leading to this compound has yet to be fully elucidated. Iridoids are a class of monoterpenoids found in many medicinal plants. They are derived from iridodial whose chemical structure consists of a cyclopentane ring that is fused to a six-membered hemiacetal (Figure 1.9). Iridomyrmecin, which is a well-known member of this family of secondary metabolites is often used to exemplify the chemical structure of iridoids (Figure 1.9). The first committed step in the biosynthesis of secologanin involves the hydroxylation of geraniol by geraniol-10-hydroxylase (Figure 1.9). Feeding studies suggest that 10-hydroxygeraniol, iridodial, and iridotrial are intermediates in the biosynthesis of secologanin.

[53,54] Iridotrial is oxidized to form a carboxylic acid which undergoes an esterification reaction to yield the corresponding methyl ester. Subsequent glycosylation of this hemiacetal gives deoxyloganin which is further hydroxylated to generate loganin. Secologanin synthase performs the oxidative cleavage of loganin to generate the final product, secologanin (Figure 1.9). [55]

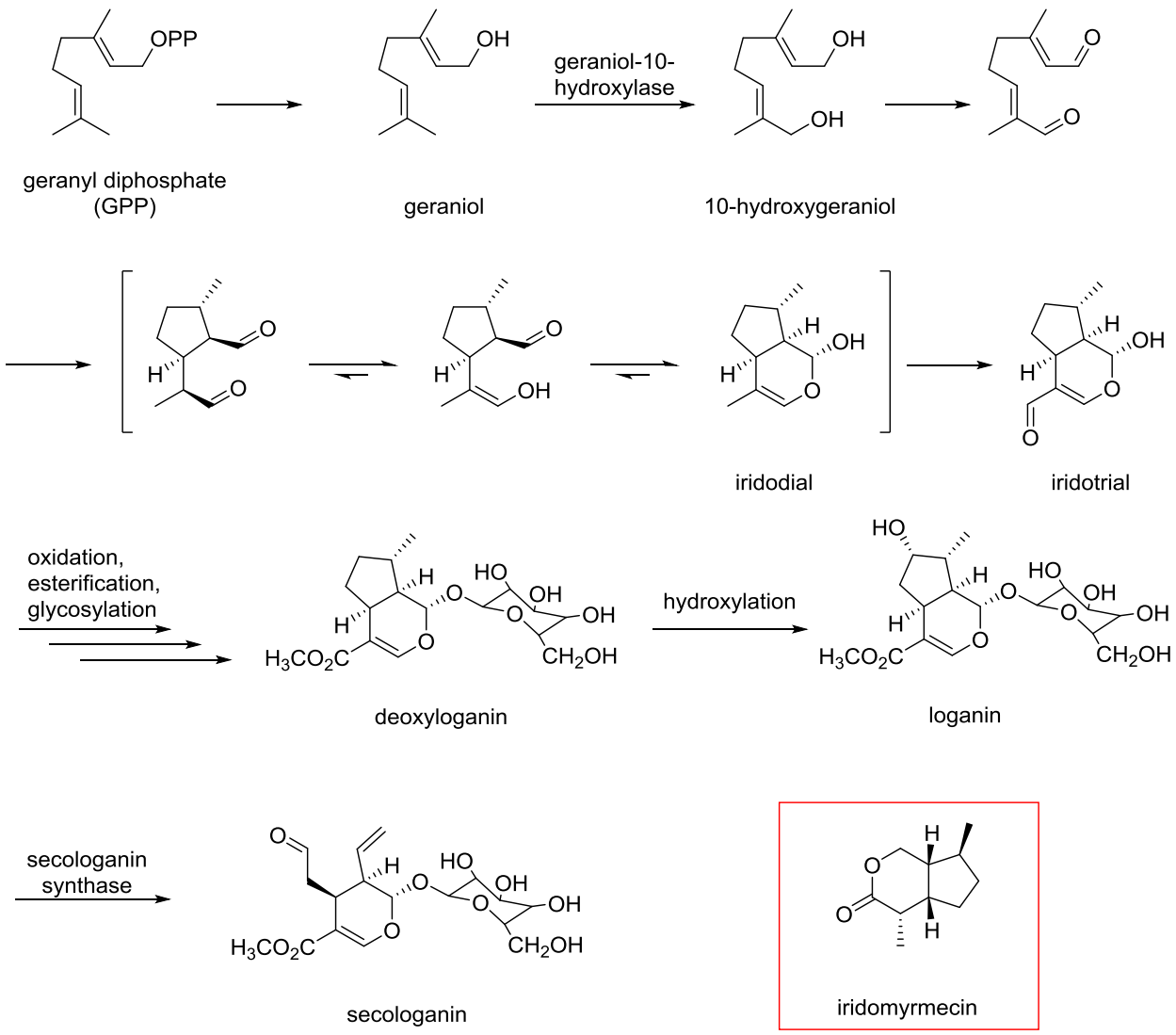

Figure 1.9 Biosynthesis of secologanin from geranyl diphosphate (GPP). The inset shows the structure of a common iridoid: iridomyrmecin.

1.4 Prenylated Indole Alkaloids

Indole alkaloids carrying 3,3-dimethylallyl (prenyl) or 1,1-dimethylallyl (*tert*-prenyl) substituents comprise a large family of natural products found in plants, fungi, and bacteria.[56,57,58] The prenyl moiety may add in a "normal" manner where the primary carbon of the dimethylallyl group connects to the indole ring, or in a "reverse" manner where the tertiary carbon is added to the molecule (Figure 1.10).[57] This prenylation process can further increase the structural diversity of alkaloids by either making them more lipophilic or by providing a carbon skeleton that will ultimately become a part of the final structure.[57] Prenyl donors are allylic diphosphates and the enzymes that catalyze this process are indole prenyltransferases, which have attracted significant interest over the past few decades.[57]

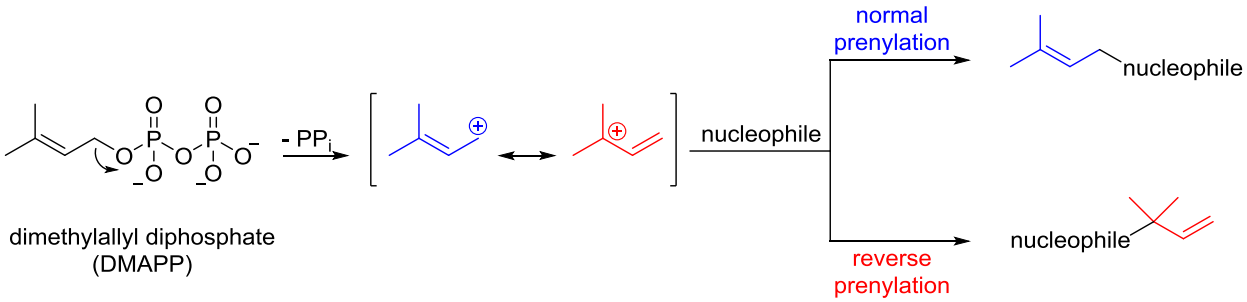

Figure 1.10 Normal and reverse prenylation with dimethylallyl diphosphate (DMAPP) as the isoprenyl donor. (Nucleophile represents a nucleophilic nitrogen or carbon of the indole ring)

Tryptophan is a key primary metabolite from which numerous indole alkaloids are biosynthesized. In a few cases, the indole core is synthesized from indole-3-glycerol phosphate. Carbons of the prenyl group are attached to either the periphery as seen in echinulin and roquefortine C, or can eventually become part of the core of the final alkaloid product as can be seen with ergotamine and brevianamide B (Figure 1.11).[57]

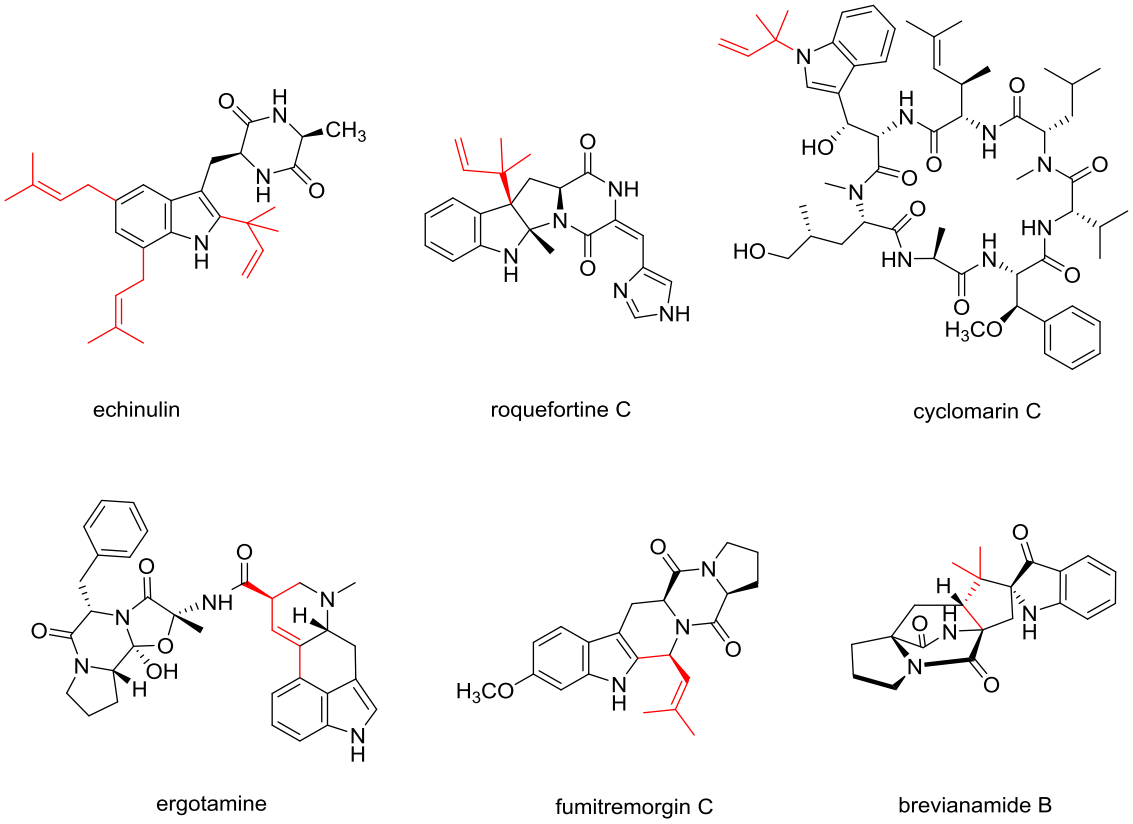

Figure 1.11 Examples of prenylated indole alkaloids. (Bonds shown in red represent the prenyl moieties)

In a few cases prenylation occurs on tryptophan itself, however, in most cases, the dimethylallyl moiety is installed onto a more complex molecule. Generally, a second amino acid is condensed with a tryptophan subunit to form a cyclic dipeptide with a diketopiperazine structure. Proline, phenylalanie, alanine, histidine, or a second tryptophan molecule, are the most common amino acids used to generate the cyclic dipeptide. [56] Echinulin, which is isolated from *Aspergillus amstelodami* and *Aspergilus schinulatus*, is a triisoprenylated cyclic dipeptide with tryptophan and alanine as its bulding blocks. Roquefortine C on the other hand, is derived from the oxidative cyclization of tryptophan, histidine, and dimethylallyl diphosphate. It is a neurotoxic mold metabolite that was first isolated from *Penicillium roqueforti*. [59] Fumitremorgin

C is a mold metabolite isolated from *Aspergillus fumigates*. The amino acids involved in its formation include tryptophan, proline and methionine (as the source of the aromatic methyl ether carbon). Brevianamides and austamides constitute a small but structurally interesting family of indole alkaloids. [59] Brevianamide B, for example, was first isolated from the fungus *Penicillium brevicompactum*, and is comprised of a tryptophan, a proline, and an isoprene unit.

Prenylation of indole alkaloids is not limited to the addition of a five-carbon dimethylallyl moiety, despite this being the most common type of prenylation. Examples of the addition of larger prenyl groups with a higher number of carbons can be found in the literature. One example includes the biosynthesis of lyngbyatoxins in which a ten-carbon geranyl group is added. Lyngbyatoxin A is a potent skin irritant produced by *Lyngbya majuscule*. It causes a skin condition known as "Swimmer's Itch" off Oahu, Hawaii. [60,61] Moreover, the addition of a twenty-carbon geranylgeranyl group has been reported in the biosynthesis of paxilline, a potassium channel blocker (Figure 1.12). [62]

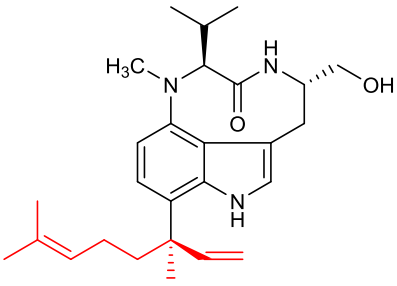

Lyngbyatoxin A

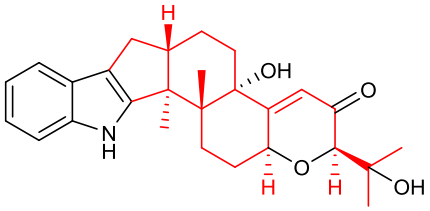

Paxilline

Figure 1.12 Structures of lyngbyatoxin A and paxilline. (Bonds colored in red show the ten-carbon geranyl and twenty-carbon geranylgeranyl groups)

1.5 Prenyltransferase Enzymes

In Nature, prenylation refers to the transfer of isoprenyl moieties to acceptor molecules, resulting in the formation of C-C, C-S, and C-N bonds. These reactions are catalyzed by enzymes called prenyltransferases (PTs). PTs are ubiquitously distributed among eukaryotes and prokaryotes, and are involved in many important physiological functions, including cell signaling and protein trafficking. Prenylation is also considered as a fundamental process in the biosynthesis of numerous natural products in many different systems. Many of these prenylated natural products possess a wide range of biological activities. Some have been exploited as medicinal agents while others have shown toxic and/or hallucinogenic effects as can be seen with certain ergot alkaloids. [63] Since PTs play an important role in such interesting transformations, widespread attention has been focused on studying them in different organisms.

In a prenylation reaction catalyzed by a prenyltransferase, an electron-rich nucleophile serves as an acceptor, and is alkylated by an isoprenyl diphosphate to form a prenylated compound and pyrophosphate (PP_i) as products (Figure 1.13). One way in which PTs can be categorized is based on the type of reaction they catalyze; whether it is the synthesis of an isoprenyl diphosphate, the prenylation of a protein or the prenylation of an aromatic substrate. Consequently, PTs have been classified into three main groups as follows: isoprenyl diphosphate synthases, protein prenyl transferases, and aromatic prenyl transferases. [63,64]

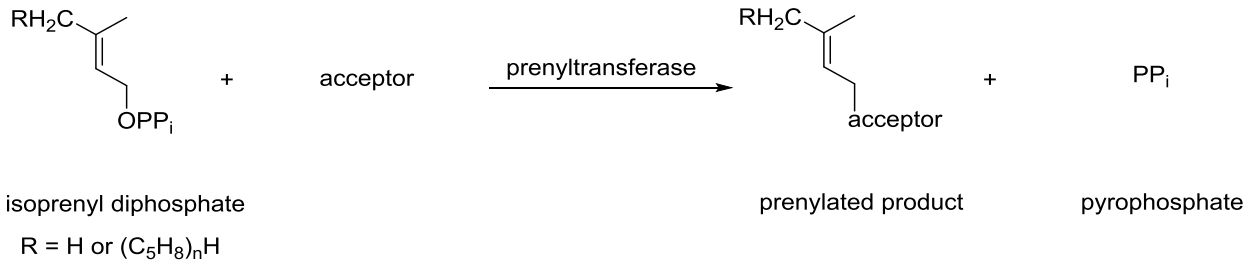

Figure 1.13 The reaction catalyzed by prenyltransferases.

The mechanism of prenylation by many of these PTs has been thoroughly investigated. The following sections will present these studies.

1.5.1 Isoprenyl Diphosphate Synthases: *trans*-Farnesyl Diphosphate Synthase

Isoprenyl diphosphate synthases (IPPSs) comprise a family of PTs that catalyze the elongation of allylic diphosphate substrates (Figure 1.14). These enzymes are versatile enough to accept a variety of isoprenyl diphosphates as electrophiles, thus generating an array of allylic diphosphates by the addition of simple five carbon building blocks.

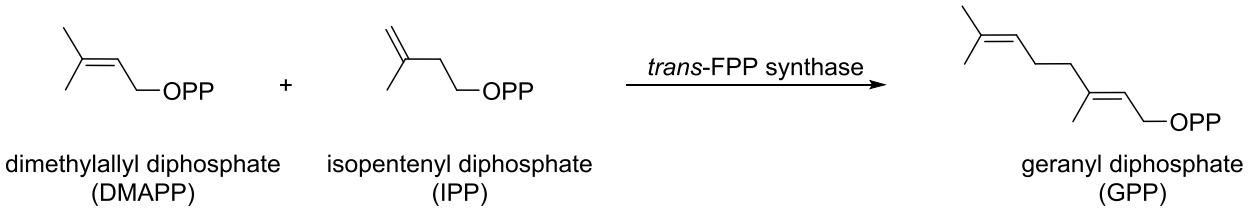

Figure 1.14 The first half of the overall reaction catalyzed by an isoprenyl diphosphate synthase: *trans*-farnesyl diphosphate synthase.

All members of the IPPS family show amino acid sequence homology and contain two aspartate-rich DDxxD motifs that are highly conserved. This suggests that they have evolved from a common origin. Individual members of the IPPS family differ from one another in the

allylic substrate they accept to initiate the elongation reaction and in the chain length of the product. For instance, geranyl diphosphate synthase (GPPS) and farnesyl diphosphate synthase (FPPS) catalyze the synthesis of geranyl diphosphate (C_{10}) and farnesyl diphosphate (C_{15}), respectively. IPPSs responsible for the linear synthesis of allylic diphosphates can be further subdivided into *cis*- and *trans*- isoprenyl diphosphate synthases according to the stereochemistry of the reaction products. [64] One of the most thoroughly studied PT is farnesyl diphosphate synthase (FPPS) which is the first PT to be discovered and participates in the biosynthesis of cholesterol in humans. [65]

Early work on the isolation and initial characterization of *trans*-FPP synthase originated from the research groups of Porter and Popák in the 1960s. [66,67] *trans*-FPP Synthase catalyzes two consecutive 1'-4 (head-to-tail) condensation reactions (Figure 1.15). In the first reaction, the five-carbon chain of dimethylallyl diphosphate (DMAPP, R=H) is linked to isopentenyl diphosphate (IPP) and inorganic pyrophosphate is released from DMAPP. The resultant C-10 geranyl diphosphate (GPP) undergoes a second condensation reaction with another molecule of IPP to give the C-15 FPP. Additionally, the presence of a divalent cation, either Mg^{2+} or Mn^{2+}, was found to be essential for the activity of the enzyme. [67] The metal ion chelates to the aspartate residues in the Asp-rich DDxxD motifs, and acts by facilitating the binding of the diphosphate substrates. [64]

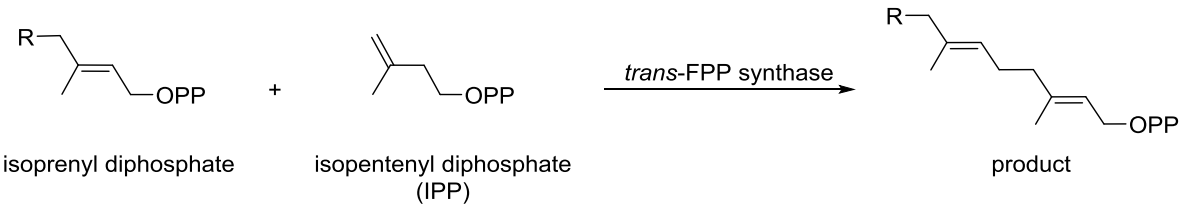

trans-FPP synthase	R	isoprenyl diphosphate	overall reaction
first reaction	H	DMAPP	DMAPP + IPP ⟶ GPP
second reaction	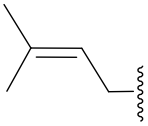	GPP	GPP + IPP ⟶ FPP

Figure 1.15 Two sequential reactions catalyzed by *trans*-FPP synthase.

Among all members of the prenyltransferase family, the crystal structure of avian FPP synthase was the first to be solved (Figure 1.16). [64,68] The enzyme shows a novel fold consisting of 13 α-helices, 10 of which form a large central cavity that surrounds the active site. There are two aspartate rich motifs (DDxxD) on opposite walls of this cavity that are located 12 Å apart from one another. This creates the substrate-binding pockets for IPP and DMAPP/GPP. Moreover, these two conserved Asp-rich motifs are chelated to a divalent metal ion such as Mg^{2+}, which coordinate to the diphosphate moieties of the substrates. The structure of *trans*-FPP synthase in complex with GPP and IPP clearly reveals that the DDxxD motif closer to the N-terminus is responsible for the binding of allylic substrate GPP and that closer to the C-terminus is the binding site of the homoallylic substrate IPP. Site-directed mutagenesis studies showed that the substitution of these aspartate residues with alanine reduced the k_{cat} values by 4-5 orders of magnitude. [69] Interestingly, the X-ray structure of *trans*-FPP synthase suggested that the aromatic residue Phe 112 plays a key role in determining the ultimate length of the hydrocarbon chain in the product. This residue is located at a distance of approximately 12 Å from the first DDxxD motif that binds the GPP substrate. This motif is near a large hydrophobic pocket that

contains the growing hydrocarbon tail of the product. The size of the active site hydrophobic pocket can be altered to conveniently accommodate an increasing number of isoprene units. For instance, replacement of the phenylalanine with smaller amino acids such as alanine and serine, shifted the product specificity from C_{15} (farnesyl diphosphate) to C_{20} (geranylgeranyl diphosphate) and C_{25} (geranylfarnesyl diphosphate), respectively. [70]

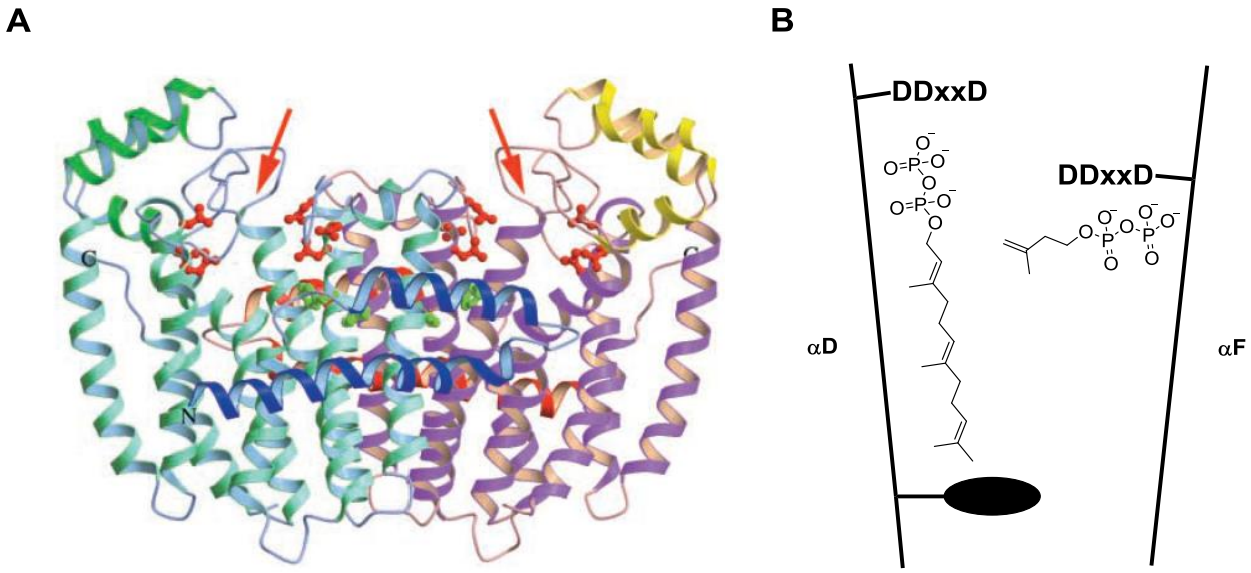

Figure 1.16 Crystal structure of *trans*-FPP synthase and graphic representation of the active site with FPP and IPP bound. A) refers to the model of avian FPP synthase and orange arrows refer to the location of active site. B) is the graphic representation of the enzyme active site showing DDxxD motifs, and the black circle represents Phe112. Diagram obtained from the crystallographic report on the enzyme. [64]

An S_N1 mechanism, which is also referred to as an 'ionization-condensation-elimination' mechanism, was proposed by Poulter for the transformation catalyzed by *trans*-FPP synthase. [71,72] Using fluorinated substrates, it was concluded that the first step in catalysis involves the dissociation of the diphosphate moiety from DMAPP (or GPP) forming a tertiary allylic

carbocation (Figure 1.17). A nucleophilic attack of the double bond of IPP onto the allylic carbocation generates a new tertiary carbocation intermediate which undergoes a deprotonation step to yield GPP (or FPP). [71,72]

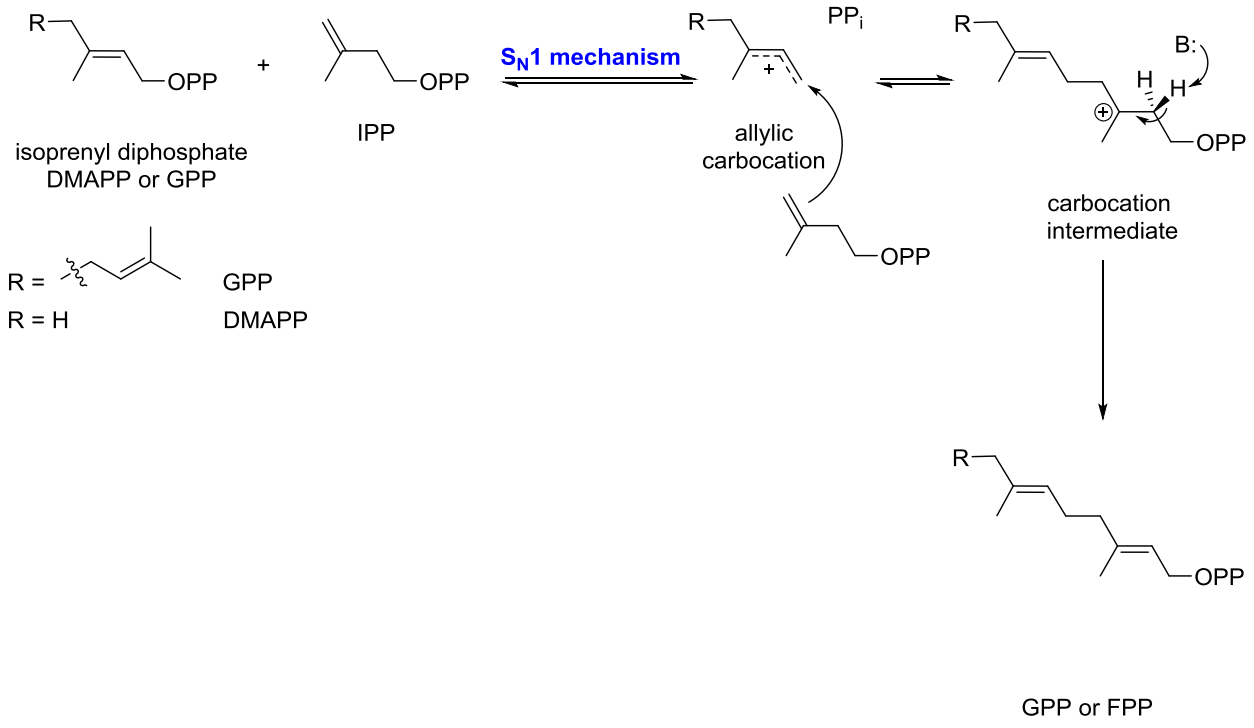

Figure 1.17 Proposed S_N1 mechanism for *trans*-farnesyldiphosphate synthase.

1.5.2 Protein Prenyltransferases: Protein Farnesyltransferase

Protein prenyltransferases belong to the second family of PTs, and they catalyze the attachment of a lipophilic isoprenyl group to a cysteine residue of a protein substrate (Figure 1.18). This cysteine residue is part of a CaaX tetrapeptide motif, where a's are aliphatic residues and X is often methionine, serine, or glutamine depending on the type of protein prenyltransferase. Protein prenylation is considered as an important post-translational

modification for a variety of proteins, such as members of the Ras and G protein families that are essential in a number of cell signaling systems. Approximately 0.5-2% of mammalian proteins are modified by the attachment of either a 15-carbon farnesyl or a 20-carbon geranylgeranyl group (Figure 1.18). [73] This isoprenoid modification is generally essential for the localization of the prenylated protein within the appropriate cellular membrane. The hydrocarbon chain of farnesyl group for instance, serves as an anchor on the membrane and promotes the localization of the prenylated proteins through hydrophobic interactions. This modification is crucial for the function of these proteins as well as their interaction with other proteins at a sub-cellular level. [74] The activities of protein PTs are dependent on the presence of a Zn^{2+} ion cofactor that coordinates with the cysteine thiolate of a protein substrate. Furthermore, the active site in these enzymes lack the Asp-rich DDxxD motif commonly associated with the binding of Mg^{2+}-diphosphate that is found in other prenyltransferases such as *trans*-FPP synthase. Notably, there is no sequence homology between the genes encoding for any of the isoprenyl diphosphate synthases and the protein FTs, suggesting a different mechanism for catalysis. A substantial amount of research has been directed towards the study of mammalian protein farnesyltransferase, presumably due to the fact that farnesylated Ras proteins are present in nearly 30% of human cancers. Since posttranslational modification of Ras through farnesylation is required for its full cellular function, inhibitors of protein farnesyltransferase have attracted significant interest as potential anti-tumor pharmaceutics. [75]

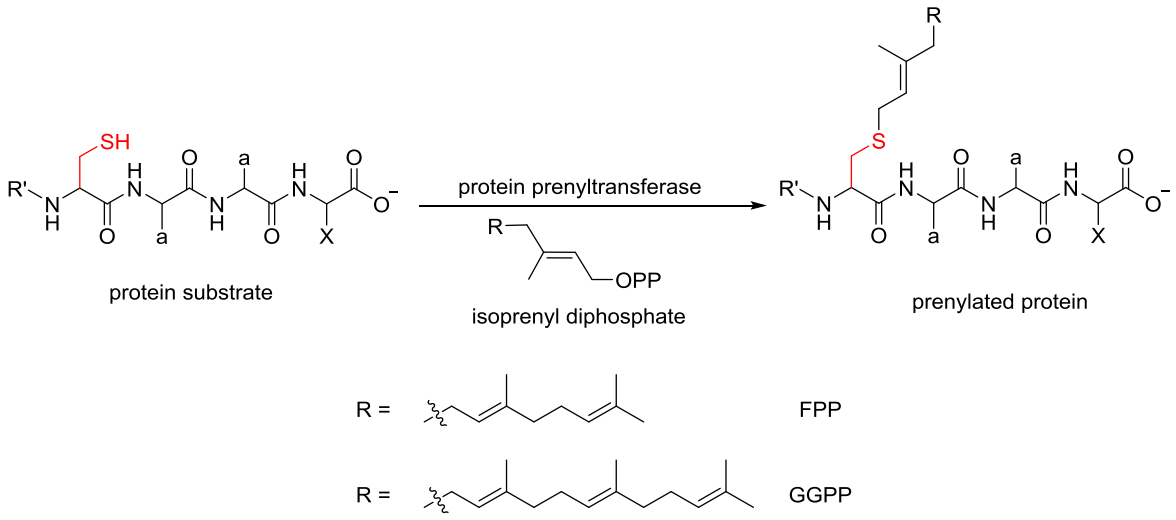

Figure 1.18 Reactions catalyzed by protein prenyltransferases. (Bonds colored in red represent the conserved cysteine residue)

Protein farnesyltransferase catalyzes the alkylation of the sulfur atom in the protein substrate through a substitution reaction between FPP and the cysteine residue of the protein. It requires both Zn^{2+} for cysteine activation and Mg^{2+} for diphosphate binding (although it lacks the DDxxD motif). Two distinct mechanistic pathways, S_N1 (dissociative) and S_N2 (associative), have been proposed for the catalysis (Figure 1.19). [76] Both mechanisms are initiated by the deprotonation of the cysteine thiol group which is subsequently coordinated to the Zn^{2+} ion in the active site pocket. The dissociative mechanism (S_N1) proceeds through the cleavage of diphosphate from FPP generating the corresponding allylic carbocation intermediate. The cysteine thiolate anion is then added to the positively charged C1 of the intermediate to yield the farnesylated protein. The associative mechanism (S_N2) on the other hand, proceeds through a single transition state, in which the steps involving the cleavage of diphosphate and the attack of nucleophilic thiolate occur simultaneously. [76,77] Whether protein farnesyltransferase employs an associative or a dissociative mechanism has been the subject of much speculation. To elucidate

the mechanism, fluorinated FPP analogs were employed as alternative substrates and their impact on the reaction rates were monitored. [77] It was hypothesized that the fluorine substitution would destabilize the corresponding allylic carbocations and consequently, reduce the reaction rates. The catalytic rates were depressed using fluorinated FPP, suggesting that significant carbocationic character is generated in the allylic group of FPP during catalysis. However, the magnitude of the rate depressions were less severe than those of the corresponding methanesulfonate derivatives in the non-enzymatic hydrolysis. To further investigate the mechanism, a deuterium-labeled FPP, [1,1-$^{2}H_{2}$]-FPP, was prepared and employed in the measurement of a kinetic isotope effect (KIE). [78] A large secondary isotope effect would be anticipated if the ionization of FPP was rate-determining (S_N1). An isotope effect near unity was observed that is more consistent with an S_N2 mechanism. It is now generally accepted that the mechanism involves an S_N2-like transition state, where there is considerable development of positive charge in the allylic moiety of FPP. [73]

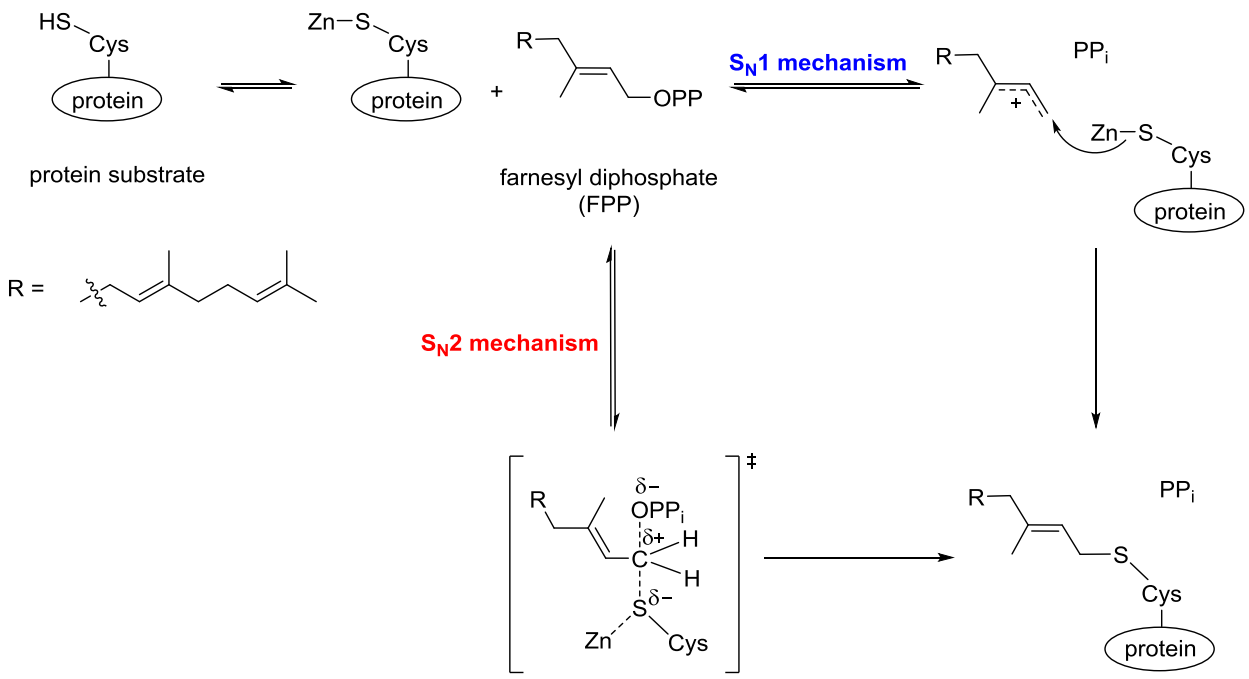

Figure 1.19 Proposed S_N1 and S_N2 mechanisms catalyzed by protein farnesyltransferase.

1.5.3 Small-Molecule Aromatic Prenyltransferases

The final category of PTs discussed here is the small-molecule aromatic prenyltransferase group. These enzymes accept aromatic substrates for prenylation and can be further subdivided into membrane-associated aromatic PTs and the soluble aromatic PTs (Figure 1.20). [63] The former group is involved in the biosynthesis of ubiquinones and menaquinones, phenolic secondary metabolites in plants, and the biosynthesis of membrane lipids in prokaryotes and archaea. Interestingly, they carry the same DDxxD motif for Mg^{2+}-mediated diphosphate binding that is present in the *trans*-FPP synthase. [79,80] Other than this motif, however, members of this family share no obvious sequence similarity with other known PTs. The latter group comprise the focus of this thesis and will be discussed in greater detail. Members of the soluble aromatic PT family (except NphB) catalyze their corresponding reactions in the absence of a divalent

metal cation. The crystal structures of these enzymes possess a unique antiparralel β/α-barrel peptide (α-β-β-α) fold that is characteristic of this family and distinctively sets it apart from the tertiary structure of the previously investigated PTs. [63] Hence, additional experiments need to be performed on this new class of soluble aromatic PTs to provide more insight into their structure, mechanism, and substrate specificity. Based on their amino acid sequences, the soluble aromatic PTs discovered to date can be further divided into two remotely related sub-categories, the PTs of bacterial origin and those of fungal origin.

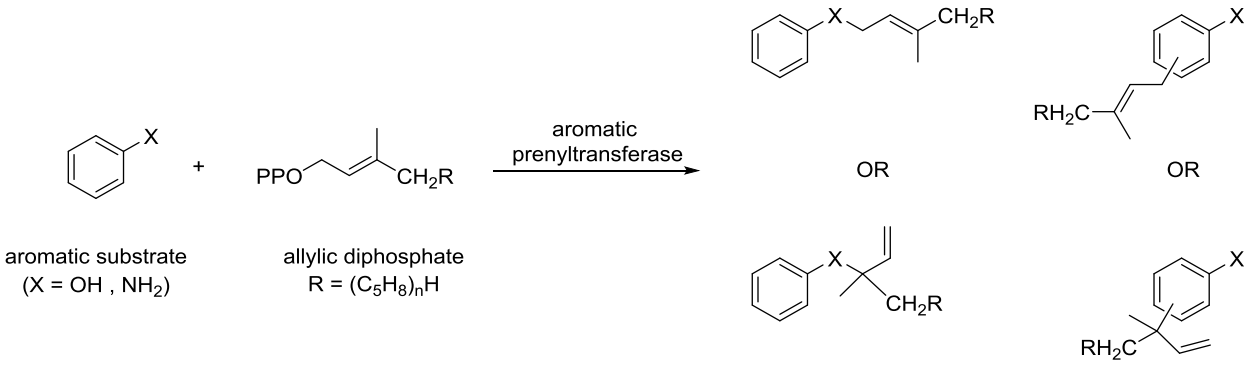

Figure 1.20 Reactions catalyzed by aromatic prenyltransferases.

1.5.3.1 Bacterial Aromatic Prenyltransferases

This first subclass of soluble aromatic PTs have recently been discovered in a number of species including the Gram positive soil bacteria *Streptomyces* sp. and the marine bacteria *Salinispora arenicola.* [63,81] X-ray crystallographic studies of these enzymes revealed a novel protein structure that contains an α-β-β-α pattern, and are therefore described as the ABBA family and/or the PT-barrel enzymes. [63] The first ABBA enzyme to be identified and characterized was CloQ that is involved in the biosynthesis of the antibiotic clorobiocin.

Moreover, the closely related NovQ protein is speculated to participate in the biosynthesis of another antibiotic, novobiocin. Finally, NphB is shown to play an important role in the biosynthesis of the anti-oxidant naphterpin (Figure 1.21). [63,82,83]

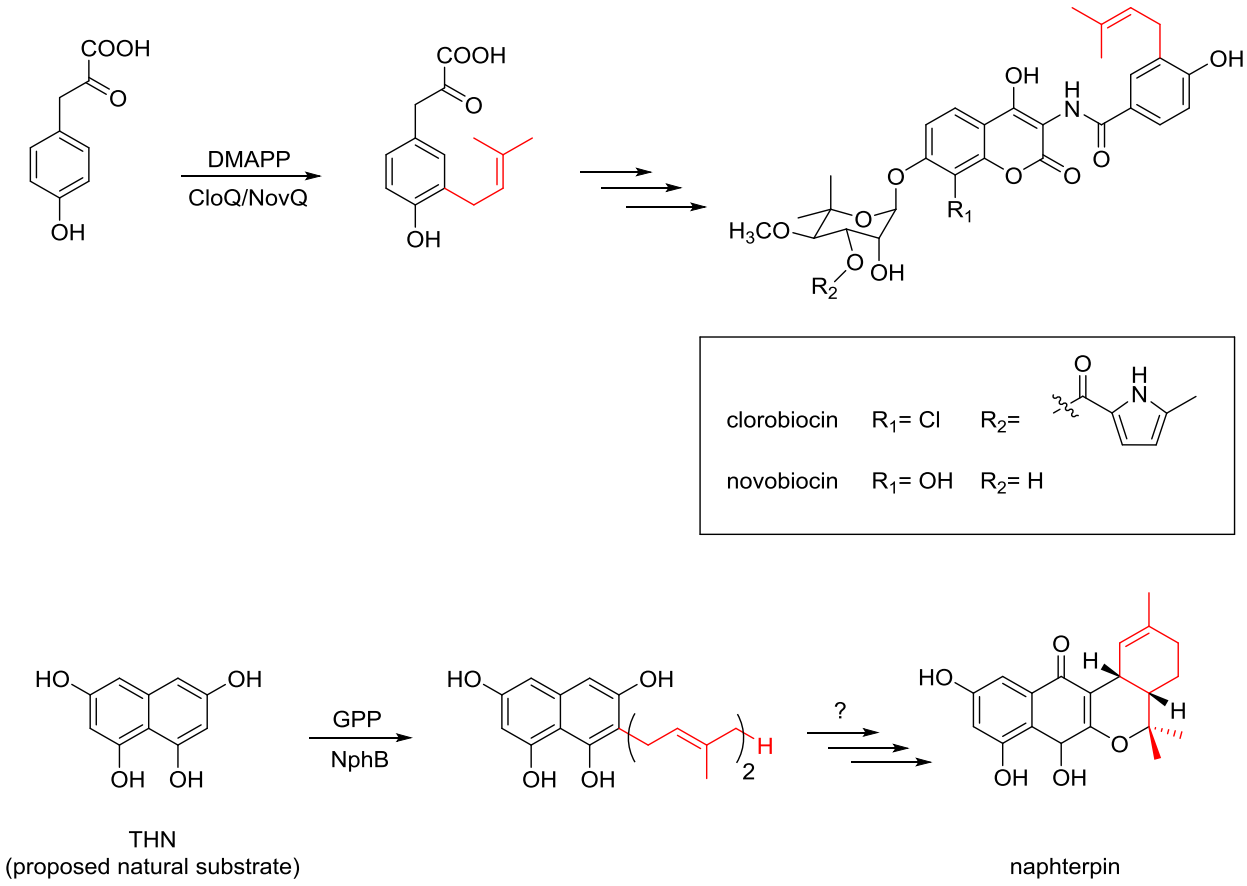

Figure 1.21 Reactions catalyzed by aromatic prenyltransferases, CloQ, NovQ and NphB. (Red denotes the chemical bonds derived from the prenyl groups)

NphB exhibits diverse substrate selectivity and can catalyze the transfer of a geranyl or farnesyl group onto a variety of small aromatic organic compounds *in vitro*. [84,85] Although the true physiological substrate of NphB is still a matter of much speculation, it has been shown to play a key role in the biosynthesis of the anti-oxidant naphterpin where it catalyzes the addition

of a 10-carbon geranyl moiety onto the aromatic substrate, 1,3,6,8 b-tetrahydroxynaphtalene (THN). Despite sharing a moderate sequence homology with other soluble aromatic prenyltransferases, NphB is the only enzyme in this family to require a Mg^{2+} cofactor for its activity. The crystal structure of NphB in complex with 1,6-dihydroxynaphtalene(1,6-DHN) and a non-hydrolysable GPP analog, geranyl *S*-thiolodiphosphate (GSPP) was obtained and the characteristic PT barrel, or ABBA arrangement, for this class of enzyme was observed (Figure 1.22). The PT barrel is a cylindrical β-sheet this is surrounded by several α-helices. This arrangement is reminiscent of the classical TIM barrel observed in the structure of triosephosphate isomerase; however, the central core in the PT barrel is comprised of ten anti-parralel β-strands instead of the parallel β-strands. Therefore, the connectivity of the secondary structure elements in the PT barrel differs considerably from that observed in the TIM barrels. [63,84]

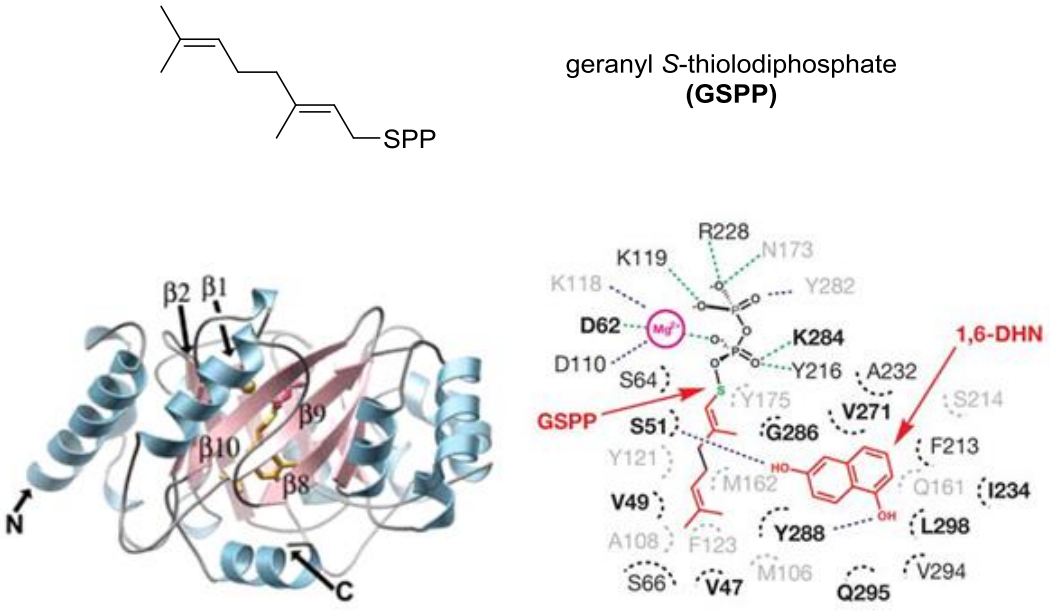

Figure 1.22 Crystal structure of NphB in complex with GSPP and 1,6-DHN and representation of the active site. Diagram was obtained from the crystallographic study of NphB (Note: the structure of GSPP shown in the active site is incorrect). [84]

There are uncertainties regarding the mechanism employed by NphB; however, crystallographic studies lead to the proposal of two distinct pathways for the prenylation. In the dissociative S_N1 pathway, the cleavage of the pyrophosphate moiety from GPP results in the formation of a geranyl carbocationic intermediate which is subsequently attacked by THN to yield a keto-intermediate (Figure 1.23). Rearomatization of this keto-intermediate occurs through a deprotonation step that yields the prenylated aromatic product. In the associative S_N2 pathway, the dissociation of the pyrophosphate moiety and the nucleophilic attack by THN occurs simultaneously to give the same keto-intermediate. [84] The crystallographic studies show that the distance between the nucleophilic carbon of the aromatic substrate and the C-1 of the thiol analog GSPP is approximately 4 Å. Since the distance between the two reacting carbon atoms is too long for a nucleophilic attack to take place, the authors suggested that the reaction follows a dissociative S_N1 mechanism where the cleavage of pyrophosphate moiety from GPP happens first. [63,84] Moreover, computational studies were also in favor of the S_N1 mechanism. [85] The free energy profile leading to the keto-intermediate showed two energy barriers that were separated by an intermediate state. The first energy barrier, which corresponded to the generation of an allylic carbocation, was shown to be the rate-limiting step for prenylation. The carbocationic intermediate was stabilized via cation-π interactions with two tyrosine residues that are located in the aromatic-rich binding pocket of NphB, thereby supporting a dissociative mechanism. [85]

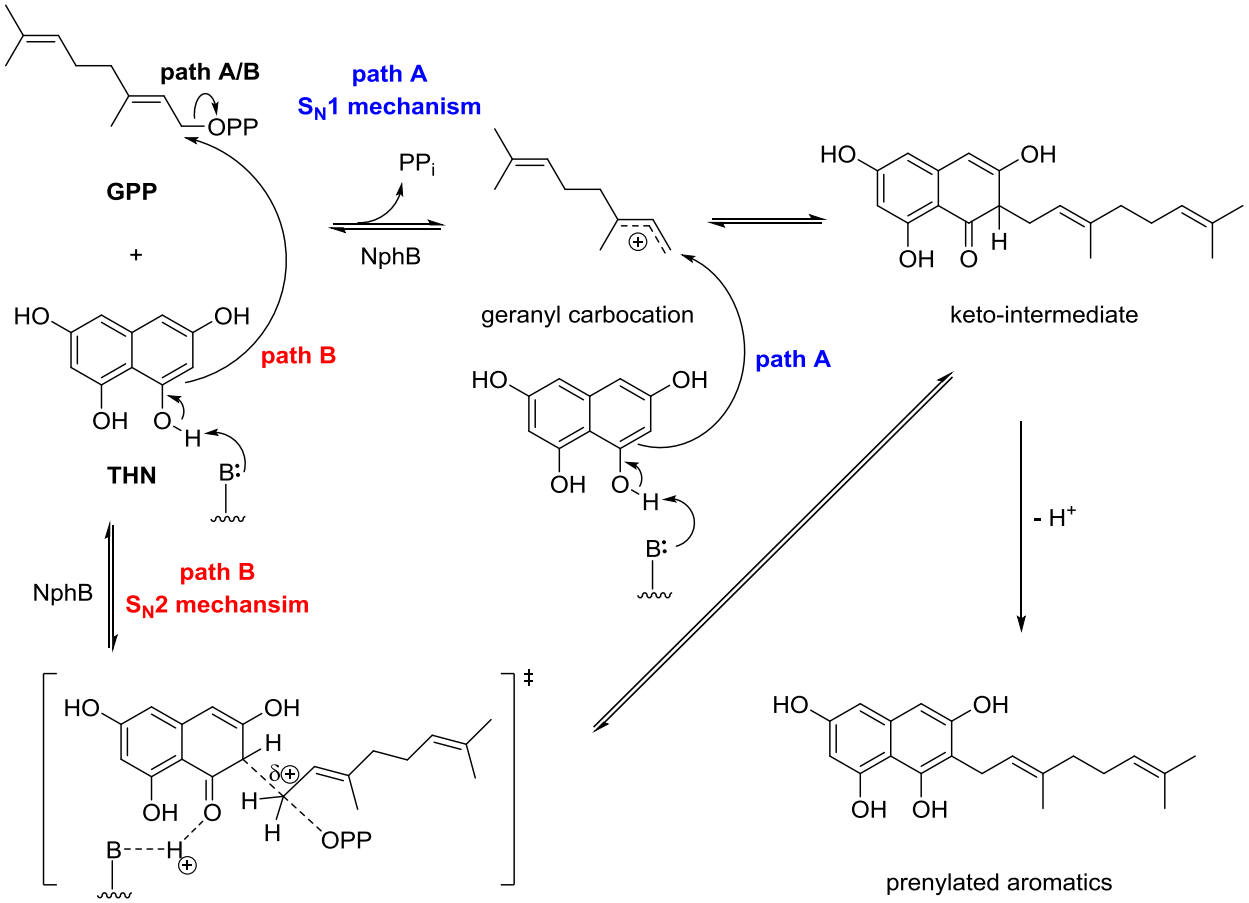

Figure 1.23 The proposed S_N1 and S_N2 mechanisms for the prenylation reaction catalyzed by NphB.

1.5.3.2 Fungal Indole Prenyltransferases: 4-Dimethylallyltryptophan Synthase

The second subcategory of soluble aromatic PTs is the indole PTs of fungal origin, which are remotely related to the soluble aromatic PTs of bacterial origin (~15-20% sequence identity). These enzymes have been identified in several fungal species and they catalyze the addition of a prenyl group to a large variety of aromatic substrates carrying an indole ring-system. [63,86,87] One example, 4-dimethylallyltryptophan synthase (DmaW) was isolated from *Claviceps purpurea* and was shown to catalyze the first committed step in the biosynthesis of the ergoline core found

in agroclavine. This is a precursor of ergotamine which is used to treat migraines and of the semi-synthetic compound, lysergic acid diethylamide (LSD) that is used in psychedelic therapy as well as a recreational drug, (Figure 1.24). Other examples of fungal indole PTs include, but are not limited to, fumigaclavine C synthase (FgaPT1) and another 4-dimethylallyltryptophan synthse (FgaPT2) that were isolated from *Aspergillus fumigates.* Both of the latter enzymes are involved in the biosynthesis of fumigaclavin C, which was initially believed to be a toxin but was later shown to possess potential therapeutic properties in protection against cardiovascular diseases. [86,87,88,89] Another indole PT isolated from *A. fumigates* is 7-dimethylallyltryptophan synthase (raction not shown), but its role in nature is still unclear. [90] All of these enzymes share high sequence similarities (26-35%) and retain their activity in the absence of a divalent metal ion. [82,83,86,87,89,90] Another category of indole prenyltransferases has recently been isolated from *A. fumigates,* which catalyzes the prenylation of cyclic dipeptide substrates. These enzymes will be discussed in detail in later sections.

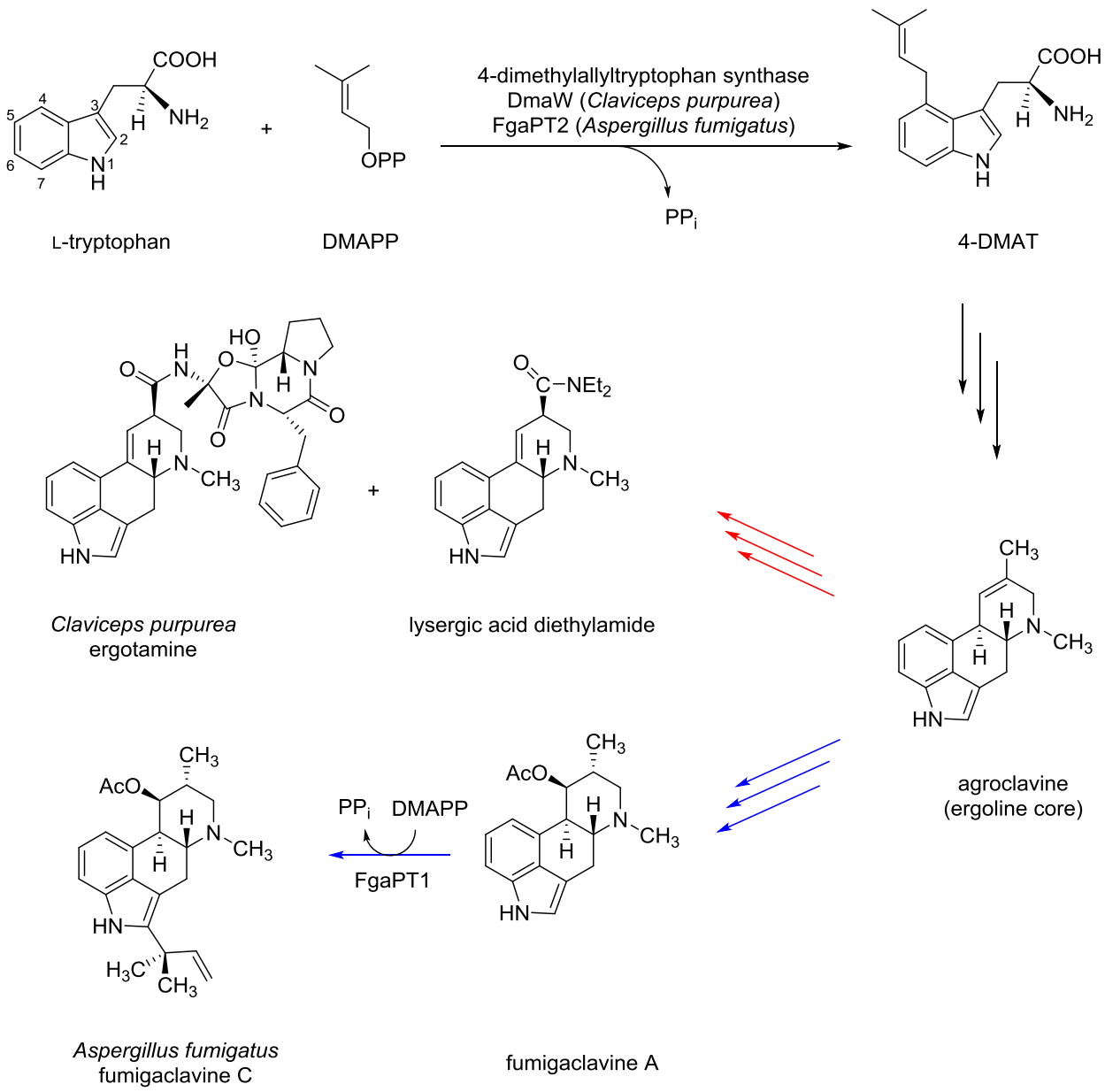

Figure 1.24 Reactions catalyzed by different fungal indole prenyltransferases. (Red arrows are indicative of the steps involved in the biosynthesis of lysergic acid in *Claviceps purpurea*, and blue arrows shows the biosynthesis of fumigaclavine C in *Aspergillus fumigates*)

4-Dimethylallyltryptophan synthase, including DmaW and FgaPT2 (which are generalized as 4-DMATS hereafter), is perhaps the most thoroughly studied fungal indole PT among all that have been discovered thus far. 4-DMATS catalyzes a Friedel-Crafts type reaction

by installing the prenyl moiety of DMAPP onto the C-4 position of L-tryptophan. The product of the reaction, 4-dimethylallyltryptophan (4-DMAT), is of biosynthetic value as it provides the carbon skeleton required for the formation of ergoline backbone (Figure 1.24); hence, 4-DMATS catalyzes the first committed step in the biosynthesis of the ergot alkaloids. This enzyme is generally produced in several fungal species of the genera *Claviceps*, *Aspergillus*, and *Penicillium* and its biochemical properties have been a matter of much investigation by several research groups. [91,92,93]

Two mechanisms have been proposed for the electrophilic aromatic substitution reaction catalyzed by 4-DMATS (Figure 1.25). The dissociative S_N1 pathway involves an initial ionization of DMAPP to form the pyrophosphate/dimethylallyl carbocation ion pair. The C-4 position of L-tryptophan then adds to the allylic carbocation to yield an arenium intermediate which is rearomatized through a final deprotonation step at H-4 generating 4-DMAT. [91,94] In the associative S_N2 pathway, the same arenium ion intermediate is formed; however, the nucleophilic attack by the aromatic ring onto DMAPP and the dissociation of pyrophosphate occurs simultaneously, via an associative transition state. [91]

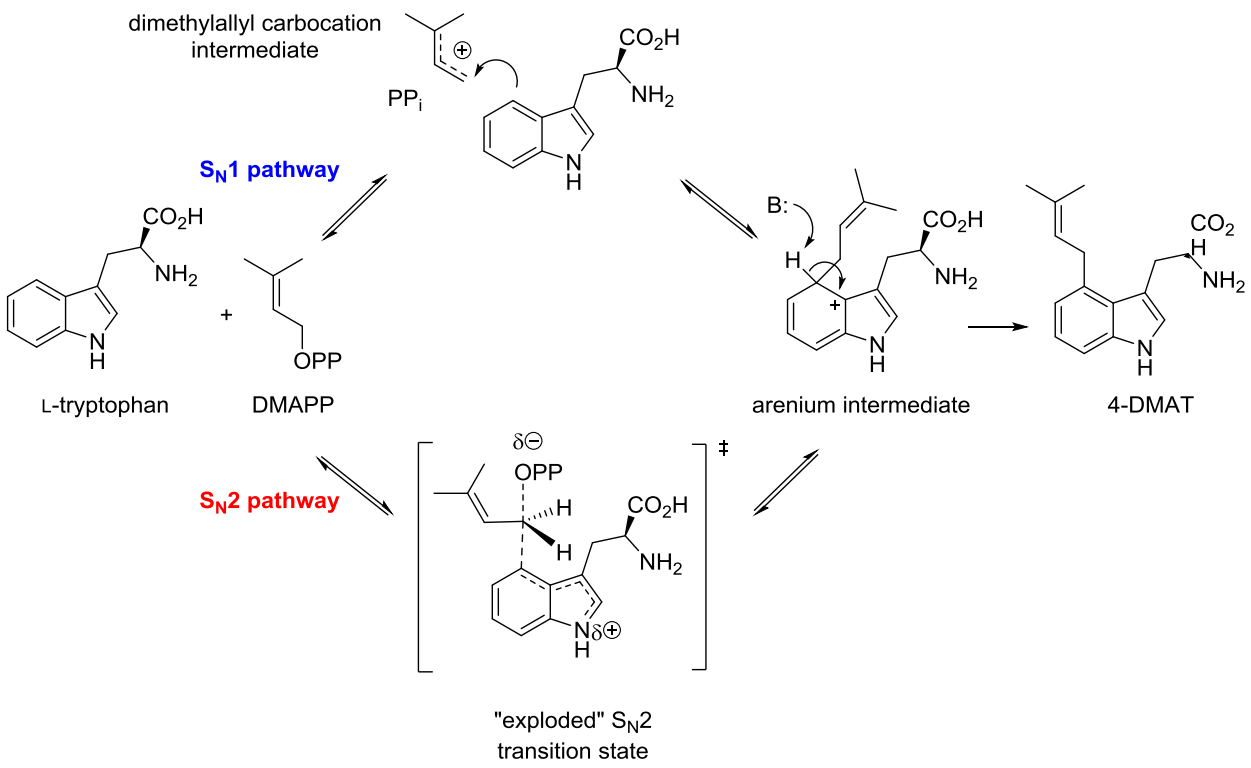

Figure 1.25 Two proposed mechanisms for the reaction catalyzed by 4-DMATS.

Poulter and his co-workers investigated the mechanism by examining the effects of substituting electron withdrawing groups onto either substrate. The reaction rates were measured using CH_2F- and CHF_2-analogs of DMAPP, as well as 7-substituted derivatives of L-tryptophan bearing F, CF_3, and NO_2 groups.[94] In both cases, the reaction was slowed down considerably. This observation was consistent with an electrophilic addition mechanism where a significant carbocationic character was developed in both the prenyl and indole groups. These results can be explained by either a dissociative mechanism or an associative mechanism that proceeds through an "exploded" transition state where considerable carbocationic character is developed on the dimethylallyl moiety of DMAPP.[95]

Additional insight into whether a discrete carbocation intermediate is formed during catalysis was gained by running a positional isotope exchange (PIX) experiment in our group.[96] When performing a PIX experiment, one follows the movement of an isotope, ^{18}O in this case, from a specific position in the starting material to a different position within the recovered starting material after a partial reaction. To perform this experiment, the synthetic [1-^{18}O]-DMAPP, which carries an ^{18}O-isotope at the position bridging the dimethylallyl and pyrophosphate moieties, was employed (Figure 1.26). After approximately 57% of the labeled substrate had been converted to product, the remaining starting material was analyzed for isotopic scrambling using ^{31}P NMR spectroscopy. According to the NMR results, 15% of the recovered DMAPP carried an ^{18}O isotope that had scrambled to a non-bridging position ([α-^{18}O]-DMAPP). This observation indicates that the cleavage of the C-O bond in DMAPP is a reversible process that occurs via a dissociative S_N1 mechanism and that the lifetime of the allylic carbocation is sufficient for bond rotation to occur in the pyrophosphate intermediate.

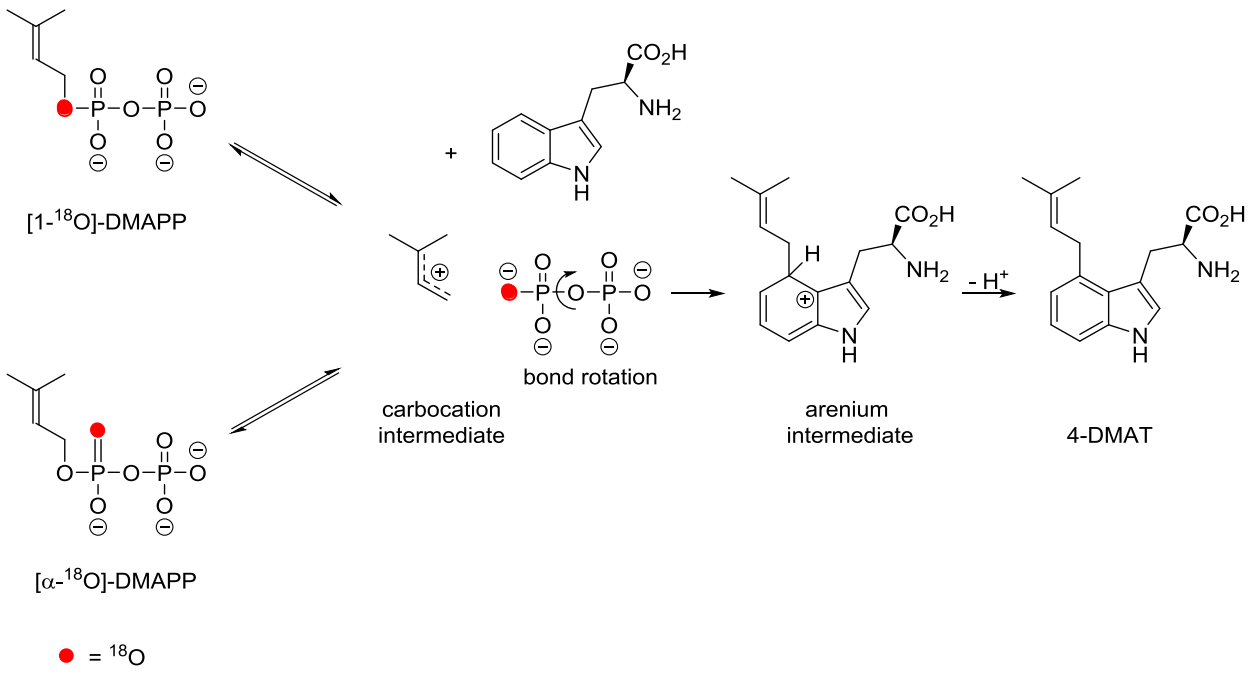

Figure 1.26 The positional isotope exchange experiment with 4-DMATS. (Solid red circle represent ^{18}O label)

The 2009 report of the crystal structure of 4-DMATS was a highlight in the understanding of indole prenyltransferases.[97] 4-DMATS was shown to adopt the rare ABBA fold (or prenyltransferase (PT) barrel fold), which was first seen with the aromatic PT, NphB that catalyzes the prenylation reaction of naphterpin. The crystal structure of 4-DMATS was obtained in complex with L-tryptophan and an unreactive thiol analog of DMAPP (Figure 1.27).[97] Three positive arginine and two lysine residues were found to interact with the diphosphate moiety of DMAPP. An additional network of hydrogen-bonds between the diphosphate group of DMAPP and a series of tyrosine residues are considered to be beneficial for the binding of the substrate as well as stabilizing the carbocationic intermediates via π-cation interactions.[97] In particular, the dimethylallyl group is sandwiched between the indole ring of L-tryptophan and the phenyl ring of Tyr345.

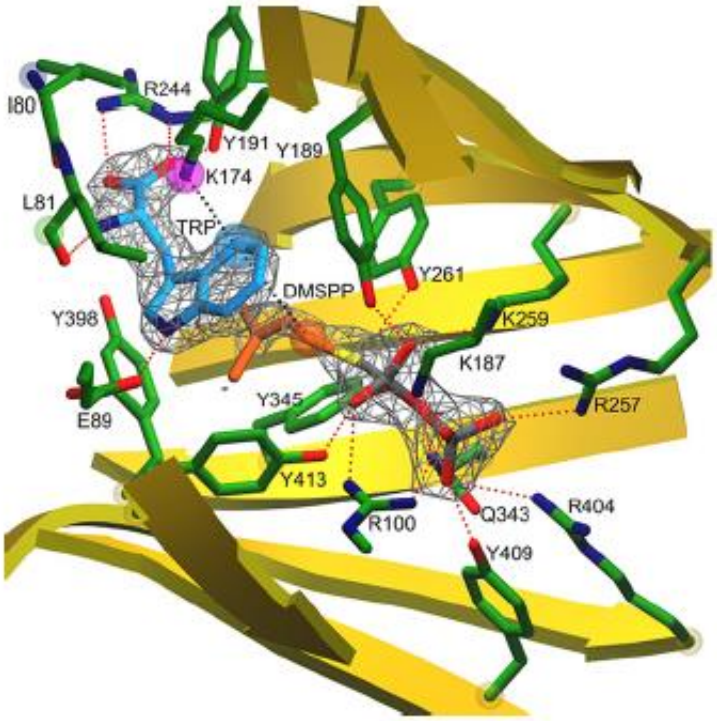

Figure 1.27 The structure of DMATS in complex with the thiol analog of DMAPP and L-Trp. Color code: nitrogen, blue; oxygen, red; phosphate, gray, and sulfur, yellow. Diagram obtained from the crystallographic report on the enzyme. [97]

Glu89 and Lys 174 were proposed to act as acid-base residues during catalysis. The carboxylate group of Glu89 was hydrogen-bonded to the indole NH, presumably increasing the nucleophilicity of C-4 via either deprotonation or the formation of a charged H-bond (Figure 1.28). When Glu89 was mutated to an alanine residue, no catalytic activity could be observed. Furthermore, the amine group of Lys174 was proposed to carry out the deprotonation of the arenium intermediate leading to the formation of 4-DMAT. Surprisingly, this lysine residue was found to be less important for catalysis as its mutation to a glutamine residue resulted in only a 60% loss in activity. It is possible that due to the low pK_a of the hydrogen being abstracted, the

glutamine residue in the mutant is still capable of acting as a strong enough base to carry out the re-aromatization of the arenium intermediate. [97,98]

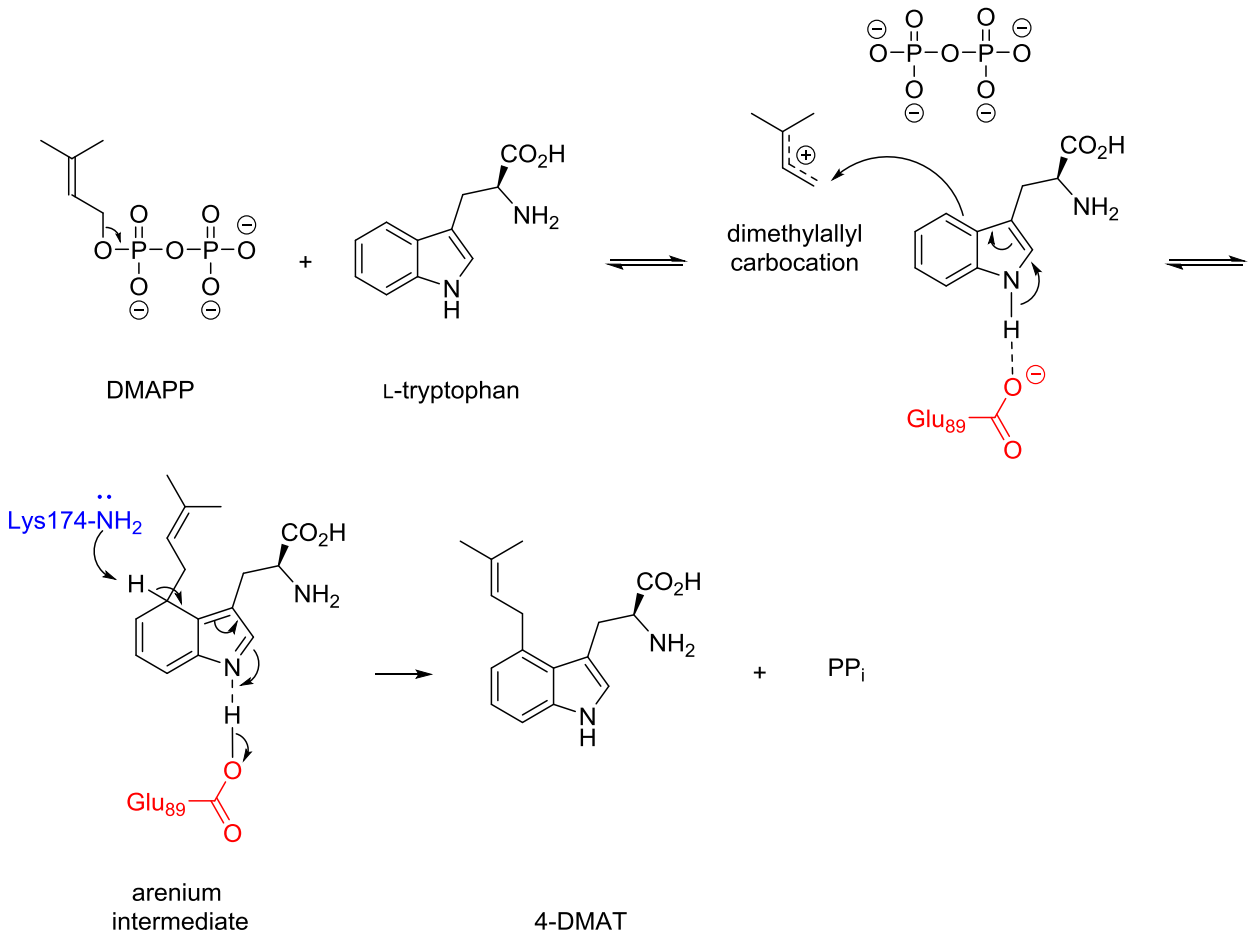

Figure 1.28 The proposed roles of Glu89 and Lys174 in the reaction catalyzed by 4-DMATS.

Analysis of the product of the reaction catalyzed by the Lys174Ala mutant afforded insight into an alternate possible mechanism for 4-DMATS. [98] It was found that the main product of this reaction was a reverse prenylated species **1** instead of 4-DMAT (Figure 1.29). Based on this observation, a mechanism involving a Cope rearrangement was proposed. Formerly, several groups have considered this mechanism as a way to explain how prenylation is directed towards

a less nucleophilic C-4 position of indole ring, but since no non-enzymatic precedence for the rearrangement was available, it was eventually disregarded. [37,99] This mechanism initiates with reverse prenylation at the C-3 position of the indole ring to yield an iminium intermediate. This initial step is strongly supported by the data obtained from the 4-DMATS crystal structure. The dimethylallyl moiety of DMAPP is coplanar with the indole ring of L-tryptophan, and the distance between the C-4 of the indole ring and the C-1 of DMAPP is 3.8 Å whereas that between the C-3 of the indole ring and the C-3 of DMAPP is 3.5 Å. [97] Given that these distances are similar and the C-3 position of an indole is far more nucleophilic than the C-4 position, one would expect that an attack from C-3 will predominate. [100] The C-3 reverse prenylated iminium intermediate would then undergo a reversible Cope rearrangement to generate a C-4 normal prenylated arenium ion. This step is achieved owing to the ability of the enzyme to hold the prenyl group in a position that resembles the transition state for the rearrangement. As shown in the crystal structure of 4-DMATS, the prenyl moiety is coplanar with the indole ring and is positioned in a manner that its C-1 and C-3 carbons are directly located above the C-4 and C-3 carbons of the indole ring, respectively. The final step of catalysis involves the deprotonation of the arenium intermediate by Lys174. In case of the Lys174Ala mutant, this deprotonation does not occur and instead the observed product **1** is formed through a ring closure of the C-3 reverse prenylated indole involving the α-amino group of tryptophan. [98]

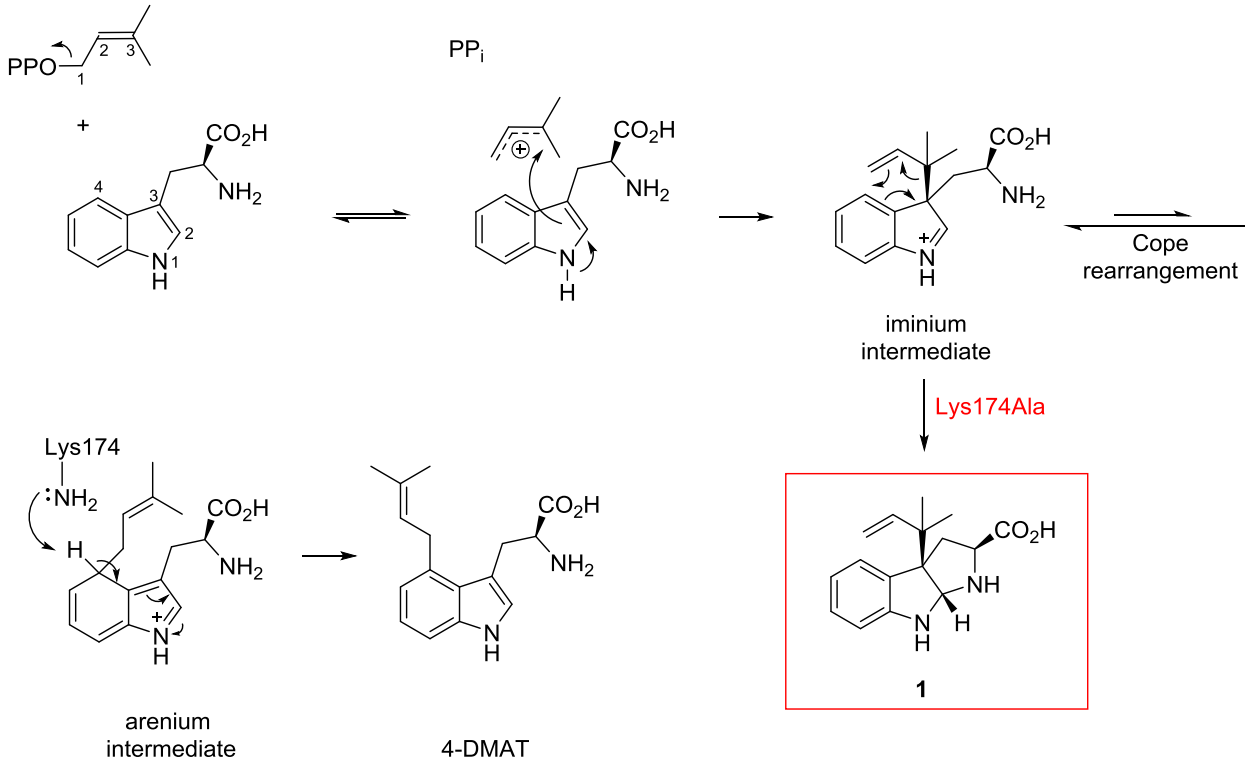

Figure 1.29 A Cope rearrangement mechanism proposed for the reaction catalyzed by 4-DMATS. (Red box represents the product of the reaction catalysed by Lys174Ala mutant)

1.5.4 C-3 Reverse Prenyl Transferase: Cyclic Dipeptide *N*-Prenyltransferase (CdpNPT)

The cyclic dipeptide *N*-prenyltransferase (CdpNPT) catalyzes the reverse C-3 prenylation of a variety of cyclic dipeptides and benzodiazepinediones (Figure 1.30). One might find it confusing for CdpNPT to be called a cyclic dipeptide *N*-prenyltransferase when it catalyzes the reverse prenylation at a carbon atom. This nomenclature was in fact the result of an initial missassignment of the product by the laboratory of Shu-Ming Li which will be discussed later.[101] The identity of the natural substrate of CdpNPT remains unknown; however, it has been shown to catalyze the reverse C-3 prenylation of a variety of benzodiazepinediones, tryptophan-containing cyclic dipeptides, as well as tryptophan itself (Figure 1.30). Benzodiazepinediones are

compounds with remarkable pharmacological potential in cancer therapy, and small-molecule inhibitors carrying this motif have been shown to suppress human tumor proliferation *in vitro*. [102,103,104] CdpNPT catalyzes the prenylation of both the (*S*)- and (*R*)-isomers of benzodiazepinedione **2**, and generates (2*S*, 3*R*)-aszonalenin exclusively when the (*S*)-enantiomer is used as the substrate (Figure 1.30). [105,106]

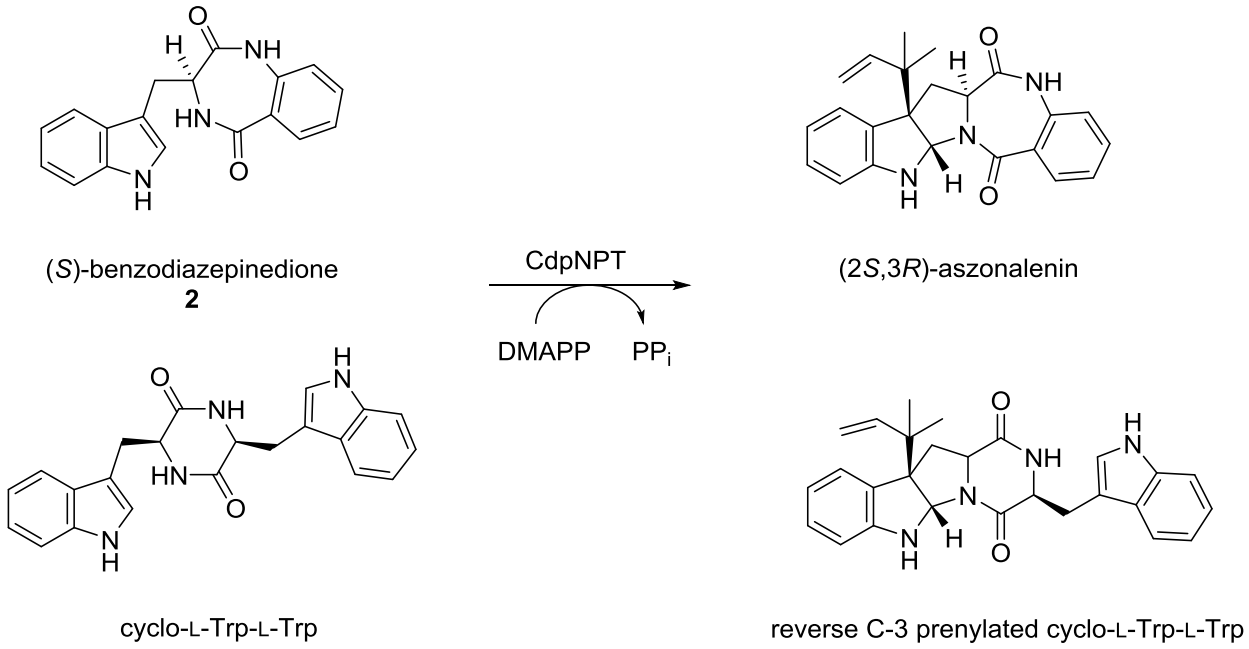

Figure 1.30 Reverse C-3 prenylation reaction catalyzed by CdpNPT prenyltransferase enzyme.

In the first ever report on CdpNPT, the product of the prenylation of cyclo-L-Trp-L-Trp was identified as the N-1 normal prenylated cyclo-L-Trp-L-Trp **4** (Figure 1.31). [101] Later studies by the same research group proposed that the true product of this catalysis is the reverse N-1 prenylated cyclo-L-Trp-L-Trp **3** which undergoes a non-enzymatic rearrangement to generate the previously observed normal N-1 prenylated cyclo-L-Trp-L-Trp **4** when treated with trichloroacetic acid (TCA). [107] This had occurred since TCA was used during protein

precipitation and termination of the enzymatic reaction. Therefore, the authors suggested that the initial observation of the normal N-1 prenylated product **4** was in fact an artefact due to rearrangement of the true enzymatic product, which was proposed to be the reverse N-1 prenylated cyclic dipeptide **3**. Use of methanol instead of TCA avoided the unwanted rearrangement. [107]

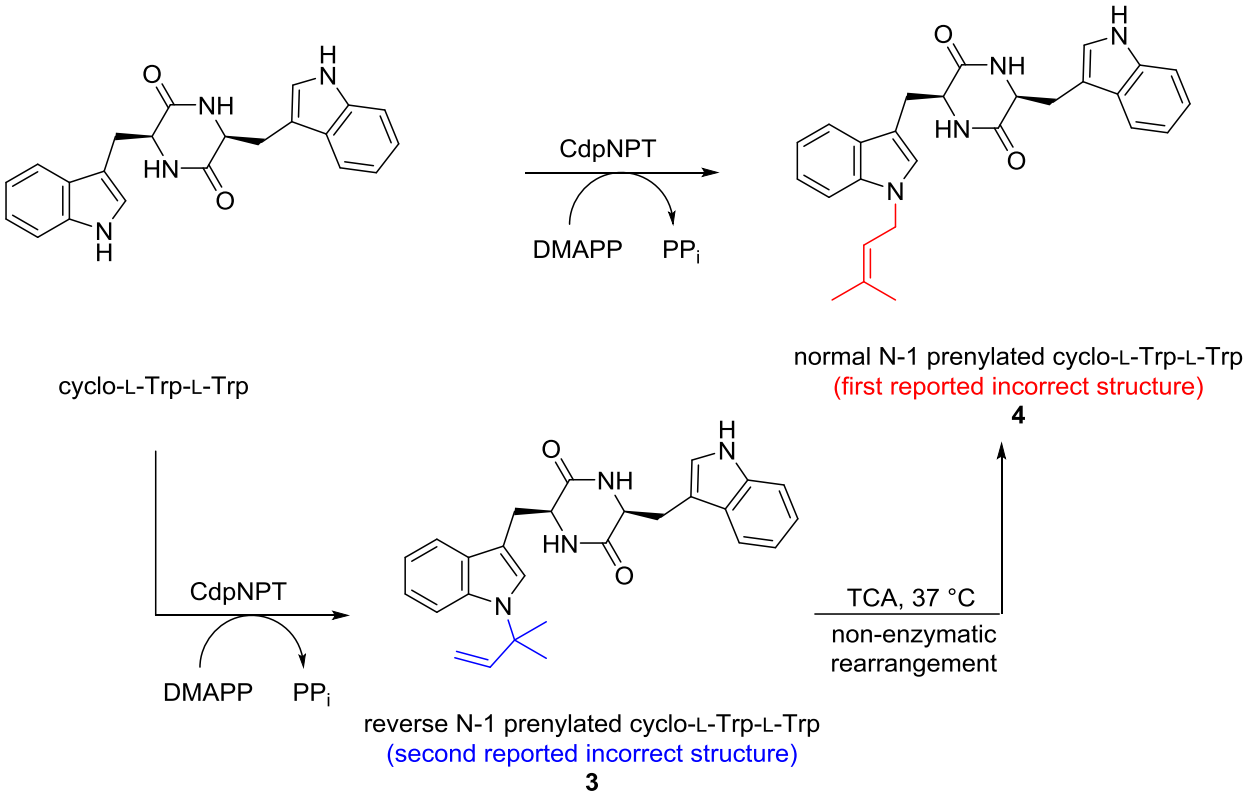

Figure 1.31 Initial incorrect reports on the structure of the product formed in the reaction catalyzed by CdpNPT.

When we carefully inspected the reported ^{1}H NMR spectrum of the product **3**, we noticed that the reported chemical shifts did not match with the proposed structure (Figure 1.32). The signal that appeared at a chemical shift of 5.52 ppm was assigned to the C-2 proton of the reverse prenylated indole ring. The C-2 proton of the unmodified indole ring on the other hand, appeared

at the chemical shift value of 7.11 ppm. Furthermore, the sp^2 hybridized C-2 protons of L-tryptophan and *N*-DMAT appear at 7.26 and 7.48 ppm, respectively. [81] Although the latter two chemical shifts are reported in a different solvent from that of compound **3**, the observed upfield shift in the C-2 proton signal in **3** is most likely due to its different hybridization (possibly sp^3) from that of L-Trp and *N*-DMAT (sp^2).

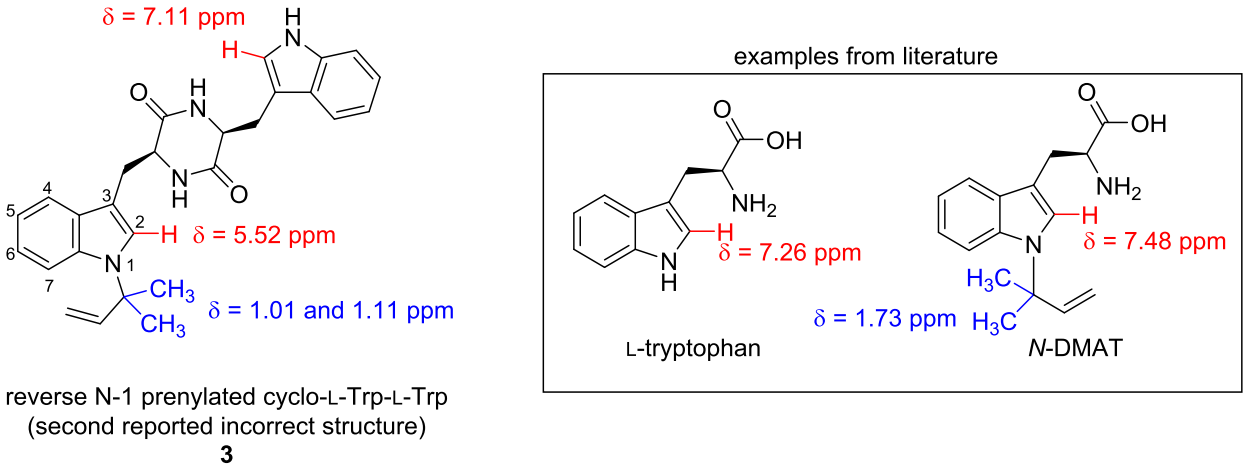

Figure 1.32 A comparision between the chemical shifts of the reported product of CdpNPT 3 (in CD_3OD) and some examples from literature (in D_2O). The inset shows the structure of L-Trp and the synthetic *N*-DMAT.

Most importantly, a previous study in our lab focusing on the mechanistic studies of the indole prenyltransferase 4-DMATS, led us to suspect that the correct product of the CdpNPT-catalyzed reaction contains a hexahydropyrroloindole structure that is reverse prenylated at the C-3 position (Figure 1.33). When the ^1H NMR spectrum of compound **3** was compared to that of the hexahydropyrroloindole **1**, we noticed a remarkable resemblance between the two spectra. [98] The methyl protons of the prenyl group in compound **3** appeared at a chemical shift very similar to that of compound **1** (at about 1.00 ppm). Three alkene signals were observed which is

characteristic of a compound that has been reverse prenylated. Finally, the observation that the C-2 proton signal has been shifted upfield provides further evidence for the existence of a hexahydropyrroloindole in the product of CdpNPT reaction.

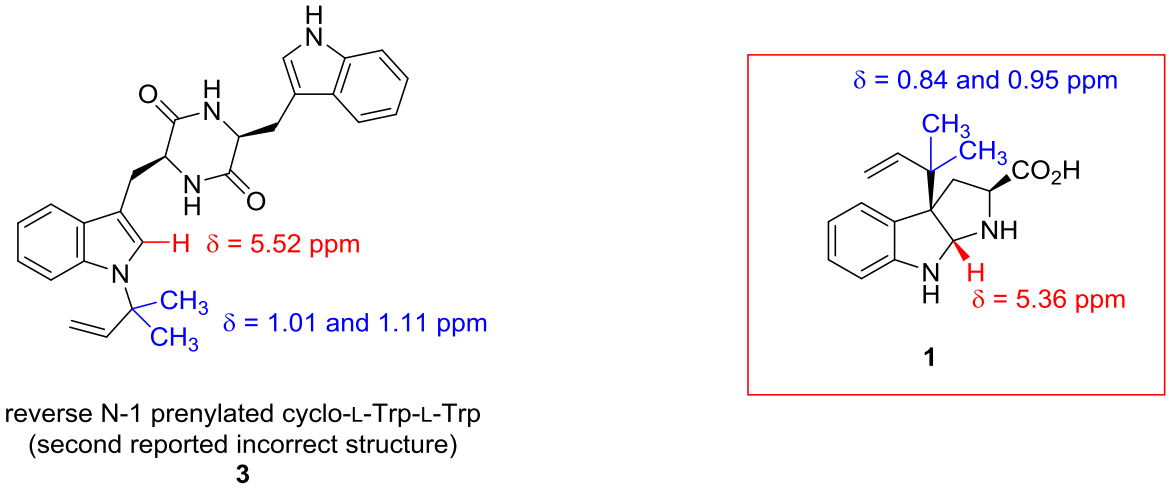

Figure 1.33 A comparision between the chemical shift values of the reported incorrect product of the CdpNPT reaction 3 with those of compound 1.

The first part of Chapter 2 identifies the structure of the true product of the CdpNPT reaction as reverse C-3 prenylated and proposes a mechanism for this transformation. The possibility of a TCA-promoted aza-Cope rearrangement that converts this reverse prenylated product into the N-1 normal prenylated compound **4** is also explored as a part of the second chapter.

1.5.5 C-2 Normal Prenyltransferase: Brevianamide F Prenyltransferase (FtmPT1)

Brevianamide F prenyltransferase (FtmPT1), also known as tryprostatin B synthase, catalyzes the normal C-2 prenylation of the cyclic dipeptide, cyclo-L-Trp-L-Pro (brevianamide F), to generate tryprostatin B, which will ultimately form fumitremorgin B (Figure 1.34).

Tryprostatin B is a biologically active molecule that inhibits cell cycle progression in the G2/M phase and has been found to exhibit cytotoxicity towards different cancer cell lines. It is also the biosynthetic precursor to fumitremorgin B, which is a mycotoxin with tremorgenic activity. [108,109] FtmPT1 was first isolated from *Aspergillus fumigates* and was characterized by the Shu-Ming Li group in 2005. [104] It shows a relaxed substrate specificity and accepts a variety of cyclic dipeptides as its substrate. Furthermore, the catalytic activity of the enzyme was found to be independent of the presence of a metal.

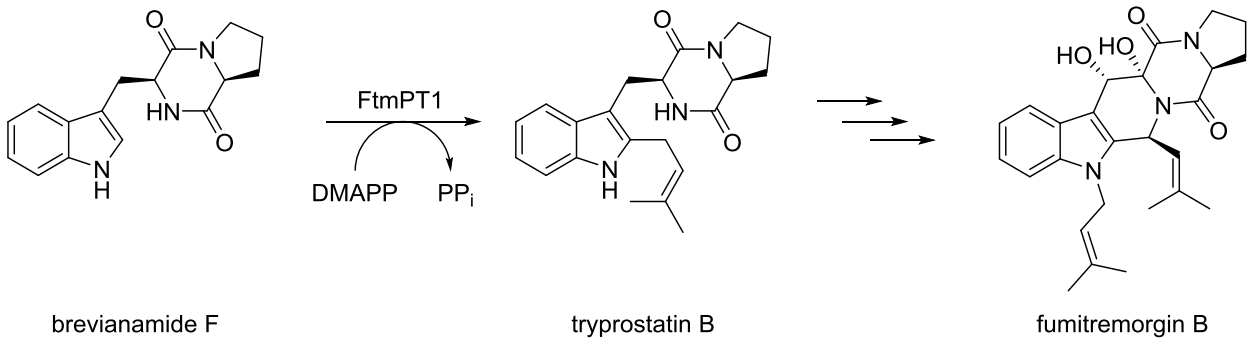

Figure 1.34 Prenylation reaction catalyzed by FtmPT1 to form tryprostatin B. The structure of fumitremorgin B is also shown.

In 2010, the structure of FtmPT1 was solved in complex with its substrate, brevianamide F, and the non-hydrolyzable thiol analog of DMAPP, dimethylallyl *S*-thiolodiphosphate or DMSPP. [110] It shows significant similarity to the crystal structure of 4-DMATS and contains the common PT barrel fold that is observed with many fungal indole prenyltransferases (Figure 1.35). The indole NH is linked by a hydrogen bond to the carboxylate group of a glutamate residue (E102), which is conserved in all fungal indole prenyltransferases and its mutation to a glutamine abolished formation of any product. The terminal phosphate of DMSPP is anchored by two positively charged arginine and lysine residues, R113 and K294, while the α-bridging

phosphate group hydrogen bonds to the hydroxyl groups of two tyrosine residues, Y203 and Y450. Additionally, four tyrosine residues in combination with a phenylalanine (Y203, Y269, F280, Y382, and Y450) form a ring-shaped tyrosine shield that likely protects the dimethylallyl cation intermediate from nucleophilic attack by water or solvent. The DMAPP binding site is highly conserved in both 4-DMATS and FtmPT1, while the substrate binding pocket is substantially enlarged in FtmPT1 to accommodate the larger cyclo-L-Trp-L-Pro substrate. This increase in size is achieved through a replacement of a threonine residue with a smaller glycine (Gly115) and an arginine residue with a histidine (His279). This also accounts for differences in the locations of two substrates. The relative orientation of the prenyl moiety and the indole ring is surprisingly similar to that observed in 4-DMATS; however, the position of the indole ring is shifted by 1 Å further into the binding pocket when compared to that of L-Trp in 4-DMATS. This shift is primarily due to the exchange of G115 for T102 as the absence of a side chain in glycine 115 makes space for the indole ring to slide deeper into the binding pocket. Furthermore, the indole ring of brevianamide F is tilted away from the dimethylallyl moiety by 180° as compared to that of 4-DMATS. This observation can possibly be the result of the substitution of leucine 81 in 4-DMATS by methionine 94 in FtmPT1. [110]

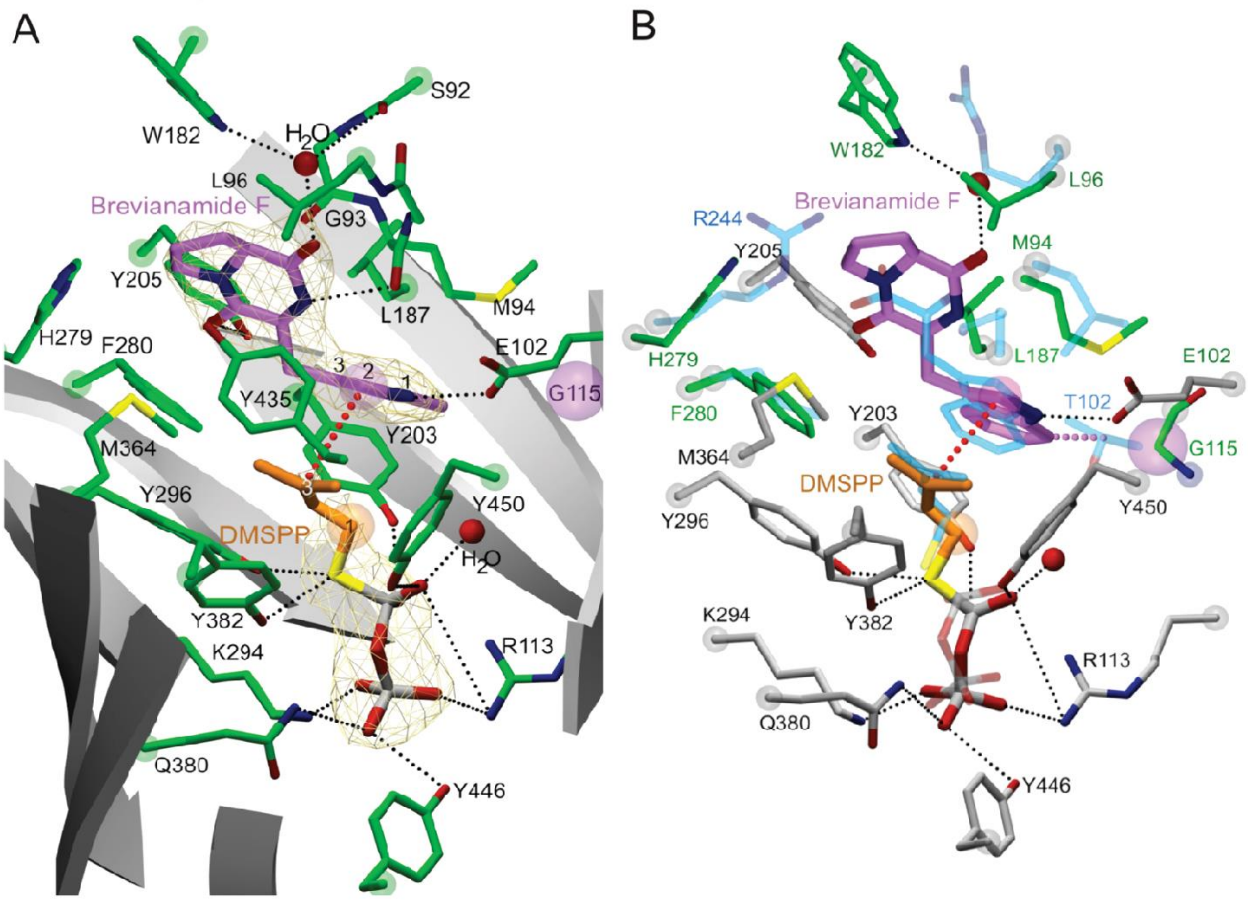

Figure 1.35 The structure of FtmPT1 in complex with brevianamide F (violet) and DMSPP (orange). (A) Cross section of the active site with the bound substrates. (B) Comparison of substrate binding in FtmPT1 and 4-DMATS. Equivalent amino acids are shown in gray. Carbon atoms of residues that differ between FtmPT1 and 4-DMATS are shown is green and blue, respectively. Diagram obtained from crystallographic report on the enzyme. [110]

FtmPT1 catalyzes a Friedel-Crafts type reaction that is similar to the electrophilic alkylation reaction catalyzed by 4-DMATS, although it exhibits a different regioselectivity. Since the relative orientation of the prenyl group and the indole ring in the active site of FtmPT1 is remarkably similar to that observed in 4-DMATS, the Shu-Ming Li group suggested that a similar dissociative mechanism is employed by FtmPT1. [110] This similarity is quite surprising

given that FtmPT1 catalyzes the transfer of a prenyl group onto the C-2 position of the indole ring, which is 5.2 Å away from the C-1 position of DMAPP (Figure 1.36).

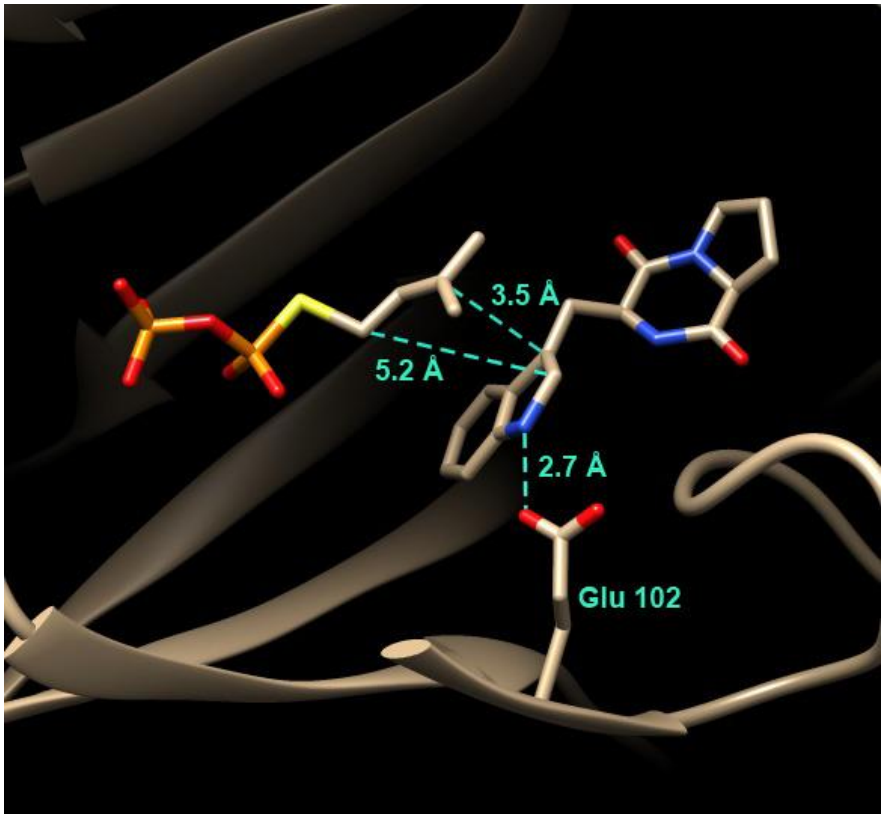

Figure 1.36 Active site structure of FtmPT1 showing the relative positions of the thiol analog of DMAPP and the indole ring of brevianamide F. A key active site residue (E102) is also shown (Data was taken from PDB ID : 302K).

Since the positioning of the two substrates does not seem to account for the formation of the observed product, the authors invoked a mechanism in which ionization of DMAPP initially occurs to form pyrophosphate and the free dimethylallyl cation, and then the cation undergoes a 180° rotation, which is referred to as a "cation-flip". This reorientation will position the primary carbon of the dimethylallyl cation in close proximity of the C-2 of the indole ring and thus, the prenylation at C-2 can occur. A final deprotonation step restores the aromaticity and generates the product, tryprostatin B (Figure 1.37). Mutagenesis studies suggest that glutamate E102 serves

as a key residue in catalysis. It not only serves to activate the indole ring for nucleophilic attack through hydrogen bonding to the N-H group, but also may act as a base in the final deprotonation step. The mutation of this glutamate residue to glutamine (E102Q) reduced the formation of tryprostatin B to undetectable amounts. [110]

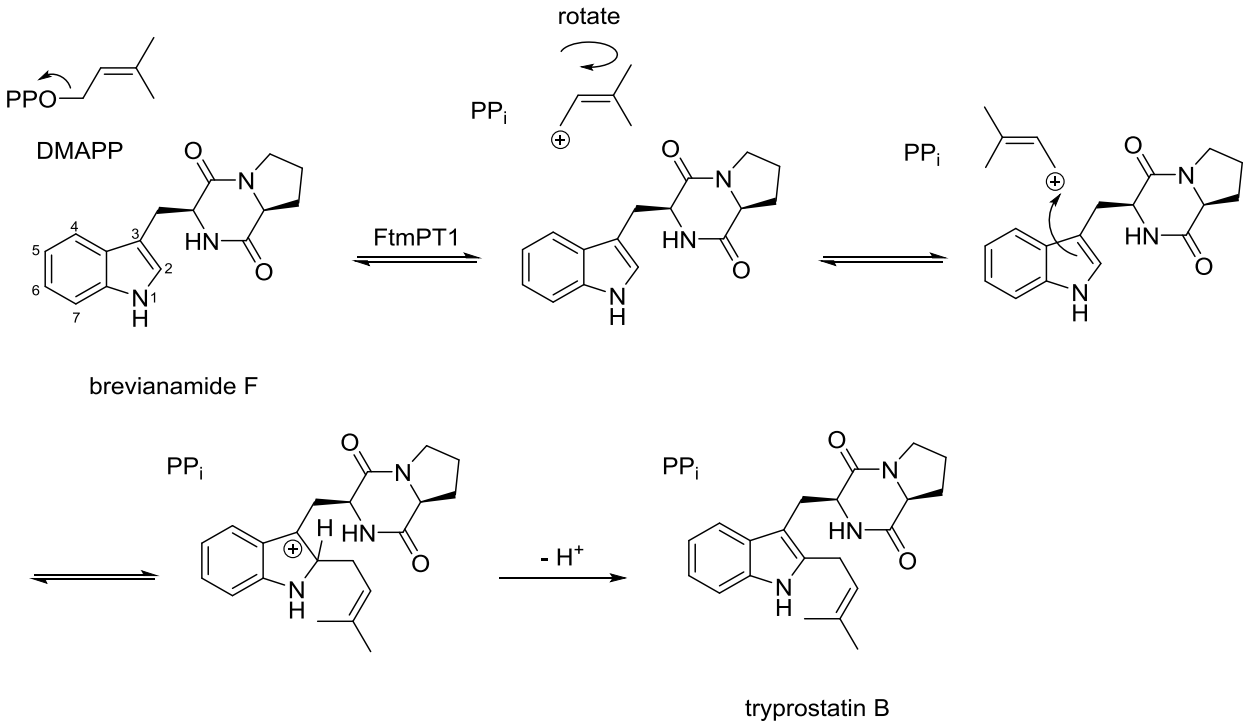

Figure 1.37 A direct alkylation mechanism for the reaction catalyzed by FtmPT1 involving a "cation-flip" step.

While the C-2 position of the indole is fairly nucleophilic and the "cation-flip" mechanism is certainly plausible, it seems rather unlikely for an enzyme like FtmPT1 to employ a mechanism in which a highly reactive intermediate is required to undergo a dramatic reorientation in the active site. A closer look at the active site reveals that the C-3 of the indole ring is in a much more favorable position for a nucleophilic attack since it is only 3.5 Å away from the C-3 of DMSPP (Figure 1.36). This observation suggests that an alternative mechanism

involving a C-3 prenylation may be responsible for the formation of the observed product (Figure 1.38).

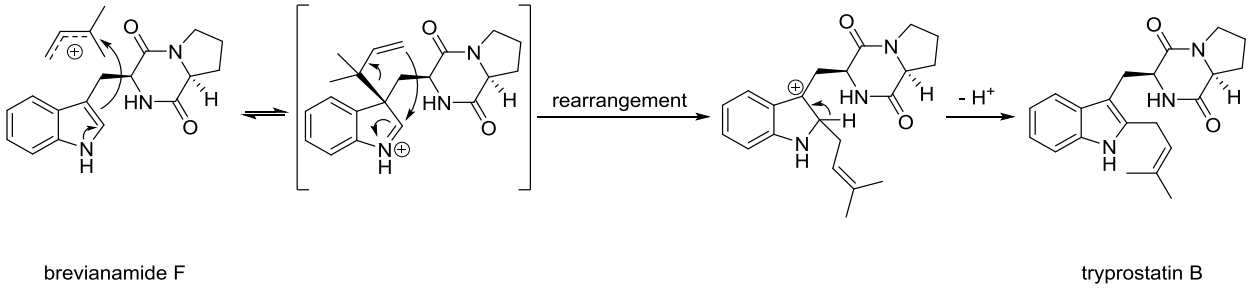

Figure 1.38 Alternative mechanism for FtmPT1 involving a C-3 reverse prenylation.

Apart from the structural analysis, recent studies have indicated that FtmPT1 is capable of catalyzing reactions that form C-3 reverse prenylated products. [110,111] For instance, it was reported that the Gly115Thr mutant of FtmPT1 forms a different product **5** that is reverse prenylated at the C-3 position of the indole ring (Figure 1.39). Interestingly, this compound has an analogous structure to that of compound **1** formed by the Lys174Ala mutant of 4-DMATS (Figure 1.29). The Gly115 residue had been mutated in an attempt to convert FtmPT1 into a 4-DMATS as one of the main differences in the active sites is the substitution of the Gly115 in FtmPT1 with Thr102 in 4-DMATS. This mutation might have imposed an increased steric bulk on the system which could have resulted in the mis-positioning of the indole ring and consequently, an unusual C-3 reverse prenylation. An alternative explanation suggests that the enzyme normally catalyzes a reverse C-3 prenylation as its first step followed by a rearrangement to give normal C-2 prenylation. The mutated FtmPT1 may no longer be capable of facilitating the rearrangement step and as a result, compound **5** represents an intermediate that has been released into solution, and subsequently cyclizes.

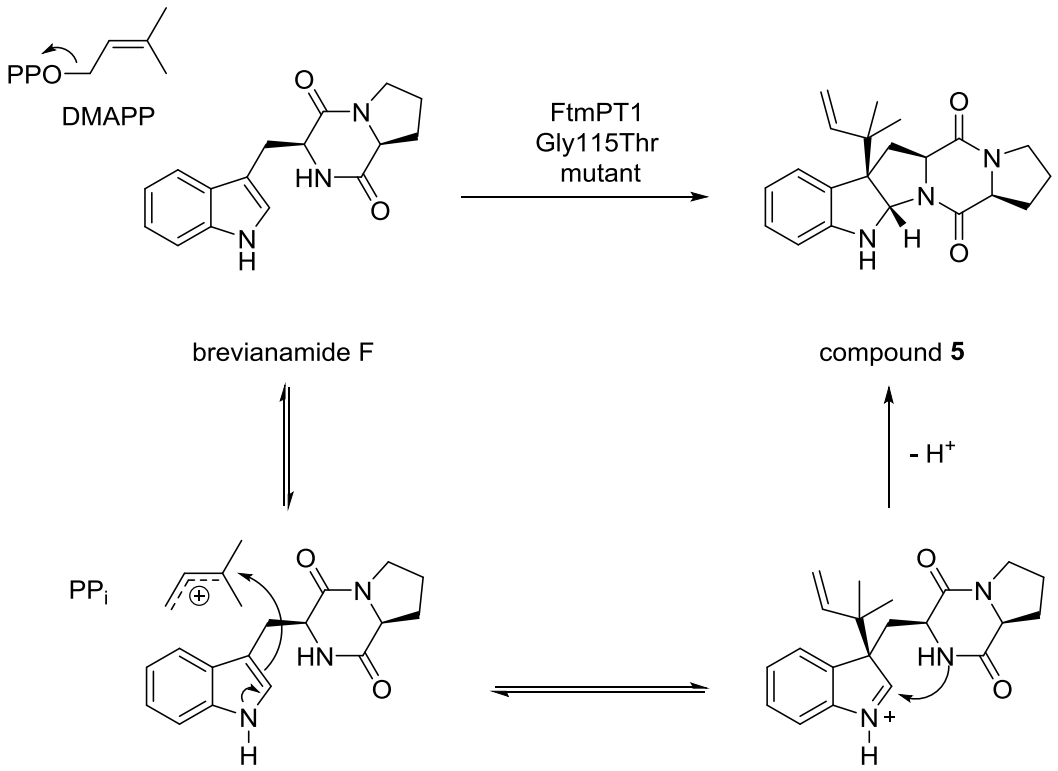

Figure 1.39 The reaction of brevianamide F catalyzed by the Gly115Thr mutant of FtmPT1.

Another example involved the use of an indole butanone derivative **6** as an alternate substrate in the reaction catalyzed by FtmPT1. [111] Interestingly, the product **7** of this reaction was found to be prenylated at a non-aromatic alkene position in a normal fashion. Two distinct pathways were proposed for the formation of compound **7** (Figure 1.40). One possibility involves the direct prenylation at the α-position of the α,β-unsaturated carbonyl compound **6** (Figure 1.40A), which is similar to the direct "cation-flip" mechanism. Alternatively, the catalysis can be initiated with a reverse prenylation at the C-3 position of the indole moiety followed by a Cope rearrangement to install the prenyl group on to a nonaromatic alkene position (Figure 1.40B).

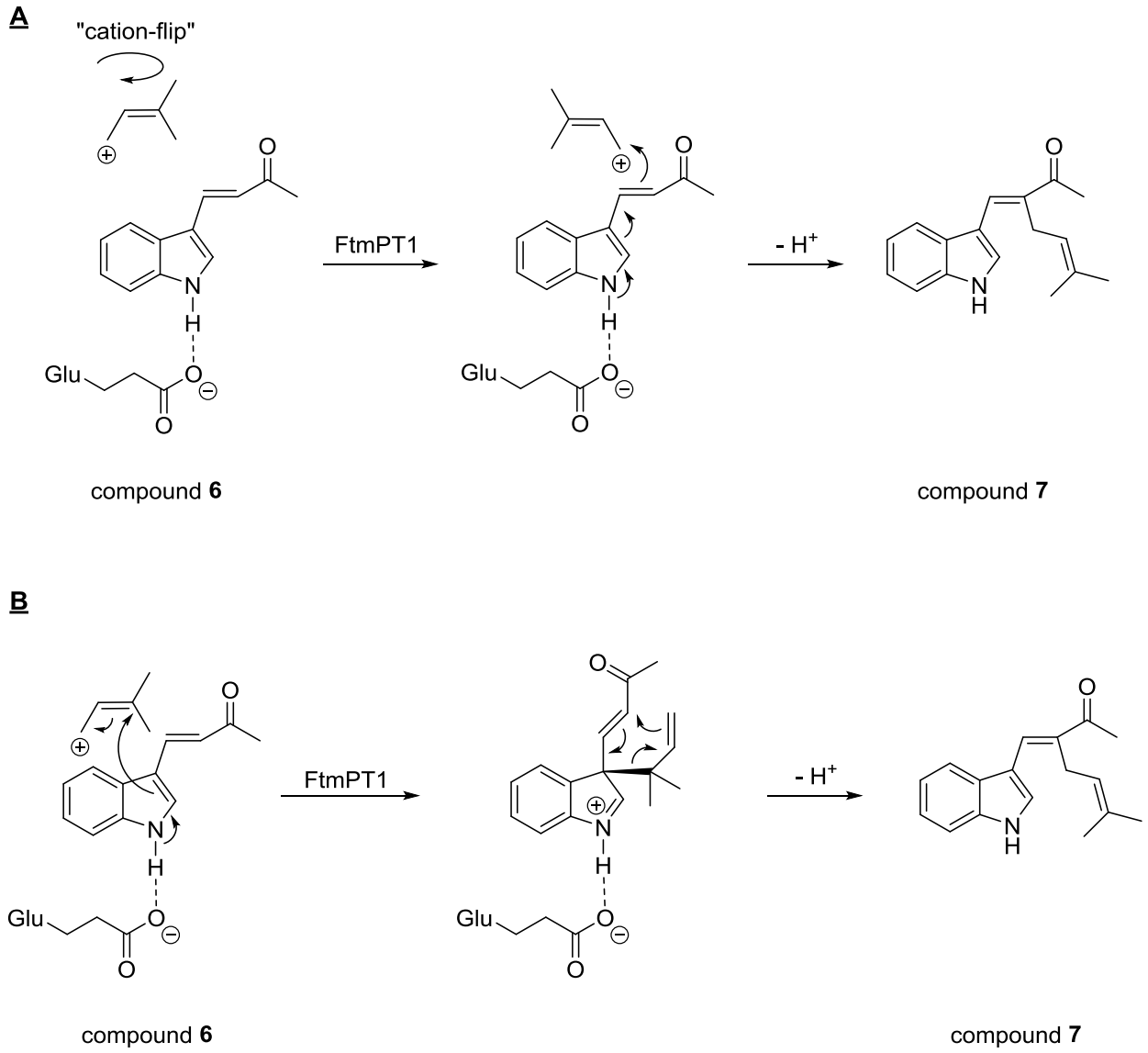

Figure 1.40 The reaction of indolylbutenone 6 catalyzed by FtmPT1. (A) Direct mechanism. (B) Reverse C-3 prenylation followed by a Cope rearrangement mechanism.

The second part of chapter two will present alternate potential mechanisms for FtmPT1that involve initial C-3 prenylation and experiments designed to probe this possibility.

1.6 Mechanism-Based Inhibitors

The third chapter of this thesis focuses on the development of prenyltransferase inhibitors so a brief introduction to mechanism-based inhibitors will be presented at this point. A powerful strategy towards obtaining selective and potent inhibitors is to design compounds based on the mechanism employed by the enzyme. These inhibitors are stable molecules that mimic the electronic and structural characteristics of the intermediate or transition state generated during the enzymatic reaction; hence, they have a great affinity for the enzyme. The reason a transition state analog can be such a potent inhibitor of an enzyme is that it can benefit from the same favorable interactions that lower the activation energy of the reaction. For enzymatic reactions that involve the development of a positive charge in their transition states, introducing positively charged atoms into an analogous position in a stable molecule has been an excellent strategy towards obtaining potent inhibitors. In the following sections, we will describe the strategies employed to inhibit a few examples of the enzymes that develope a positive charge in their transition states.

1.6.1 Inhibition Studies of Glycosidases

Glycosyl hydrolases, also known as glycosidases, catalyze the hydrolysis of glycosidic bonds, resulting in the release of a sugar hemiacetal that carries either the same configuration as the substrate (retention) or, less commonly, the opposite configuration (inversion). Glycosidases are involved in numerous important biological processes such as the breakdown of food carbohydrates, viral and bacterial infections, and post-translational modification of glycoproteins. [112] Since the enzyme-catalyzed hydrolysis of carbohydrates occurs extensively in biological systems, glycosidase inhibitors have found applications as agrochemicals and

pharmaceuticals, and it is no surprise that extensive research has been focused on developing new inhibitors of glycosidases. [113] In 1953, Koshland proposed that retaining glycosidases function by a double-displacement mechanism involving an enzyme or substrate nucleophile, whereas inverting glycosidases employ a single-displacement mechanism in which the aglycon portion is displaced by a nucleophilic water molecule (Figure 1.41). [114] Each step is thought to proceed via a transition state with considerable oxocarbenium ion character and may or may not form a discrete oxocarbenium ion intermediate. [115,116]

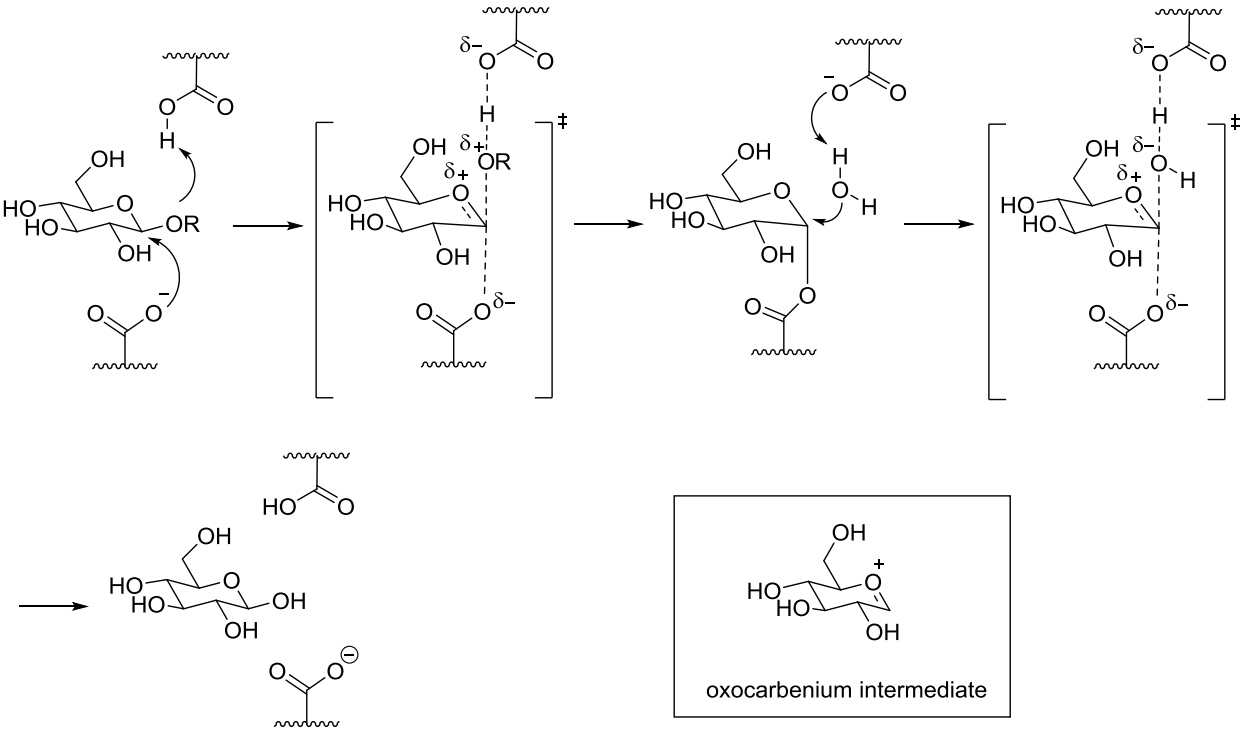

Figure 1.41 Catalytic mechanism employed by configuration-retaining glycosidases. (The inset shows the structure of a putative oxocarbenium intermediate)

Because of their therapeutic potential, developing new glycosidase inhibitors has been the subject of much reseaerch. [113] The reversible inhibitors of glycosidases can be classified as substrate analogs, transition state analogs, and product analogs. As described in section 1.6,

strong inhibition is expected for transition state analogs or high energy intermediate analogs, and consequently numerous inhibitors mimicking the oxocarbenium ion with a flattened chair conformation and positive charge have been synthesized. A classic example of an inhibitor that contains a trigonal, planar configuration at C-1 is the aldonolactone **8**, which inhibits the β-glucosidase from almonds with a K_i value of 0.2 mM at pH 6.2 (Figure 1.42). [117,118,119] In addition to structural similarity, the dipole moment of the lactone accounts for considerable electrostatic interaction with a nearby catalytic carboxylate residue, resulting in favorable binding of the inhibitor in the active site. [118] Measurement of inhibition constants has proven to be difficult for 1,5-lactones as they can undergo hydrolytic ring opening under mildly basic conditions and conversion into 1,4-lactones under acidic conditions. This has led to the development of new classes of inhibitors which are not only stable, but also more potent.

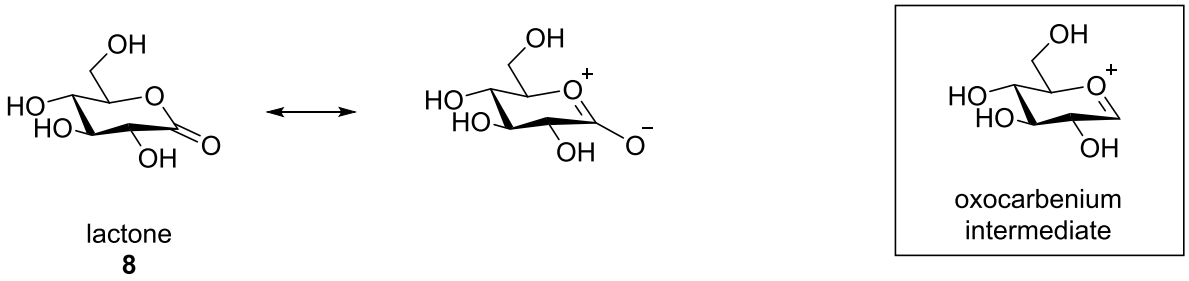

Figure 1.42 Resemblance between the lactone and oxocarbenium intermediate. (The inset shows the structure of the oxocarbenium ion intermediate)

1.6.1.1 Amino-Sugars as Cationic Inhibitors of Glycosidases

Several potent natural and synthetic inhibitors of glycosidases carry basic nitrogens in their chemical structures (Figure 1.43). [120] Polyhydroxylated piperidines and iminosugars for instance, play an important role in inhibiting carbohydrate-processing enzymes. Nojirimycin from *Streptomyces* sp. was the first nitrogen-containing glucose analog that was found to inhibit α-, and β-glucosidases from various organisms. [121,122] The more stable version of nojirimycin is

1-deoxynojirimycin (DNJ), which lacks the hydroxyl group at C-1. It was initially isolated from the roots of the mulberry tree and exhibited excellent inhibitory activity against α-glucosidases *in vitro*. [123] Another example of an α-glucosidase inhibitor is the indolizine alkaloid castanospermine, which was isolated from the seeds of the Australian plant *Castanospermum australe* (Figure 1.43). [124] When compared to the previously discussed aldonolactone **8**, these polyhydroxylated piperidines show less conformational resemblance to the oxocarbenium ion due to their sp^3-hybridized anomeric carbon atom. However, these piperidines exist in their protonated form under physiological pH conditions and are believed to bind the enzyme through electrostatic interactions with negatively charged catalytic carboxylate groups. These basic amino sugars are relatively potent glycosidase inhibitors, mimicking the developing charge of an oxocarbenium ion-like transition state. Thus, they are often regarded as transition state mimics, although they do not closely mimic the conformation of the transition state.

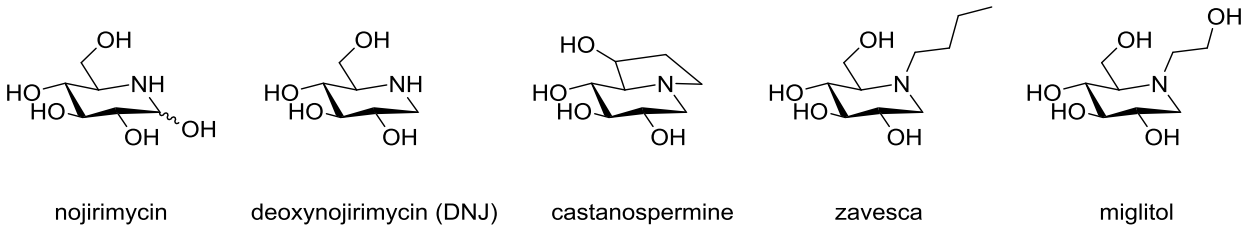

Figure 1.43 Structures of the natural and the synthetic amino-sugars used as glycosidase inhibitors. (The amine group is shown in its neutral form rather than the protonated form)

The natural amino-sugars served as leads for the development of therapeutic agents, and much research has been focused on preparing new derivatives that can serve as better glycosidase inhibitors. *N*-Butyl-1-deoxynojirimycin (zavesca) and *N*-hydroxyethyl-1-deoxynojirimycin (miglitol), for instance, are highly biologically active compounds that have completed clinical trials for type I Gaucher disease and lysosomal storage disorder (Figure 1.43).

[125] Further modification of amino sugar inhibitors was achieved by preparing glucose-derived fused imidazoles **9**, triazoles **10**, and tetrazoles **11** (Figure 1.44). The imidazole analog **9** inhibits the β-glucosidase from almonds with a K_i value of 0.1 μM. The triazole **10** and tetrazole **11** analogs inhibit the same enzyme with much higher K_i values, 19 μM and 150 μM, respectively. These inhibitors presumably have a half-chair conformation due to their fusion with the aromatic ring and may also be protonated to bear a positive charge. [126,127]

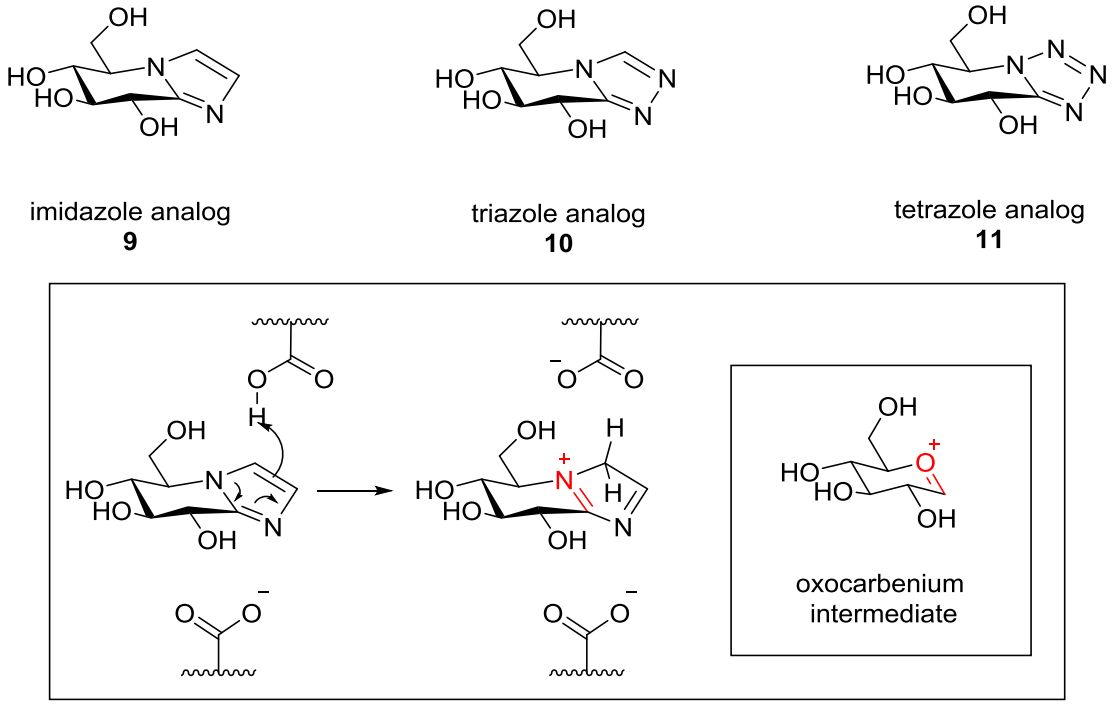

Figure 1.44 Structures of the imidazole, triazole, and tetrazole analogs of amino-sugar inhibitors. (The inset shows the protonation of the imidazole moiety by a catalytic carboxylic acid residue. The structure of the oxocarbenium intermediate is also given to facilitate comparison between the positively charged species)

1.6.2 Inhibition Studies of Isomerases, Cyclases, and Prenyltransferases

Similar to the work with glycosidase inhibitors, ammonium containing compounds have been reported to inhibit a variety of enzymes that proceed via carbocationic intermediates. Isopentenyldiphosphate isomerase for instance, catalyzes the isomerisation of IPP to DMAPP

through a two step mechanism involving the formation of a tertiary carbocation intermediate (Figure 1.45). Abeles and Poulter studied the inhibitory effect of the ammonium-containing inhibitor **12** on catalysis. Inhibitor **12** contains a positively charged nitrogen atom positioned appropriately to mimic the intermediate carbocation. As expected, compound **12** inhibited the isopentenyldiphosphate isomerase from baker's yeast with a K_i value of 2.0 μM. [128,129]

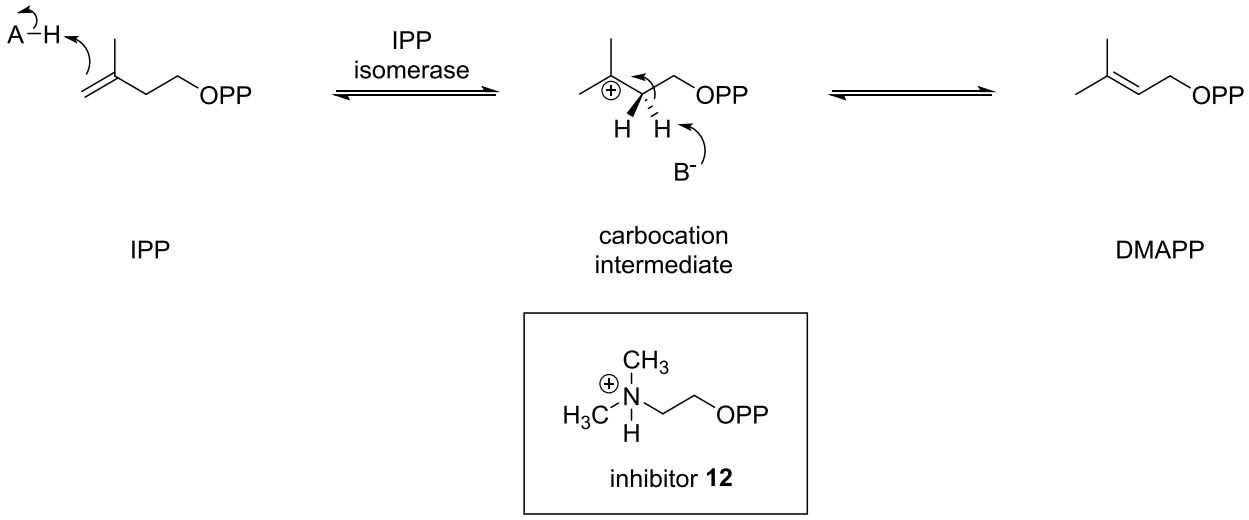

Figure 1.45 Isomerisation reaction catalyzed by isopentenyldiphosphate isomerase. A-H and B represent a general catalytic acid and base, respectively. (The inset shows the structure of inhibitor **12**)

Another example that highlights the application of N-containing intermediate analogs is observed with trichodiene synthase. This terpene cyclase catalyzes the cyclization of farnesyldiphosphate (FPP) to trichodiene (Figure 1.46). [130] Trichodiene is an important precursor in the biosynthesis of a large family of mycotoxins generated by several genera of phytopathogenic fungi, also known as trichothecenes. [131] Mechanistic and stereochemical studies have supported a cyclization mechanism in which the bisabolyl cation is one of the intermediates. [130] Cane *et al.* tested the aza analog of the bisabolyl cation as an inhibitor of trichodiene synthase in the presence of inorganic pyrophosphate. Both (*R*)- and (*S*)-stereoisomers

of inhibitor **13** inhibited trichodiene synthase with K_i values of 0.51 and 0.47 μM, respectively.[132] The ammonium analog of the bisabolyl cation acts as an intermediate analog that mimics the positive charge on the high energy intermediate (Figure 1.46). A similar strategy has been employed to inhibit a variety of terpenoid metabolizing enzymes, such as squalene synthase.[133,134]

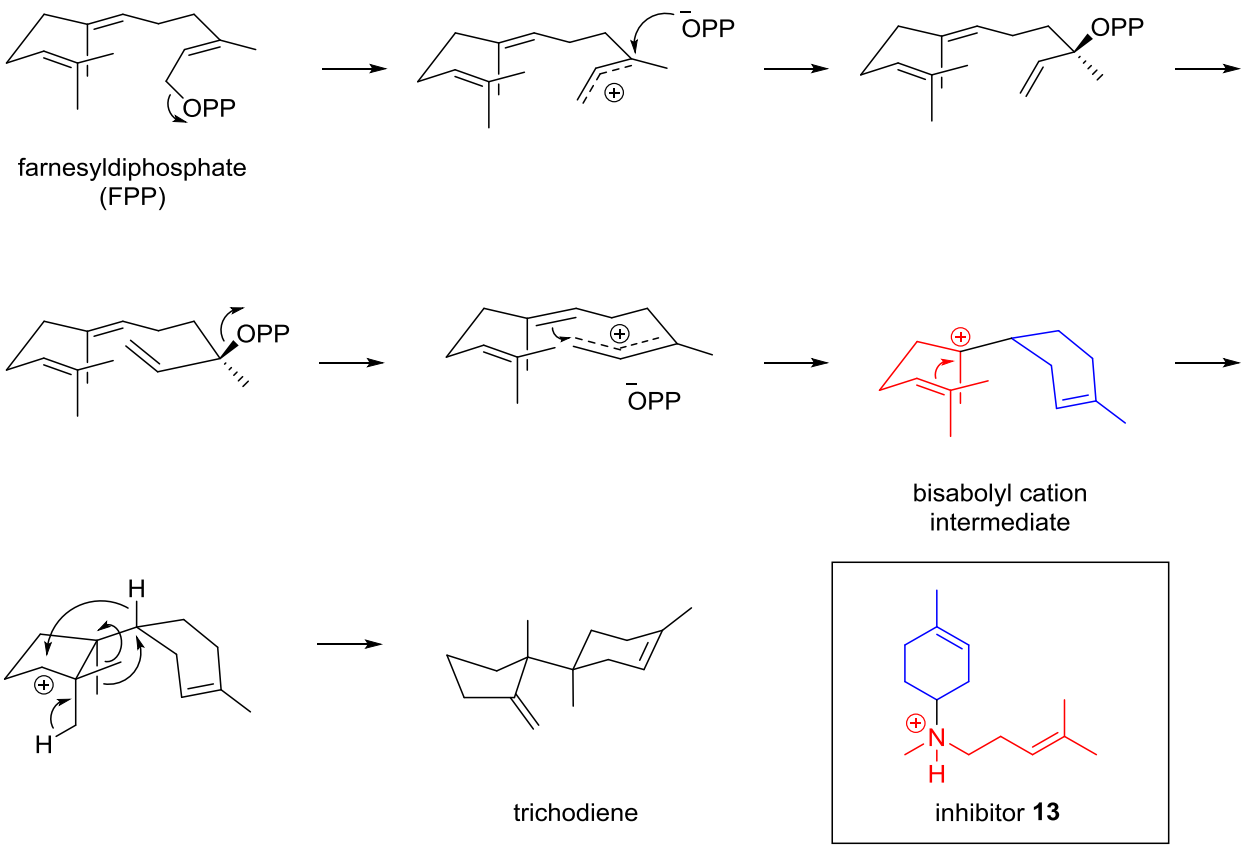

Figure 1.46 Cyclization reaction catalyzed by trichodiene synthase. Blue and red colored bonds are used to show structural similarity between the intermediate and the inhibitor. (The inset shows the structure of inhibitor **13**)

A more recent example that further expands the application scope of N-containing inhibitors is observed with geranylgeranyl diphosphate synthase (GGPP synthase) from rat liver.[135,136] GGPP synthase catalyzes the condensation reaction of farnesyl diphosphate (FPP) with a

molecule of isopentenyl diphosphate (IPP) to form geranylgeranyl diphosphate (GPP) (Figure 1.47). 3-Azageranylgeranyl diphosphate **14** was designed by Steiger *et al.* as an intermediate analog for the GGPP synthase reaction (Figure 1.47). [136] Inhibitor **14** is presumably bound in its protonated form and therefore mimics the positive charge on the high energy carbocation intermediate. When compound **14** was tested as an inhibitor of GGPP synthase, a 90% inhibition was observed at the concentration of 0.9 µM. [135]

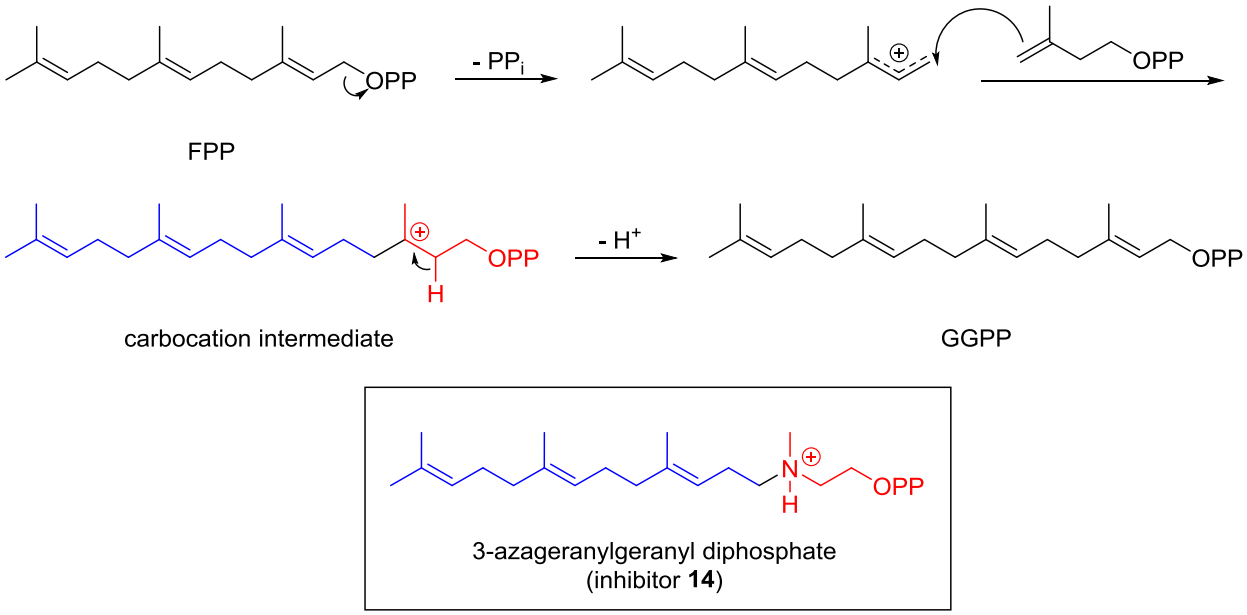

Figure 1.47 Condensation reaction catalyzed by geranylgeranyl diphosphate synthase (GGPP synthase). (The inset shows the protonated form of inhibitor **14**)

In the following section, we will describe a short history of bisphosphonates and the strategies that have been used to improve the inhibitory properties of these compounds.

1.6.3 Bisphosphonate Inhibitors

Bisphosphonates are serendipitous inhibitors of metal-dependent prenyltransferases. They were initially used to treat bone-related diseases but were later found to inhibit farnesyl diphosphate (FPP) and geranylgeranyl diphosphate (GGPP) synthase. [137] Inhibition of these enzymes ultimately results in decreased prenylation of proteins such as Ras and subsequent impairment of cell survival signaling pathways. Since prenylated Ras proteins are present in nearly 30% of human cancers, both the protein farnesyltransferase (FTase) and the farnesyl diphosphate synthase (FPP synthase) are important drug targets for developing new anticancer therapeutic.

The history of bisphosphonates BPs dates back to the 19th century when they were used as complexing agents in the textile, fertilizer, and oil industries, as well as antiscaling and anticorrosive agents. [138,139] In the late 1960s, the potential of bisphosphonates as therapeutic agents was explored and their ability to treat different bone-related diseases became evident. These compounds have been used to prevent the loss of bone mass associated with osteoporosis [140], Paget's disease of bone [141] and hypercalcaemia. [142] Bisphosphonates acts by restraining the digestion of bone by osteoclast bone cells, thereby, slowing the process of bone loss. Methylenebisphosphonates, commonly referred to as bisphosphonates, are analogs of the naturally occurring inorganic pyrophosphate where a carbon atom replaces the bridging oxygen atom between the two phosphate groups (Figure 1.48). Early studies by Fleisch *et al.* suggested that pyrophosphate was capable of impairing the formation and dissolution of calcium phosphate crystals *in vitro*. [143] Likewise, geminal bisphosphonates were proposed to modulate calcification both *in vitro* and *in vivo*, when used in high doses. [144] The replacement of the oxygen atom in the P-O-P bond of pyrophosphates with a carbon atom in bisphosphonates opened up the possibility

of attaching two different side chains, R_1 and R_2. Early efforts to prepare novel BPs focused on changing these two substituents on the methylene carbon. Not surprisingly, bisphosphonate derivatives carrying a hydroxyl group on the bridging carbon (R_1=OH) exhibited increased affinity for calcium. Hydroxylated bisphosphonates bind the bone calcium ions through the alcohol and two neighboring phosphate groups, which is commonly referred to as the tridentate "bone hook". The nature of the R_2 group also plays a crucial role for the optimization of BPs as potent inhibitors of bone resorption. Etidronic acid, for instance, is a first-generation bisphosphonate that carries a simple methyl substituent in the R_2 position (Figure 1.48). [145] It is one of the first BPs that was used successfully in the clinic in the 1970s and 1980s but its potency was only moderate. [146]

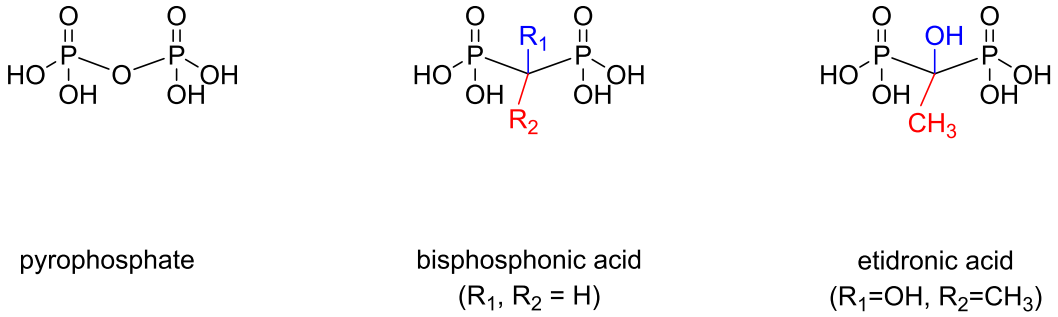

Figure 1.48 Structures of pyrophosphate, bisphosphonate and the first-generation bisphosphonate inhibitor etidronic acid. All molecules are shown in their protonated forms.

The second-generation bisphosphonates demonstrated improved inhibitory properties via the incorporation of a basic aminoalkyl group onto the bisphosphonate scaffold. The first member of the nitrogen-containing bisphosphonate (N-BP) family was pamidronate (Figure 1.49). It was originally synthesized by Henkel as a detergent additive but was later licensed to Ciba-Geigy for further application as a pharmaceutical agent. [147] It has been used clinically for treatment of patients suffering from Paget's disease, tumor-induced hypercalcaemia, and

osteolytic bone metastases caused by breast cancer. [147] Other examples of N-BPs in clinical use include alendronate and ibandronate (Figure 1.49).

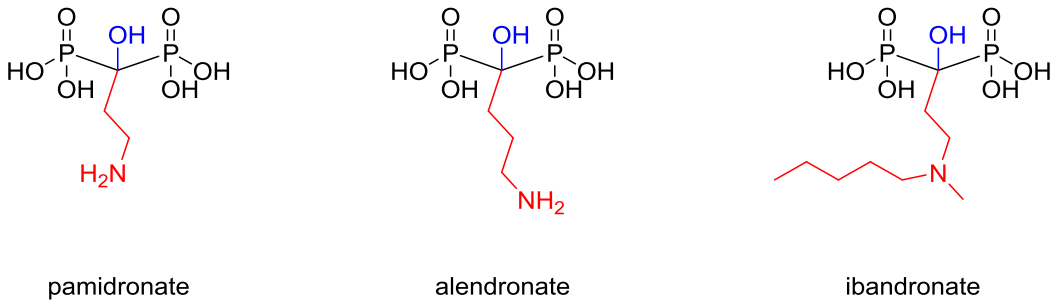

Figure 1.49 Structures of common second-generation nitrogen-containing bisphosphonates. (Blue denotes the hydroxyl substituent and red denotes the aminoalkyl substituent)

Bisphosphonates have been used to treat diseases characterized by excessive bone resorption for over 30 years; but surprisingly, it was not until the early 2000s that their mechanism of action came to light. All BPs have high affinity for bone mineral and are capable of chelating calcium ions owing to their P-C-P backbone structure. [148] It is now generally accepted that at the cellular level, BPs target osteoclasts, the type of bone cell that resorbs bone tissue. [149,150] At the molecular level, on the other hand, it is evident that once bound to the bone, nitrogen-containing bisphosphonates inhibit their molecular target which is believed to be farnesyldiphosphate synthase (FPP synthase) (Figure 1.50). [151,152] FPP is required for the post-translational modification of signaling proteins such as Ras. Farnesylated Ras proteins have been found in a number of human cancers and the prenylation appears to be essential for the full function of these proteins. Therefore, inhibition of FPP synthase prevents the protein prenylation and subsequently, disrupts vital signaling and causes cell death. [153] Both the FPP synthase and the FTase enzymes are drug targets and have attracted a great deal of interest for developing anti-cancer drugs.

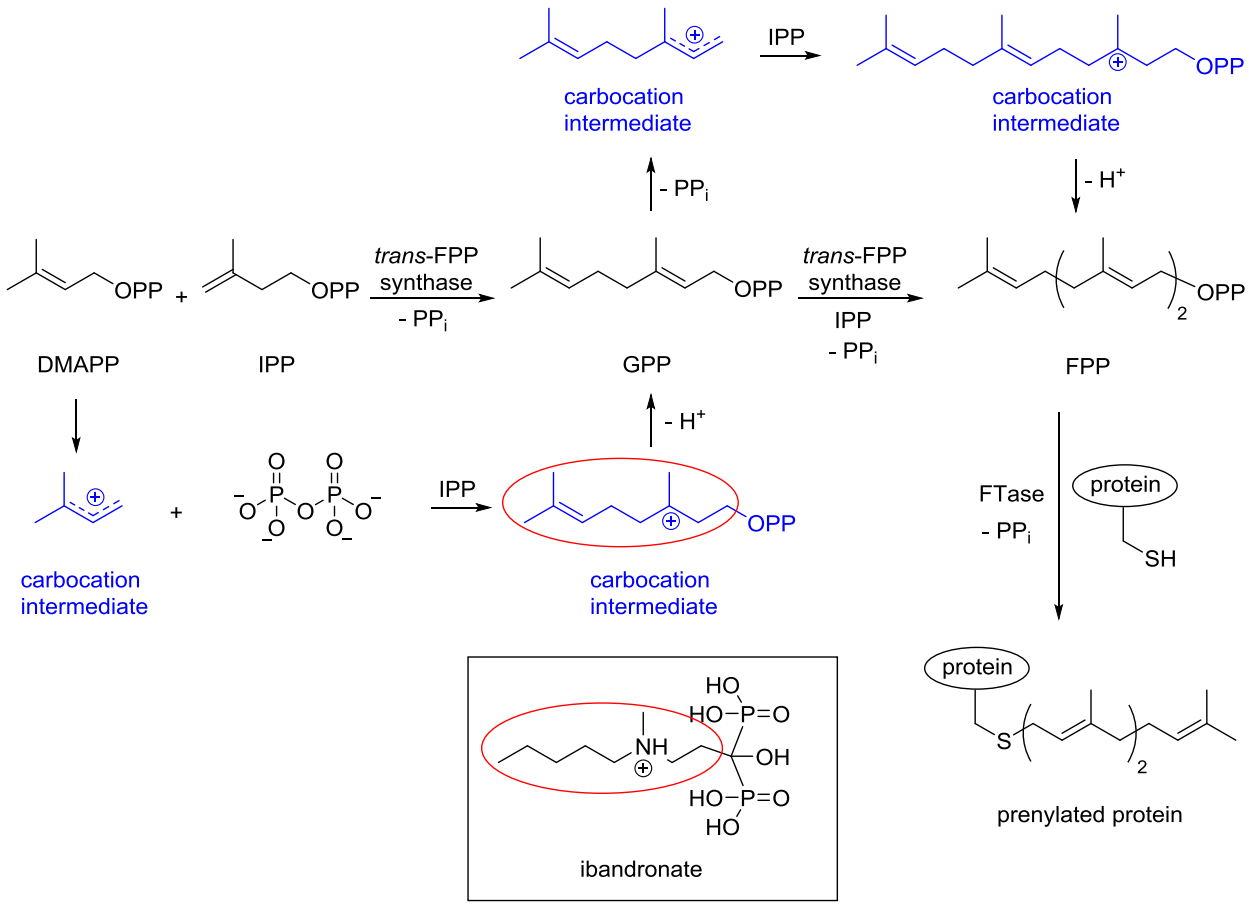

Figure 1.50 Prenylation reactions catalyzed by *trans*-farnesyldiphosphate synthase (*trans*-FPP synthase) and protein farnesyltransferase (FTase). Reaction intermediates are shown in blue. The inset shows the structure of ibandronate with the carbocation side-chain analog circled in red.

As described in section 1.5.1, FPP biosynthesis proceeds via reactive carbocation intermediates (Figure 1.50). Bisphosphonates containing positively charged nitrogens are intermediate analogs that mimic the high energy carbocation intermediates. [154] The side chain containing the ammonium ion mimics the cationic centers of the reactive intermediates, and the bisphosphonate backbone provides a hydrolytically stable analog of the pyrophosphate moiety (Figure 1.50). This surely contributes to the enhanced inhibitory potency of N-BPs that was

observed with human FPP synthase when compared with bisphosphonates lacking a nitrogen atom. [155]

The first-generation BP etidronic acid is a weak inhibitor of human farnesyldiphosphate synthase as it has an IC_{50} value of 80 μM (Figure 1.48). [156] The second-generation bisphosphonates that carry a basic aminoalkyl side chain show improved inhibitory properties. Pamidronate, alendronate, and ibandronate, for instance, inhibit human farnesyldiphosphate synthase with IC_{50} values of 500 nM, 460 nM, and 20 nM, respectively (Figure 1.49). [156,157] The more recently-developed aminobisphosphonate inhibitors contain heteroatomic rings with one or more nitrogen atoms as components of their side chains (R_2). Risedronate, for instance is a potent inhibitor of human farnesyldiphosphate synthase and it shows an IC_{50} value of 6 nM (Figure 1.51). Moreover, zoledronate and minodronate both have IC_{50} values of 3 nM and are considered as some of the most potent N-containing BP inhibitors. [158,157]

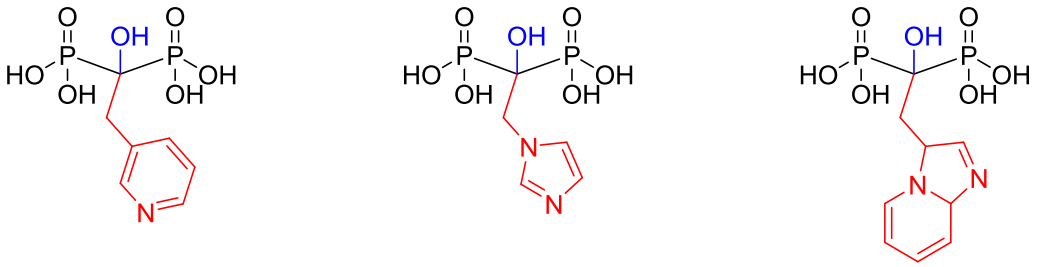

Figure 1.51 Structures of potent third-generation nitrogen-containing bisphosphonates. Blue denotes the hydroxyl substituent and red denotes the side chains carrying heteroatomic rings (R_2).

Although bisphosphonates have found extensive applications in treating bone-related diseases, there are certain drawbacks to their use in different clinical settings. Because of their highly charged nature, bisphosphonates exhibit poor cell-membrane permeability resulting in

low bioavailability. Moreover, they are rapidly (< 1 hour) removed from bloodstream due to their tight interactions with bone minerals. [137,159,160] The tridentate "bone hook" that is comprised of two phosphate groups and the R_1 hydroxyl group is responsible for the observed localization of bisphosphonates onto the bone. To address some of these issues, the hydroxyl groups in risedronate and zoledronate were replaced with a variety of hydrophobic side chains yielding compounds BPH-811 and BPH-703, respectively (Figure 1.52). [137,161] These novel bisphosphonates demonstrate enhanced cellular uptake, which can be attributed to their increased lipophilicity and to the lack of hydroxyl group on the bridging methylene, resulting in weaker binding to bone minerals. These two novel bisphosphonates were found to be potent inhibitors of the malarial enzyme, geranylgeranyldiphosphate synthase from *Plasmodium falciparum*. [161] Both compounds were tested in mice and a major decrease in mortality and parasitemia was observed. This new finding is of great interest as it indicates that overcoming the cell penetration and bone localization problem of current bisphosphonates is certainly a possibility and that these new lipophilic bisphosphonates can potentially be used in cancer chemotherapy. [137,161]

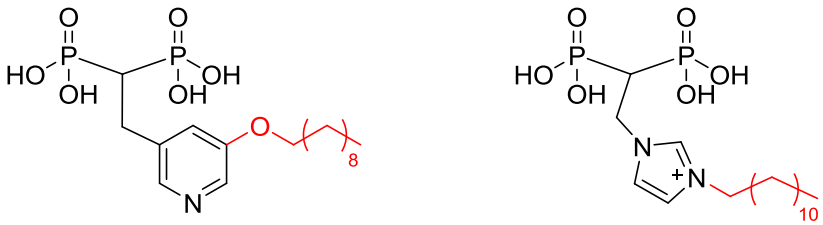

Figure 1.52 Structures of novel lipophilic bisphosphonates. Red bonds denote the lipophilic side chains added to the non-hydroxylated zoledronate and risedronate.

1.7 Project Goals

The second chapter of this thesis focuses on the study of two prenyltransferase enzymes, CdpNPT and FtmPT1. In the first part of Chapter two, we aim to prove that the structure of the product of the CdpNPT-catalyzed reaction is the C-3 reverse prenylated compound **15**. Next, we wish to study whether this compound undergoes a Cope rearrangement onto either the C-4 position (compound **16**) or the N-1 position (compound **4**) under acidic conditions (Figure 1.53). A Cope rearrangement of a C-3 reverse prenylated intermediate onto the C-4 position has been proposed in the mechanism of the prenyltransferase 4-DMATS [98]; hence, we wish to examine whether a similar rearrangement can occur non-enzymatically in a similar system.

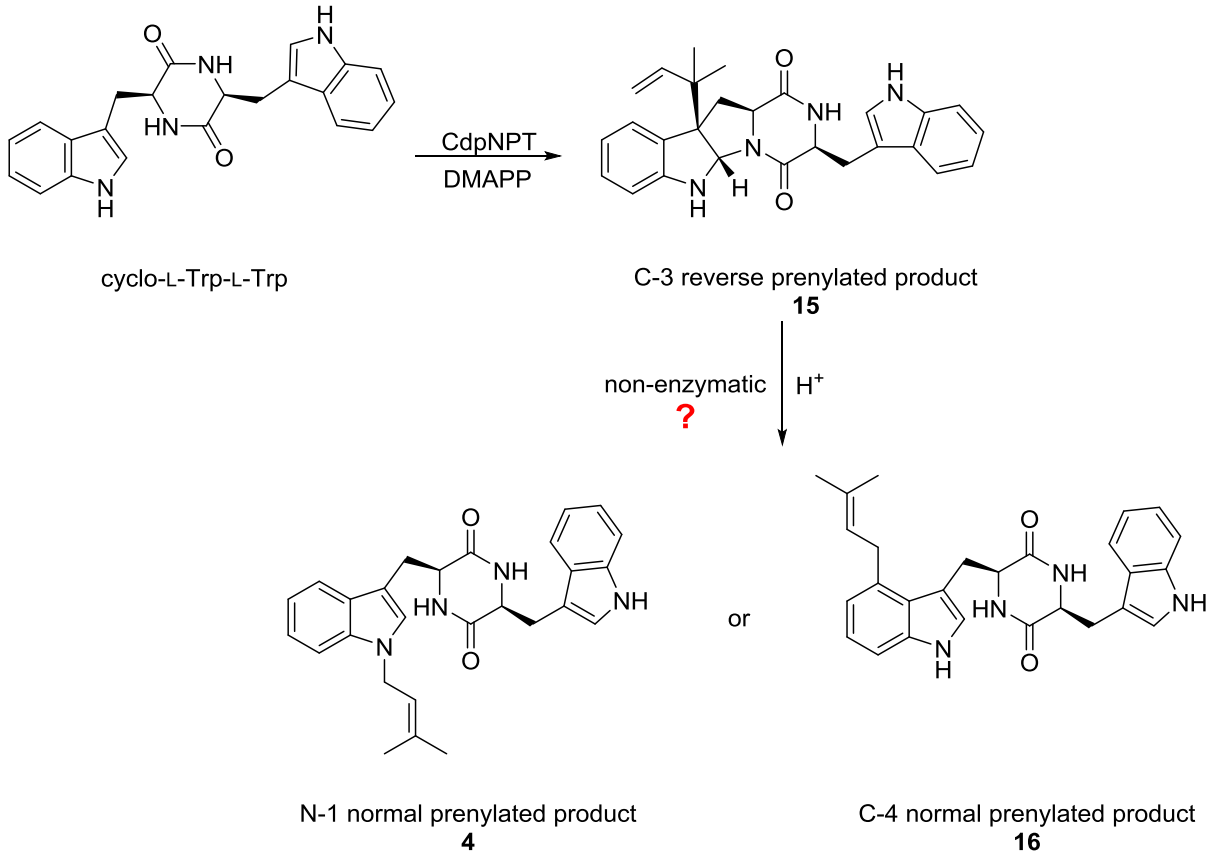

Figure 1.53 Structure of the expected product of the CdpNPT reaction and the structures of the potential rearrangement products when treated with acid.

The second part of Chapter two contains the details of the research performed on the prenyltransferase FtmPT1. We found the previously proposed mechanism for FtmPT1 unlikely as it involves an unusual rotation of a high-energy carbocation intermediate in the active site. Therefore, we will investigate alternative mechanisms for this enzyme, one of which involves an initial C-3 reverse prenylation. This mechanism is highly supported by the crystal structure of FtmPT1 and the relative orientations of the substrates in the active site. We will also examine whether a mechanism involving an initial C-3 normal prenylation is possible for FtmPT1. The design, synthesis, and testing of two substrate analogs will be undertaken to examine whether C-3 normal/reverse prenylation is operative as the first step of catalysis. We anticipate that the use of these substrate analogs will enable us to isolate reaction intermediates that could no longer undergo rearrangements, thus providing indirect support for a particular mechanism (Figure 1.54).

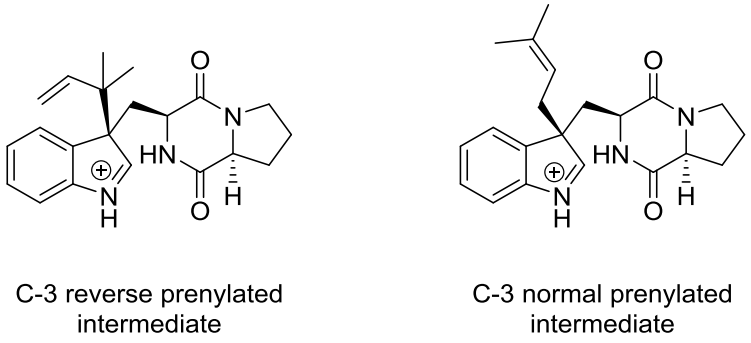

Figure 1.54 Structures of the potential intermediates formed during the FtmPT1-catalyzed reaction.

We will synthesize 2 substrate analogs, 5-hydroxybrevianamide F **17** and 2-methylbrevianamide F **18** to test our hypothesis (Figure 1.55). We anticipate that the presence of the 5-hydroxy group will activate the indole ring for nucleophilic attack, and, given the geometry shown in the X-ray crystal structure, products arising from either a C-3 or C-4 attack would be

expected to be produced. We will next probe the products of the reaction with 2-methylbrevianamide F **18**. We anticipate that blocking the C-2 position with a methyl group will lead to the formation of a C-3 modified product that would not rearrange and could be isolated. This would provide evidence in favor of either the reverse or normal C-3 prenylation mechanisms.

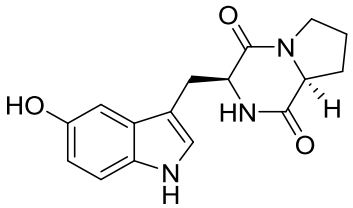

5-hydroxybrevianamide F
17

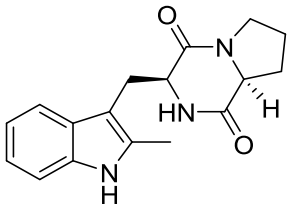

2-methylbrevianamide F
18

Figure 1.55 Structures of the alternate substrates 5-hydroxybrevianamide F 17 and 2-methylbrevianamide F 18.

The third chapter of this thesis focuses on the design of an inhibitor of 4-dimethylallyltryptophan synthase (4-DMATS). Since 4-DMATS portrays a model case for an enzyme that generates an allylic carbocation during a rate-limiting step of catalysis, we chose to target it for rational inhibitor design and test whether we could mimic the properties of the transition state/intermediate with a small molecule (Figure 1.56). We chose to incorporate a guanidinium moiety onto the phosphorylated phosphonate back bone to generate inhibitor **19** (Figure 1.56). This inhibitor mimics the structural and electronic characteristics of the transition state/intermediate closely. The phosphorylated phosphonate group is similar to the pyrophosphate and the guanidinium moiety acts as a close mimic of the allylic carbocation. Besides the fact that this guanidinium moiety provides the desired positive charge, it is sp^2 hybridized and possesses resonance structures that delocalizes the positive charge over more that

one atom. If this compound acts as a potent inhibitor of 4-DMATS, one can imagine that it can also bind tightly to other carbocation forming prenyltransferases, such as farnesyldiphosphate synthase (FPP synthase) and inhibit these enzymes effectively.

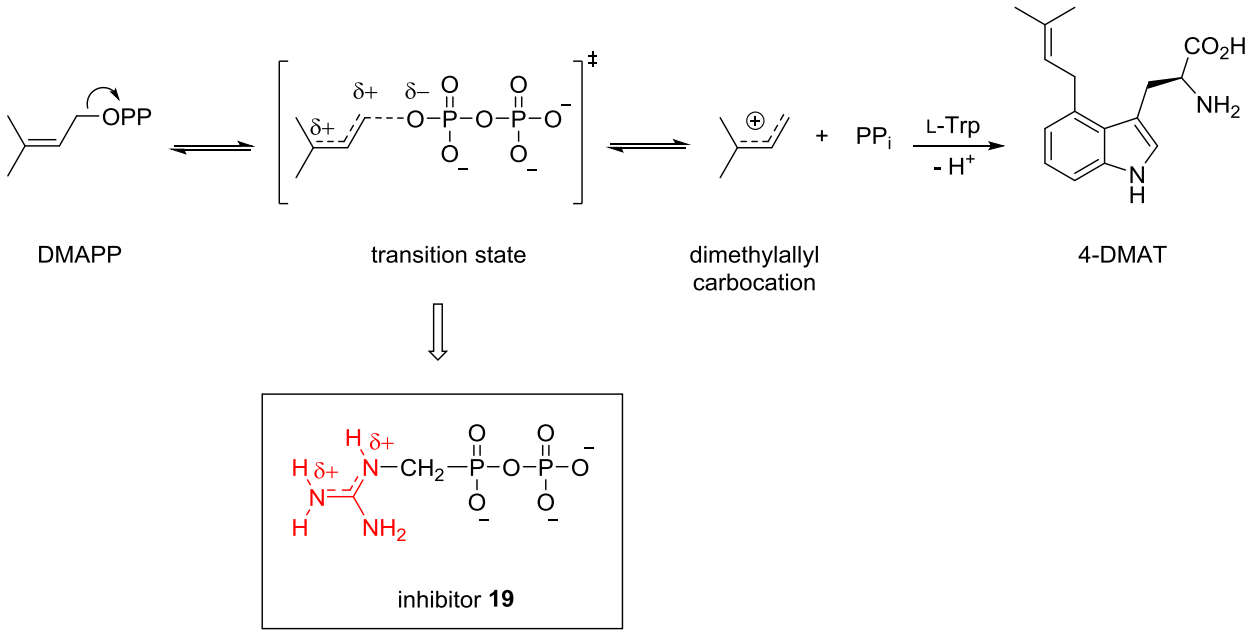

Figure 1.56 Structures of the transition state/intermediate formed during the 4-DMATS reaction. The inset shows the structure of inhibitor **19**.

In the third chapter, we will describe our efforts towards the synthesis and purification of inhibitor **19**. Moreover, the results of the inhibition studies of the synthesized inhibitor **19** with 4-DMATS will be presented.

Chapter 2: Mechanistic Studies on the Cyclic Dipeptide *N*-Prenyltransferase CdpNPT and the Indole Prenyltransferase FtmPT1

The first part of this chapter focuses on our research efforts towards the identification of the true product of the cyclic dipeptide *N*-prenyltransferase (CdpNPT) reaction. A mechanism for the CdpNPT-catalyzed reaction is then proposed and discussed. Next, the product of the CdpNPT-catalyzed reaction is used to examine non-enzymatic Cope and aza-Cope rearrangements. ^{1}H NMR spectroscopy and mass spectrometry are employed to examine the structure of the products. Synthesis of authentic samples is undertaken to verify the structures of the rearrangement products when the purification of these compounds is not feasible using convential methods. Finally, a mechanism is proposed for the observed aza-Cope rearrangement and the literature precedent supporting our observation is discussed.

The second part of this chapter details our mechanistic studies on the reaction catalyzed by FtmPT1. Through the synthesis and testing of the natural substrate and several substrate analogs, a wide range of products are obtained. The structures of the products are examined using ^{1}H NMR spectroscopy and mass spectrometry. The results of the substrate analog studies are then used to propose alternative mechanisms for the FtmPT1-catalyzed reaction. Literature precedent in support of each meachanism is then presented and discussed. Finally, the chapter is concluded with a summary of the two individual projects.

2.1 Mechanistic Studies on the Cyclic Dipeptide *N*-Prenyltransferase (CdpNPT)

The first enzyme we wished to examine was the cyclic dipeptide *N*-prenyltransferase CdpNPT. When we began our studies, little was known regarding the mode of action of this

enzyme. Our knowledge was limited to the information provided by two papers published by the Shu-Ming Li group in 2007 and 2008. [101,107] As described in section 1.5.4 of Chapter 1, CdpNPT normally acts on benzodiazepinedones, but it has also been shown to accept a variety of cyclic dipeptides including cyclo-L-Trp-L-Trp. The first report on a CdpNPT-catalyzed reaction between DMAPP and cyclo-L-Trp-L-Trp identified the product as an N-1 normal prenylated compound **4** (Figure 2.1). [101] Shortly after, a re-examination of the enzymatic reaction suggested that the observed N-1 prenylated product **4** was in fact the result of a non-enzymatic rearrangement that occured at room temperature under acidic work-up conditions. [107] When we started our studies, CdpNPT was believed to catalyze a reverse N-1 prenylation and the product was thought to be the N-1 reverse prenylated cyclic dipeptide **3** (Figure 2.1).

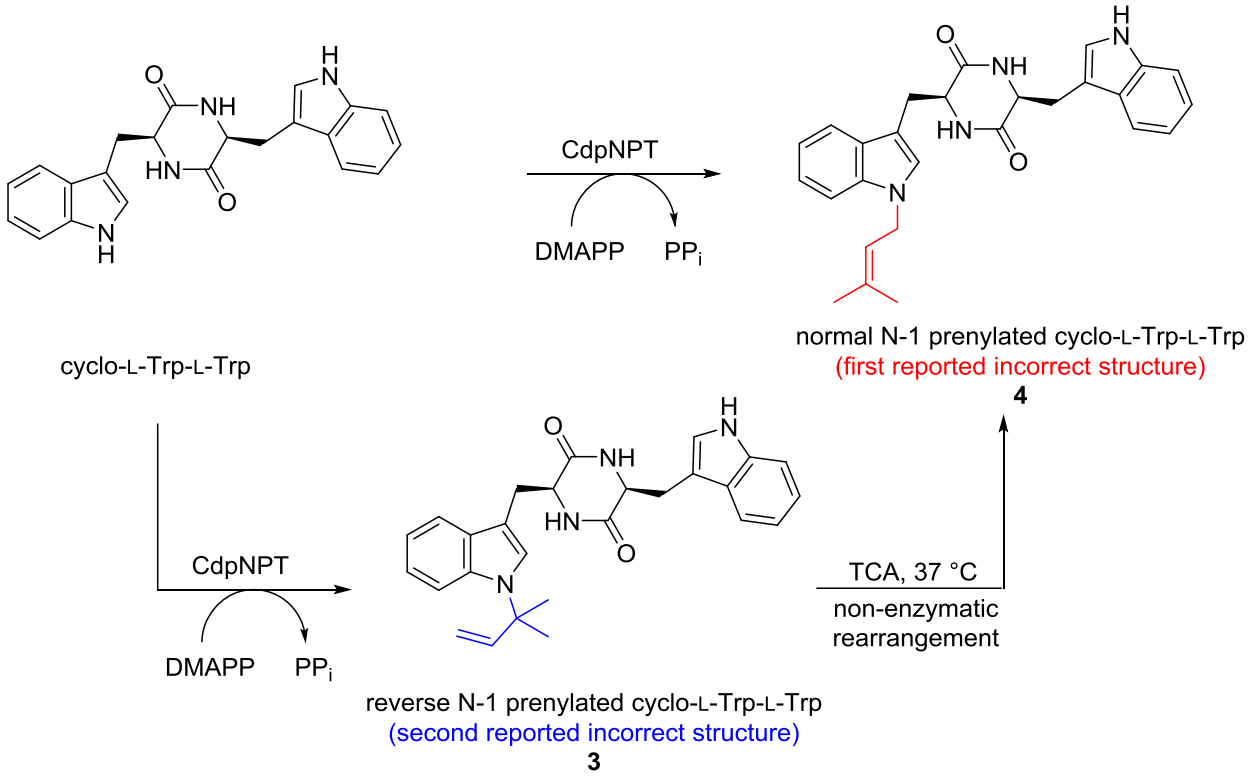

Figure 2.1 Previously reported incorrect structures for the product of the CdpNPT-catalyzed reaction.

2.1.1 Analysis of the Structure of the Previously Reported Product of CdpNPT

Upon careful inspection of the reported ^{1}H NMR spectrum of the product **3**, we noticed that the reported chemical shifts do not match the proposed structure. The signal that appeared at the chemical shift of 5.52 ppm was assigned to the C-2 proton (Figure 2.2). Compound **3** carries a second L-tryptophan in its structure that is unmodified during the prenylation reaction. The C-2' proton signal of this second indole ring appeared at the chemical shift of 7.11 ppm. We found this difference in the chemical shift values of these two similar C-2 protons rather strange as they are both attached to sp^2 hybridized carbons. We felt that it is unlikely that the reverse prenylation at the N-1 of the indole ring could cause the C-2 proton signal to shift this far upfield, so we compared the chemical shift value to that of a structurally relevant molecule.

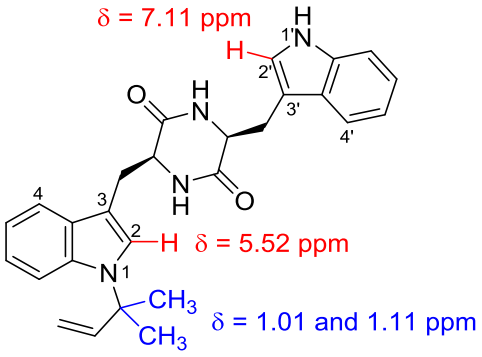

reverse N-1 prenylated cyclo-L-Trp-L-Trp
(second reported incorrect structure)
3

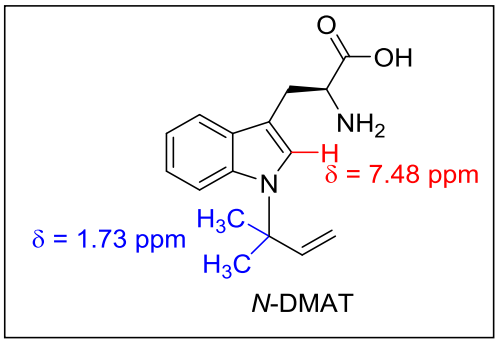

Figure 2.2 A comparision between the chemical shift values of compound 3 and those of the N-1 reverse prenylated L-tryptophan (*N*-DMAT). The inset shows the structure of *N*-DMAT.

A previous study in our lab focusing on the mechanistic studies of CymD gave us access to a similarly N-1 reverse prenylated compound. [162] CymD is a prenyltransferase that catalyzes the reverse N-prenylation of L-tryptophan to give *N*-(1,1-dimethyl-1-allyl)tryptophan, *N*-DMAT (Figure 2.2). The C-2 proton of *N*-DMAT appears at the chemical shift of 7.48 ppm, which is

significantly higher than that of compound **3**. [81] The observation that the chemical shift of the C-2 proton in **3** appears further upfield led us to believe that this difference is most likely due to a different hybridization (possibly sp^3) of C-2 in the correct structure of compound **3**. Furthermore, the signals for the six protons of the two methyl groups in *N*-DMAT appear at a higher chemical shift (1.73 ppm) when compared to those of the proposed compound **3** (1.01 and 1.11 ppm) implying that the prenyl group is possibly connected to a carbon atom rather than a nitrogen atom. The results of this analysis clearly showed that the product of the CdpNPT reaction is not the reported N-1 reverse prenylated compound **3**.

Fortunately, our lab has been working on several indole prenyltransferases in the past and as a result, we had access to the ^{1}H NMR spectra of a number of normal/reverse prenylated indole-containing molecules. The results of a previous mechanistic study on the indole prenyltransferase 4-DMATS, led us to believe that the correct product of the CdpNPT reaction contains a hexahydropyrroloindole structure that is reverse prenylated at the C-3 position. [98] The Lys174Ala mutant of 4-DMATS generates the C-3 reverse prenylated hexahydropyrroloindole **1** in the reaction between L-tryptophan and DMAPP. [98] When the ^{1}H NMR spectrum of compound **3** was compared to that of the compound **1**, we noticed a remarkable resemblance (Figure 2.3). [98] The methyl signals in compound **3** appeared at the chemical shifts of 1.01 and 1.11 ppm, which are very similar to those of compound **1** (0.84 and 0.95 ppm). The presence of three alkene signals at the chemical shifts of 5.96, 5.12, and 5.07 ppm observed in the CdpNPT product is characteristic of a molecule that has been reverse prenylated at a carbon atom. A similar pattern for the alkene signals can be found in compound **1** (5.84, 5.02, and 4.97 ppm). Finally, the appearance of the C-2 proton signal at 5.52 ppm is consistent with an sp^3 hybridized C-2 (5.36

ppm in compound **1**), which provides further evidence for the existence of a ring-closed hexahydropyrroloindole structure.

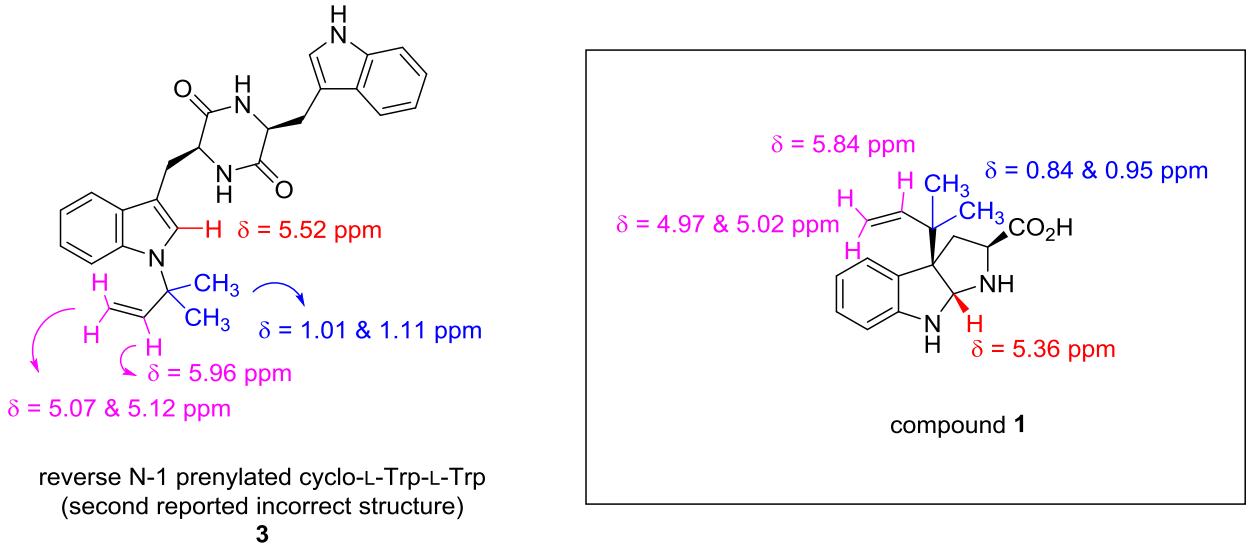

Figure 2.3 A comparision between the chemical shifts values of incorrectly assigned compound 3 (in $CDCl_3$) and those of compound 1 (in D_2O) shown in the box. Compound **1** is generated in the reaction between L-tryprophan and DMAPP catalyzed by the Lys174Ala mutant of 4-DMATS.

All the described analyses provided us with evidence that the structure of the product of the CdpNPT reaction had been missassigned even after the published reinvestigation. [107] We predicted that the true product is a C-3 reverse prenylated hexahydropyrroloindole **15** (Figure 2.4). To prove our hypothesis, we began our studies with the purification of the enzyme CdpNPT and employing it in the reaction between cyclo-L-Trp-L-Trp and DMAPP.

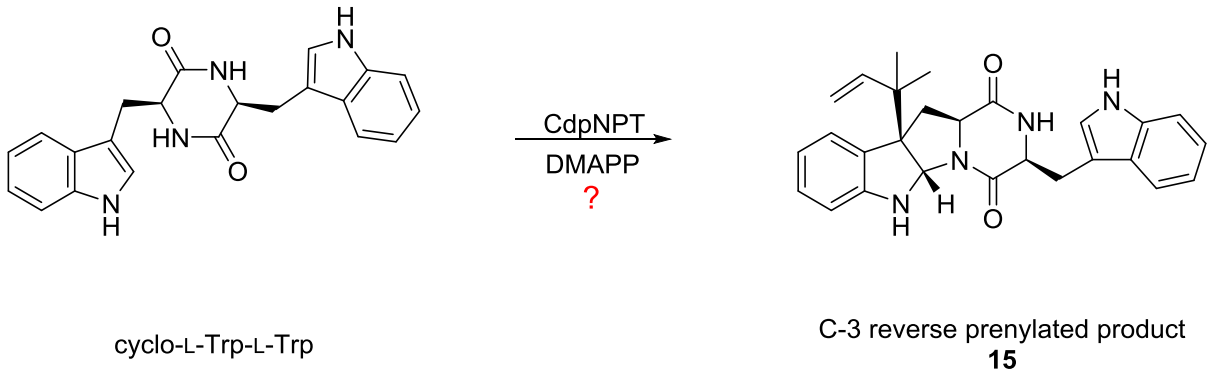

Figure 2.4 Proposed structure of the product of the CdpNPT reaction.

2.1.2 Expression and Purification of the Cyclic Dipeptide *N*-Prenyltransferase CdpNPT

The gene encoding for cyclic dipeptide *N*-prenyltransferase, *cdpNPT* from *Aspergillus fumigatus*, was synthesized by GenScript® with codon optimization for expression in *E. coli*. It was then cloned into a pET28 vector (Figure 2.5). We opted for the pET28a system as it offers several useful cloning features. This includes a sequence encoding for a C-terminal histidine (His) tag that allows for protein purification, a kanamycin resistance gene that facilitates the selection of transformed bacteria and a T7 promoter/lac operon system for IPTG induction and protein expression. [163] A modification of the protocol described by Steffan and his co-workers was employed to overproduce the enzyme. [86]

GGATCCATGGACGGTGAAATGACGGCTTCCCCGCCGGATATTAGCGCGTGTGATAC
GAGTGCAGTGGACGAACAAACGGGCCAAAGTGGTCAGAGCCAGGCGCCGATTCCG
AAAGATATCGCCTATCATACCCTGACGAAAGCACTGCTGTTTCCGGATATTGACCAG
TACCAACACTGGCATCACGTTGCGCCGATGCTGGCCAAAATGCTGGTCGATGGCAA
ATATAGCATCCATCAGCAATATGAATACCTGTGCCTGTTCGCACAGCTGGTCGCTCC
GGTGCTGGGTCCGTATCCGTCACCGGGTCGTGACGTGTACCGCTGTACCCTGGGCGG
TAACATGACGGTTGAACTGTCGCAGAATTTTCAACGTAGCGGCTCTACCACGCGCAT
TGCTTTCGAACCGGTGCGTTACCAGGCGTCTGTTGGTCATGATCGTTTTAACCGCACC
AGTGTGAATGCCTTTTTCTCCCAGCTGCAACTGCTGGTTAAATCAGTCAACATCGAA
CTGCATCACCTGCTGTCGGAACACCTGACCCTGACGGCGAAAGATGAACGTAACCT
GAATGAAGAACAGCTGACCAAATATCTGACGAATTTTCAGGTCAAAACCCAATACG
TGGTTGCCCTGGACCTGCGCAAAACGGGCATTGTGGCAAAAGAATATTTCTTTCCGG
GTATCAAATGCGCAGCAACCGGTCAGACGGGTTCAAACGCGTGTTTCGGCGCAATTC
GTGCTGTTGATAAAGACGGTCATCTGGATAGCCTGTGCCAACTGATTGAAGCTCACT
TTCAGCAATCTAAAATCGATGACGCCTTCCTGTGCTGTGATCTGGTCGACCCGGCCC
ATACCCGCTTTAAAGTCTATATTGCAGACCCGCTGGTGACCCTGGCGCGTGCCGAAG
AACACTGGACCCTGGGCGGTCGCCTGACGGATGAAGACGCAGCTGTGGGCCTGGAA
ATTATCCGTGGTCTGTGGAGTGAACTGGGCATTATCCAGGGTCCGCTGGAACCGTCC
GCAATGATGGAAAAAGGCCTGCTGCCGATTATGCTGAATTATGAAATGAAAGCGGG
TCAGCGCCTGCCGAAACCGAAACTGTACATGCCGCTGACCGGCATCCCGGAAACGA
AAATTGCGCGTATCATGACCGCCTTTTTCCAGCGCCATGATATGCCGGAACAAGCTG
AAGTTTTCATGGAAAACCTGCAGGCGTATTACGAAGGTAAAAATCTGGAAGAAGCA
ACCCGCTATCAAGCTTGGCTGTCGTTCGCTTACACCAAAGAAAAAGGTCCGTATCTG
TCCATCTACTACTTCTGGCCGGAATAA**CCCGATAAGCTT**

Figure 2.5 DNA sequence of *cdpNPT* codon optimized for overexpression in *E. coli*. (Bases shown in red are non-coding regions used during cloning).

The plasmid *cdpNPT*/pET28a was transformed into Rosetta (DE3) pLysS *E. coli* cells and the bacteria were grown in Terrific Broth (TB) medium until an optical density (OD_{600}) of 0.6 was reached. The *E. coli* cells were induced for overexpression by addition of IPTG and left growing at 24 °C for an additional 24 hours. Cells were harvested and lysed with a French press, and the lysate was applied to a column filled with immobilized metal ion affinity resin that was charged with a solution of $NiSO_4$. The column was washed with eluting buffer containing varying concentrations of imidazole and the hexahistidine-tagged CdpNPT was collected. Typically, ~15 mg of enzyme was obtained from 1 L of culture. The SDS-PAGE of the isolated recombinant protein is shown in Figure 2.6.

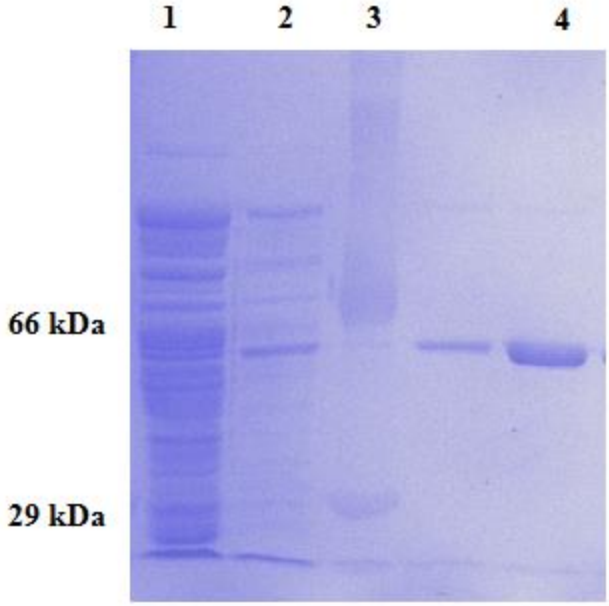

Figure 2.6 SDS-PAGE gel showing the purification of CdpNPT. Lane 1: column extracts with eluting buffer containing 5 mM imidazole; Lane 2: column extracts with eluting buffer containing 100 mM imidazole; Lane 3: molecular weight standards of 66 kDa (bovine serum albumin) and 29 kDa (carbonic anhydrase); Lanes 4 & 5: purified CdpNPT.

2.1.3 Product Studies with Cyclo-L-Trp-L-Trp

A stock solution of commercially available cyclo-L-Trp-L-Trp (25 mM) was prepared in MeOH. We tried to carry out the enzymatic reaction in pure Tris-HCl buffer, pH 7.5, but the substrate showed very poor solubility. Hence, it is crucial to use 20% MeOH to ensure sufficient solubility. The substrates cyclo-L-Trp-L-Trp and dimethylallyl diphosphate (DMAPP) were incubated with the enzyme CdpNPT at 37 °C for 20 hours. After the reaction was complete, the precipitate was removed through centrifugation and the resulting solution was extracted with ethyl acetate. Removal of the solvent gave a residue which was purified by silica gel column chromatography. No decomposition was observed during the course of purification.

The ^{1}H NMR spectrum of the product, taken in CD_3OD, clearly shows two alkene signals at 5.58 and 4.92 ppm which is the characteristic of reverse prenylation (Figure 2.7). Furthermore, the C-2 proton signal was observed at 5.24 ppm which is lower than the corresponding proton in the starting material. This is expected for a reverse prenylated hexahydropyrroloindole structure as the change in hybridization at C-2 from sp^2 in cyclo-L-Trp-L-Trp to sp^3 in the cyclized product results in an upfield shift (Figure 2.7).

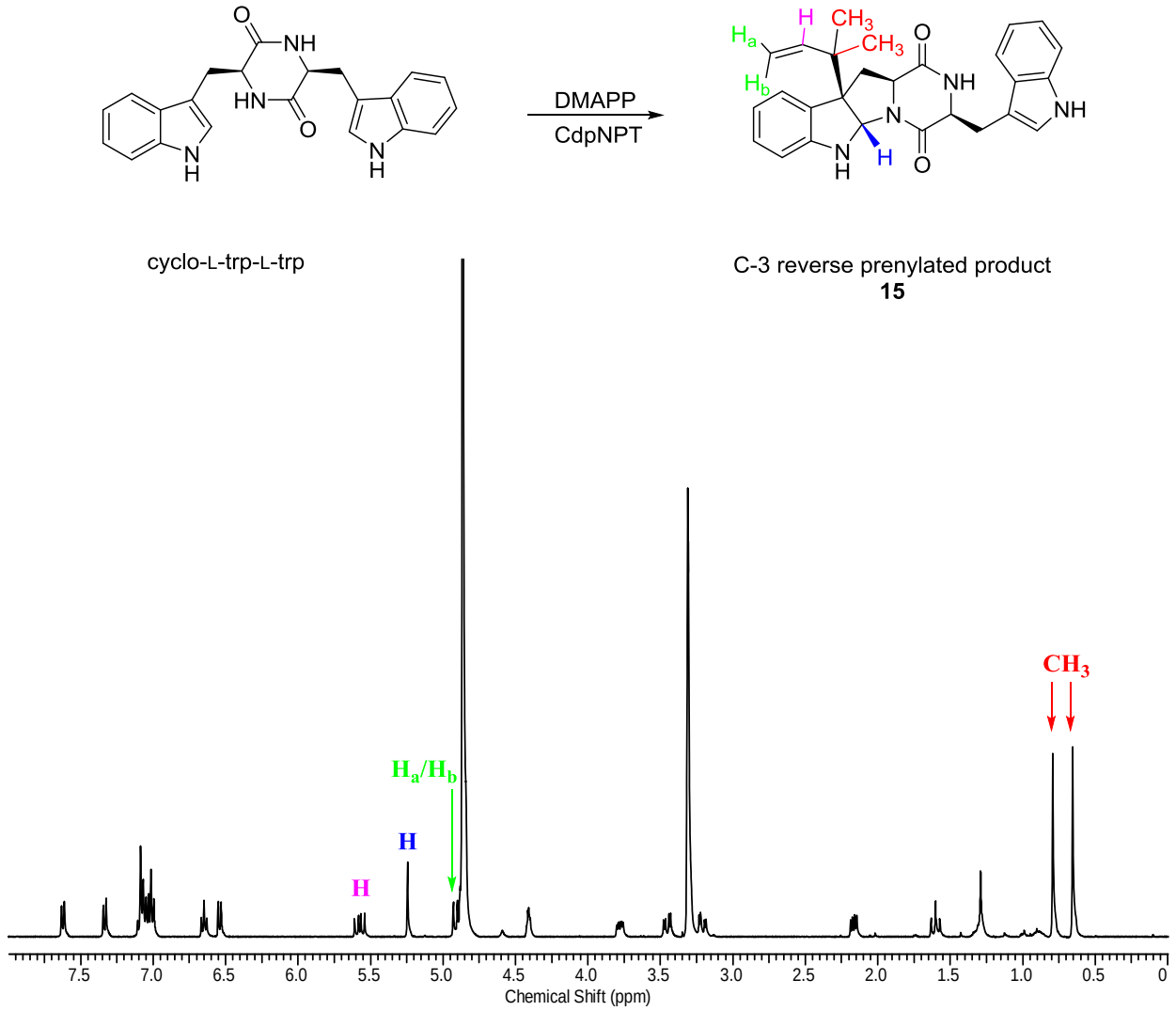

Figure 2.7 Corrected structure of the product of the CdpNPT reaction based on the results from the ^{1}H NMR spectrum. (CD_3OD, 400 MHz)

Moreover, the HMBC spectrum showed a correlation between the proton signals from the two methyl groups of the prenyl moiety and the carbon signal of the C-3 atom of the indole ring (Figure 2.8). These correlations would be missing in the previously reported N-1 reverse prenylated compound **3**. [101,107] Thus, we concluded that the product of the CdpNPT is a C-3 reverse prenylated compound **15** (Figure 2.7).

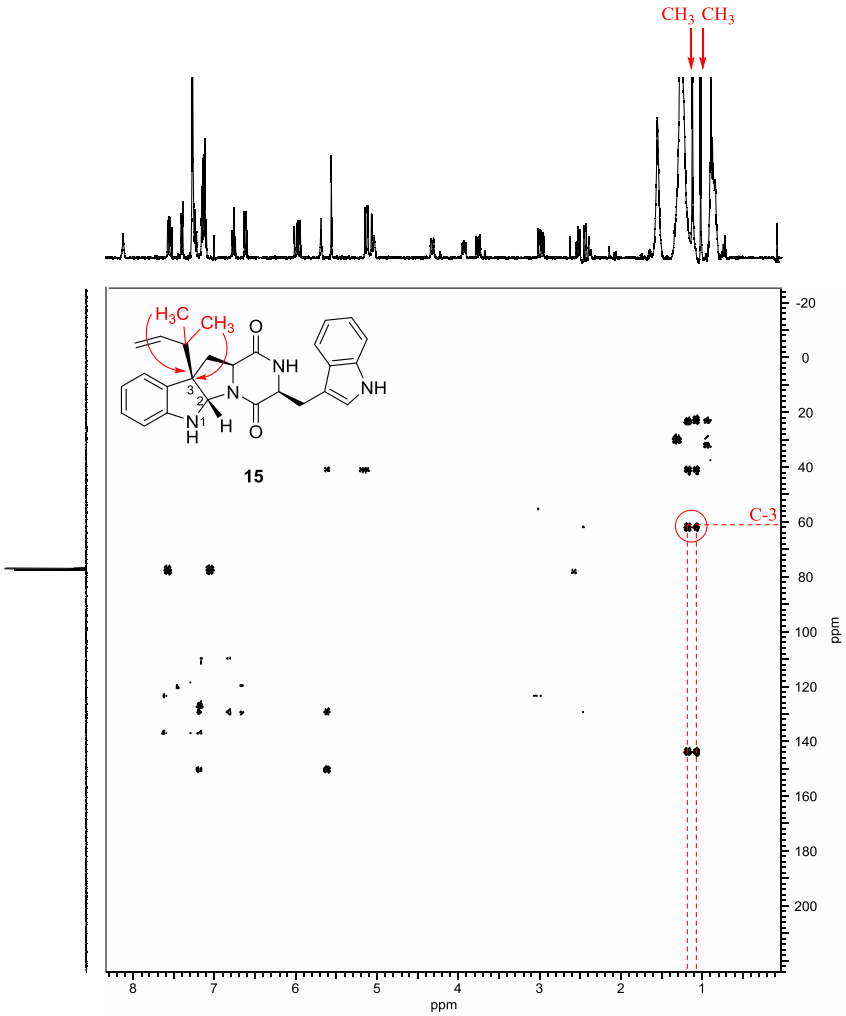

Figure 2.8 HMBC spectrum of compound 15 showing the correclation between the methyl proton signals and the C-3 carbon signal. ($CDCl_3$, 400 MHz)

We propose that the first step in the CdpNPT-catalyzed reaction is similar to that of the indole prenyltransferase 4-DMATS. The prenylation reaction is initiated with the dissociation of the diphosphate moiety, generating a dimethylallyl carbocation (Figure 2.9). Given that the active site of CdpNPT is similar to that of 4-DMATS, the C-3 position of the dimethylallyl carbocation would sit right above the C-3 position of the indole ring of cyclo-L-Trp-L-Trp,

facilitating a C-3 attack to form an imminium intermediate. This is chemically reasonable given the high nucleophilicity of the C-3 of the indole ring. This intermediate can then undergo a ring closure by an attack from the neighboring amide N-H, which is followed by a deprotonation step to yield the product **15** (Figure 2.9).

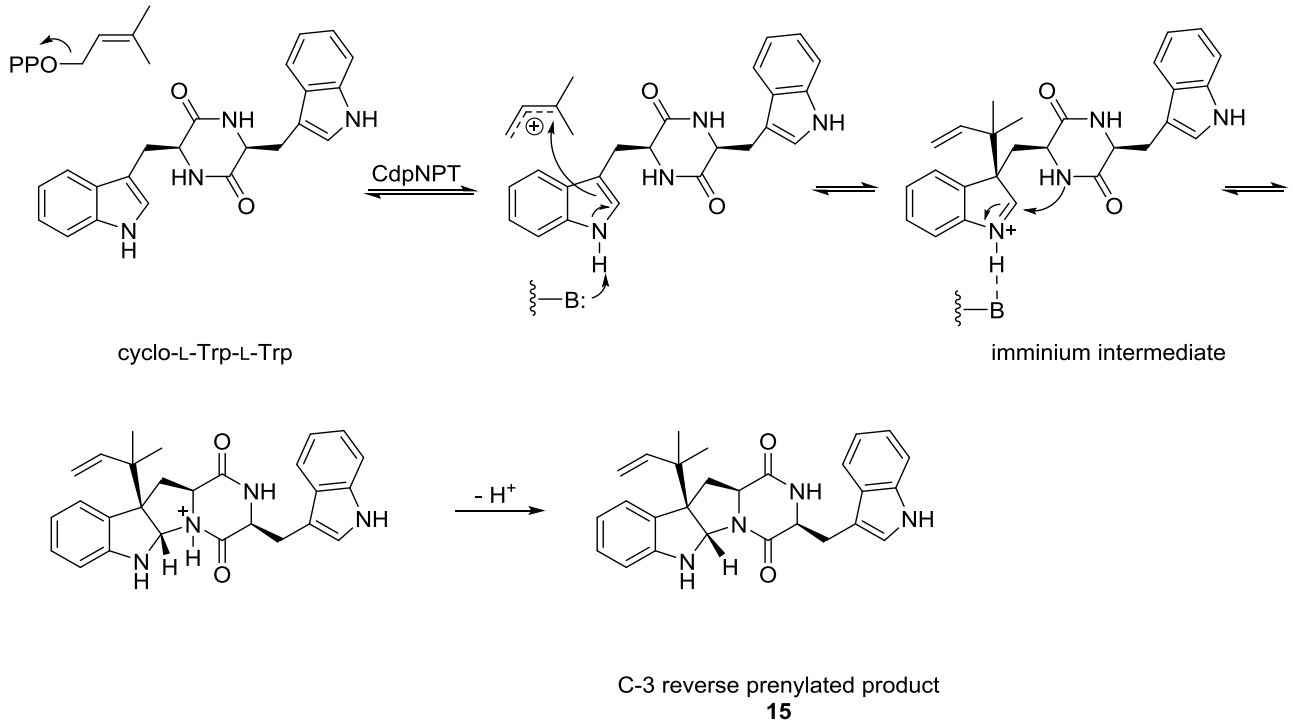

Figure 2.9 Proposed mechanism for the reaction catalyzed by CdpNPT.

As we were preparing a report to publish our findings, the Shu-Ming Li group published a second correction that finally indicated that the true product of the CdpNPT reaction with cyclo-L-Trp-L-Trp was the C-3 reverse prenylated compound **15**. [102] The crystal structure of CdpNPT was also reported in this same paper.

2.1.4 The X-Ray Crystal Structure of CdpNPT

The crystal structure of CdpNPT was determined in complex with (*S*)-benzodiazepinedione **2** and thiolodiphosphate (SPP), which is the hydrolyzed version of the thio analog of DMAPP (DMSPP) (Figure 2.10). [102] The crystallographic results showed that the enzyme adopts the familiar PT barrel that is the characteristic feature of all members of the ABBA family of aromatic prenyltransferases. [164] CdpNPT is similar in size, as well as structure, to the fungal 4-DMATS. The highly conserved DMAPP binding site is located near the center of the β-barrel. The terminal phosphate group of the prenyl substrate is anchored by three positively charged arginine and lysine residues (R129, R284, and K286). The phosphate group that is connected to the sulfur atom is surrounded by a ring of four tyrosine residues (Y221, Y288, Y366, and Y435) that hold the diphosphate moiety in place. These tyrosine residues also serve as a shield to protect the emerging dimethylallyl carbocation during catalysis. The indole substrate binding pocket is mainly hydrophobic in character and is somewhat enlarged when compared to 4-DMATS in order to accommodate the larger substrate. Notably, the C-3 position of the indole substrate appears to sit directly next to the C-3 position of DMAPP. Moreover, the glutamate residue (E116) that is highly conserved in all fungal PTs forms a hydrogen bond with the indole NH. It is likely that this glutamate residue serves to increase the nucleophilicity of the indole ring, similar to its role in 4-DMATS. [102]

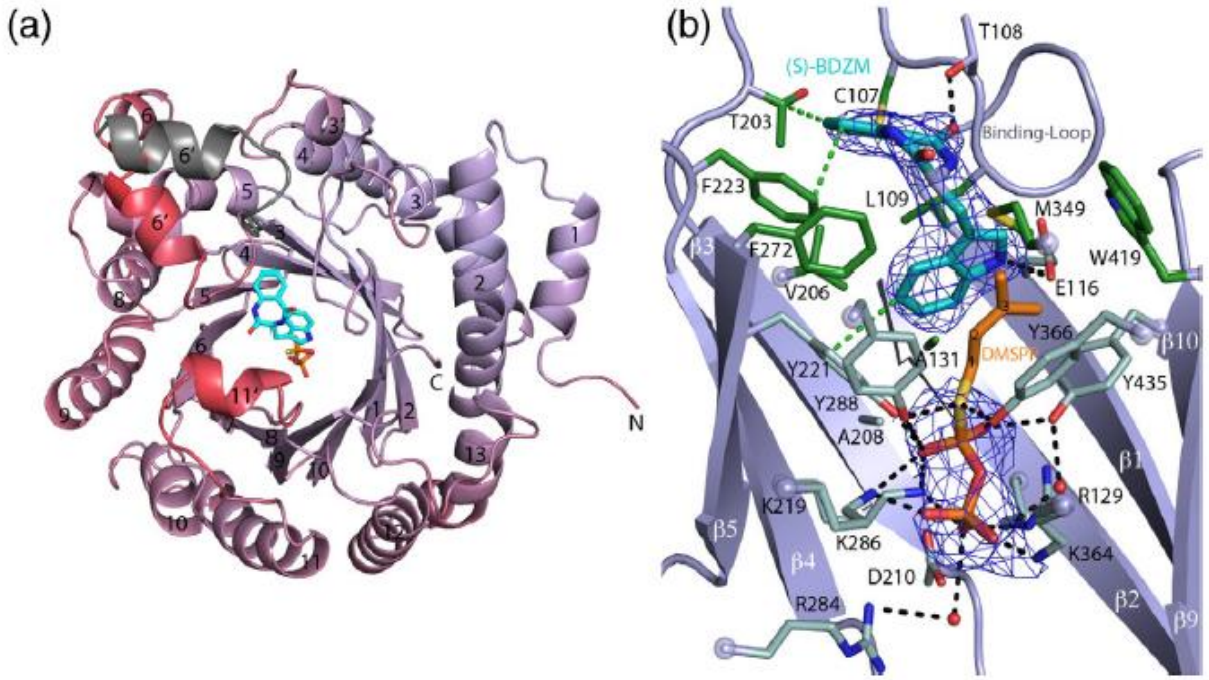

Figure 2.10 The structure of CdpNPT in complex with (*S*)-benzodiazepinedione 2 and thiolodiphosphate (SPP). (A) The ABBA fold with active site in the center. (*S*)-benzodiazepinedione **2** shown in cyan and SPP shown in orange. (B) The active site with key amino acid residues displayed. The prenyl moiety has been modeled into the active site. Diagram obtained from crystallographic report on the enzyme. [102]

Since CdpNPT shares a high sequence similarity with 4-DMATS from different fungi (~28-31%), a similar dissociative mechanism was proposed by the Shu-Ming Li group (Figure 2.11). It was suggested that prenylation is initiated with the cleavage of the diphosphate moiety, resulting in the generation of a dimethylallyl carbocation. Since the C-3 atom of the indole moiety is the most nucleophilic position, it attacks the C-3 position of the dimethylallyl carbocation. The nucleophilicity of C-3 is further enhanced by the H-bonding between the indole NH and glutamate 116. The resultant iminium intermediate then undergoes a nucleophilic attack by the nitrogen atom of the amide bond in the benzodiazepindione moiety and a deprotonation

step yields the product (Figure 2.11). The crystal structure shows that the distance between the amide nitrogen and the C-2 atom of the indole ring is 3.2 Å which makes this attack feasible. [102]

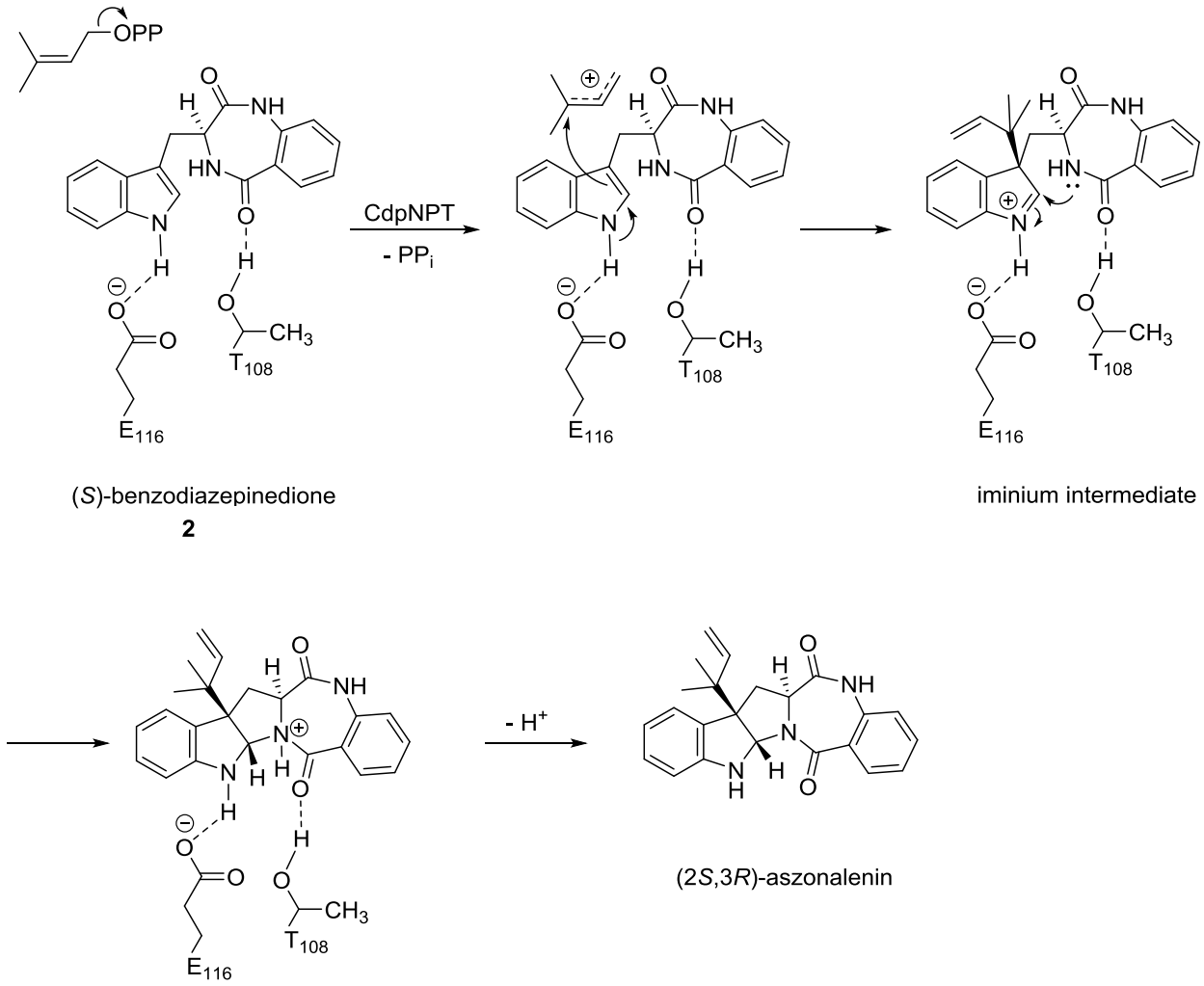

Figure 2.11 Proposed mechanism for CdpNPT catalysis. (*S*)-benzodiazepinedione **2** is shown as the substrate.

As we described in section 2.1, the second paper published on CdpNPT described a rearrangement of the product **3**, then incorrectly thought to be an N-1 reverse prenylated compound, to an N-1 normal prenylated **4** under acidic conditions. [107] Following the

identification of the true product of CdpNPT as the C-3 reverse prenylated compound **15**, we wished to re-examine this rearrangement and verify the structure of any products formed (Figure 2.12). If the structure of an N-1 normal prenylated compound **4** was assigned correctly as the product of the rearrangement, this would represent an aza-Cope rearrangement of a C-3 reverse prenylated species. As described in the section on 4-DMATS, it would also be very interesting to see if the reverse C-3 prenylated species could undergo a Cope rearrangement to give the C-4 normal prenylated product **16**. This would produce excellent non-enzymatic precedence for the Cope rearrangement described for 4-DMATS. [98] We will describe our experiments investigating the non-enzymatic Cope and aza-Cope rearrangements in the following section.

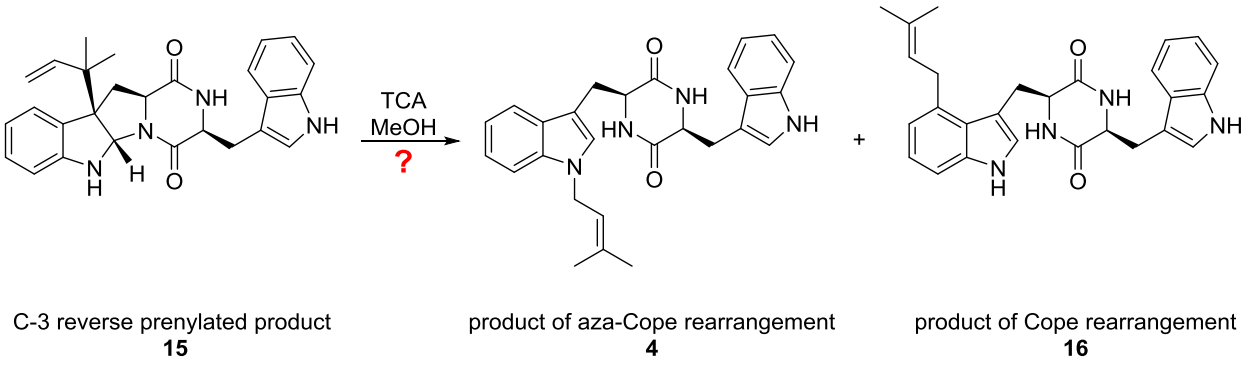

Figure 2.12 Structures of the expected products of compound 14 following the Cope/aza-Cope rearrangements.

2.2 Non-Enzymatic Cope and Aza-Cope Rearrangement Studies with Compound 15

The reactions of C-3 reverse prenylated indoles undergoing Cope or aza-Cope rearrangements has been the subject of much interest to those studying indole prenyltransferase mechanisms. [37,98,165] Since the energy barrier to some Cope rearrangements is quite high, we wished to investigate whether the non-enzymatic reactions would occur at reasonable rates and

temperatures. To start our study, a purified sample of **15** was dissolved in MeOH and TCA (136 mM) was added. All the starting material was consumed after stirring at 37 °C for a period of 48 hours.

^{1}H NMR analysis of the crude mixture indicated that a predominant product along with several minor by-products had formed (Figure 2.13). The major product was assigned to be normal prenylated as the signals corresponding to the two methyl groups were shifted from 0.79 and 0.66 ppm in the starting material to higher chemical shifts of 1.81 and 1.69 ppm in the product (Figure 2.13). This downfield shift is expected for the two methyl groups as they are connected to an sp^2 hybridized carbon, which is a clear indication of a normal prenylation. The absence of the C-2 proton signal at 5.2 ppm suggested that the hexahydropyrroloindole core is no longer present in the molecule. Instead, several signals appeared around 6.0 – 6.5 ppm that possibly corresponded to the C-2 protons of the observed products. This downfield shift suggested that the C-2 proton was connected to an sp^2 hybridized carbon rather than an sp^3 hybridized carbon as in the starting material **15**. Furthermore, integration of the aromatic region showed that all protons of the indole ring were present in the ^{1}H NMR spectrum implying that the prenyl group is attached to the indole NH, consistent with a structure such as compound **4**.

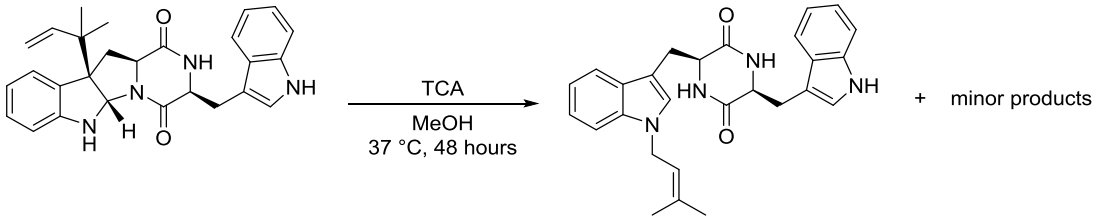

C-3 reverse prenylated product **15**

N-1 normal prenylated product **4** (major)

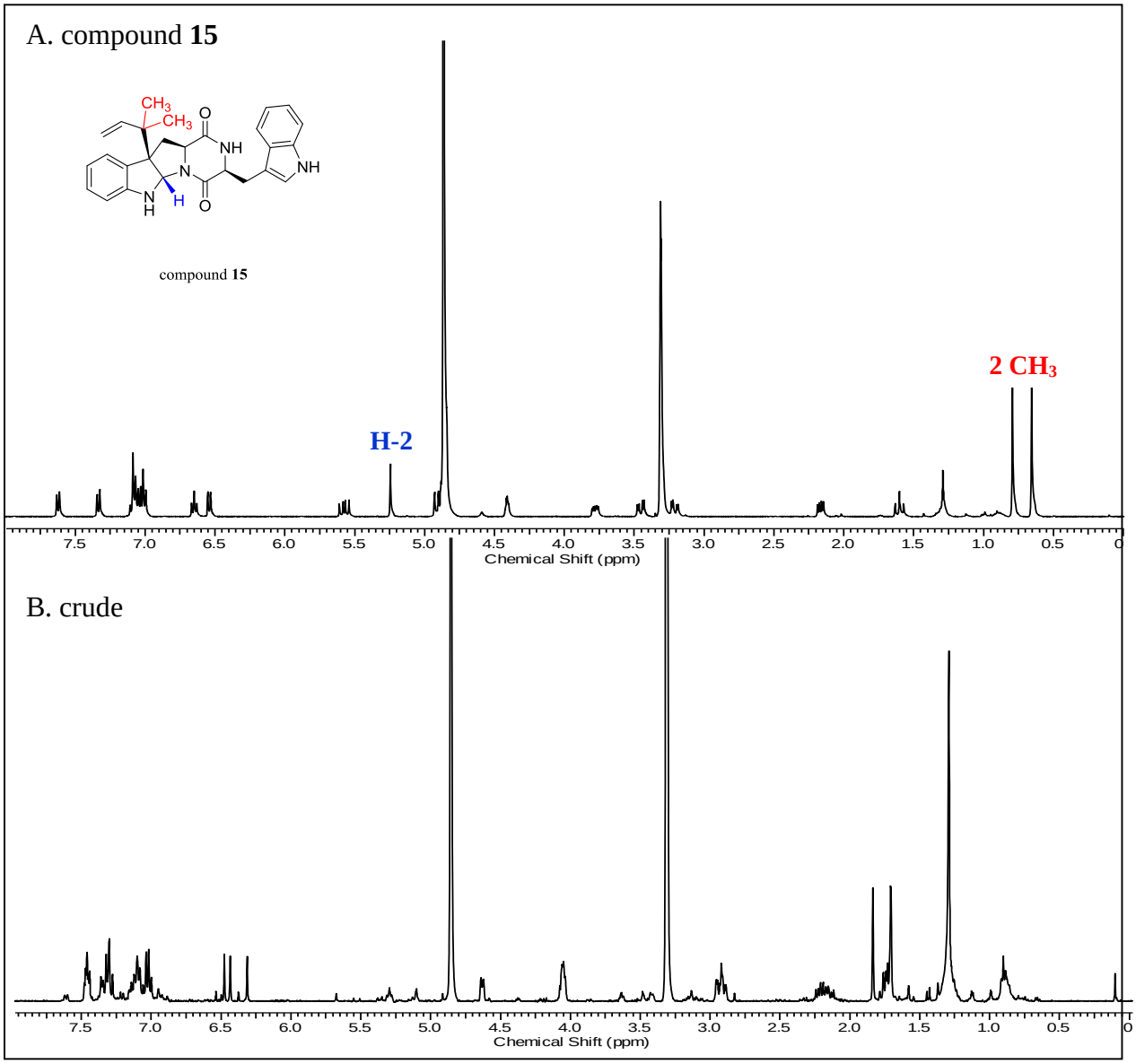

Figure 2.13 The non-enzymatic aza-Cope rearrangement of 15 to 4 under acidic condition. (CD_3OD, 400 MHz) A. Purified product of CdpNPT reaction, compound **15**. B. Crude reaction mixture from incubation of compound **15** with TCA at 37 °C.

Since our efforts towards purifying compound **4** from the crude reaction mixture were unsuccessful using conventional silica gel chromatography, we decided to undertake the chemical synthesis of compound **4** to prove the structure.

2.2.1 Synthesis of *N*-Prenyl Cyclo-L-Tryptophan-L-Tryptophan (4)

Starting with L-tryptophan, the amine group was protected with a Boc group in a reaction with di-*tert*-butyl dicarbonate $(Boc)_2O$ to give the literature known Boc-protected L-tryptophan **20**. [166] Compound **21** was prepared via a nucleophilic substitution reaction of the indole N-H with 3,3-dimethylallyl bromide (Figure 2.14). [167] Compound **21** was used in the next step without further purification as the purification process proved to be challenging. However, a small portion of **21** was transformed into the corresponding methyl ester **22** for characterization purposes. Methyl esterification of compound **21** was achived by the reaction with trimethylsilyldiazomethane in MeOH and the product was purified using silica gel column chromatography. The coupling reaction between the amine of **21** and the carboxylic acid of the L-tryptophan methyl ester **23** was mediated by 1,3-dicyclohexylcarbodiimide (DCC) to generate compound **24**. Cleavage of the Boc protecting group was achieved with trifluoroacetic acid and the cyclization occurred after the addition of 2-hydroxypyridine. The product was purified by using silica gel column chromatography to give pure **4** in 34% yield (Figure 2.14).

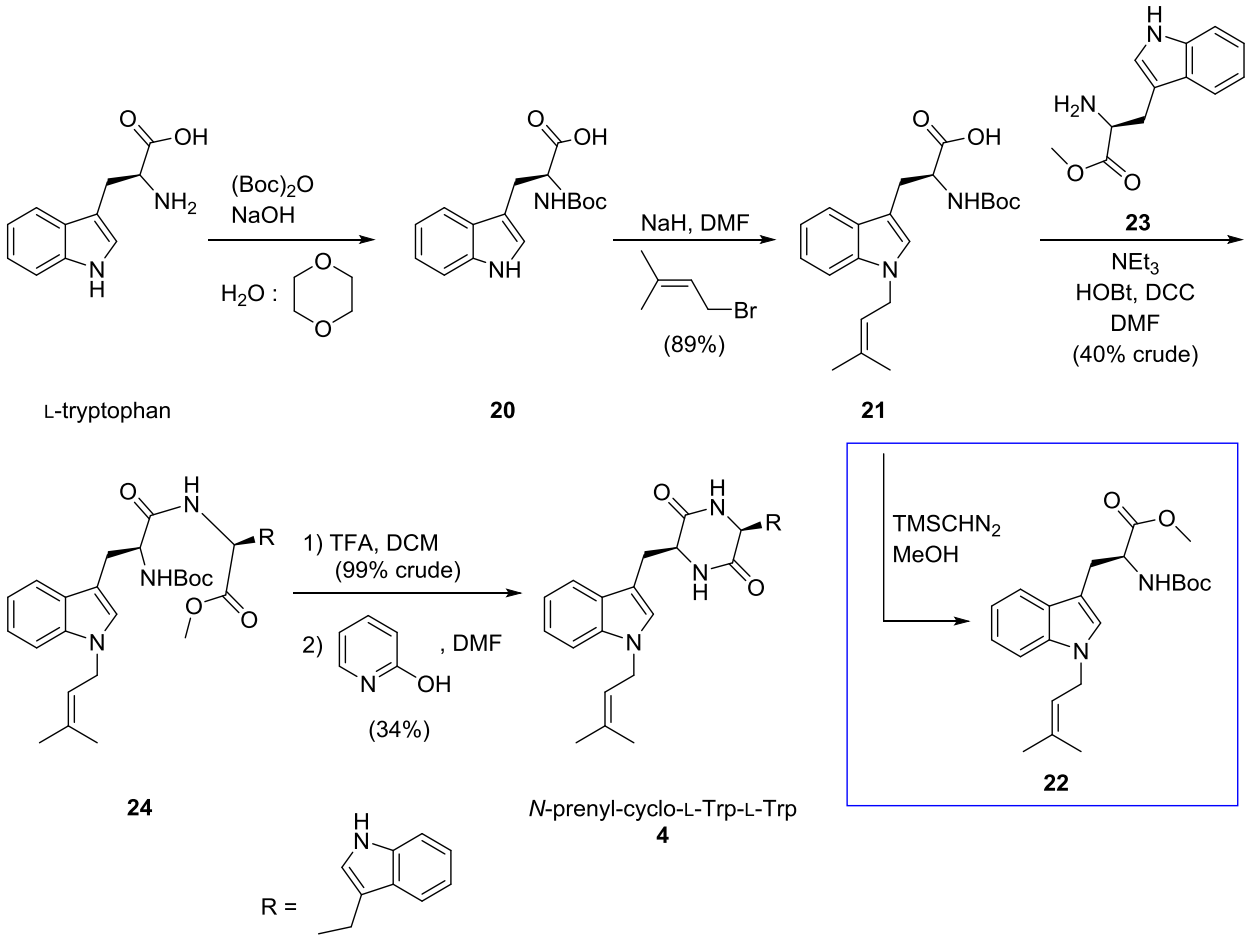

Figure 2.14 Chemical synthesis of compound 4.

A comparison between the ^{1}H NMR spectrum of the authentic synthetic compound **4** and that of the enzymatic reaction mixture confirmed that **4** was the major reaction product (Figure 2.15). The signals corresponding to the two methyl groups of the prenyl moiety appear at higher chemical shifts suggesting since they are no longer attached to an sp^3 hybridized carbon. The new chemical shift values are consistent with those observed for the N-1 prenylated indole. Moreover, two signals corresponding to the H-2 protons have shifted downfield indicating that the hexahydropyrroloindole system is not longer present in the molecule, and the H-2 protons are both connected to an sp^2 hybridized carbon.

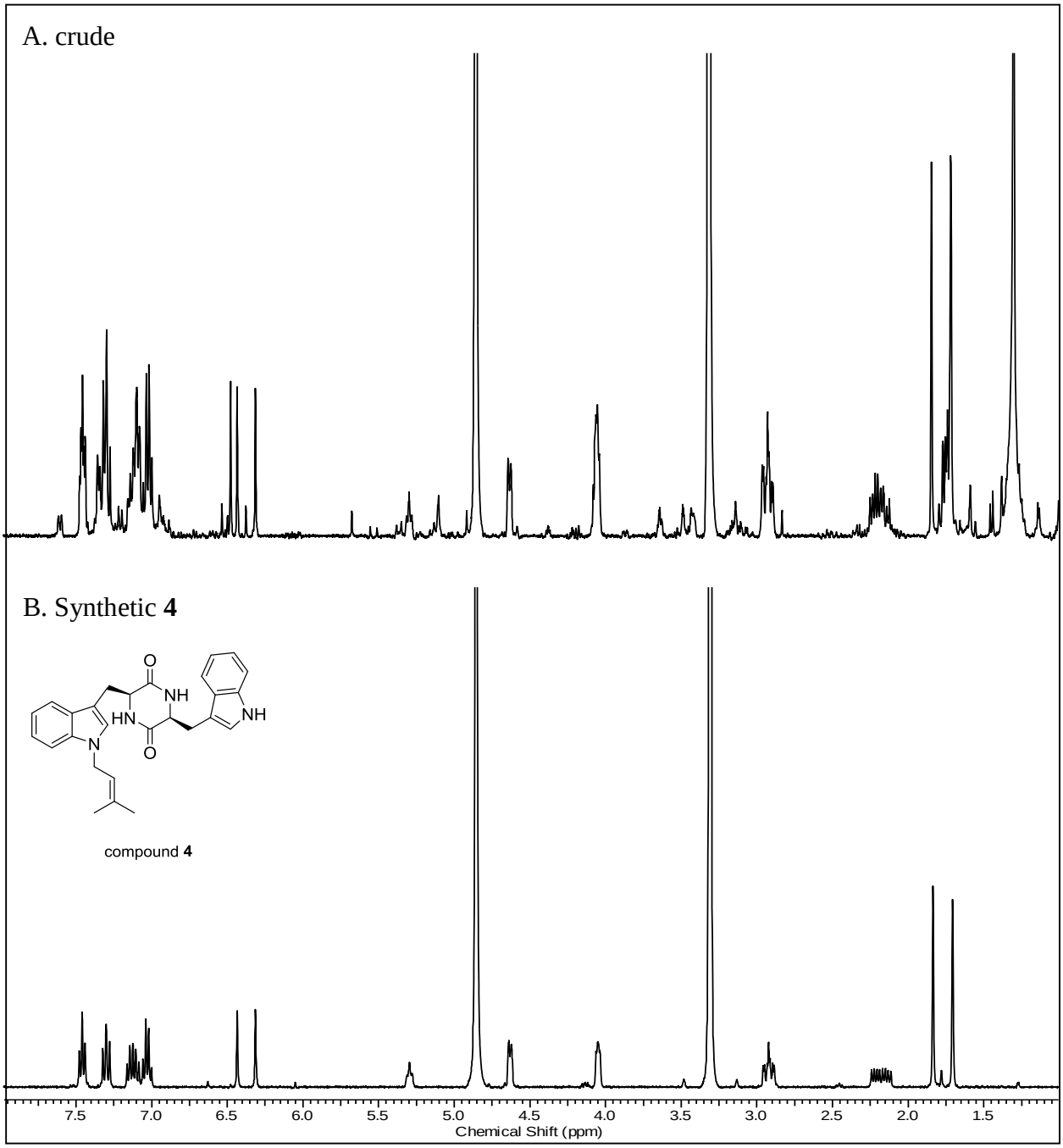

Figure 2.15 Identification of compound 4 by ^{1}H NMR spectroscopy (CD_3OD, 400 MHz). A. Crude reaction mixture from incubation of compound **15** with TCA at 37 °C. B. Synthetic compound **4**.

The observation that an N-1 normal prenylated indole **4** is the major product of the reaction indicates that an aza-Cope rearrangement of a C-3 reverse prenylated indole **15** to an N-1 normal prenylated indole **4** can occur readily at 37 °C. Furthermore, given that the reaction took place in neat methanol, it is likely that it proceeds via a concerted mechanism rather than in a stepwise fashion via a carbocation (Figure 2.16). One would expect a high energy carbocation to be trapped by a high concentration of a nucleophile, such as MeOH, to give an ether. We next wished to examine whether compound **15** also undergoes a Cope rearrangement onto the C-4 position of the indole ring under acidic conditions and whether **16** was present as a minor product in the rection mixture (Figure 2.16).

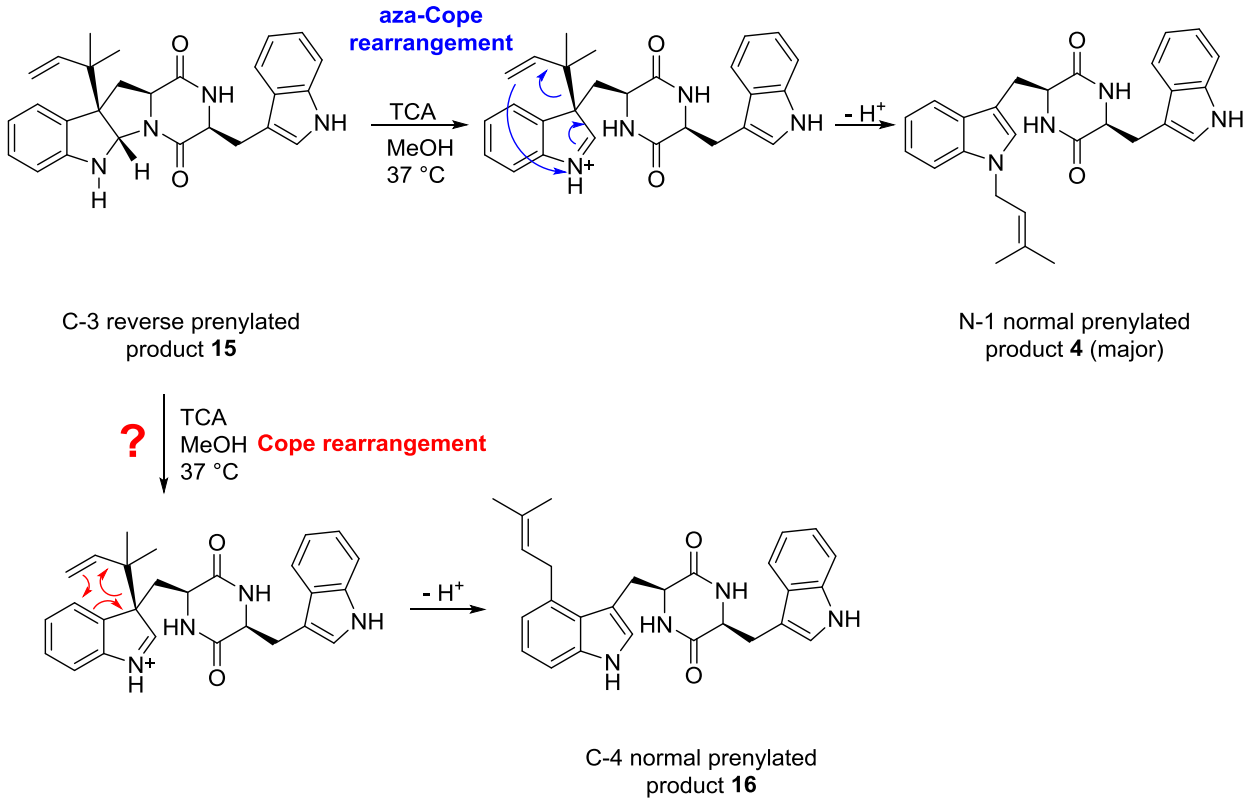

Figure 2.16 Proposed aza-Cope and Cope rearrangement mechanisms for the transformation of compound 15 to compounds 16 and 4.

Since the chemical synthesis of compound **16** would be challenging, we opted for an enzymatic approach where cyclo-L-Trp-L-Trp is C-4 normal prenylated by the action of the enzyme CpaD. [168] CpaD, cyclo-acetoacetyl-L-tryptophan dimethylallyltransferase, is one of the three pathway-specific enzymes, including CpaS, CpaD and CpaO, involved in the assembly of the fungal neurotoxin α-cyclopiazonic acid (α-CPA) (Figure 2.17). It catalyzes the normal C-4 prenylation of cyclo-acetoacetyl-L-tryptophan (cAATrp) to give β-cyclopiazonic acid (β- CPA). In addition, CpaD has been shown to accept tryptophan-containing diketopiperazines as substrates for C-4 prenylation. [168]

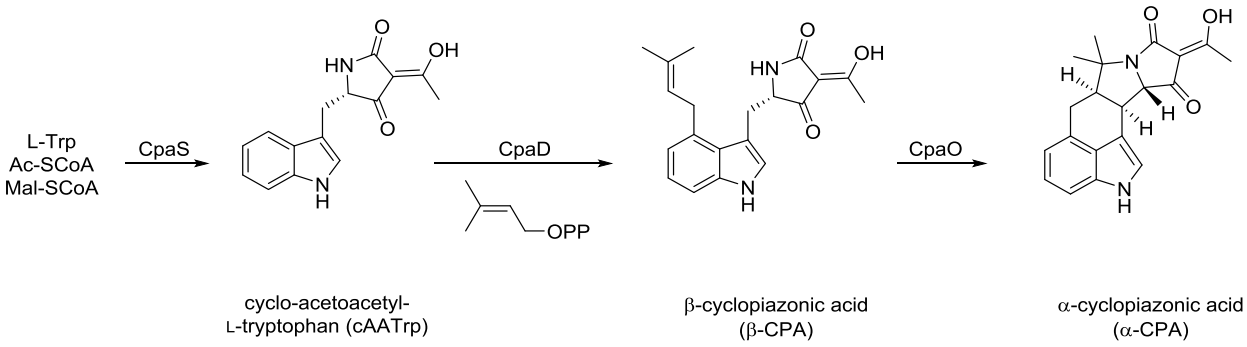

Figure 2.17 Biosynthesis of cyclopiazonic acid (CPA) in *Aspergillus* sp.

2.2.2 Enzymatic Synthesis of C-4 Normal Prenylated Cyclo-L-Trp-L-Trp (16)

2.2.2.1 Expression and Purification of the Prenyltransferase CpaD

The gene encoding for cyclo-acetoacetyl-L-tryptophan dimethylallyltransferase, *cpaD* from *Aspergillus oryzae*, was synthesized by GenScript® with codon optimization for overexpression in *E. coli* and cloned into a pET28 vector under similar conditions as described

earlier for *cdpNPT* gene (Figure 2.18). A modification of the protocol described by Steffan and his co-workers was employed to overproduce the enzyme. [86]

GGATCCATGGAAATCTCGAAGAAAGCGGCAACCCTGCTGCCGAAACCGTTTTACGT
CCTGAGCCAAGCCCTGAACCTGAGCAATAAGGATCACACCAAATGGTGGTATAGCA
CGGCACCGATGTTCGCTACCATGATGGCGGGCGCCGGTTATGATGTGCATGCACAGT
ACAAATTTCTGTGCATTCACCGTGAAGTTATTATCCCGGCGCTGGGCCCGTATCCGG
AAAAAGGTCAACCGATGCATTGGAAGTCACACCTGACCCGTTTTGGCCTGCCGTTCG
AACTGTCGTTTAACTACAGCAAGTCTCTGCTGCGCTTTGCGTTCGAACCGCTGGGCT
CACTGACCGGTACGAAAGATGACCCGTTCAATACCCAGGCGATCCGCCCGGTCTTAC
AGGATCTGAAGGCGATGGTGCCGGGCCTGGATCTGGAATGGTTTGACCATTTCACGA
AAGCACTGGTGGTTTCGGAAGAAGAAGCGCGTACCCTGCTGGATCGCGACATTGAA
ATCCCGGTCTTTAAAACGCAGAACAAGCTGGCGGCCGATCTGGAACCGAGCGGTGA
CATTGTGCTGAAAACCTATATCTACCCGCGTATTAAGTCTATCGCGACCGGCACGCC
GAAAGAACGCCTGATGTTCGATGCCATTAAAGCAGCTGACAAATTTGGCAAGGTGG
CGACGCCGCTGGCCATTCTGGAAGAATTTATCGCAGAACGTGCTCCGACCCTGCTGG
GCCACTTTCTGAGTTGCGATCTGGTTAAACCGAGTGAATCCCGTATCAAGGTCTATT
GTATGGAACGCCAGCTGGATCTGGCCTCCATTGAAGGCATCTGGACGCTGAACGGTC
GTCGCAATGACCCGGAAACCCTGGATGGTCTGGACGCACTGCGCGAACTGTGGCAG
CTGCTGCCGGTTACCGAAGGTCTGTGCCCGCTGCCGAACTGTTTTTATGAACCGGGC
ACGAGCCCGCAGGAACAACTGCCGTTCATTATCAATTTTACCCTGAGCCCGAAGTCT
GCACTGCCGGAACCGCAGATTTACTTTCCGGCTTTCGGCCAAAACGATAAAACGATC
GCAGAAGGTCTGGCTACCTTTTTCGAAAGCCGTGGCTGGGGCGGTCTGGCCAAAAGT
TATCCGGCGGATCTGGCCTCCTATTACCCGGATGTGGATCTGCAAACGGCGAATCAT
CTGCAAGCCTGGATTTCATTTTCGTACAAAGGCAAAAAGCCGTATATGTCTGTCTAC
CTGCACACCTTTGAAGCGTTTTCTGCTGCTGCCCAGGAAGTTGCGATGTGTCACGAC
GGTCATAACCCGTAG**CCCGATAAGCTT**

Figure 2.18 Synthetic DNA sequence of *cpaD* codon optimized for overexpression in *E. coli*. (Bases shown in red are non-coding regions used during cloning)

The plasmid *cpaD*/pET28a was transformed into Rosetta (DE3) pLysS *E. coli* cells and the bacteria were grown in Terrific Broth (TB) medium until an optical density (OD_{600}) of 0.6

was reached. The *E.coli* cells were induced for overexpression by addition of IPTG and left growing at 24 °C for an additional 24 hours. Cells were harvested and lysed with a French press, and the lysate was applied to a column filled with immobilized metal ion affinity resin that was charged with a solution of $NiSO_4$. The column was washed with eluting buffer containing varying concentrations of imidazole and the hexahistidine-tagged CpaD was collected. The SDS-PAGE of the isolated recombinant protein is shown in Figure 2.19.

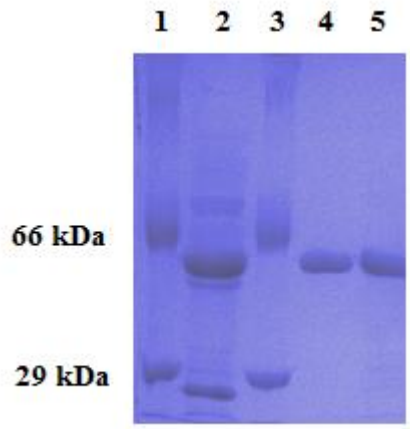

Figure 2.19 SDS-PAGE gel showing the purification of CpaD. Lane 1 & 3: molecular weight standards of 66 kDa (bovine serum albumin) and 29 kDa (carbonic anhydrase); Lane 2: crude cell extract after induction with IPTG; Lane 4 & 5: purified CpaD.

2.2.2.2 Synthesis of Compound 16 Using the CpaD Enzyme

Starting with the commercially available cyclo-L-Trp-L-Trp, a stock solution of the dipeptide (15 mM) was prepared in MeOH. As described previously in section 2.1.3 for the CdpNPT-catalyzed reactions, the substrate shows very poor solubility in aqueous buffer. Therefore, it is crucial to use 20% MeOH to ensure solubility. The substrates cyclo-L-Trp-L-Trp and dimethylallyl diphosphate (DMAPP) were incubated with the enzyme CpaD at 37 °C for 20 hours. After extracting the product with ethyl acetate, silica gel column chromatography was

used to purify the C-4 normal prenylated cyclo-L-Trp-L-trp **16** (Figure 2.20). No diprenylated compound was detected indicating that one indole ring must be unmodified for binding to the active site.

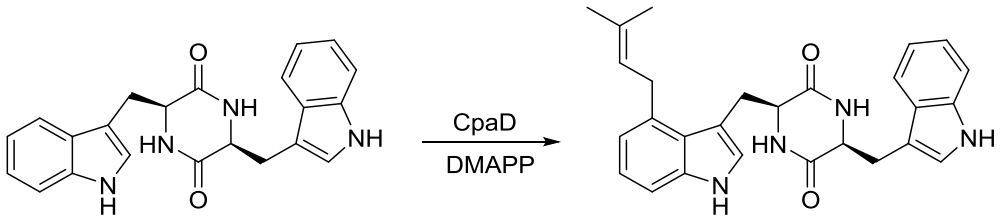

cyclo-L-Trp-L-Trp

C-4 normal prenylated cyclo-L-Trp-L-Trp
16

Figure 2.20 Synthesis of compound 16 using the enzyme CpaD.

A comparison between the ^{1}H NMR spectrum of compound **16** with that of the crude reaction mixture of **15** indicated that the C-4 normal prenylated compound **16** was not generated to any detectable extent (Figure 2.21). As described earlier for the indole prenyltransferase 4-DMATS, the Cope rearrangement has been proposed to occur onto the C-4 position in the active site of the enzyme. [98] Based on our findings in this study, it was concluded that in the absence of the enzyme active site, the aza-Cope rearrangement occurs more readily onto the indole nitrogen rather than a Cope rearrangement onto the C-4 position. Literature precedent for the preferred occurrence of the non-enzymatic Cope rearrangement onto the N-1 position instead of the C-4 position is available and will be described in the following section. [169]

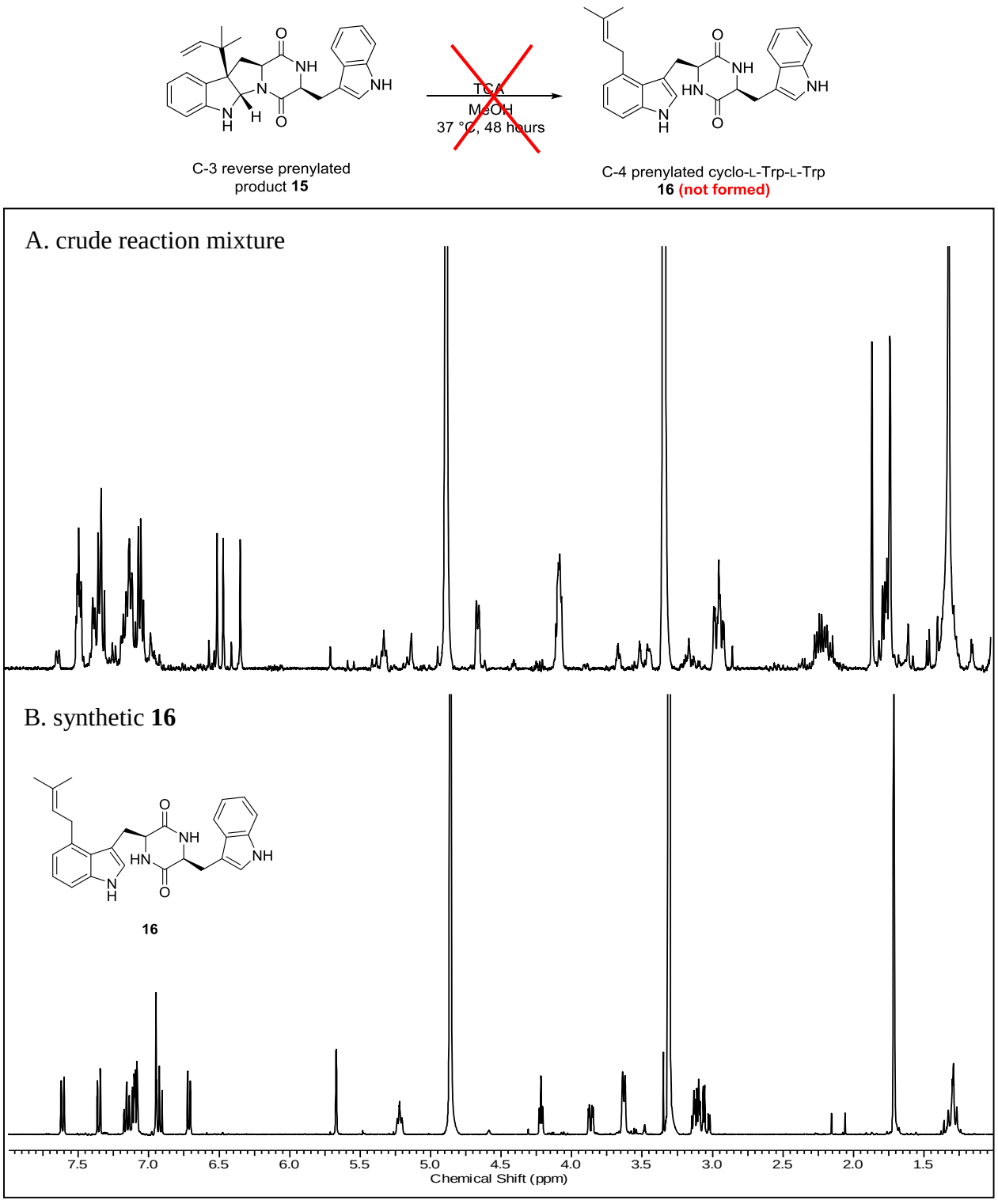

Figure 2.21 Identification of compound 16 by ^{1}H NMR spectroscopy (CD_3OD, 400 MHz). A. Crude reaction mixture from incubation of compound **15** with TCA at 37 °C. B. Synthetic compound **16**.

2.2.3 Examples of Non-Enzymatic Cope Rearrangement

The findings of Voûte *et al* showed that compound **25** undergoes a Claisen rearrangement to give compound **26** when heated to reflux in toluene (Figure 2.22 A). [169] Further heating in toluene generated a mixture of **27** and **28** in 72% and 12% yield, respectively. This observation indicates that the Cope rearrangement of allyl group onto C-4 can be in competition with the aza-Cope rearrangement onto N-1 in a structurally similar system.

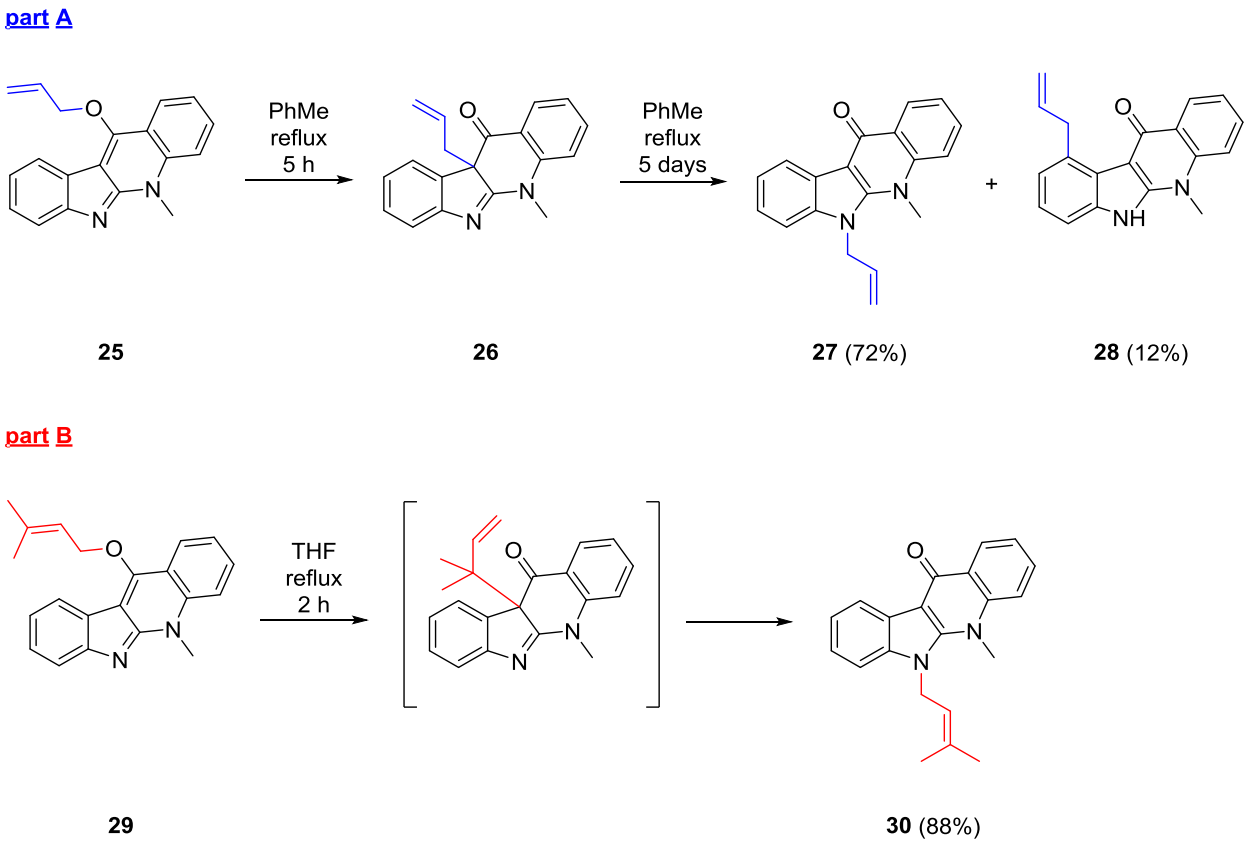

Figure 2.22 Examples of non-enzymatic Claisen, Cope, and aza-Cope rearrangements.

In the same study, the effect of alkyl substitution on the rate of migration was investigated (Figure 2.22B). They showed that these rearrangements occur significantly faster with dimethylallyl groups as a result of the gem-dimethyl effect. [169,170] Refluxing compound **29**

in THF for 2 hours gave **30** in 88% yield. Surprisingly, no C-4 substituted product was observed in this case. This is presumably due to the higher regioselectivity of the process as a result of the lower temperature.

Our studies used a closer analog to the iminium intermediate formed in the 4-DMATS reaction, and we found that the rearrangement occurred at an even lower temperature. In our case we saw that only the aza-Cope rearrangement occurs, indicating that this is the preferred reaction. If the Cope rearrangement is operative in 4-DMATS, the enzyme must be restricting the orientation of the prenyl group to direct it specifically to C-4.

As we completed our studies with the CdpNPT enzyme, we decided to focus on the prenyltransferase FtmPT1 that catalyzes a C-2 normal prenylation reaction. Since the crystal structure of FtmPT1 shows significant similarity to that of 4-DMATS, we wished to examine whether the two enzymes employ a similar mechanism that involves an initial C-3 reverse prenylation. The second part of chapter two describes our studies on this enzyme.

2.3 Mechanistic Studies on the Brevianamide F Prenyltransferase FtmPT1

As described in section 1.5.5 of Chapter 1, brevianamide F prenyltransferase from *Aspergillus fumigates* (FtmPT1) catalyzes the C-2 normal prenylation of brevianamide F (cyclo-L-Trp-L-Pro). A previous study on FtmPT1 proposed a mechanism involving a direct C-2 attack of the indole ring onto the primary carbon of the incipient dimethylallyl cation. [104] The crystal structure of FtmPT1 clearly shows that the primary carbon of the dimethylallyl cation is pointing away from the C-2 position of the indole ring, and instead the tertiary carbon of the allylic carbocation sits directly above the C-3 position of the indole ring. [110] To rationalize the formation of the product, it was proposed that the allylic carbocation undergoes a 180° rotation

in the enzyme active site in order to relocate the primary carbon of allylic carbocation in proximity to the C-2 position of the indole ring. Since the reorientation of the highly reactive carbocationic intermediate seems somewhat unlikely, we sought to further investigate the mechanism of FtmPT1. Reports with mutant enzyme and alternate substrates showed that FtmPT1 could produce C-3 reverse prenylated products and we therefore suspected that a mechanism involving an initial C-3 reverse prenylation may be operative (Figure 2.23). This will generate an iminium intermediate which must undergo a rearrangement to give the C-2 normal prenylated benzylic cation. This rearrangement is technically a [3,5]-sigmatropic shift, and is therefore unlikely to be a concerted process as it is symmetry forbidden. [171] Instead it could proceed in a stepwise fashion by a secondary cation (not shown here). The final step involves the deprotonation of the benzylic cation to give tryprostatin B.

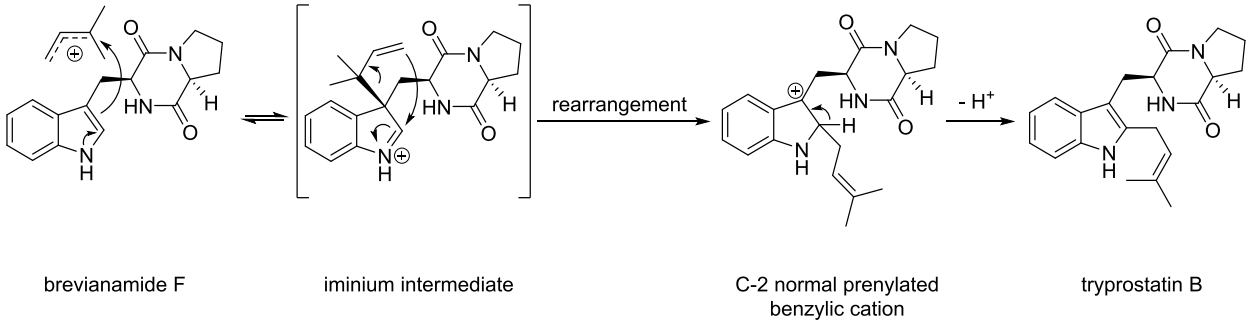

Figure 2.23 Proposed mechanism for FtmPT1 involving an initial C-3 reverse prenylation.

In the following sections, we describe the design and synthesis of the natural substrate and two substrate analogs. The testing of these compounds was used to probe the mechanism employed by FtmPT1. To begin our studies, we wished to regenerate the previously reported results by synthesizing brevianamide F and incubating it with the enzyme. [104]

2.3.1 Expression and Purification of the Prenyltransferase FtmPT1

The gene encoding for brevianamide F prenyltransferase, *ftmPT1* from *Aspergillus fumigatus*, was synthesized by GenScript® with codon optimized for overexpression in *E. coli* and cloned into a pET28 vector under similar conditions as described earlier for *cdpNPT* and *cpaD* genes (Figure 2.24). A modification of the protocol described by Steffan and his co-workers was employed to overproduce the enzyme. [86]

GGATCCATGCCGCCGGCCCCGCCGGATCAGAAACCGTGTCATCAACTGCAACCGGC
TCCGTACCGTGCCCTGAGTGAATCAATCCTGTTTGGTAGTGTGGATGAAGAACGTTG
GTGGCATAGTACCGCGCCGATTCTGTCCCGCCTGCTGATCAGCTCTAACTATGATGT
GGACGTTCAGTATAAATACCTGTCTCTGTATCGTCACCTGGTTCTGCCGGCACTGGG
TCCGTACCCGCAGCGTGATCCGGAAACCGGTATTATCGCTACGCAATGGCGCTCAGG
CATGGTCCTGACCGGTCTGCCGATTGAATTTTCGAACAATGTTGCACGTGCTCTGATT
CGCATCGGTGTTGATCCGGTTACCGCAGACAGCGGTACGGCACAGGACCCGTTCAA
CACCACGCGTCCGAAAGTGTATCTGGAAACCGCAGCACGTCTGCTGCCGGGTGTTG
ACCTGACGCGCTTTTACGAATTCGAAACCGAACTGGTTATTACGAAAGCGGAAGAA
GCCGTCCTGCAGGCGAATCCGGACCTGTTTCGCAGCCCGTGGAAATCTCAGATCCTG
ACCGCCATGGACCTGCAAAAATCCGGCACGGTCCTGGTGAAAGCATATTTCTACCCG
CAACCGAAATCAGCTGTGACCGGTCGTTCGACGGAAGATCTGCTGGTGAACGCCATT
CGCAAAGTTGACCGTGAAGGCCGCTTTGAAACCCAGCTGGCAAATCTGCAACGTTAT
ATCGAACGTCGCCGTCGCGGTCTGCATGTCCCGGGTGTGACCGCAGATAAACCGCC
GGCTACGGCAGCTGATAAAGCATTTGACGCTTGCAGCTTTTTCCCGCATTTCCTGTCT
ACCGATCTGGTCGAACCGGGTAAAAGTCGTGTGAAATTTTATGCATCCGAACGCCAC
GTTAATCTGCAGATGGTCGAAGATATTTGGACGTTCGGTGGTCTGCGTCGCGATCCG
GACGCACTGCGTGGTCTGGAACTGCTGCGCCACTTTTGGGCCGATATCCAAATGCGT
GAAGGTTATTACACCATGCCGCGCGGCTTTTGCGAACTGGGTAAAAGTTCCGCGGGC
TTCGAAGCCCCGATGATGTTTCATTTCCACCTGGATGGCTCACAGTCGCCGTTTCCGG
ACCCGCAAATGTATGTTTGTGTCTTCGGTATGAACAGCCGCAAACTGGTGGAAGGCC
TGACCACGTTTTACCGTCGCGTTGGTTGGGAAGAAATGGCCTCTCATTATCAGGCAA
ACTTTCTGGCTAATTACCCGGATGAAGACTTCGAAAAAGCGGCCCACCTGTGTGCGT
ATGTGAGCTTCGCCTACAAAAATGGCGGTGCGTATGTGACCCTGTATAATCATTCAT
TCAATCCGGTTGGCGATGTGTCGTTCCCGAACTGA**CCCGATAAGCTT**

Figure 2.24 Synthetic DNA sequence of *ftmPT1* codon optimized for overexpression in *E. coli*. (Bases shown in red are non-coding regions used during cloning)

The plasmid *ftmPT1*/pET28a was transformed into Rosetta (DE3) pLysS *E. coli* cells and the bacteria were grown in Terrific Broth (TB) medium until an optical density (OD_{600}) of 0.6

was reached. The *E. coli* cells were induced for overexpression by addition of IPTG and left growing at 24 °C for an additional 24 hours. Cells were harvested and lysed with a French press, and the lysate was applied to a column filled with immobilized metal ion affinity resin that was charged with a solution of $NiSO_4$. The column was washed with eluting buffer containing varying concentrations of imidazole and the hexahistidine-tagged FtmPT1 was collected. Typically, ~25 mg of enzyme was obtained from 1 L of culture. The SDS-PAGE of the isolated recombinant protein is shown in Figure 2.25.

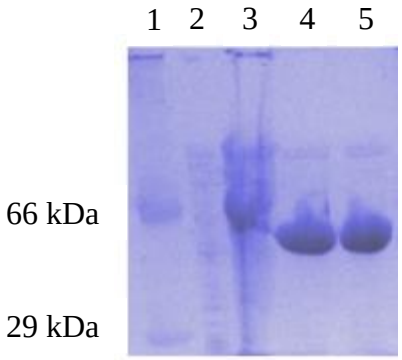

Figure 2.25 SDS-PAGE of the purified His-tagged FtmPT1. Lane 1: molecular weight standards of 66 kDa (bovine serum albumin) and 29 kDa (carbonic anhydrase); Lane 2: crude cell extract before induction; Lane 3: crude cell extract after induction with IPTG; Lane 4&5: purified FtmPT1.

2.3.2 Characterization of the Products of FtmPT1-Catalyzed Reactions

2.3.2.1 Product studies with the Natural Substrate of FtmPT1: Brevianamide F

Brevianamide F was synthesized from its two amino acid building blocks, L-tryptophan and L-proline through a coupling reaction. A common procedure for the formation of a peptide bond often involves the activation of the carboxylic acid of one amino acid by a peptide-coupling reagent, followed by coupling with the amine group of the second amino acid (Figure 2.26).

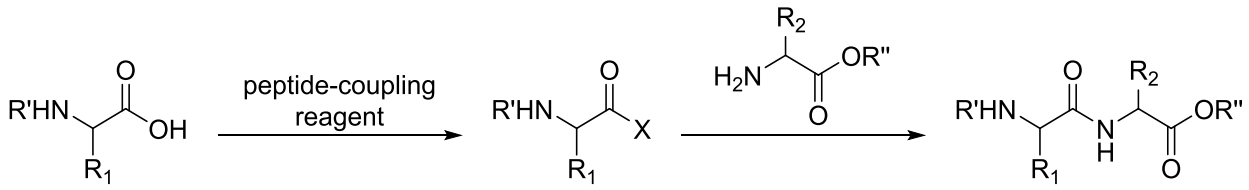

Figure 2.26 A general representation of a peptide bond formation reaction.

The use of protecting groups is fairly common in peptide bond formation reactions to avoid undesired products and side reactions. The carboxylic acid is commonly protected as an alkyl or aryl ester. A methyl ester for instance, is stable under most coupling conditions and can be easily removed by base hydrolysis. The amine group is most commonly protected with a carbamate, such as *tert*-butyloxycarbonyl (Boc) or 9-fluorenylmethyloxycarbonyl (Fmoc). Boc protected amines are prepared by reaction with *tert*-butyl dicarbonate. This protecting group is unstable under acidic condition and therefore, it is removed by treatment with trifluoroacetic acid at room temperature. To prepare the Fmoc protected amines, the free amine is allowed to react with Fmoc-Cl. In contrast to Boc protecting group, the cleavage of Fmoc can be achieved under mild basic conditions.

Starting from the commercially available L-proline, the carboxylic acid was protected as a methyl ester in a reaction with thionyl chloride in methanol, generating the hydrochloric salt of **31** quantitatively (Figure 2.27). Amide bond formation between the amine moiety of L-proline methyl ester **31** and the carboxylic acid of Boc protected L-tryptophan **20** was mediated by the coupling reagent 1,3-dicyclohexylcarbodiimide (DCC), generating the protected dipeptide **32** in 58% yield. Cleavage of the Boc protecting group was achieved under acidic conditions (TFA) to release the free amine **33** in 43% yield. The final cyclization of the amino methyl ester **33** with 2-

hydroxypyridine provided brevianamide F in 98% yield, which was purified by silica gel column chromatography. [167]

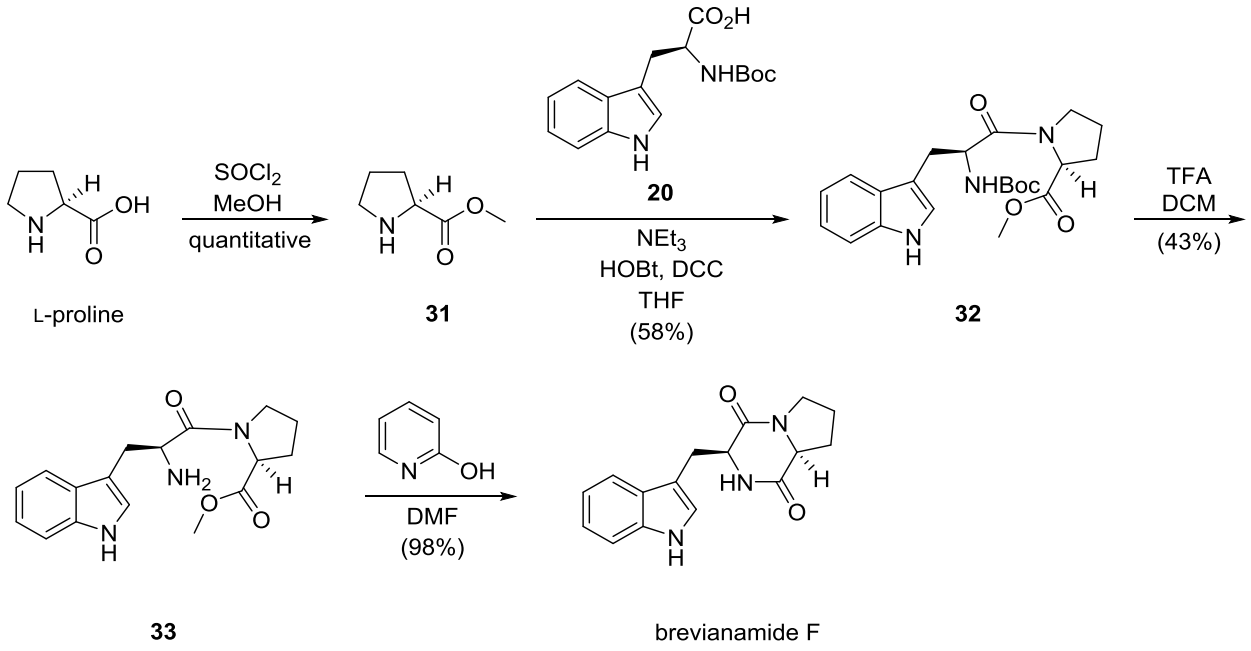

Figure 2.27 Synthesis of the natural substrate of FtmPT1, brevianamide F.

The substrates brevianamide F (cyclo-L-Trp-L-Pro) and dimethylallyl diphosphate (DMAPP) were incubated with the enzyme FtmPT1 at 37 °C for 20 hours. After the reaction was complete, the precipitate was removed through centrifugation and the resulting solution was extracted with ethyl acetate. Removal of the solvent gave a residue which was purified by silica gel column chromatography. Analysis by mass spectrometry and NMR spectroscopy indicated that a predominant product was formed with a mass corresponding to that of monoprenylated brevianamide F. The ^{1}H NMR spectrum was missing the key signal in the aromatic region that corresponded to the C-2 proton of brevianamide F (7.08 ppm) (Figure A.3) and it fully agreed with that of synthetic tryprostatin B. [172] We therefore concluded that the product of the FtmPT1

reaction between brevianamide F and DMAPP is indeed prenylated at the C-2 position (Figure 2.28).

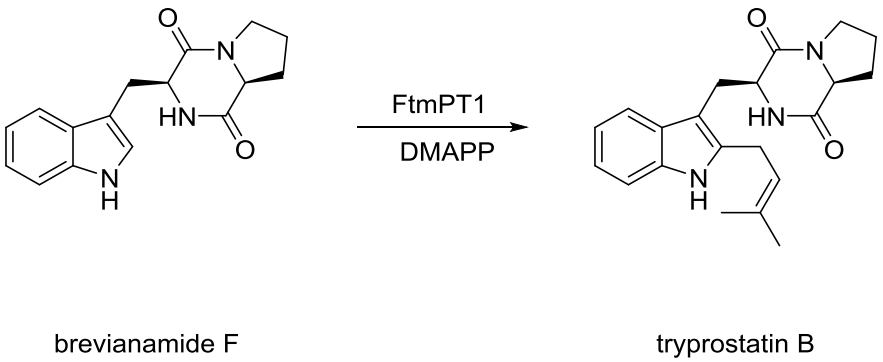

Figure 2.28 Reaction catalyzed by the prenyltransferase FtmPT1.

2.3.2.2 Product Studies with L-Tryptophan

We next investigated the FtmPT1-catalyzed reaction between L-tryptophan and DMAPP. A previous study by the Shu-Ming Li group reported that the product of this reaction was reverse prenylated at the N-1 position and was identified as *N*-(1,1-dimethyl-1-allyl)-tryptophan (*N*-DMAT) (Figure 2.29). [173] A previous study in our lab that focused on elucidating the mechanism of the prenyltransferase CymD, gave us access to the ^{1}H NMR spectrum of the enzymatically synthesized *N*-DMAT. [162] When we compared the ^{1}H NMR spectrum of *N*-DMAT generated in a CymD-catalyzed reaction to that of the compound obtained from the FtmPT1 reaction, it became obvious that the two compounds were not identical (Figure 2.29). The signal corresponding to the methyl groups of the authentic *N*-DMAT appears at 1.73 ppm while the similar methyl groups in the product of FtmPT1-catalyzed reaction appear at 0.99 and 1.10 ppm. Moreover, the signal for the C-2 proton appeared at 7.48 ppm in the authentic sample of *N*-DMAT while that of *N*-DMAT synthesized by FtmPT1 appeared at 5.46 ppm in a similar solvent. [162] The inconsistency between the chemical shift values of the reported product and those of the

enzymatically synthesized *N*-DMAT indicated that the structure of the product was missassigned.

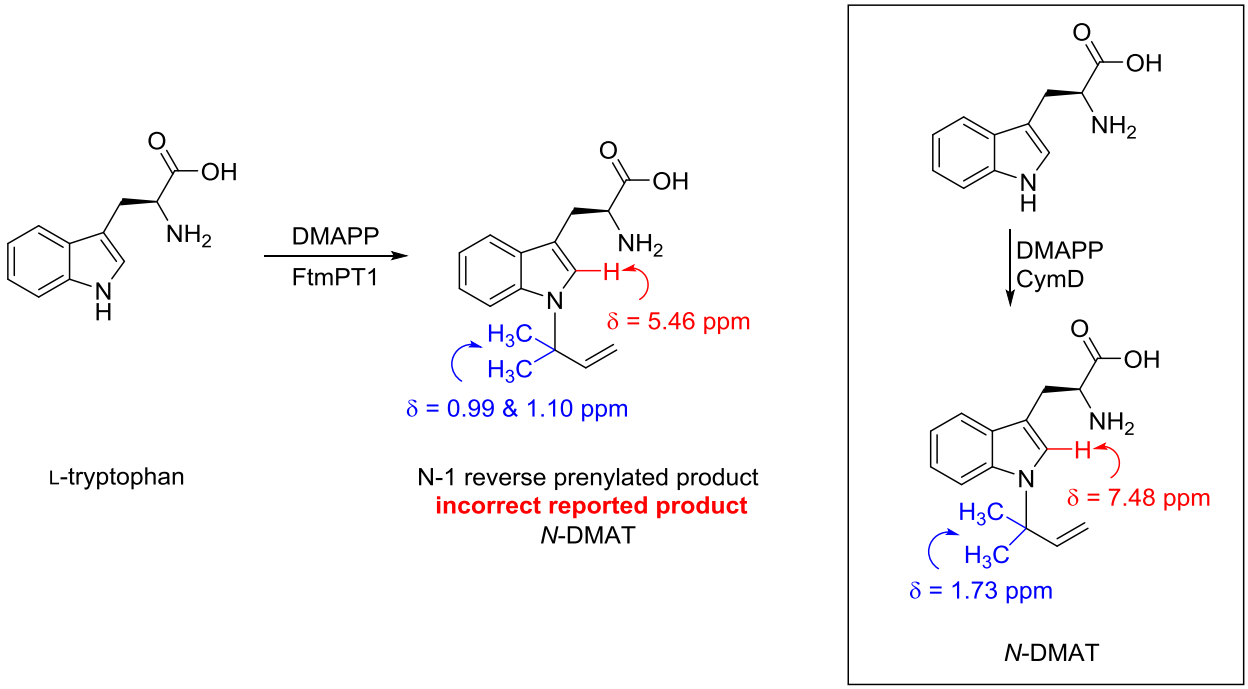

Figure 2.29 Incorrect reported structure of the product of FtmPT1-catalyzed reaction between L-tryptophan and DMAPP (in D_2O). The inset shows the reaction catalyzed by CymD and the chemical shift values of the authentic sample of *N*-DMAT in D_2O.

Another study in our lab focusing on the mechanistic studies of 4-DMATS led us to believe that the structure of the product is reverse prenylated at the C-3 position of the indole ring. [98] As described in section 1.5.3 of chapter one, the Lys174Ala mutant of 4-DMATS catalyzes the reaction between L-tryptophan and DMAPP, to give a C-3 reverse prenylated hexahydropyrroloindole **1** (Figure 2.30). Qi Qian, a PhD student in our group, synthesized **1** following a literature procedure to confirm the predicted structure of the Lys174Ala product. [98] This gave us access to an authentic synthetic sample of **1**. A quick comparison between the chemical shift values of the reported product by the Shu-Ming Li group to those of the authentic

synthetic **1** raised the possibility that the true product is also C-3 reverse prenylated (Figure 2.30).

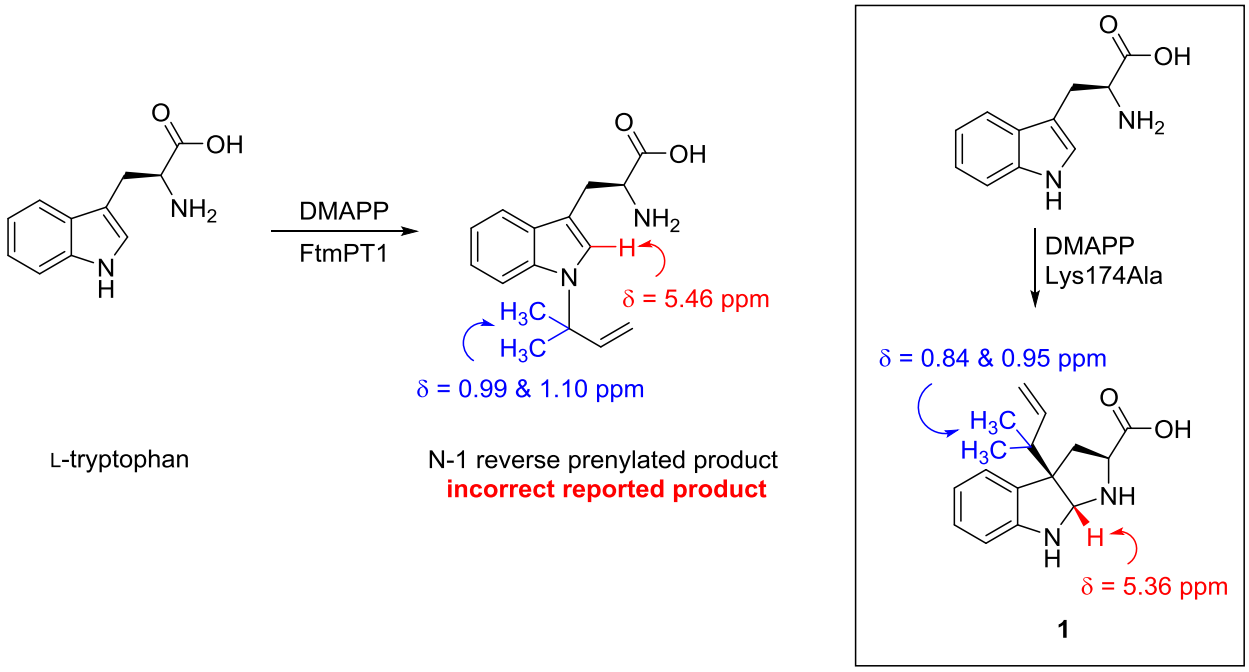

Figure 2.30 Comparision between the chemical shift values of the reported product of the FtmPT1-catalyzed reaction and those of the authentic synthetic 1 in D_2O. The inset shows the reaction catalyzed by the Lys174Ala mutant of 4-DMATS and the chemical shift values of the authentic synthetic sample of **1**.

To examine this hypothesis, we incubated L-tryptophan and DMAPP with FtmPT1 in a deuterated phosphate buffer and monitored the reaction directly by ^{1}H NMR spectroscopy. The progress of the reaction was slow and despite extended incubation, only approximately 18% conversion was observed. However, analysis of the mixture by ^{1}H NMR spectroscopy clearly indicated that a reverse prenylated product was formed. The appearance of three alkene signals at chemical shifts of 5.90, 5.07, and 5.01 is indicative of the generation of a reverse prenylated product (Figure 2.31A). We then compared the spectrum of the crude reaction mixture with that of an authentic synthetic sample of compound **1** with known stereochemistry to confirm that the

product of the reaction was C-3 reverse prenylated (Figure 2.31B). [98,174] Since a close resemblance between these two spectra was observed, we concluded that the true product of FtmPT1 with L-tryptophan is reverse prenylated at the C-3 position, compound **1** (Figure 2.32).

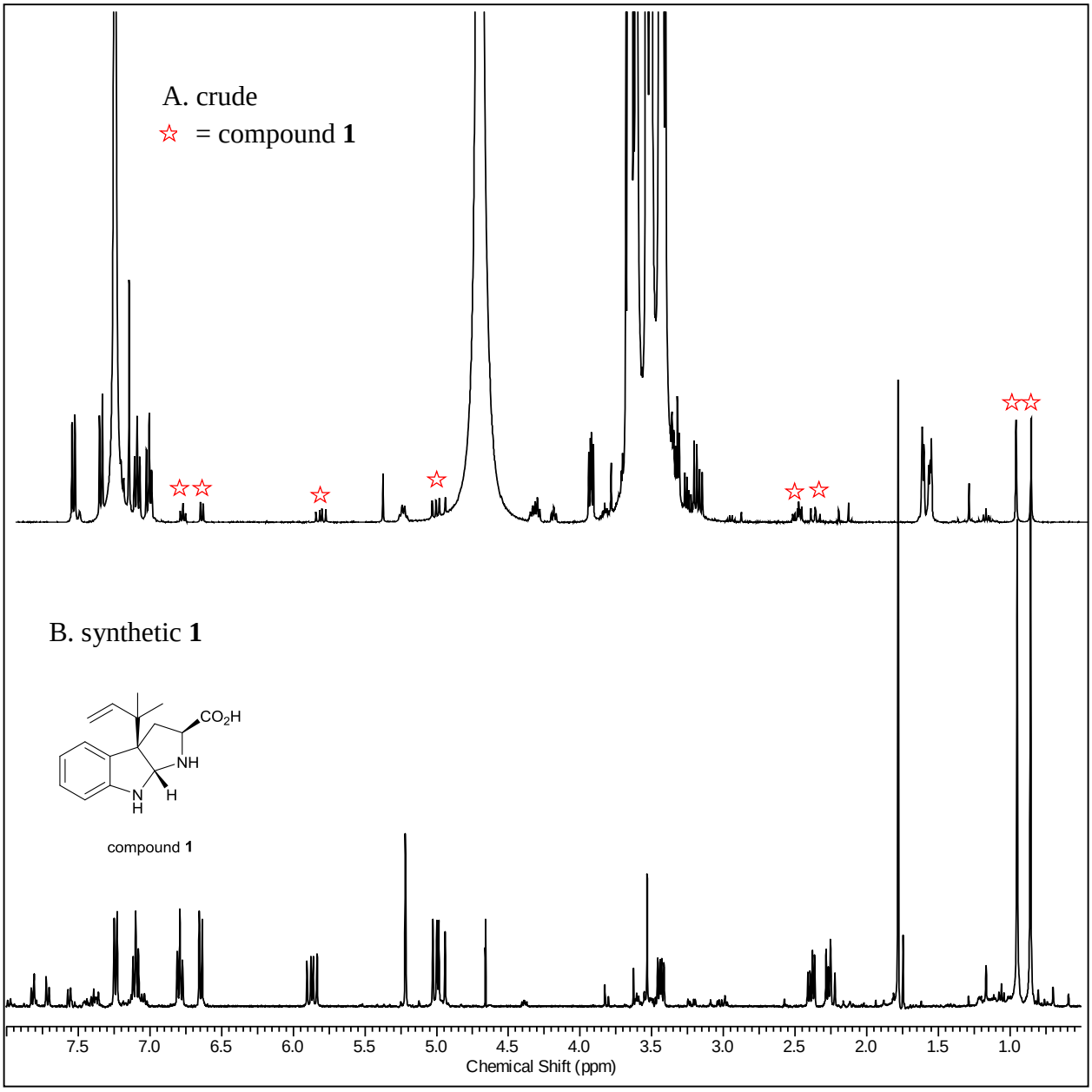

Figure 2.31 Identification of compound 1 by ^{1}H NMR spectroscopy (D_2O, 400 MHz). A. Crude reaction mixture from incubation of L-Trp with DMAPP and FtmPT1. B. Synthetic compound **1**.

We made no attempts to isolate the enzymatically formed C-3 reverse prenylated hexahydropyrroloindole **1**, as previous studies in our lab had indicated that it underwent decomposition when subjected to purification by high pressure liquid chromatography (HPLC).

The observation that wild-type FtmPT1 was capable of catalyzing a reverse C-3 prenylation reaction further supports our theory that this is potentially the first step in catalysis. In the case of L-tryptophan, it is conceivable that the primary amine functionality captures this intermediate by cyclization before any further rearrangement can occur (Figure 2.32).

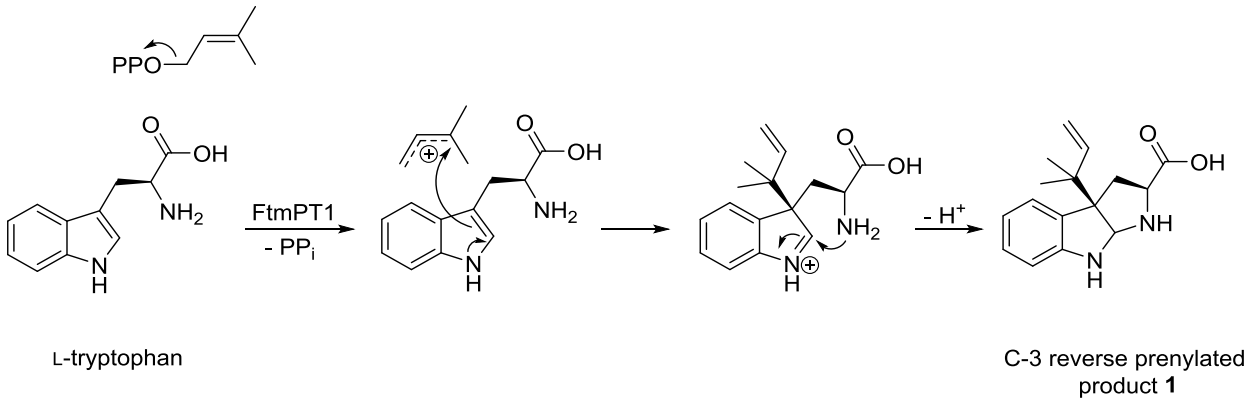

Figure 2.32 Proposed mechanism for the formation of C-3 reverse prenylated product 1 in the reaction catalyzed by FtmPT1 with L-tryptophan.

2.3.2.3 Product Studies with Cyclo-L-Trp-L-Trp

The observation that the product of the FtmPT1-catalyzed reaction between L-tryptophan and DMAPP was C-3 reverse prenylated triggered our curiosity and led us to investigate the FtmPT1 reaction with cyclo-L-Trp-L-Trp. A previous study by the Shu-Ming Li group reported that the C-2 normal prenylated cyclo-L-Trp-L-Trp **34** was isolated as the only product (Figure 2.33). [104] Given the similarity between the active sites of 4-DMATS and FtmPT1, we suspected that a C-3 reverse prenylated product **15** might have formed as the minor product during the reaction but has not been detected and isolated in the previous report (Figure 2.33).

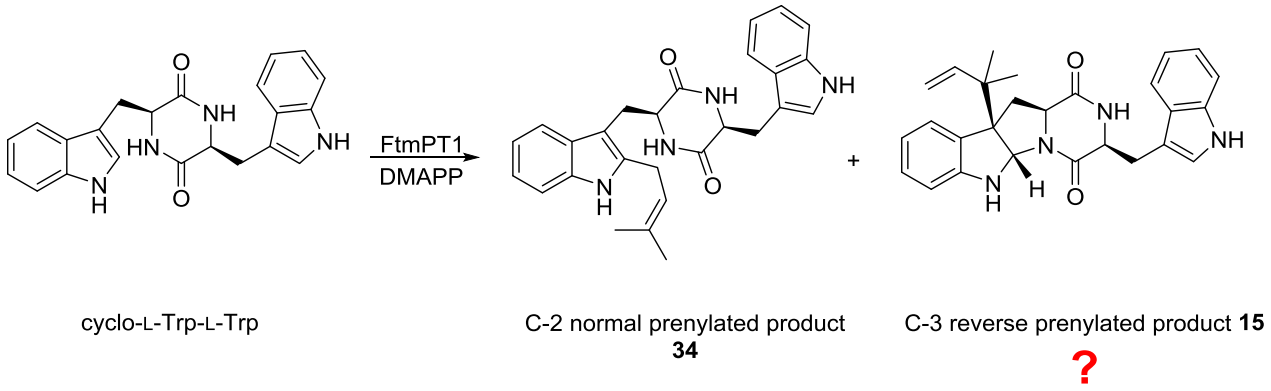

Figure 2.33 Structure of the product of the FtmPT1-catalyzed reaction of cyclo-L-Trp-L-Trp. The structure of the suspected minor product is also shown.

To test this hypothesis, a stock solution of cyclo-L-Trp-L-Trp was prepared in MeOH (25 mM). The substrates cyclo-L-Trp-L-Trp and dimethylallyldiphosphate (DMAPP) were incubated with FtmPT1 at 37 °C for 20 hours. After extraction with ethyl acetate and purification using silica gel column chromatography, two compounds were isolated in addition to the unreacted cyclo-L-Trp-L-Trp. Analysis by mass spectrometry indicated that these two products had a mass corresponding to that of monoprenylated cyclo-L-Trp-L-Trp. Further analysis by NMR spectroscopy indicated that the major product (60%) was the C-2 normal prenylated product **34** while the structure of the minor product (30%) was ultimately assigned as the C-3 normal prenylated compound **35** (Figure 2.34).

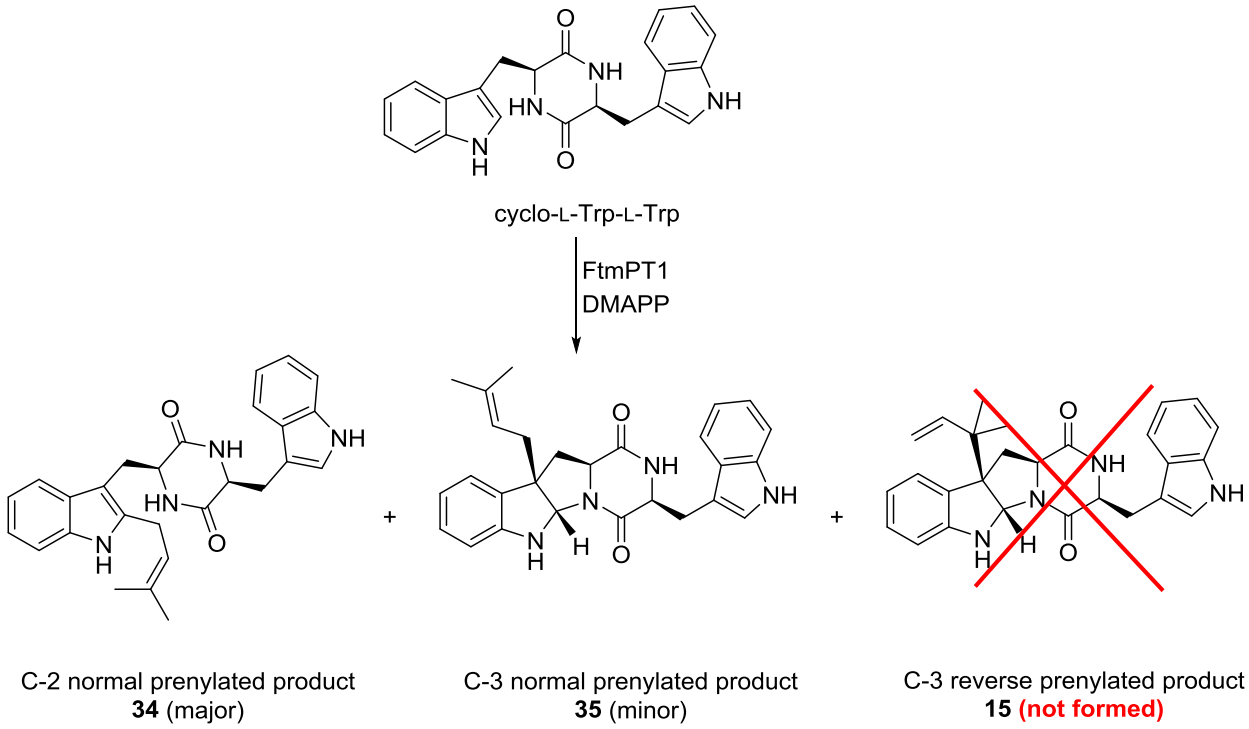

Figure 2.34 Reaction of FtmPT1 with cyclo-L-Trp-L-Trp and DMAPP.

The ^{1}H NMR spectrum of the major product **34** agreed fully with that of the previously reported enzymatically formed C-2 normal prenylated cyclo-L-Trp-L-Trp. [104] Presence of only one alkene signal (5.31 ppm) is indicative of a normal prenylation (Figure A.4). Furthermore, integration of the aromatic region showed that one of the protons of the indole rings was missing implying that the prenyl group is attached to the indole ring. The absence of the C-2 proton at 7.10 ppm suggests that the prenylation had occurred at the C-2 position of the indole ring to give compound **34**.

Surprisingly, the ^{1}H NMR spectrum of the minor product **35** showed only one alkene signal at 5.15 ppm suggesting that normal prenylation has occurred, which was opposed to our initial hypothesis that a C-3 reverse prenylated product was formed (Figure 2.35). The signal corresponding to the C-2 proton appeared at 5.34 ppm which was lower than that of the starting

material (7.10 ppm). This is consistent with an sp^3 hybridized C-2, suggesting that a hexahydropyrroloindole structure is present. Moreover, the integration of the aromatic region showed that all protons of the indole ring were present implying that the prenyl group is either connected to the C-3 position or to the indole NH. Presence of three signals (8.13, 5.66, and 5.08 ppm) that corresponded to the NH protons suggested that the prenyl group is connected to the C-3 position. In order to fully characterize the structure of compound **35** and assign the peaks present in the spectrum, we decided to take a COSY spectrum of compound **35**.

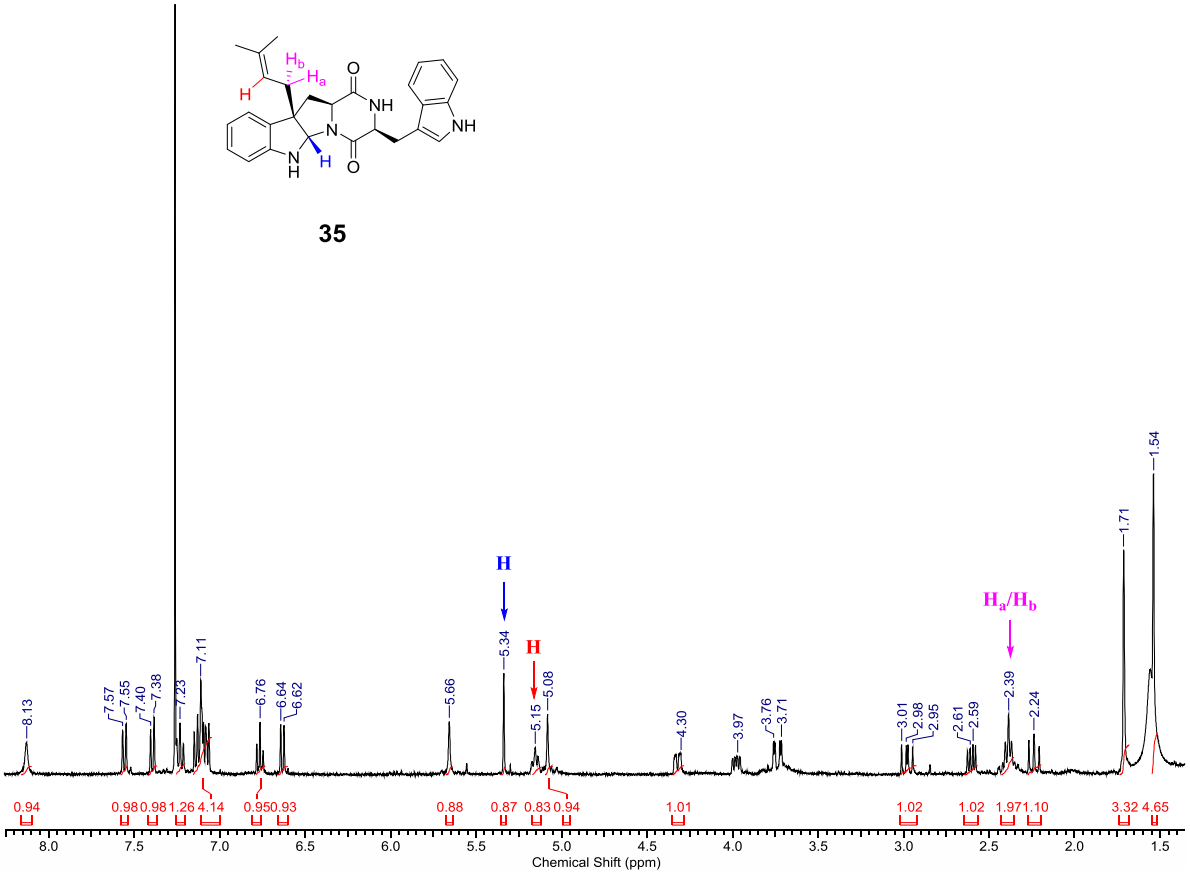

Figure 2.35 ^{1}H NMR spectrum of compound 35 (400 MHz, $CDCl_3$).

Analysis of the COSY spectrum of compound **35** indicated that the signal at the chemical shift of 2.39 ppm belonged to the methylene (C-1') protons of the prenyl group. This assignment was made based on the observation of two correlations (Figure 2.36). The first of these correlations was with the two signals corresponding to the methyl protons (1.54 and 1.71 ppm) while the second was with the alkene signal (5.15 ppm).

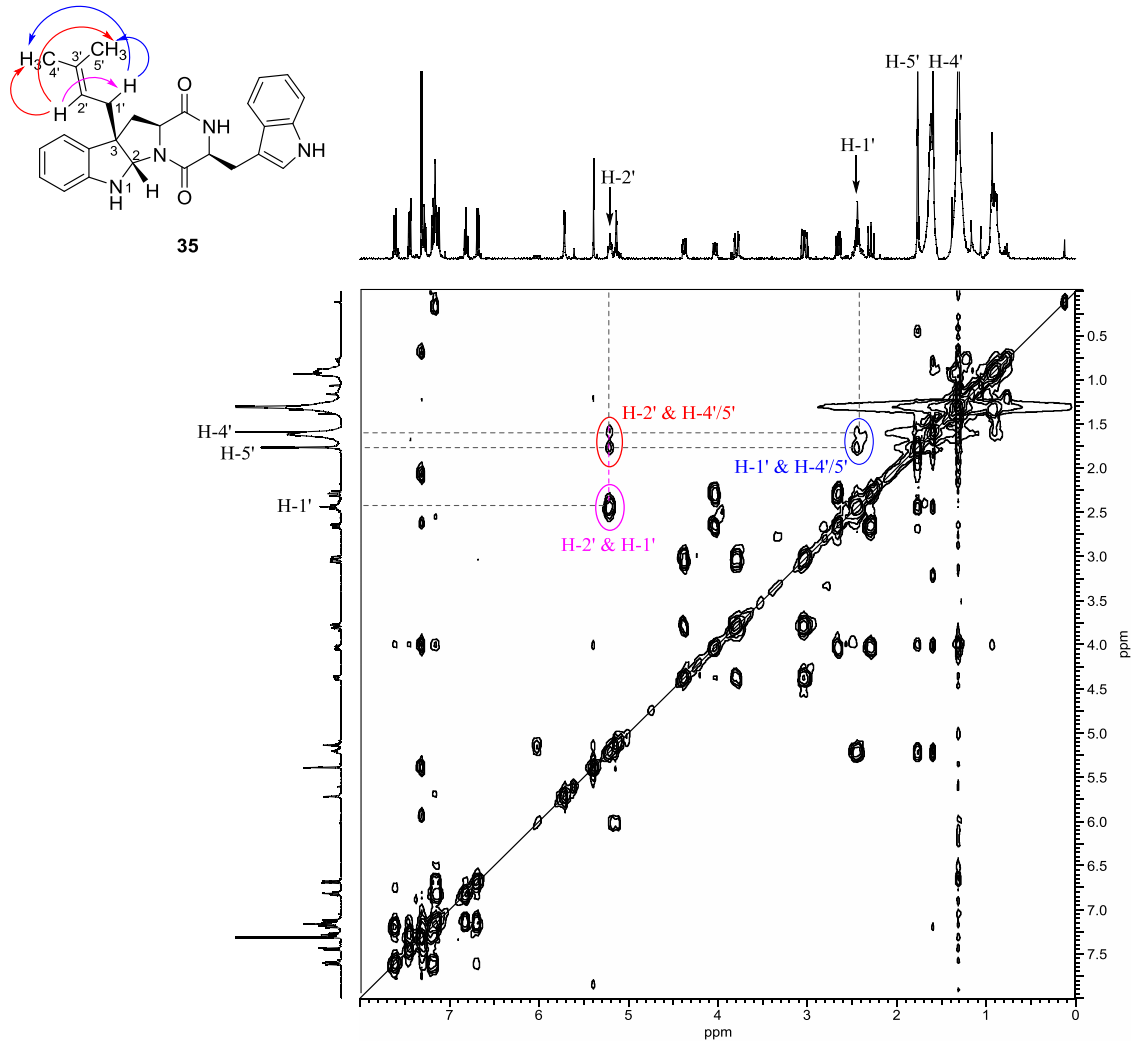

Figure 2.36 COSY spectrum of compound 35 ($CDCl_3$, 400 MHz).

An HSQC spectrum of compound **35** was also taken to determine the chemical shift values corresponding to the C-1', C-2, and C-2' signals of compound **35** (Figure 2.37). Based on the observed correlations, the signals at the chemical shift values of 35, 80, and 118 ppm were assigned to C-1', C-2, and C-2', respectively.

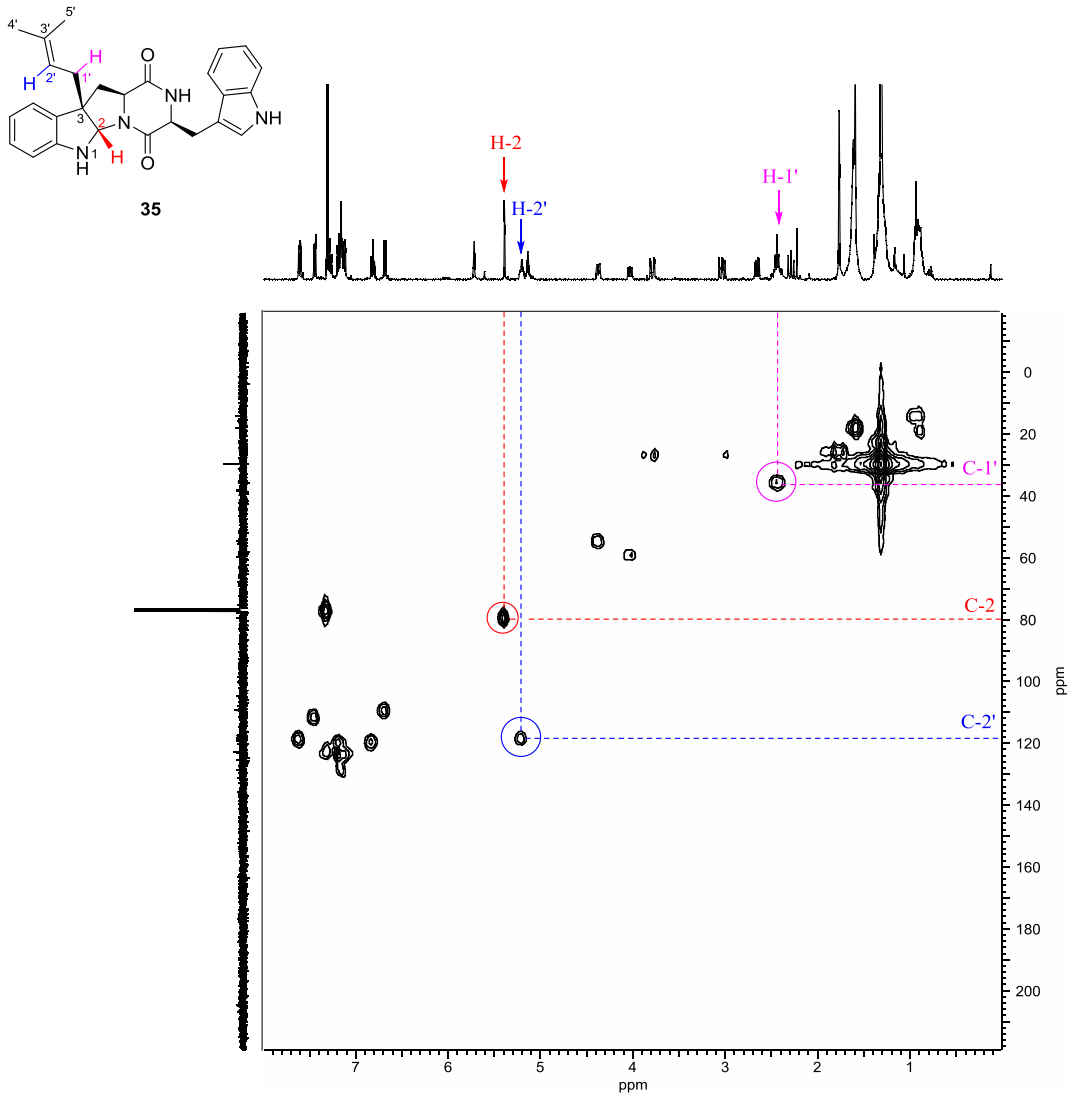

Figure 2.37 HSQC spectrum of compound 35 ($CDCl_3$, 400 MHz).

Lastly, we took an HMBC spectrum of compound **35** which showed a correlation between the C-2 proton signal at 5.34 ppm and the C-1' signal at 38 ppm (Figure 2.38). All these analyses led us to conclude that the structure of the minor product is a C-3 normal prenylated compound **35** (Figure 2.34).

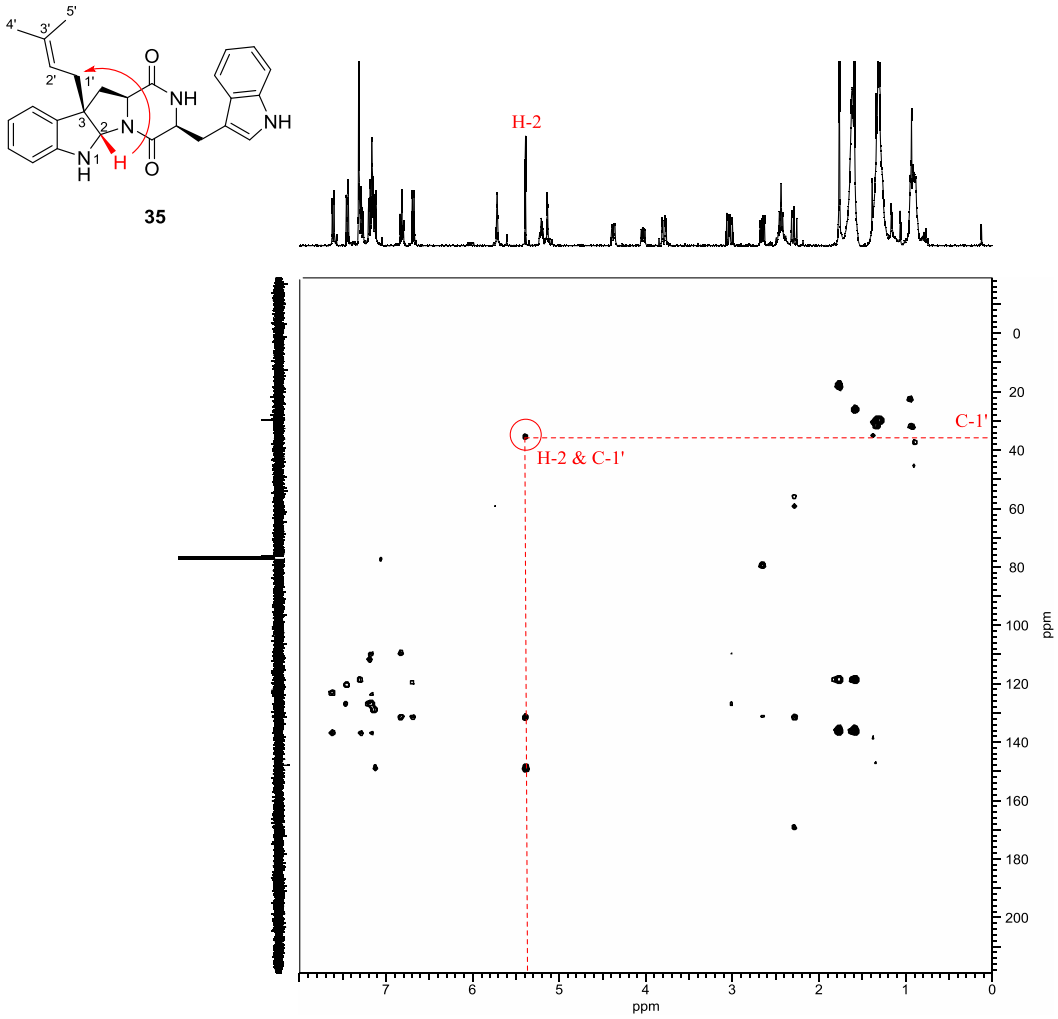

Figure 2.38 HMBC spectrum of compound 35 ($CDCl_3$, 400 MHz).

The observation of the C-3 normal prenylated product **35** in addition to the expected C-2 normal prenylated product **34** suggested that an alternate mechanism might be operative. We

therefore suggested that FtmPT1 may utilize a mechanism involving a C-3 normal prenylation as the first step of catalysis and the C-3 normal prenylated product **35** represent the released reaction intermediate that cyclized in solution (Figure 2.39). In this scenario, the C-3 normal prenylated intermediate would have to undergo a 1,2-alkyl shift to generate the C-2 prenylated intermediate and a final deprotonation would give compound **34**. Such 1,2-alkyl rearrangements are well known in indole chemistry and have been called Plancher rearrangements. [175,176,177] This exact rearrangement has been used in the chemical synthesis of tryprostatin B. [172]

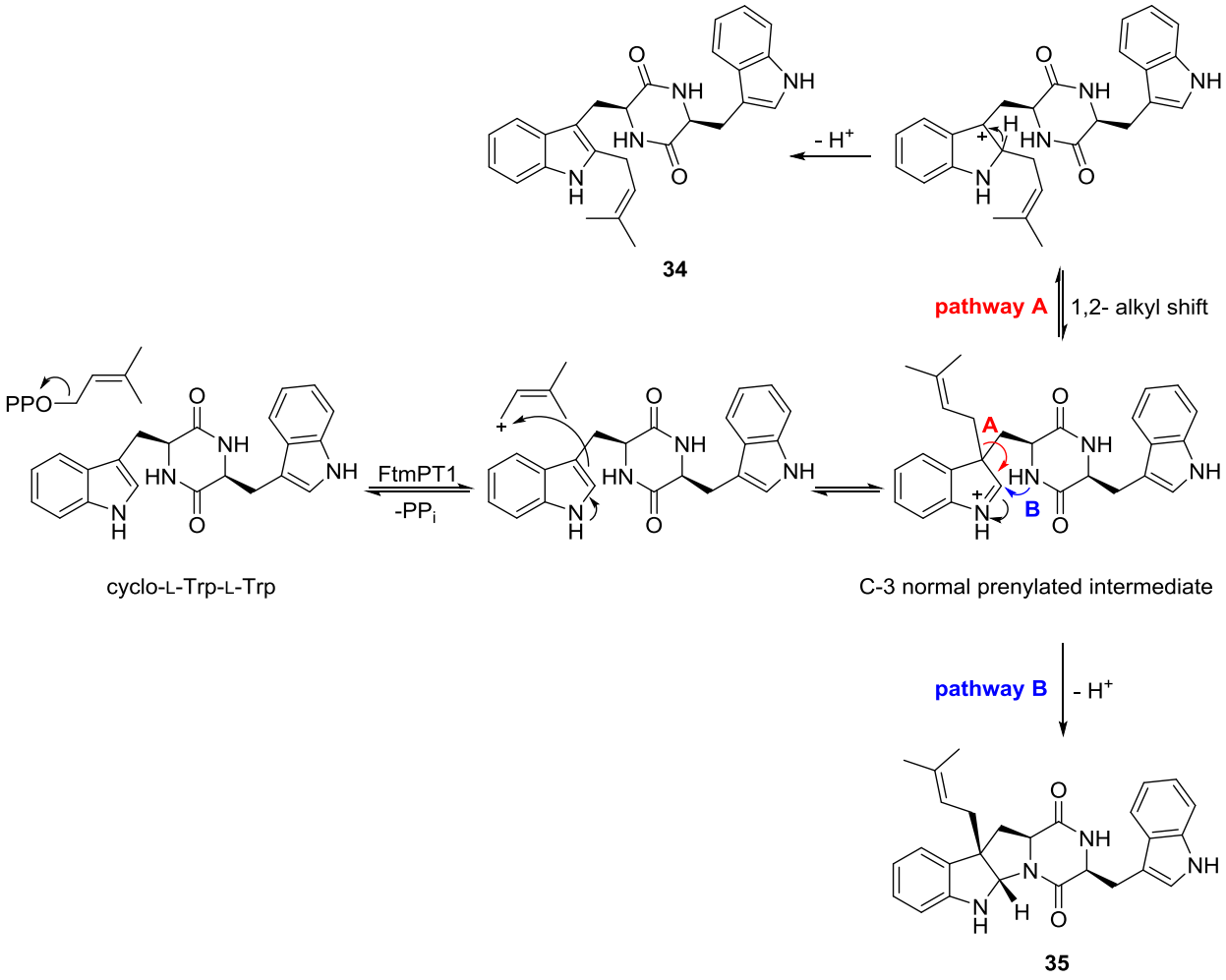

Figure 2.39 A normal C-3 prenylation mechanism for the reaction catalyzed by FtmPT1.

As we completed our studies on cyclo-L-Trp-L-Trp, a report was published by the Shu-Ming Li group which also indicated that when the proline residue of brevianamide F is exchanged for other amino acids, an unexpected side product is formed in addition to the predominant normal C-2 prenylated product (Figure 2.40). [178] Treatment of cyclo-L-Trp-L-Tyr, cyclo-L-Trp-L-Ala, cyclo-L-Trp-L-Gly, and cyclo-L-Trp-L-His with FtmPT1 and DMAPP generated the corresponding normal C-2 prenylated cyclic dipeptides as the predominant product. However, normal C-3 prenylated species have also been detected that made up for as much as 30% of the isolated products.

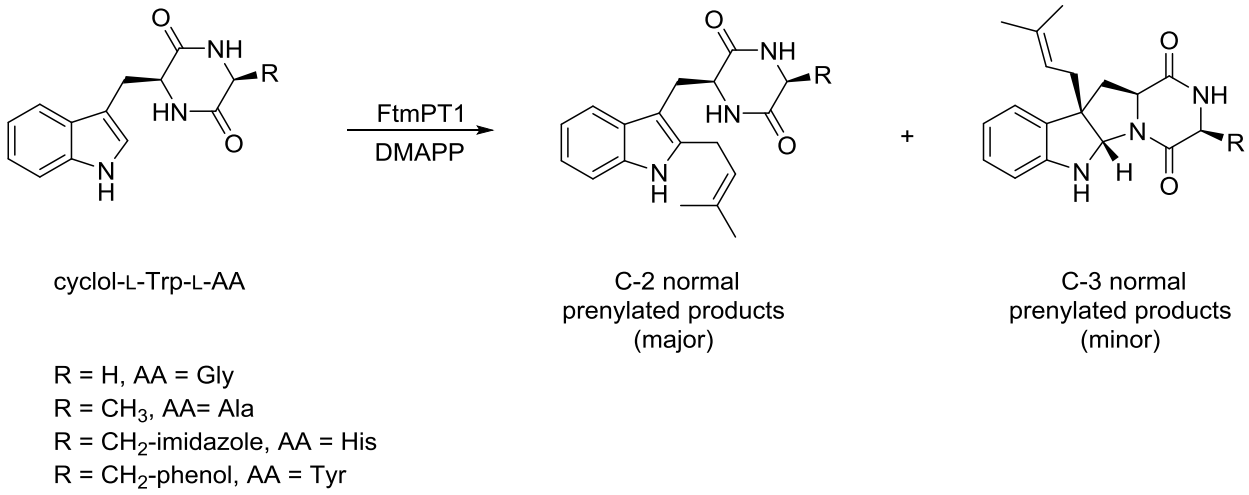

Figure 2.40 Products formed from the reaction of FtmPT1 and a series of cyclic dipeptides.

It is possible that replacement of the proline residue with a different amino acid can cause the enzyme to lose its spatial control over the carbocation within the active site and allow both C-2 and C-3 attacks to take place. However, one can also imagine that the observation of the C-3 normal prenylated products is due to the formation of these compounds as reaction intermediates that were released into solution before further rearrangements could occur. This demonstrates

that normal C-3 prenylation is possible in the FtmPT1 active site and indirectly supports a potential mechanism involving an initial C-3 prenylation followed by a 1,2-alkyl shift (Figure 2.39 – Pathway A).

In order to further investigate the mechanism of FtmPT1, we synthesized two substrate analogs, 5-hydroxybrevianamide F **17** and 2-methylbrevianamide F **18**, and tested them with FtmPT1 to obtain evidence supporting either an initial C-3 reverse or C-3 normal prenylation mechanism. The results of our studies with these two compounds will be described in the following sections.

2.3.2.4 Product Studies with 5-Hydroxybrevianamide F (17)

In many of the previously reported cases where FtmPT1 formed C-3 prenylated products, substrates with significant alterations to the brevianamide F core structure were employed. We decided to examine substrate analogs that retained the L-proline component of brevianamide F, to see whether this segment of the substrate plays a crucial role in proper positioning of the molecule in the active site. The first substrate analog we designed was 5-hydroxybrevianamide F, compound **17**. The 5-hydroxy group on the L-tryptophan portion of the substrate activates the indole ring for nucleophilic attack. Based on the crystal structure of FtmPT1 and the relative geometry of the substrates in the active site, products arising from either a C-3 or C-4 attack would be expected to be formed. The 5-hydroxy group should dramatically accelerate C-4 attack and thus, provide evidence that the orientation in the X-ray structure is relevant to product formation.

To begin the synthesis of compound **17**, the amine group of 5-hydroxytryptophan **36** was protected with di-*tert*-butyl dicarbonate $(Boc)_2O$ to give compound **37** (Figure 2.41). The methyl

ester of L-Pro **31** was coupled with the N-Boc protected 5-hydroxytryptophan **37** in a DCC mediated reaction to give dipeptide **38** in 77% yield. Following the purification of compound **38** by silica gel column chromatography, the Boc protecting group was removed under acidic condition to release the free amine, which was used in the next reaction without further purification. The final cyclization step was accomplished using 2-pyridone to give 5-hydroxybrevianamide F **17**, which was purified by silica gel column chromatography (26% yield over two steps) (Figure 2.41).

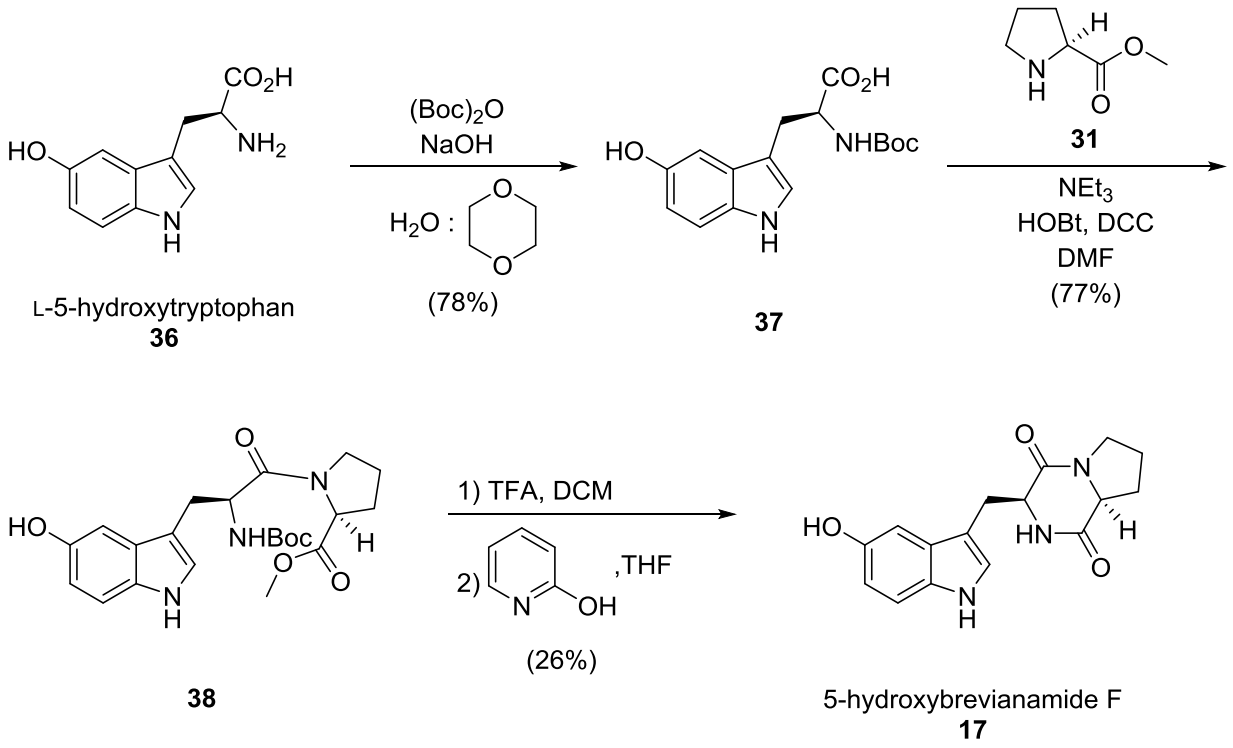

Figure 2.41 Synthesis of 5-hydroxybrevianamide F 17.

5-Hydroxybrevianamide F **17** was incubated with DMAPP and FtmPT1 under similar conditions to those described for brevianamide F. After the reaction was complete, the precipitate was removed via centrifugation and the resulting solution was extracted with ethyl acetate. Analysis by mass spectrometry and NMR spectroscopy indicated that only unreacted

starting material **17** and a single monoprenylated product **39** was formed. The structure of **39** was ultimately assigned as a C-4 normal prenylated product (Figure 2.42). The ^{1}H NMR spectrum of **39** showed only one alkene signal, suggesting that normal prenylation has occurred. Moreover, three signals were detected in the aromatic region. Two of these aromatic signals demonstrated *ortho*-coupling with a coupling constant of 8.7 Hz and were assigned to the C-6 and C-7 protons, while the third signal appeared as a doublet with a coupling constant of 2.4 Hz. To investigate the identity of the third signal, a COSY spectrum of compound **39** was taken in deuterated chloroform. Based on the observation of a correlation between the N-1 proton signal of the indole amine and the third proton signal in the aromatic region, we concluded that this signal can be attributed to the C-2 proton and therefore, the prenyl group is attached to the C-4 position (Figure 2.42).

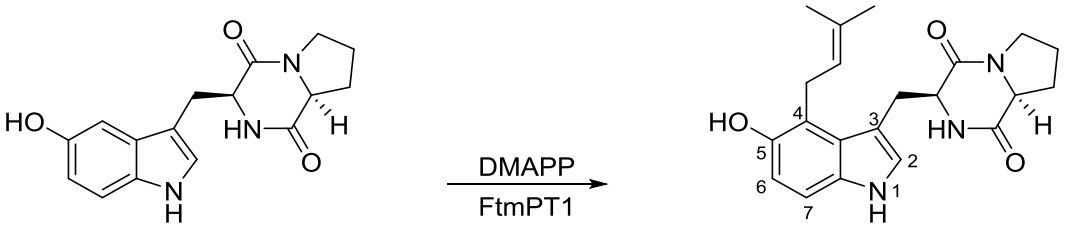

5-hydroxybrevianamide F
17

C-4 normal prenylated product
39

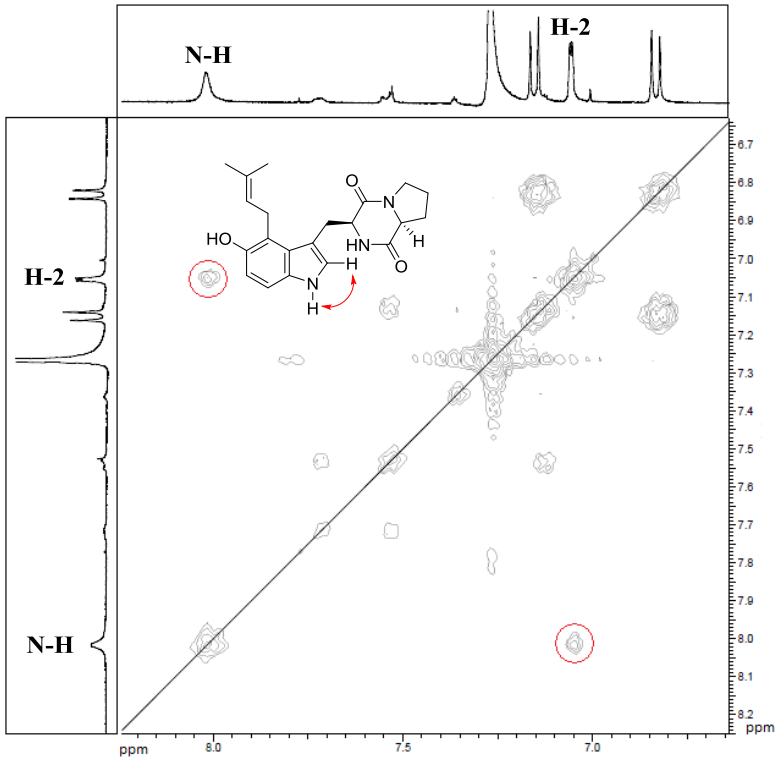

Figure 2.42 Reaction of 5-hydroxybrevianamide F 17 with DMAPP catalyzed by FtmPT1. The COSY spectrum with the correlation between C-2 proton and indole N-H is also presented ($CDCl_3$, 400 MHz).

We envisioned two scenarios for the formation of the observed product (Figure 2.43). One scenario involves a direct normal prenylation at the C-4 position followed by a deprotonation step (path A). The second of the two possible scenarios suggests an initial reverse prenylation at C-3 followed by a Cope rearrangement and then a deprotonation step (path B). A

similar Cope rearrangement onto the C-4 position has been proposed for the 4-DMATS-catalyzed reaction between DMAPP and L-tryptophan. [96]

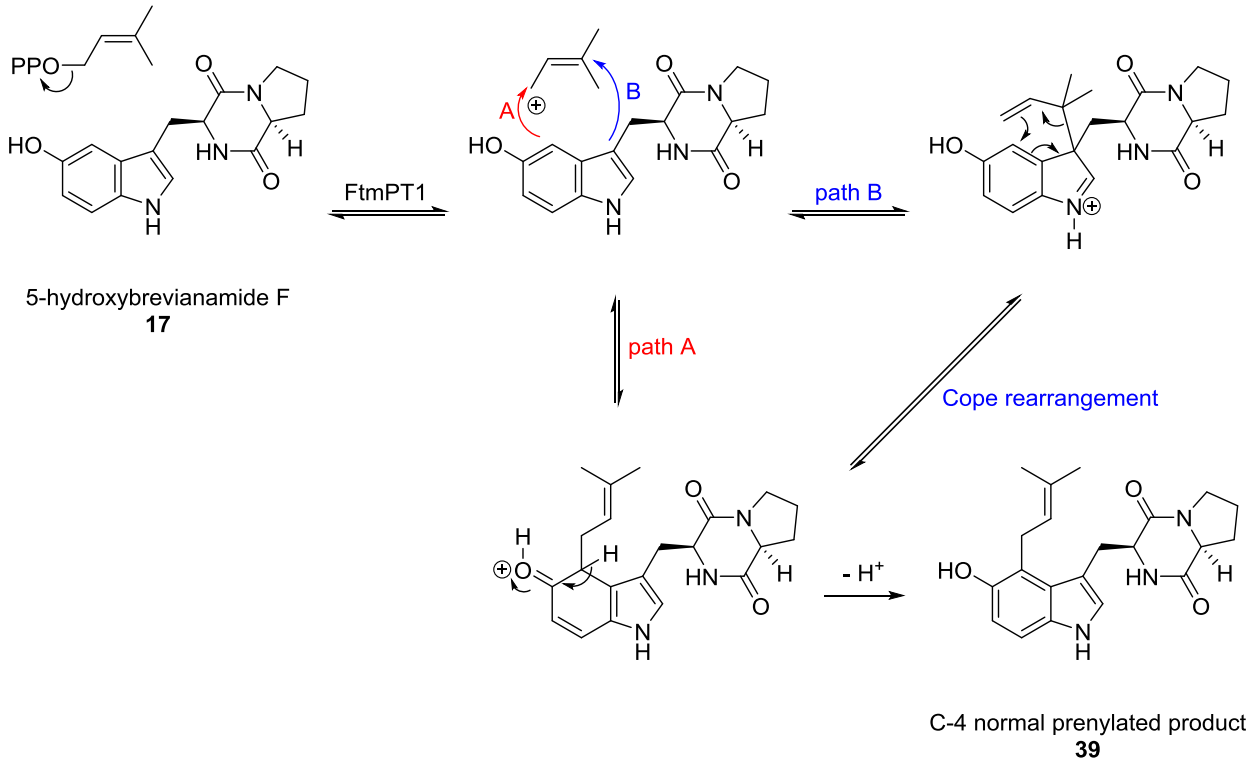

Figure 2.43 Proposed mechanisms for the formation of compound 39 from 5-hydroxybrevianamide F 17. Path A: direct C-4 prenylation mechanism; Path B: C-3 reverse prenylation mechanism followed by a Cope rearrangement.

Analysis of the enzyme structure reveals that the C-3 and C-4 positions of L-tryptophan in brevianamide F are proximal to the C-3 and C-1 positions of the incipient dimethylallyl cation, respectively (Figure 2.44). Assuming that the substrate analog 5-hydroxybrevianamide F **17** binds in a similar manner as the natural substrate, one can imagine that the enzyme is capable of employing either mechanism for catalysis. Furthermore, it is expected that both the C-4 direct attack and the Cope rearrangement would experience a noticeable acceleration due to the introduction of the 5-hydroxyl group.

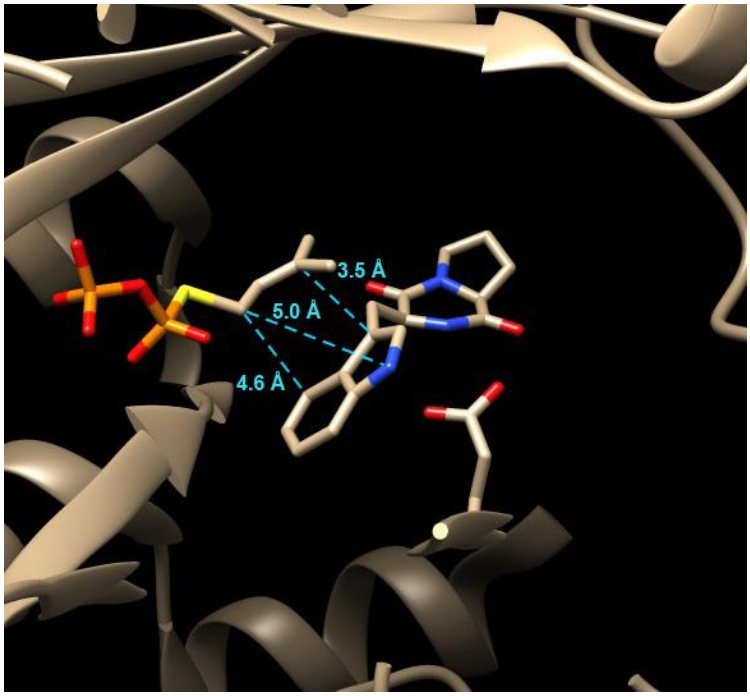

Figure 2.44 Active site structure of FtmPT1 showing the relative positions of the thiol analog of DMAPP and the indole ring of brevianamide F. A key active site residue (E102) is also shown (Data was taken from PDB ID : 302K).

A potential third mechanism involves an initial reverse prenylation on the C-5 hydroxyl group followed by a Claisen rearrangement (Figure 2.45). This mechanism was proposed based on the observation that was made with the prenyltransferase enzyme LynF which catalyzes the reverse *O*-prenylation of a tyrosine residue in macrocyclic peptides (Figure 2.45). [179] The resulting product undergoes a spontaneous non-enzymatic Claisen rearrangement to give an ortho normal prenylated product. Although this mechanism can explain the formation of the observed product in the reaction between 5-hydroxybrevianamide F **17** and DMAPP, it is considered unlikely given the relative geometry of the reacting groups in the active site.

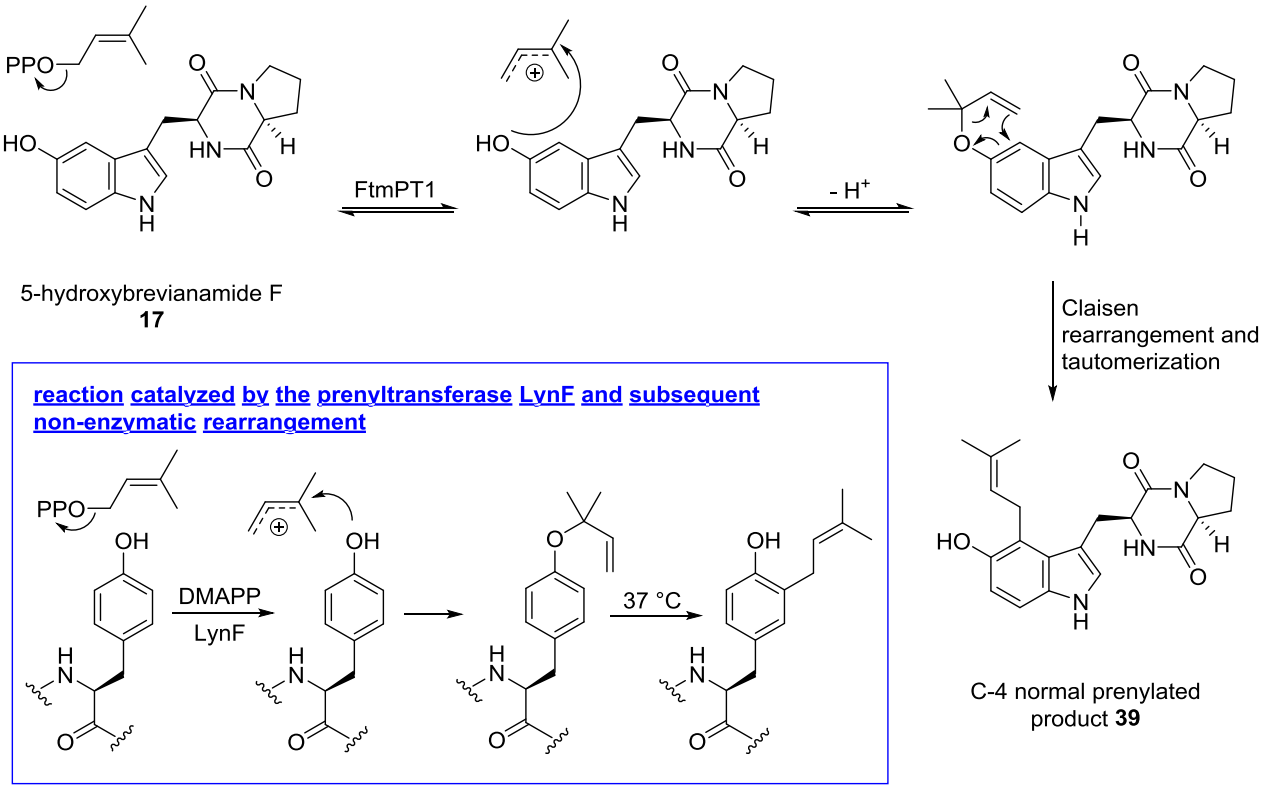

Figure 2.45 Third proposed mechanism for the FtmPT1 reaction of 5-hydroxybrevianamide F 17 involving a Claisen rearrangement. The inset represents the proposed mechanism for the reaction catalyzed by LynF and the subsequent non-enzymatic Claisen rearrangement.

Regardless of which mechanism FtmPT1 employs to catalyze the prenylation reaction, the observation that a normal C-4 prenylated product is formed from the 5-hydroxy substrate analog indicates that ionization of DMAPP is not accompanied by a dramatic reorientation of the dimethylallyl cation as was proposed previously. [104,110] Furthermore, it is clear that the relative positions of the two substrates in the X-ray structure are not misleading, but meaningful.

2.3.2.5 Product Studies with 2-Methylbrevianamide F (18)

We next investigated the reaction between the substrate analog 2-methylbrevianamide F (cyclo-L-2-methyltryptophan-L-proline) **18** and DMAPP in the presence of FtmPT1 (Figure

2.46). If a C-3 prenylation mechanism was operative, blocking the C-2 position with a methyl group should stop the reaction at the formation of a C-3 modified product that is not capable of undergoing a rearrangement. Since the structure of 2-methylbrevianamide F **18** is similar to that of the natural substrate, the results of this study could provide us with evidence favoring either the reverse or normal C-3 prenylation mechanism. The synthesis of 2-methylbrevianamide F **18** started with an enzymatic reaction to generate 2-methyltryptophan **41** (Figure 2.46). 2-Methylindole **40** was incubated with L-serine, pyridoxal phosphate (PLP), and tryptophan synthase following a previously published procedure. [180] The amine of L-2-methyltryptophan **41** was protected with a Boc group to give *N*-Boc-L-2-methyltryptophan **42** in 74% yield. It was then coupled to the methyl ester of L-Pro **31** using DCC to give the protected dipeptide **43**, which was purified by silica gel column chromatography. Despite several attempts at purifying this compound, a small amount of dicyclohexylurea impurity was detected in the fractions collected from the column, which resulted in the crude yield of 49%. This compound was used in subsequent steps without further purification. Cleavage of the Boc protecting group with TFA was followed by the 2-pyridone mediated cyclization reaction to give 2-methylbrevianamide F **18**. Purification by silica gel column chromatography gave the substrate analog **18** in 37% yield over two steps (Figure 2.46).

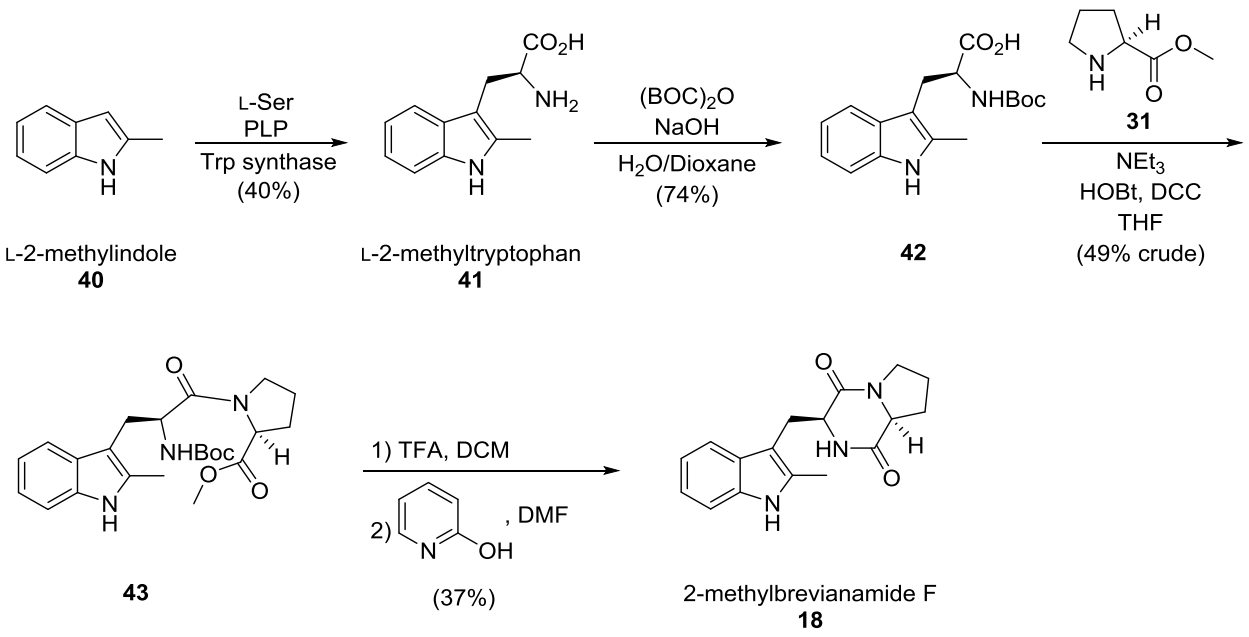

Figure 2.46 Synthesis of 2-methylbrevianamide F 18.

A stock solution of 2-methylbrevianamide F **18** was prepared in MeOH (113 mM). Substrate analog **18** was incubated with DMAPP and FtmPT1 under similar conditions as described for the natural substrate. After extraction with ethyl acetate and purification by silica gel column chromatography, two products were isolated. Analysis by mass spectrometry indicated that both products had a mass corresponding to that of monoprenylated 2-methylbrevianamide F **18**. The major product was identified as the C-3 normal prenylated compound **44** while the minor product was the N-1 normal prenylated compound **45** (Figure 2.47)

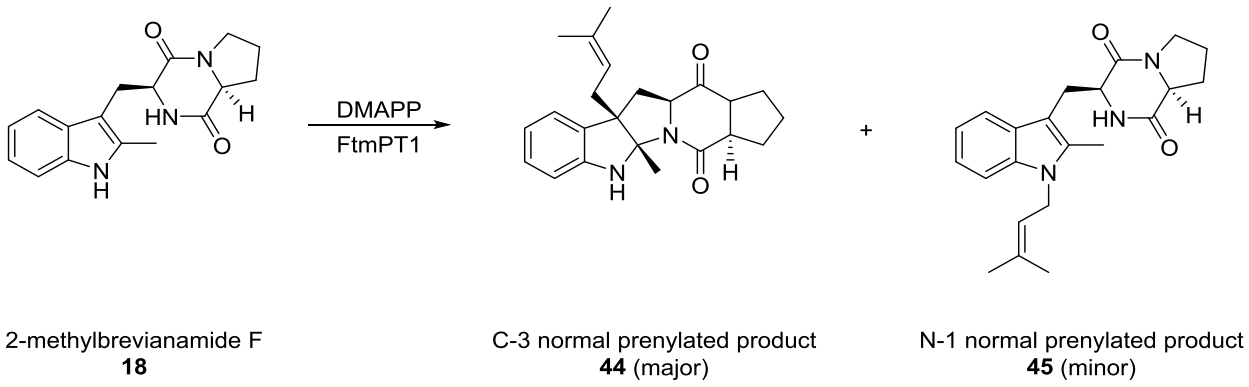

Figure 2.47 FtmPT1-catalyzed reaction of 2-methylbrevianamide F 18 with DMAPP.

Analysis of compound **44** by ^{1}H NMR spectroscopy clearly indicated that this compound is a hexahydropyrroloindole that contains a normal prenyl group at the C-3 position of the indole ring (Figure 2.48). Five proton signals were present in the aromatic region that belonged to the phenyl moiety and the indole NH. A single vinylic proton signal that appears at 5.15 ppm indicates that normal prenylation had occurred (Figure 2.48). The signal corresponding to the C-2 methyl group in the starting material **18** appears at 2.43 ppm; in the product **44** however, the signal was observed at 1.40 ppm. This change in chemical shift is due to the hybridization change at the C-2 atom. In 2-methylbrevianamide F **18**, the methyl group is connected to an sp^2 hybridized carbon, which results in a higher chemical shift. In the C-3 normal prenylated product **44** on the other hand, the methyl group is connected to an sp^3 hybridized center and therefore, the methyl signal moves upfield.

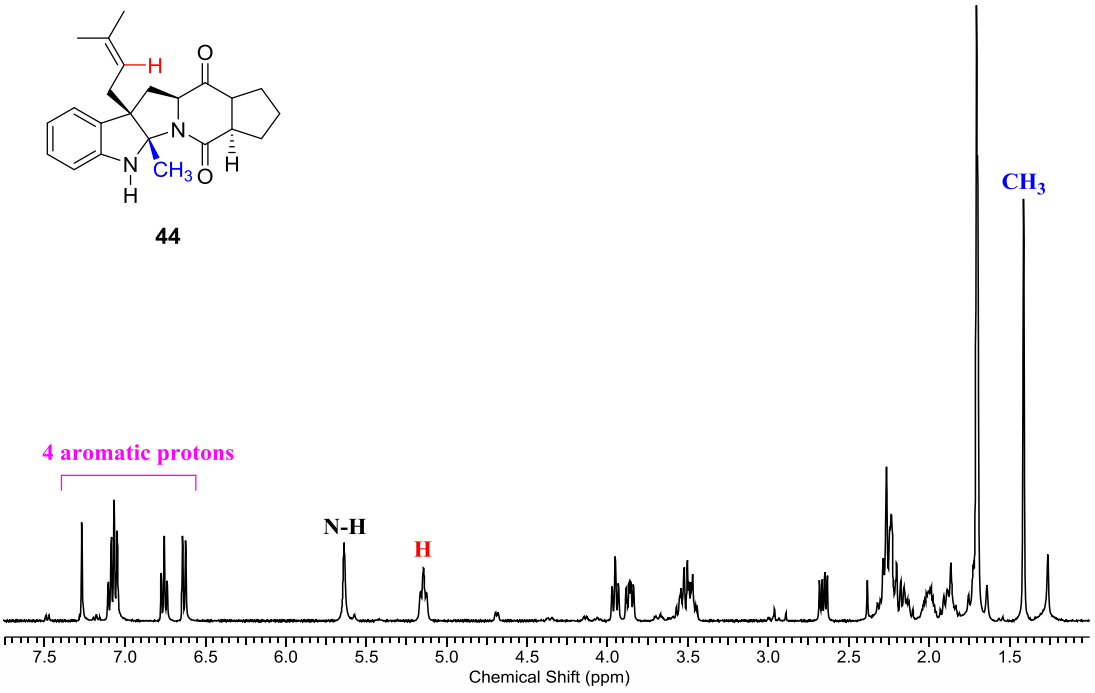

Figure 2.48 ^{1}H NMR spectrum of compound 44 ($CDCl_3$, 400 MHz).

To further investigate the structure of compound **44**, we obtained a NOSEY spectrum. A clear correlation between the signals from the methylene of the prenyl group and those of the C-2 methyl group was observed (Figure 2.49). This correlation is expected given the proximity and the *cis* relationship of these groups.

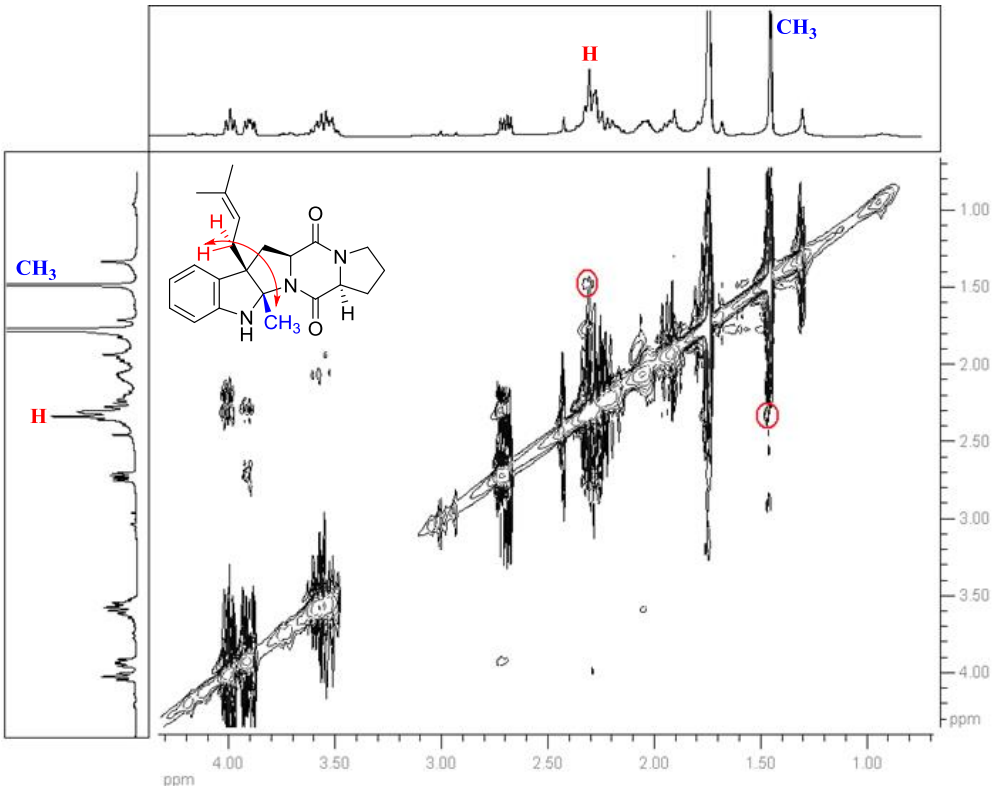

Figure 2.49 NOESY spectrum of compound 44 ($CDCl_3$, 400 MHz). The correlation between the C-2 methyl and the methylene protons of the prenyl group is shown.

The minor product was identified as the N-1 normal prenylated compound **45**. A single vinylic proton signal that appears at 5.11 ppm indicates that normal prenylation had occurred (Figure 2.50). ^{1}H NMR spectroscopy showed that four proton signals were present in the aromatic region that belonged to the phenyl moiety; but the singlet corresponding to the indole NH was missing.

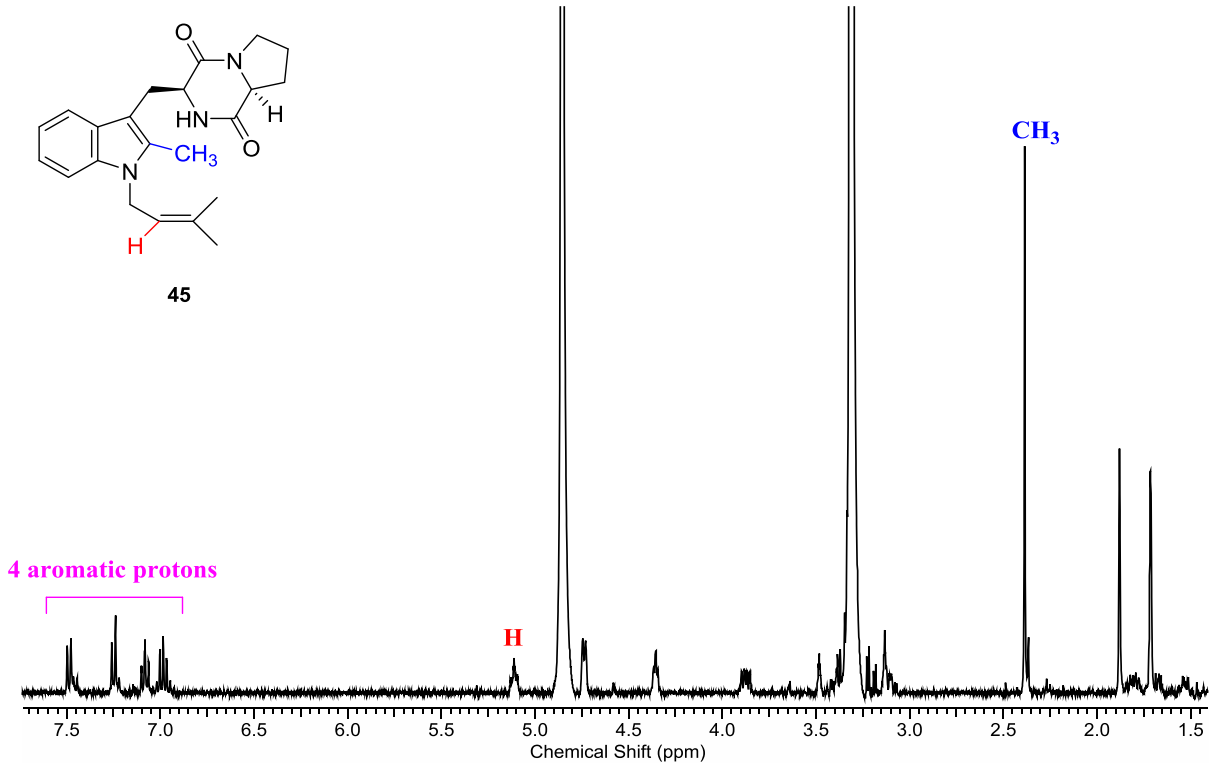

Figure 2.50 ^{1}H NMR spectrum of compound 45 (CD_3OD, 400 MHz).

The NOESY spectrum of compound **45** showed correlations between the signal from the methylene protons of the prenyl group and those from both the C-7 phenyl proton and the C-2 methyl protons (Figure 2.51).

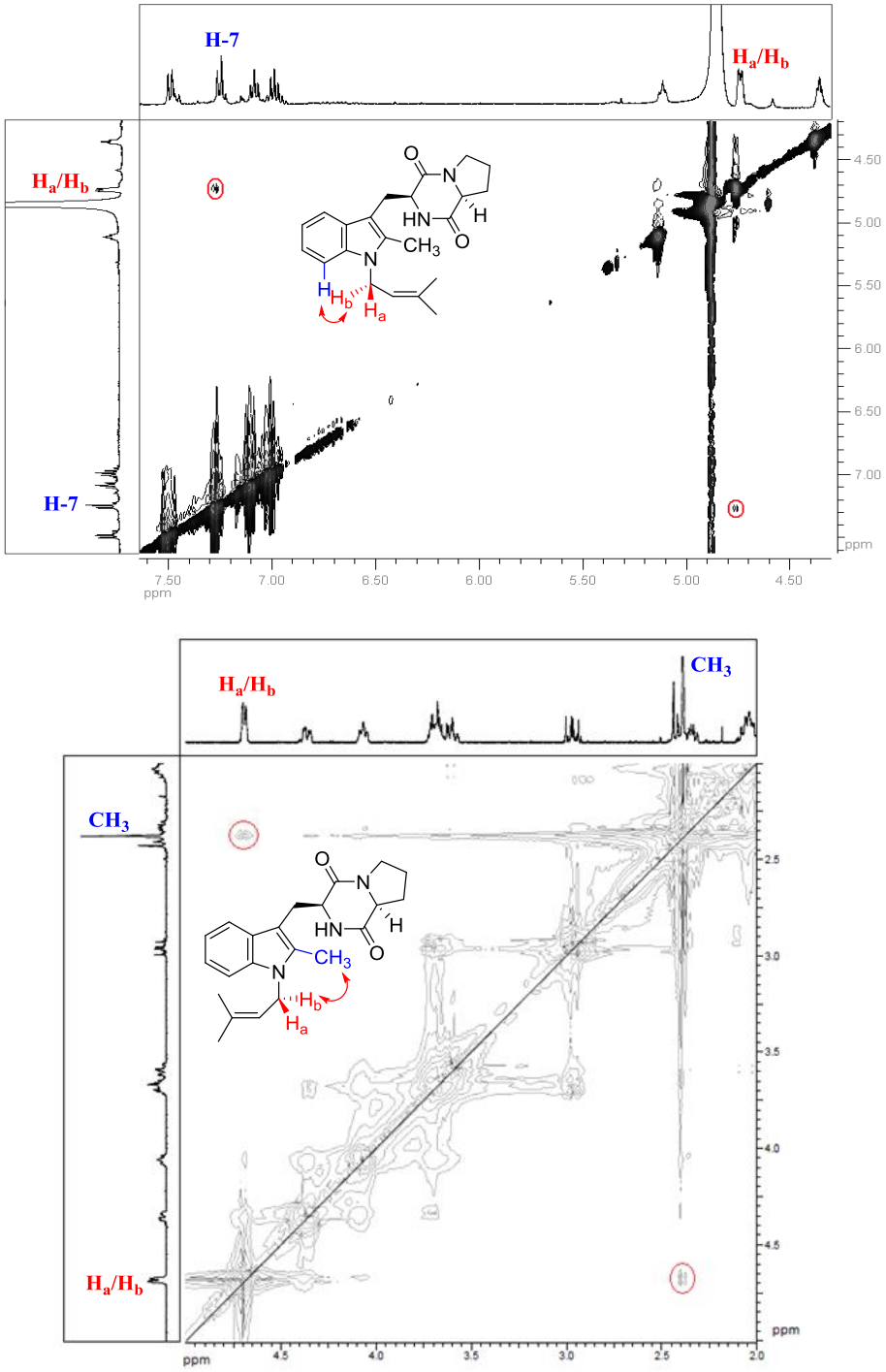

Figure 2.51 NOESY spectra of compound 45 in two solvents ($CD_3OD/CDCl_3$, 400 MHz). The correclation between the prenyl methylene protons and the C-7 phenyl proton is shown in the top spectrum (in CD_3OD). The bottom spectrum shows the correlation between the prenyl methylene protons and the C-2 methyl protons (in $CDCl_3$).

The formation of the C-3 normal prenylated product **44** is consistent with an FtmPT1 mechanism that involves a C-3 normal prenylation as the first step of catalysis (Figure 2.52 – Pathway A). In this case, the subsequent 1,2-alkyl shift would not lead to the formation of a stable product as the final deprotonation step could no longer occur. This observation demonstrates that C-3 normal prenylation can occur on substrates that closely resemble the structure of the natural substrate and contain an L-proline as a portion of their cyclic dipeptide structure.

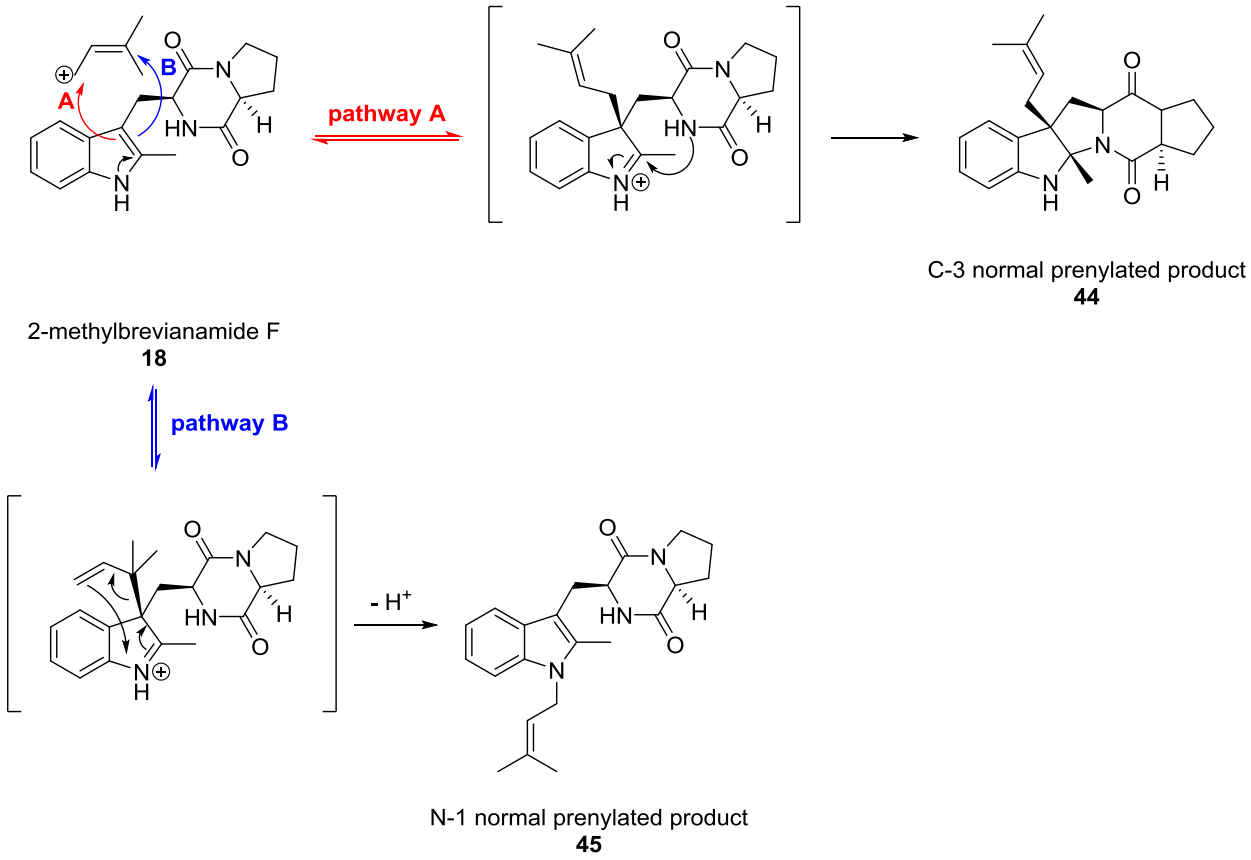

Figure 2.52 Proposed mechanisms for the formation of the C-3 and N-1 normal prenylated products in the reaction of 2-methylbrevianamide F 18.

The formation of the N-1 normal prenylated compound **45** as the minor product can be explained in two ways. Firstly, an initial reverse prenylation at C-3 followed by an aza-Cope rearrangement would generate the observed N-1 normal prenylated compound **45** (Figure 2.52 – Pathway B). This mechanism involves an attack by C-3, which is an excellent nucleophile that is positioned 3.5 Å away from the C-3 position of the incipient dimethylallyl cation. As we described in section 2.2, non-enzymatic aza-Cope rearrangement of C-3 reverse prenylated indoles can occur readily.

Alternatively, one can imagine that the dimethylallyl cation is attacked directly by the indole nitrogen atom to give the observed product (Figure 2.53). A similar mechanism involving a direct attack onto the dimethylallyl carbocation by the deprotonated indole NH has been proposed for the indole prenyltransferase CymD, which catalyzes the N-1 reverse prenylation of L-tryptophan (Figure 2.53 inset). [162] However, the nitrogen atom of the indole ring is a poor nucleophile and thus, one might not expect such a nucleophilic attack to occur given that FtmPT1 has not evolved to catalyze this reaction. Moreover, based on the crystal structure of FtmPT1, the distance between the indole N-1 and the C-1 atom of dimethylallyl cation is approximately 5 Å, which does not favor such a direct attack. Therefore, it is more likely that FtmPT1 follows the first proposed mechanism, which involves an initial C-3 reverse prenylation, followed by an aza-Cope rearrangement.

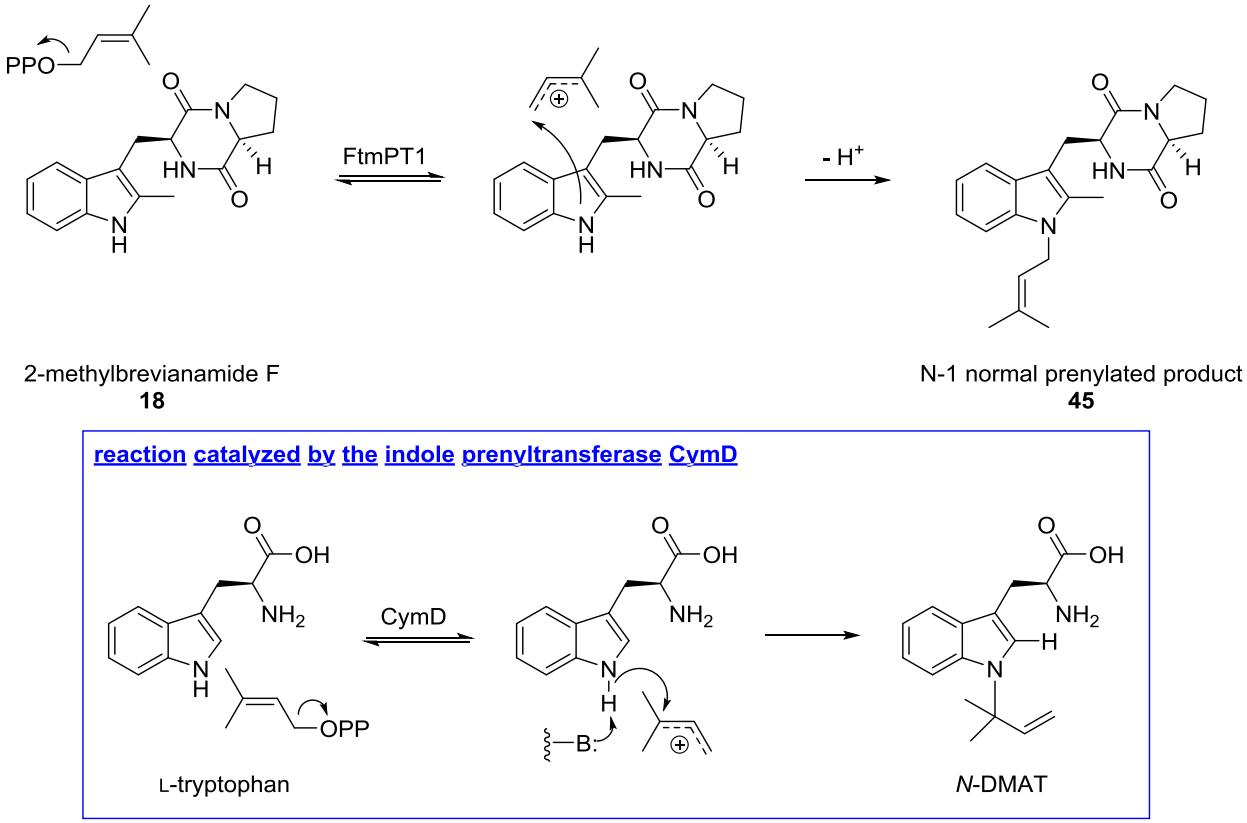

Figure 2.53 An alternate mechanism for the formation of N-1 normal prenylated 2-methylbrevianamide F 18. The blue inset shows the proposed mechanism for the reaction catalyzed by CymD.

Overall, the formation of the observed products with 2-methylbrevianamide F **18** indicates that FtmPT1 is capable of catalyzing both C-3 normal and C-3 reverse prenylations on substrate analogs containing an L-Pro residue.

2.4 Conclusion and Summary

In the first part of this chapter, we reinvestigated the CdpNPT-catalyzed reaction between cyclo-L-Trp-L-Trp and DMAPP and correctly identified the product as a C-3 reverse prenylated compound containing a hexahydropyrroloindole structure. This finding enabled us to propose a mechanism for this enzyme that involves an initial reverse prenylation at the C-3 position of the

indole ring. We then studied the acid-induced non-enzymatic Cope and aza-Cope rearrangements of this product at 37 °C. Our studies demonstrated that the energy barrier to the aza-Cope rearrangement can be relatively low and that it can readily proceed at room temperature. The C-3 reverse prenylated product of the CdpNPT was found to undergo a rearrangement onto the N-1 position (aza-Cope) rather than onto the C-4 position (Cope). Based on this observation, we concluded that in the absence of other factors, such as an enzyme active site, an aza-Cope rearrangement onto the N-1 position is favored. This has implications for 4-DMATS catalysis as it means that enzymatic control of the substrate must play a key role if a Cope mechanism is operative.

In the second part of this chapter we have detailed our studies on the mechanism of the brevianamide F prenyltransferase, FtmPT1. When incubated with different substrates, FtmPT1 produced an exceptional variety of products, including C-4 normal, C-3 normal, C-3 reverse, and N-1 normal prenylated compounds (Table 2.1). This observation greatly expands the product scope of this interesting enzyme. Formation of the C-3 reverse prenylated compound **1** from L-tryptophan is consistent with a mechanism involving an initial reverse C-3 prenylation followed by a premature release of the reaction intermediate into the solution. Similarly, the observation of compound **45** from 2-methylbrevianamide F can be explained from an initial C-3 reverse prenylation followed by an aza-Cope rearrangement. Together with previous studies on the Gly115Thr mutant (section 1.5.5) and the alternate substrate **6** (section 1.5.5), a reaction case can be made for initial C-3 reverse prenylation mechanism. We also showed that 5-hydroxybrevianamide F **17** gave exclusively C-4 normal prenylation. This suggests that the active site architecture present in the X-ray structure is significant. Such a positioning provides indirect evidence for a C-3 reverse prenylation mechanism. Since the C-3 position of the indole

is in close proximity to the C-3 of the prenyl group, without the highly activating C-5 hydroxyl group, one would expect C-3 prenylation to occur.

Substrate	Enzyme	Prenylation position
brevianamide F	WT	C-2 normal
brevianamide F	Gly115Thr	C-3 reverse
indole butenone **6**	WT	external alkene
cyclo-L-Trp-L-Gly, cyclo-L-Trp-L-Ala, cyclo-L-Trp-L-His and others	WT	C-2 normal and C-3 normal
L-Trp	WT	C-3 reverse
5-hydroxybrevianamide F **17**	WT	C-4 normal
2-methylbrevianamide F **18**	WT	C-3 normal and N-1 normal

Table 2.1 Summary of the products formed in the FtmPT1-catalyzed reactions with various indoles and DMAPP.

The observation of the products that were normal prenylated at the C-3 position indicates that such an attack is also possible in the FtmPT1 active site. In this study, we used cyclo-L-Trp-L-Trp and 2-methylbrevianamide F (where the C-2 position is blocked) and found that C-3 normal prenylated compounds were formed as the major product in each case. These findings support a mechanism involving an initial C-3 normal prenylation (Figure 2.39). In order to obtain the C-2 normal prenylated structure observed with tryprostatin B, a subsequent 1,2-alkyl migration, or Wagner Meerwein rearrangement would have to occur (Figure 2.39). Despite the fact that these product studies on their own do not allow one to conclude the mechanism that the enzyme employs for catalysis, they clearly indicate that C-3 prenylation is a feasible first step of catalysis.

2.5 Future Directions

Future studies on FtmPT1 will focus on identifying the intermediates generated during the FtmPT1-catalyzed reaction. The structures of the isolated intermediates can provide us with insight into whether the enzyme employs an initial C-3 reverse or C-3 normal prenylation mechanism. This experiment will be performed using a technique known as rapid quenching. This involves incubating stoichiometric amounts of enzyme and substrate for only a few microseconds before the reaction is stopped by the addition of a quenching reagent, such as trichloroacetic acid TCA. The reaction intermediates or the products are then isolated and analyzed by chromatographic or other analytical techniques. Formation of the C-3 reverse prenylated compound **5** will support the C-3 reverse prenylation mechanism while isolating the C-3 normal prenylated intermediate **46** will provide evidence for the C-3 normal prenylation (Figure 2.54).

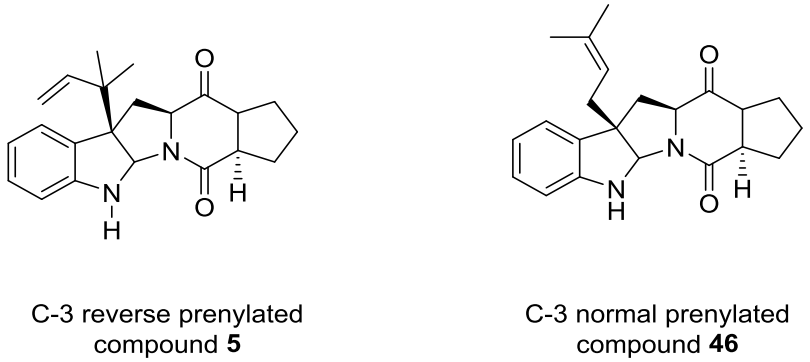

Figure 2.54 Structures of the potential intermediates formed in the FtmPT1-catalyzed reaction between brevianamide F and DMAPP.

Another experiment that could provide evidence for either mechanisms involves feeding the enzyme FtmPT1 with reaction intermediates. For instance, compound **5** can be conveniently synthesized in the CdpNPT-catalyzed reaction between brevianamide F and DMAPP (Figure

2.55). If an initial C-3 reverse prenylation mechanism is operative, compound **5** could act as a reaction intermediate and would be converted to tryprostatin B (Figure 2.55). One potential pitfall of this experiment is that the enzyme would have to catalyze ring opening of compound **5** or bind this form directly from solution.

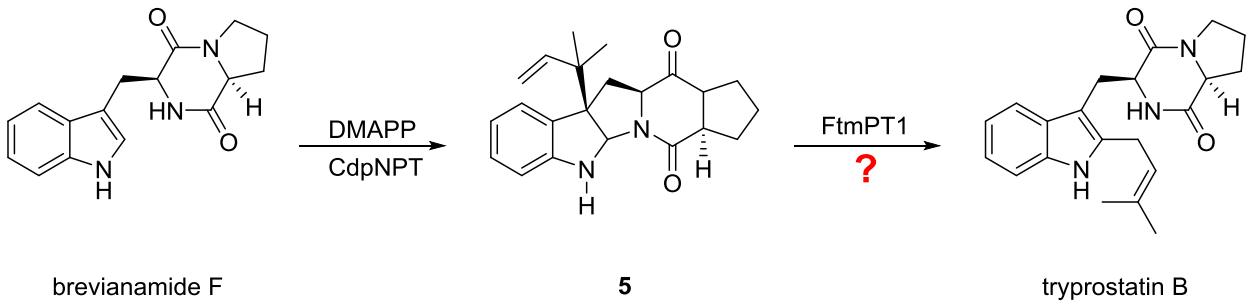

Figure 2.55 Feeding experiment with the C-3 reverse prenylated intermediate 5.

Finally, a closer investigation of the minor products of the FtmPT1 reaction on the normal substrate brevianamide F is necessary. Since only small quantities of products were formed in the previous studies, our efforts at isolating and identifying minor by-products (<10%) were unsuccessful. A possible strategy to overcome this problem involves generating larger quantities of the products through scaling up the enzymatic reaction. This would allow for running NMR analysis on the isolated by-products to see if C-3 prenylated compounds were indeed produced in the wild type reaction.

2.6 Experimental Procedures

2.6.1 Materials and Methods

All reagents were purchased from Sigma-Aldrich, Fluka, Toronto Research Chemicals Inc. (TRC), or Advanced ChemTech (Louisville, KY) and used without further purification

unless otherwise stated. Isopropyl-β-D-galactopyranoside (IPTG) was purchased from Invitrogen. D_2O (99.9%) was purchased from Cambridge Laboratories. Silica gel chromatography was performed using Silica Gel SiliaFlash (230-400 mesh, Silicycle). Pyridine, triethylamine, methylene chloride, and methanol were distilled over CaH_2 under an atmosphere of argon. Tetrahydrofuran (THF) was distilled from sodium and benzophenone.

^{1}H NMR spectra were recorded on a Bruker AV400 at a field strength of 400 MHz. Proton-decoupled ^{13}C NMR spectra were recorded on a Bruker AV400 spectrometer at field strengths of 100 MHz, respectively. Mass spectrometry was performed by electrospray ionization (ESI-MS) using an Esquire LC mass spectrometer. Neutral compounds were detected as positive ions, and negatively charged compounds were detected as negative ions.

2.6.2 Synthesis of *N*-Prenyl-Cyclo-L-Tryptophan-L-Tryptophan (4)

2.6.2.1 Syntheses of *N*-Boc-L-Tryptophan (20)

Compound **20** was prepared from L-tryptophan using a literature procedure. [166] To a stirred solution of L-tryptophan (5.1 g, 24.9 mmol) in 1:1 water-1,4-dioxane (100 mL) was added 1M NaOH (25 mL) followed by addition of di-*tert*-butyl dicarbonate $(Boc)_2O$ (5.4 g, 24.9 mmol, 1.0 equiv). The mixture was stirred at room temperature for 24 h and then the pH was adjusted to 2.4 by the addition of aqueous HCl. The resulting mixture was extracted with EtOAc (3×100 mL) and dried over anhydrous $MgSO_4$. Removal of the solvent under reduced pressure gave *N*-Boc-L-tryptophan **20** (6.0 g, 79% yield) as white solid. ^{1}H NMR and ESI-MS data were identical to those reported in the literature. [166]

2.6.2.2 Synthesis of *N*-Prenyl-*N'*-Boc-L-Tryptophan (21)

To a stirred solution of *N*-Boc-L-tryptophan **20** (2.05 g, 6.72 mmol) in 10 mL anhydrous DMF at 0 °C was added NaH (733 mg f a 55% oil suspension, 16.8 mmol, 2.5 equiv.) under an Ar atmosphere. The mixture was stirred at 0 °C for 10 minutes before 3,3-dimethylallyl bromide (1.50 g, 10.08 mmol, 1.5 equiv., 1.17 mL) was added. The reaction mixture was stirred at 0 °C for one more hour followed by stirring at room temperature for an additional 2 hours. The reaction was quenched by the addition of 50 mL water and was washed with 25 mL of hexane. The aqueous layer was acidified by $NaHSO_4$ solution (1.0 M) until the pH value of 3.0 was reached. The acidified solution was extracted with CH_2Cl_2 (3×25 mL) and the organic layers were combined, washed with water (2×25 mL) and dried over $MgSO_4$. The solvent was removed under reduced pressure to give 2.24 g of compound **21** as light brown oil (89% crude yield). Since the purification of compound **21** proved to be difficult, a small portion was converted into its corresponding methyl ester and purified for the purpose of characterization.

2.6.2.3 Synthesis of *N*-Prenyl-*N'*-Boc-L-Tryptophan Methyl Ester (22)

To a stirred solution of crude compound **21** (133 mg, 0.35 mmol) in 1.0 mL MeOH at 0 °C was added a solution of $TMSCHN_2$ (2.0 M in hexane) until the yellow color was persistent and the evolution of N_2 gas ceased (~ 0.7 mL). The solvent was removed under reduced pressure and the resultant residue was purified by silica gel column chromatography, using toluene:EtOAc (16:1) as eluent. ^{1}H NMR and ESI-MS data were identical to those reported in the literature. [167]

2.6.2.4 Synthesis of *N*-Prenyl-*N'*-Boc-L-Tryptophan-L-Tryptophan Methyl Ester (24)

To a stirred solution of *N*-prenyl-*N'*-Boc-L-tryptophan **21** (2.24 g, 6.01 mmol) in 20 mL of anhydrous DMF was added the commercially available L-tryptophan methyl ester hydrochloride (3.06 g, 12.02 mmol, 2 equiv). The mixture was cooled to 0 °C and NEt_3 (1.34 g, 13.2 mmol, 2.2 equiv, 1.84 mL) was added dropwise. To this mixture was added 1-hydroxybenzotriazole (920 mg, 6.01 mmol, 1 equiv) followed by DCC (1.30 g, 6.31 mmol, 1.05 equiv). The ice bath was removed and the reaction was left stirring at room temperature overnight. Solids were removed by filtration and washed with Et_2O (5×20 mL). The filtrate was combined with the washings and the solvents were removed under reduced pressure. The residue was dissolved in 200 mL EtOAc and then washed with 5% aqueous $NaHCO_3$ (50 mL), 10% aqueous citric acid (50 mL), 5% aqueous $NaHCO_3$ (50 mL), and brine (50 mL). The organic phase was dried over anhydrous $MgSO_4$ and solvent was removed under reduced pressure. The crude reaction product was dissolved in EtOAc (40 mL) and solids were formed upon the addition of hexane (50 mL). The resulting precipitates were collected by filtration and rinsed with hexane to give 1.4 g of pure protected dipeptide **24** as white solid (40% yield). ^{1}H NMR (DMSO-d_6, 400 MHz): δ ppm 8.25 (d, 1H, J = 7.3 Hz), 7.57 (d, 1H, J = 7.6 Hz), 7.48 (d, 1H, J = 7.3 Hz), 7.34 (dd, 2H, J = 8.1, 2.6 Hz), 7.17 (s, 1H), 7.07 (m, 2H), 7.03 (s, 1H), 6.98 (m, 2H), 6.75 (d, 1H, J = 8.5 Hz), 5.27 (m, 1H), 4.66 (d, 2H, J = 6.7 Hz), 4.56 (q, 1H, J = 6.4 Hz), 4.23 (m, 1H), 3.56 (s, 3H), 3.13 (dd, 2H, J = 11.9, 6.7 Hz), 3.01 (dd, 1H, J = 10.7, 3.7 Hz), 2.86 (m, 1H), 1.79 (s, 3H), 1.69 (s, 3H), 1.30 (s, 9H). ESI-MS (+) *m/z* 595 $[M+Na]^+$.

2.6.2.5 Synthesis of *N*-Prenyl-Cyclo-L-Tryptophan-L-Tryptophan (4)

To a stirred solution of protected dipeptide **24** (1.3 g, 2.27 mmol) in 20 mL anhydrous CH_2Cl_2 at 0 °C was added 2.8 mL of TFA under an atmosphere of Ar. The mixture was allowed to stir for 6 h. The solvent was removed under reduced pressure at 0 °C and the resulting residue was taken up in 200 mL of EtOAc. The solution was washed with 5% aqueous Na_2CO_3 (50 mL), brine (50 mL) and dried over anhydrous $MgSO_4$. Removal of the solvent under reduced pressure gave 1.06 g of crude reaction product that was used directly in the subsequent step (99% crude yield). A solution of crude unprotected dipeptide (400 mg, 0.48 mmol) was prepared in 10 mL of anhydrous DMF. To this solution was added 2-hydroxypyridine (0.1 equiv, 0.084 mmol, 8.1 mg) at 0 °C under an atmosphere of Ar. The resulting solution was refluxed for 6 h. The solvent was removed under reduced pressure and the resulting residue was purified by means of silica gel column chromatography, using CH_2Cl_2:MeOH (50:1) as eluent to give 120 mg of the pure diketopiperazine **4** (34% yield). ^{1}H NMR (CD_3OD, 400 MHz): δ ppm 7.46 (t, 2H, *J* = 7.6 Hz), 7.30 (t, 2H, *J* = 9.3 Hz), 7.12 (m, 2H), 7.03 (q, 2H, *J* = 7.7 Hz), 6.44 (s, 1H), 6.31 (s, 1H), 5.29 (t, 1H, *J* = 6.9 Hz), 4.64 (d, 2H, *J* = 6.7 Hz), 4.05 (t, 2H, *J* = 5.5 Hz), 2.92 (m, 2H), 2.21 (dd, 1H, *J* = 14.3, 7.0 Hz), 2.15 (dd, 1H, *J* = 14.0, 7.3 Hz), 1.84 (s, 3H), 1.71 (s, 3H). ESI-MS (+) *m/z* 463 $[M+Na]^+$.

2.6.3 Synthesis of Cyclo-L-Tryptophan-L-Proline (Brevianamide F)

2.6.3.1 Synthesis of L-Proline Methyl Ester Hydrochloride (31)

The procedure for the methyl esterification of L-proline was adapted from an existing literature methodology. [181] Thionyl chloride (3.5 mL, 48.7 mmol, 1.1 equiv.) was slowly added

to a stirred solution of L-proline (5.1 g, 44.3 mmol) in anhydrous methanol (30 mL) at 0 °C under an atmosphere of Ar. The ice-bath was removed and the reaction mixture was refluxed for 3 hours. Removal of the solvent under reduced pressure gave a yellow residue which was subsequently dissolved in toluene (30 mL) and concentrated to dryness to remove residual thionyl chloride and methanol to yield compound **31** as a colorless oil (7.9 g, quant.). ^{1}H NMR and ESI-MS data were identical to those reported in the literature. [182]

2.6.3.2 Synthesis of *N*-Boc-L-Tryptophan-L-Proline Methyl Ester (32)

N-Boc-L-tryptophan **20** was prepared according to a previously described procedure. To a stirred solution of *N*-Boc-L-tryptophan **20** (1.14 g, 3.75 mmol) in 10 mL of dry THF was added L-proline methyl ester hydrochloride (1.24 g, 7.49 mmol, 2 equiv). The mixture was cooled to 0 °C and NEt_3 (835 mg, 8.25 mmol, 2.2 equiv, 1.15 mL) was added dropwise. To this mixture was added 1-hydroxybenzotriazole (574 mg, 3.75 mmol, 1 equiv) followed by DCC (812 mg, 3.94 mmol, 1.05 equiv). The ice bath was removed and the reaction was left stirring at room temperature overnight. Solids were removed by filtration and washed with Et_2O (5×10 mL). The filtrate was combined with the washings and the solvents were removed under reduced pressure. The residue was dissolved in 100 mL EtOAc and then washed with 5% aqueous $NaHCO_3$ (125 mL), 10% aqueous citric acid (125 mL), 5% aqueous $NaHCO_3$ (125 mL), and brine (125 mL). The organic phase was dried over anhydrous $MgSO_4$ and the solvent was removed under reduced pressure to give compound **32** as white solid (907 mg, 58%) ^{1}H NMR and ESI-MS data were identical to those reported in the literature. [183]

2.6.3.3 Synthesis of Cyclo-L-Tryptophan-L-Proline (Brevianamide F)

To a stirred solution of protected dipeptide **32** (705 mg, 1.69 mmol) in 5.0 mL anhydrous CH_2Cl_2 at 0 °C was added 2.0 mL of TFA (26.1 mmol, 15.4 equiv) under an Ar atmosphere. The mixture was allowed to stir for 6 h. The solvent was removed under reduced pressure at 0 °C and the resulting residue was taken up in 100 mL of EtOAc. The solution was washed with 5% aqueous Na_2CO_3 (50 mL), brine (50 mL) and dried over anhydrous $MgSO_4$. Removal of the solvent under reduced pressure gave 310 mg of crude reaction product that was used directly in the subsequent step (99% crude yield). A solution of crude unprotected dipeptide (310 mg, 0.98 mmol) was prepared in 10 mL of anhydrous DMF. To this solution was added 2-hydroxypyridine (0.1 equiv, 0.098 mmol, 9.3 mg) at 0 °C under an Ar atmosphere. The resulting solution was refluxed for 6 h. The solvent was removed under reduced pressure and the resulting residue was purified by means of silica gel column chromatography, using CH_2Cl_2:MeOH (50:1) as eluent to give 110 mg of pure brevianamide F (40% yield). ^{1}H NMR and ESI-MS data were identical to those reported in the literature. [104]

2.6.4 Synthesis of 5-Hydroxybrevianamide F (17)

2.6.4.1 Synthesis of *N*-Boc-L-5-Hydroxytryptophan (37)

To a stirred solution of L-5-hydroxytryptophan **36** (400 mg, 1.82 mmol) in 1:1 water-1,4-dioxane (20 mL) was added 1M NaOH (1.82 mL) followed by the addition of di-*tert*-butyl dicarbonate $(Boc)_2O$ (397 mg, 1.82 mmol, 1.0 equiv). The mixture was stirred at room temperature for 24 h and then the pH was adjusted to 2.4 by adding aqueous HCl. The resulting mixture was extracted with EtOAc (3×10 mL) and dried over anhydrous $MgSO_4$. Removal of the

solvent under reduced pressure gave 453 mg of *N*-Boc-L-5-hydroxytryptophan **37** (78% yield) as an off-white solid. ^{1}H NMR (CD_3OD, 400 MHz): δ ppm 7.15 (d, 1H, *J* = 8.5 Hz), 7.02 (s, 1H), 6.95 (1H, d, *J* = 2.1 Hz), 6.66 (dd, 1H, *J* = 8.7, 2.3 Hz), 4.38 (dd, 1H, *J* = 9.1, 4.9 Hz), 3.22 (dd, 1H, *J* = 14.8, 5.0 Hz), 3.04 (dd, 1H, *J* = 14.3, 7.9 Hz), 1.39 (s, 9H). ESI-MS (-) *m/z* 319 $[M-H]^-$.

2.6.4.2 Synthesis of *N*-Boc-L-5-Hydroxytryptophan-L-Proline Methyl Ester (38)

To a stirred solution of crude *N*-Boc-L-5-hydroxytryptophan **37** (1.24 g, 3.8 mmol) in 10 mL of anhydrous DMF was added L-proline methyl ester hydrochloride **31** (769 mg, 4.6 mmol, 1.2 equiv). The mixture was cooled to 0 °C and NEt_3 (500 mg, 4.94 mmol, 1.3 equiv, 0.69 mL) was added dropwise. To this mixture was added 1-hydroxybenzotriazole (582 mg, 3.8 mmol, 1 equiv) followed by DCC (823 mg, 3.99 mmol, 1.05 equiv). The ice bath was removed and the reaction was left stirring at room temperature overnight. Solids were removed by filtration and washed with Et_2O (5×10 mL). The filtrate was combined with the washings and the solvents were removed under reduced pressure. The residue was dissolved in 100 mL EtOAc and then washed with 5% aqueous $NaHCO_3$ (25 mL), 10% aqueous citric acid (25 mL), 5% aqueous $NaHCO_3$ (25 mL), and brine (25 mL). The organic phase was dried over anhydrous $MgSO_4$ and solvent was removed under reduced pressure. This gave 1.24 g of crude reaction product, which was purified by means of silica gel chromatography, using CH_2Cl_2:MeOH (50:1) as eluent (77% yield). ^{1}H NMR ($CDCl_3$, 400 MHz): δ ppm 7.98 (br, 1H), 7.20 (d, 1H, *J* = 8.8 Hz), 7.14 (s, 1H), 7.11 (dd, 1H, *J* = 8.1, 2.0 Hz), 6.83 (dd, 1H, *J* = 8.7, 2.3 Hz), 5.39 (d, 1H, *J* = 8.5 Hz), 4.78 (dd, 1H, *J* = 12.7, 7.6 Hz), 4.53 (dd, 1H, *J* = 8.5, 4.6 Hz), 3.74 (s, 3H), 3.55 (m, 1H), 3.24 (dd, 1H, *J* = 11.3, 7.9 Hz), 3.09 (dd, 2H, *J* = 13.9, 5.0 Hz), 2.14 (m, 1H), 1.83-1.96 (m, 3H), 1.43 (s, 9H). ESI-MS (+) *m/z* 543 $[M+Na]^+$.

2.6.4.3 Synthesis of Cyclo-L-5-Hydroxytryptophan-L-Proline (17)

To a stirred solution of protected dipeptide **38** (1.27 g, 2.94 mmol) in 10 mL anhydrous CH_2Cl_2 at 0 °C was added 4.5 mL of TFA under an Ar atmosphere. The mixture was refluxed for 6 h. The solvent was removed under reduced pressure and the resulting residue was taken up in 100 mL of EtOAc. The solution was washed with 5% aqueous Na_2CO_3 (25 mL), brine (25 mL) and dried over anhydrous $MgSO_4$. Removal of the solvent under reduced pressure gave 691 mg of crude reaction product which was used directly in the next step. A solution of crude dipeptide (691 mg, 2.08 mmol) was prepared using 40 mL of anhydrous THF. To this mixture was added 2-hydroxypyridine (0.1 equiv, 0.208 mmol, 19.8 mg) at room temperature under an Ar atmosphere. The resulting solution was refluxed overnight. The solvent was removed under reduced pressure and the resulting residue was purified by means of silica gel column chromatography, using CH_2Cl_2:MeOH (20:1) as eluent to give 224 mg of the pure diketopiperazine **17** (26% yield over two steps). ^{1}H NMR (CD_3OD, 400 MHz): δ ppm 7.15 (d, 1H, *J* = 8.5 Hz), 7.04 (s, 1H), 6.94 (d, 1H, *J* = 1.8 Hz), 6.67 (dd, 1H, *J* = 8.2, 1.8 Hz), 4.38 (t, 1H, *J* = 4.6 Hz), 4.02 (dd, 1H, *J* = 10.6, 7.0 Hz), 3.49- 3.56 (m, 1H), 3.24 (m, 3H), 1.96-2.02 (m, 1H), 1.70 (m, 1H), 1.55 (m, 1H), 1.01 (m, 1H). ESI-MS (+) *m/z* 322 $[M+Na]^+$.

2.6.5 Synthesis of 2-Methylbrevianamide F (18)

2.6.5.1 Synthesis of *N*-Boc-L-2-Methyltryptophan (42)

2-Methyltryptophan **41** was prepared from L-serine and 2-methylindole using tryptophan synthase. The procedure for this reaction is described in the general enzyme methods. To a stirred solution of L-2-methyltryptophan **41** (335 mg, 1.54 mmol) in 1:1 water-1,4-dioxane (20

mL) was added 1M NaOH (1.54 mL) followed by di-*tert*-butyl dicarbonate (335 mg, 1.54 mmol, 1.0 equiv). The mixture was stirred at room temperature for 24 h and then the pH was adjusted to 2.4 by adding aqueous HCl. The resulting mixture was extracted with EtOAc (3×10 mL) and dried over anhydrous $MgSO_4$. Removal of the solvent under reduced pressure gave 361 mg of *N*-Boc-L-2-methyltryptophan **42** (74% yield) as an off-white solid. ^{1}H NMR ($CDCl_3$, 400 MHz): δ ppm 7.87 (br, 1H), 7.52 (d, 1H, *J* = 7.6 Hz), 7.28 (d, 1H, *J* = 7.3 Hz), 7.12 (t, 1H, *J* = 7.0 Hz), 7.07 (t, 1H, *J* = 7.3 Hz), 5.05 (d, 1H, *J* = 7.0 Hz), 4.61 (d, 1H, *J* = 5.2 Hz), 3.28 (d, 2H, *J* = 4.6 Hz), 2.35 (s, 3H), 1.43 (s, 9H). ESI-MS (+) *m/z* 341 $[M+Na]^+$.

2.6.5.2 Synthesis of *N*-Boc-L-2-Methyltryptophan-L-Proline Methyl Ester (43)

To a stirred solution of crude *N*-Boc-L-2-methyltryptophan **42** (361 mg, 1.13 mmol) in 10 mL of anhydrous THF was added L-proline methyl ester hydrochloride **31** (374 mg, 2.26 mmol, 2 equiv). The mixture was cooled to 0 °C and NEt_3 (252 mg, 2.49 mmol, 2.2 equiv, 0.35 mL) was added dropwise. To this mixture was added 1-hydroxybenzotriazole (173 mg, 1.13 mmol, 1 equiv) followed by DCC (245 mg, 1.19 mmol, 1.05 equiv). The ice bath was removed and the reaction was left stirring at room temperature overnight. Solids were removed by filtration and washed with Et_2O (5×5 mL). The filtrate was combined with the washings and the solvents were removed under reduced pressure. The residue was dissolved in 5 mL EtOAc and then washed with 5% aqueous $NaHCO_3$ (10 mL), 10% aqueous citric acid (10 mL), 5% aqueous $NaHCO_3$ (10 mL), and brine (10 mL). The organic phase was dried over anhydrous $MgSO_4$ and the solvent was removed under reduced pressure. The resulting residue was purified by means of silica gel column chromatography, using hexane:EtOAc (3:1) as eluent to give 237 mg of **43** containing impurities of dicyclohexylurea (49% crude yield). This compound was used directly in

subsequent steps without further purification. ^{1}H NMR ($CDCl_3$, 400 MHz): δ ppm 7.82 (br, 1H), 7.50 (d, 1H, *J* = 7.6 Hz), 7.24 (d, 1H, *J* = 7.0 Hz), 7.11-7.08 (m, 2H), 5.25 (d, 1H, *J* = 8.8 Hz), 4.81 (m, 1H), 4.46 (m, 1H), 3.69 (s, 3H), 3.43 (m, 1H), 3.28 (m, 1H), 3.14 (dd, 1H, *J* = 12.5, 7.9 Hz), 3.05 (m, 1H), 2.45 (s, 3H), 2.10 (m, 1H), 1.78-1.98 (m, 3H), 1.46 (s, 9H). ESI-MS (+) *m/z* 452 $[M+Na]^+$.

2.6.5.3 Synthesis of Cyclo-L-2-Methyltryptophan-L-Proline (18)

To a stirred solution of protected dipeptide **43** (237 mg, 0.55 mmol) in 5 mL anhydrous CH_2Cl_2 at 0 °C was added 0.65 mL of TFA under an Ar atmosphere. The mixture was allowed to stir for 6 h. The solvent was removed under reduced pressure at 0 °C and the resulting residue was taken up in 20 mL of EtOAc. The solution was washed with 5% aqueous Na_2CO_3 (10 mL), brine (10 mL) and dried over anhydrous $MgSO_4$. Removal of the solvent under reduced pressure gave 164 mg of crude reaction product which was used directly in the next step. A solution of crude dipeptide (164 mg, 0.49 mmol) was prepared in 5 mL of dry DMF. The mixture was cooled to 0 °C and 2-hydroxypyridine (0.1 equiv, 0.049 mmol, 4.8 mg) was added under Ar atmosphere. The resulting solution was refluxed for 6 h. The solvent was removed under reduced pressure and the resulting residue was purified by means of silica gel column chromatography, using CH_2Cl_2:MeOH (50:1) as eluent to give 60 mg of the pure diketopiperazine **18** (37% yield over two steps). ^{1}H NMR ($CDCl_3$, 400 MHz): δ ppm 7.94 (br, 1H), 7.48 (d, 1H, *J* = 7.9 Hz), 7.32 (d, 1H, *J* = 8.2 Hz), 7.17 (t, 1H, *J* = 7.9 Hz), 7.12 (t, 1H, *J* = 7.6 Hz), 5.58 (br, 1H), 4.37 (dd, 1H, *J* = 7.6, 3.3 Hz), 4.08 (t, 1H, *J* = 7.6 Hz), 3.68 (dd, 2H, *J* = 14.9, 4.0 Hz), 3.60 (dd, 1H, *J* = 7.3, 3.0 Hz), 2.96 (dd, 1H, *J* = 16.4, 11.2 Hz), 2.44 (s, 3H), 2.35 (m, 1H), 1.89-2.09 (m, 3H). ESI-MS (+) *m/z* 298 $[M+H]^+$.

2.6.6 General Enzyme Methods

Centrifugal filters (4 mL 10 000 MWCO) were purchased from Millipore. Chelating Sepharose® Fast resin was purchased from Pharmacia Biotech. Protein concentrations were determined by the method of Bradford on a Cary 3E UV-Vis spectrophotometer using bovine serum albumin as standard. [184] All measurements were performed at room temperature. Protein purity was assessed using SDS-PAGE, stained with Coomassie blue according to Laemmli. [185] Molecular weight standards for SDS-PAGE were BSA (66 kDa) and carbonic anhydrase (29 kDa), both purchased from Sigma.

2.6.6.1 Overexpression and Purification of Prenyltransferases FtmPT1, CdpNPT, and CpaD

The genes encoding all three prenyltransferases (*ftmPT1* and *cdpNPT* from *Aspergillus fumigates*, and *cpaD* from *Aspergillus oryzae*) were synthesized by GenScript with codon optimization for expression in *E. coli*. These were cloned into pET28a vectors (Novagen/EMD Millipore) at BamH1 and HindIII restriction sites. Overexpression of the C-terminally hexahistidine-tagged enzymes was performed by using a modification of the protocol described by Steffan *et al*. [86] Rosetta(DE3) pLysS (Novagen) harboring the pET28a construct were grown at 37 °C in Terrific Broth (TB) medium containing chloramphenicol (35 μgmL^{-1}) and kanamycin (30 μgmL^{-1}) until an optical density (OD_{600}) of 0.6 was reached. The *E. coli* cells were induced for overexpression by the addition of 119 mg (0.5 mM) of isopropyl-1-thio-*β*-D-galactopyranoside (IPTG) and left growing at 24 °C for an additional 24 hours. Cells were harvested and lysed with a French press in sodium phosphate buffer (20 mM, pH 8.0) containing dithiothreitol (DTT, 2 mM), aprotinin (1 μgmL^{-1}), and pepstatin A (1 μgmL^{-1}). The lysate was

cleared by centrifugation (34 155g, 45 min) and filtering through a 0.22 mm filter. A column containing chelating Sepharose fast flow resin (GE Healthcare, 10 mL) was charged with 100 mM $NiSO_4$ and washed with sodium phosphate buffer (20 mM, pH 8.0) containing NaCl (500 mM) and imidazole (5 mM). The clarified lysate was loaded onto the column and eluted with same buffer but containing imidazole at 5, 100, and 500 mM. Glycerol (7%) was added to the resulting eluent before flash freezing with liquid N_2.

2.6.6.2 Enzymatic Synthesis of C-4-Prenyl-Cyclo-L-Trp-L-Trp (16) Using CpaD

Due to the low solubility of cyclo-L-Trp-L-Trp in aqueous buffer, a stock solution of cyclo-L-Trp-L-Trp (15 mM in MeOH) was prepared. An incubation solution of cyclo-L-Trp-L-Trp (4 mM, 4.5 mL of stock solution) and DMAPP (8 mM) was then prepared in Tris·HCl (50 mM, pH 7.5, 12.5 mL). The reaction was initiated by addition of CpaD (6 mg) in phosphate buffer (20 mM pH 7.5, 6 mL) containing imidazole (500 mM)) to the incubation solution. The mixture was incubated for 20 h at 37 °C and the precipitate was then removed by centrifugation (34155g, 30 min). The resulting solution was extracted with ethyl acetate (3×20 mL). The organic layer was dried over $MgSO_4$ and purified by silica gel column chromatography with CH_2Cl_2:MeOH (50:1) as eluent. ^{1}H NMR and ESI-MS data were identical to those reported in the literature. [89]

2.6.6.3 Preparation and Expression of Tryptophan Synthase

A sample of *E. coli* cells which were pre-transformed with a plasmid (pSTB7) expressing tryptophan synthase from *Salmonella enterica* was purchased from the American Type Culture Collection (ATCC 37845). Growth of the cells and expression of the enzyme was performed

using a slight modification of the protocol described by Goss *et al.* [180] Cells harboring the pSTB7 construct were grown at 37 °C in 10 mL of Luria-Bertani Broth (LB) medium containing ampicillin (100 μgmL^{-1}) until an optical density (OD_{600}) of 1.8 was reached. Half of this culture (5 mL) was added to 500 mL of Lysogeny Broth (LB) medium containing ampicillin (100 μgmL^{-1}) and left growing at 37 °C for an additional 20 hours. Cells were harvested and lysed with a French press in a buffer (pH 7.8) containing Tris-HCl (500 mM), EDTA (5 mM), mercaptomethanol (10 mM), phenylmethanesulfonylfluoride (PMSF) (1.0 mM), and pyridoxal-5-phosphate (PLP) (0.1 mM). The lysate was clarified by centrifugation (34 155g, 60 min) and the crude supernatant was used in the reaction without further purification.

2.6.6.4 Enzymatic Synthesis of L-2-Methyltryptophan (41)

An incubation solution of 2-methylindole **40** (160 mg, 1.21 mmol, 12 mM), L-serine (127 mg, 1.21 mmol, 12 mM), and PLP (0.8 mg, 3 μmol, 30 μM) was prepared in KH_2PO_4 buffer (100 mM, pH 7.8, 100 mL) and cooled to 0 °C. The reaction was initiated by the addition of cell lysate containing tryptophan synthase (2 mL). The reaction mixture was incubated in a shaker at 37 °C for 3 days and fresh enzyme (2 mL each time) was added on the second and third day to help with the progress of the reaction. The reaction mixture was filtered and the resulting solution was extracted with ethyl acetate (3×50 mL) to remove any unreacted 2-methylindole. The volume of the aqueous layer was reduced to 20 mL under reduced pressure prior to purification by reverse-phase chromatography. The solution was loaded onto reverse-phase silica (15.0 g) and was eluted using water. Fractions (10 mL) were collected and visualized on TLC plates using ninhydrin. Early fractions contained L-serine, and once serine was no longer detected, two further fractions were collected prior to switching to MeOH as eluent. Methanolic

fractions containing 2-methyltryptophan were combined and concentrated under reduced pressure, and then by freeze drying. ^{1}H NMR and ESI-MS data were identical to those reported in the literature. [180]

2.6.7 Product Studies with Substrate and Substrate Analogs

2.6.7.1 Product Studies with Cyclo-L-Trp-L-Trp

A stock solution containing cyclo-L-Trp-L-Trp (25 mM in MeOH) was prepared. An incubation solution containing cyclo-L-Trp-L-Trp (7 mM, 2 mL of stock solution), DMAPP (14 mM), and $CaCl_2$ (10 mM) was then prepared in Tris·HCl (50 mM, pH 7.5, 4 mL). The reaction was initiated by the addition of CdpNPT (3 mg in phosphate buffer (20 mM, pH 7.5, 3 mL) containing imidazole (500 mM)) to the incubation solution. The mixture was incubated for 20 h at 37 °C, and the precipitate was then removed by centrifugation (34 155g, 30 min). The resulting solution was extracted with ethyl acetate (3×10 mL). The organic layer was dried over Na_2SO_4 and purified by silica gel column chromatography with gradient elution, CH_2Cl_2/EtOAc (20:1 to 1:1). ^{1}H NMR spectrum of compound **15** (CD_3OD, 400 MHz): δ ppm 7.62 (d, 1H, *J* = 7.9 Hz), 7.33 (d, 1H, *J* = 7.9 Hz), 7.09 (s, 1H), 7.05-7.11 (m, 2H), 7.01 (t, 2H, *J* = 7.5 Hz), 6.65 (t, 1H, *J* = 7.2 Hz), 6.54 (d, 1H, *J* = 7.6 Hz), 5.58 (dd, 1H, *J* = 17.4, 11.0 Hz), 5.24 (s, 1H), 4.92 (d, 1H, *J* = 9.7 Hz), 4.41 (m, 1H), 3.78 (ddd, 1H, *J* = 11.8, 5.6, 2.1 Hz), 3.45 (dd, 1H, *J* = 14.8, 4.7 Hz), 3.21 (dd, 1H, *J* = 14.8, 4.1 Hz), 2.17 (dd, 1H, *J* = 11.9, 5.5 Hz), 1.60 (t, 1H, *J* = 11.9 Hz), 0.79 (s, 3H), 0.66 (s, 3H). ESI-MS (+) *m/z* 463 $[M+Na]^+$.

2.6.7.2 Non-Enzymatic aza-Cope Reaction of (15)

A solution of **15** (2.2 mM) and trichloroacetic acid (136 mM) in MeOH (0.6 mL) was incubated at 37 °C. The progress of reaction was monitored by ^{1}H NMR spectroscopy. After two days, the reaction mixture was diluted with 10% aqueous $NaHCO_3$ (3 mL) and extracted with $CHCl_3$ (3×5 mL). The organic layer was dried over Na_2SO_4, and the solvent was removed under reduced pressure.

2.6.7.3 Product Studies with Brevianamide F

A solution containing brevianamide F (12 mM), DMAPP (24 mM), and $MgCl_2$ (5 mM) were prepared in Tris·HCl (50 mM, pH 7.5, 3 mL). The reaction was initiated by addition of FtmPT1 (5 mg in phosphate buffer (20 mM, pH 7.5, 6 mL) containing imidazole (500 mM)). The mixture was incubated for 20 h at 37 °C, and the precipitate was removed by centrifugation (34 155g, 30 min). The resulting solution was extracted with ethyl acetate (3×10 mL). The organic layer was dried over $MgSO_4$ and purified by silica gel column chromatography, using CH_2Cl_2/MeOH (80:1) as eluent. ^{1}H NMR spectrum of tryprostatin B ($CDCl_3$, 400 MHz): δ ppm 7.97 (br, 1H), 7.49 (d, 1H, *J* = 7.6 Hz), 7.32 (d, 1H, *J* = 7.9 Hz), 7.17 (dt, 1H, *J* = 1.4, 7.5 Hz), 7.11 (dt, 1H, *J* = 1.1, 7.8 Hz), 5.62 (br, 1H), 5.33 (t, 1H, *J* = 1.2 Hz), 4.38 (dd, 1H, *J* = 11.6, 2.7 Hz), 4.07 (t, 1H, *J* = 7.5 Hz), 3.69 (dd, 2H, *J* = 14.01, 3.96 Hz), 3.61 (dd, 1H, *J* = 8.8, 3.0 Hz), 3.49 (t, 2H, *J* = 7.3 Hz), 2.97 (dd, 1H, *J* = 15.1, 11.4 Hz), 2.34 (m, 1H), 2.02-2.09 (m, 2H), 1.89-1.96 (m, 1H), 1.80 (s, 3H), 1.77 (3H). ESI-MS (+) *m/z* 374 $[M+Na]^+$.

2.6.7.4 Product Studies with L-Trp

A solution containing L-Trp (9 mM), DMAPP (18 mM), and $MgCl_2$ (5 mM) was prepared in Tris·HCl (50 mM, pH 7.5, 9.5 mL). The reaction was initiated by addition of FtmPT1 (3 mg in phosphate buffer (20 mM, pH 7.5, 4 mL) containing imidazole (500 mM)). The mixture was incubated for 20 h at 37 °C, and the precipitate was then removed by centrifugation (34 155g, 30 min). The sample (0.6 mL) was placed in an NMR tube, and D_2O (0.1 mL) was added. ^{1}H NMR spectra were obtained with solvent suppression.

2.6.7.5 Product Studies with Cyclo-L-Trp-L-Trp

A stock solution containing cyclo-L-Trp-L-Trp (25 mM in MeOH) was prepared. An incubation solution containing cyclo-L-Trp-L-Trp (7 mM, 2 mL of stock solution), DMAPP (14 mM), and $MgCl_2$ (10 mM) was then prepared in Tris·HCl (50 mM, pH 7.5, 4 mL). The reaction was initiated by addition of FtmPT1 (3 mg in phosphate buffer (20 mM, pH 7.5, 3 mL) containing imidazole (500 mM)) to the incubation solution. The mixture was incubated for 20 h at 37 °C, and the precipitate was then removed by centrifugation (34 155g, 30 min). The resulting solution was extracted with ethyl acetate (3×10 mL). The organic layer was dried over Na_2SO_4 and purified by silica gel column chromatography, using CH_2Cl_2/MeOH (50:1) as eluent. ^{1}H NMR spectrum of compound **34** ($CDCl_3$, 400 MHz): δ ppm 8.03 (br, 1H), 7.98 (br, 1H), 7.51 (m, 2H), 7.32 (dd, 2H, *J* = 14.5, 7.8 Hz), 7.09-7.21 (m, 4H), 6.30 (br, 1H), 5.82 (br, 1H), 5.67 (br, 1H), 5.31 (m, 1H), 4.27 (m, 1H), 4.14 (d, 1H, *J* = 9.7 Hz), 3.38 (d, 2H, *J* = 7.5 Hz), 3.22-3.33 (m, 2H), 3.03 (dd, 1H, *J* = 14.8, 7.5 Hz) 2.05 (m, 1H), 1.83 (s, 3H), 1.78 (s, 3H). ESI-MS (+) *m/z* 463 $[M+Na]^+$. ^{1}H NMR spectrum of compound **35** ($CDCl_3$, 400 MHz): δ ppm 8.14 (s, 1H), 7.57 (d, 1H, *J* = 8.2 Hz), 7.40 (d, 1H, *J* = 8.2 Hz), 7.24 (t, 1H, *J* = 7.6 Hz), 7.07-7.16

(3H, m), 7.12 (s, 1H), 6.77 (t, 1H, *J* = 7.3 Hz), 6.64 (d, 1H, *J* = 7.9 Hz), 5.67 (s, 1H), 5.35 (s, 1H), 5.16 (t, 1H), 5.09 (s, 1H), 4.34 (m, 1H), 3.99 (dd, 1H, *J* = 10.8, 5.9 Hz), 3.75 (dd, 1H, *J* = 15.1, 3.5 Hz), 2.99 (dd, 1H, *J* = 15.2, 11.0 Hz), 2.61 (dd, 1H, *J* = 12.6, 5.9 Hz), 2.40 (m, 2H), 2.25 (t, 1H, *J* = 11.0, Hz), 1.72 (s, 3H), 1.55 (s, 3H). ESI-MS (+) *m/z* 463 $[M+Na]^+$.

2.6.7.6 Product Studies with 5-Hydroxybrevianamide F (17)

A solution containing 5-hydroxybrevianamide F **17** (12 mM), DMAPP (24 mM), and $MgCl_2$ (5 mM) was prepared in Tris·HCl (50 mM, pH 7.5, 3 mL). The reaction was initiated by addition of FtmPT1 (5 mg in phosphate buffer (20 mM, pH 7.5, 6 mL) containing imidazole (500 mM)). The mixture was incubated for 20 h at 37 °C, and the precipitate was removed by centrifugation (34 155g, 30 min). The resulting solution was extracted with ethyl acetate (3×10 mL). The organic layer was dried over $MgSO_4$ and purified by silica gel column chromatography with elution gradient CH_2Cl_2/MeOH (60:1 to 25:1). ^{1}H NMR spectrum of compound **39** ($CDCl_3$, 400 MHz): δ ppm 8.02 (s, 1H), 7.15 (d, 1H, *J* = 8.7 Hz), 7.06 (d, 1H, *J* = 2.4 Hz), 6.83 (d, 1H, *J* = 8.7 Hz), 5.79 (br, 1H), 5.24 (t, 1H, *J* = 6.4 Hz), 4.27 (d, 1H, *J* = 9.7 Hz), 4.09 (t, 1H, *J* = 7.9 Hz), 3.95 (dd, 1H, *J* = 15.4, 3.2 Hz), 3.77 (m, 1H), 3.60-3.70 (m, 3H), 2.93 (dd, 1H, *J* = 15.4, 11.4 Hz), 2.36 (m, 1H), 2.02-2.15 (m, 3H), 1.95 (m, 1H), 1.85 (s, 3H), 1.75 (s, 3H). ESI-MS (+) *m/z* 390 $[M+Na]^+$.

2.6.7.7 Product Studies with 2-Methylbrevianamide F (18)

A stock solution of 2-methylbrevianamide F **18** (113 mm in MeOH) was prepared. An incubation solution containing **18** (12 mM, 0.25 mL of stock solution), DMAPP (24 mM), and $MgCl_2$ (5 mM) in Tris·HCl (50 mM, pH 7.5, 1.75 mL) was then prepared (final, MeOH 11 %).

The reaction was initiated by addition of FtmPT1 (3 mg in phosphate buffer (20 m/m pH 7.5, 4 mL) containing imidazole (500 mM)) to the incubation solution. The mixture was incubated for 20 h at 37 °C, and the precipitate was then removed by centrifugation (34155g, 30 min). The resulting solution was extracted with ethyl acetate (3×10 mL). The organic layer was dried over $MgSO_4$ and purified by silica gel column chromatography with CH_2Cl_2/MeOH (80:1) as eluent. ^{1}H NMR spectrum of compound **44** ($CDCl_3$, 400 MHz): δ ppm 7.07 (m, 2H), 6.76 (dt, 1H, *J* = 0.9, 7.5 Hz), 6.63 (d, 1H, *J* = 7.6 Hz), 5.64 (s, 1H), 5.15 (br, 1H), 3.95 (t, 1H, *J* = 7.9 Hz), 3.86 (dd, 1H, *J* = 10.8, 6.5 Hz), 3.54 (m, 1H), 3.49 (m, 1H), 2.66 (dd, 1H, *J* = 13.2, 6.5 Hz), 2.26-2.29 (m, 2H), 2.20-2.25 (m, 2H), 2.12-2.18 (m, 1H), 1.97-2.04 (m, 1H), 1.84-1.91 (m, 1H), 1.70 (s, 6H), 1.41 (s, 3H). ESI-MS (+) *m/z* 366 $[M+H]^+$. ^{1}H NMR spectrum of compound **45** (CD_3OD, 400 MHz): δ ppm 7.49 (d, 1H, *J* = 7.8 Hz), 7.25 (d, 1H, *J* = 8.1 Hz), 7.08 (dt, 1H, *J* = 0.98, 7.63 Hz), 6.98 (dt, 1H, *J* = 1.0, 7.0 Hz), 5.11 (tt, 1H, *J* = 6.6, 1.1 Hz), 4.74 (d, 2H, *J* = 6.3 Hz), 4.35 (t, 1H, *J* = 4.3 Hz), 3.87 (ddd, 1H, *J* = 11.5, 6.2, 1.1 Hz), 3.48 (m, 1H), 3.35-3.38 (m, 2H), 3.20 (dd, 1H, *J* = 12.3, 4.9 Hz), 3.09-3.13 (m, 2H), 2.38 (s, 3H), 1.88 (s, 3H), 1.77-1.84 (m, 1H), 1.71 (s, 3H), 1.49-1.69 (m, 2H). ESI-MS (+) *m/z* 366 $[M+H]^+$.

Chapter 3: Design and Synthesis of a Potent Inhibitor of an Indole Prenyltransferase: 4-DMATS

As discussed in section 1.6.3, the classic application of bisphosphonate inhibitors was to treat bone-related diseases; but more recently, they have been studied as a treatment for cancer. The potential of bisphosphonates to act as anti-cancer drugs originates from their ability to inhibit metal-dependent prenyltransferases such as farnesyl diphosphate (FPP) and geranylgeranyl diphosphate (GGPP) synthase, which will ultimately inhibit protein prenylation catalyzed by the the enzyme protein farnesyltransferase (FTase). [137] Initial interest in the inhibition of protein farnesyltransferase was triggered by the finding that farnesylation was required for the oncogenic forms of Ras proteins to transform cells, as Ras proteins are associated with approximately 30% of all human cancers. Ras proteins play a fundamental role in the signaling cascade in cells and their mutation results in the transformation of normal cells into malignant ones. It has been shown that unfarnesylated mutant Ras proteins do not anchor onto cell membranes and cannot induce this transformation. Consequently, post-translational modification and membrane association of mutant Ras is believed to be necessary for this transforming activity. Since the enzyme protein farnesyltransferase (FTase) catalyzes the prenylation of Ras proteins, it was considered as one of the most promising targets for cancer therapy. [186] Despite the initial promising results, FTase inhibitors have not been found to be very effective drugs, partially due to the finding that some Ras proteins can bypass the FTase inhibition through alternative prenylation by the related enzyme geranylgeranyl transferase (GGTase I). [187]

Since the direct inhibition of protein farnesyltransferase (FTase) proved to be ineffective, an alternative approach was employed that involved blocking the biosynthesis of farnesyl and/or geranylgeranyl diphosphate by inhibiting the enzymes farnesyl diphosphate (FPP) and geranylgeranyl diphosphate (GGPP) synthase. [137] As described in section 1.5.1, the biosynthesis of FPP proceeds via a dissociative mechanism with the formation of allylic carbocation intermediates. A successful strategy to inhibit FPP synthase involves the use of nitrogen-containing bisphosphonates that contain a potent metal binding functionality and also mimic the carbocationic character of the high energy intermediates. [154] Interestingly, the first step in the mechanism of all prenyltransferase reactions is believed to involve the formation of either an allylic carbocation intermediate, or an associative transition state that carries a great deal of carbocation character at the allylic position. [71,73,76,78,94,96] We decided to target 4-DMATS for rational inhibitor design as it serves an excellent example of an enzyme that generates an allylic carbocation during a rate-limiting step of catalysis. In addition, there have been no reports of inhibitors that target metal-independent prenyltransferases. We also envisioned that a potent inhibitor of 4-DMATS could serve as a general inhibitor of prenyltransferases and cyclases (including FPP synthase) given that all of these enzymes form high energy allylic carbocationic intermediates during the course of reaction. In the following section, we will provide more details regarding the mechanism of 4-DMATS and our strategy towards the design of a potent inhibitor.

3.1 Design of Inhibitor 19

As described in section 1.5.3.2, two mechanisms have been proposed for the indole prenyltransferase 4-DMATS. The first proposed mechanism suggests a direct attack by the C-4

position of tryptophan onto the primary carbon of the dimethylallyl cation. [94,165] An alternative mechanism suggests that the reaction proceeds through an initial C-3 reverse prenylation, which is followed by a Cope rearrangement to give 4-dimethylallyl tryptophan (4-DMAT). [98] Whether 4-DMATS employs a mechanism that involves a direct attack or a Cope rearrangement, the first step of catalysis is a dissociation step where a dimethylallyl cation is formed (Figure 3.1).

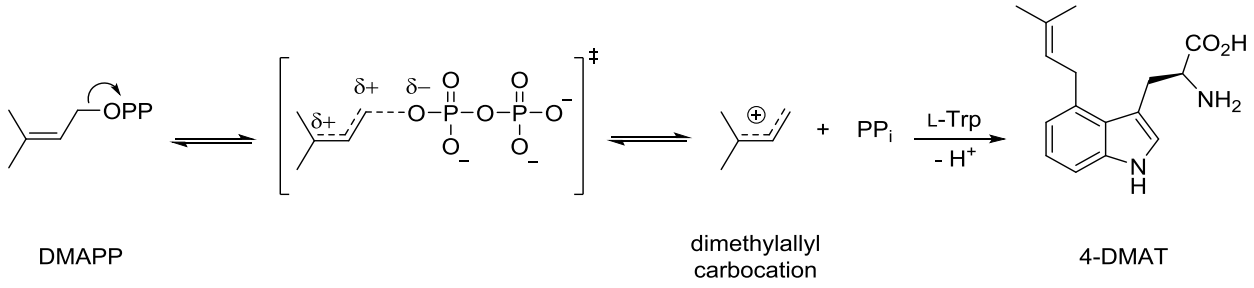

Figure 3.1 The dissociation step and the corresponding transition state in the reaction catalyzed by 4-DMATS.

As described in section 1.6, different strategies have been used for inhibiting various carbocation-forming enzymes. Among the different approaches, incorporating a protonated amine group into the structure of the inhibitors gave positive results. [128,129,132] Since our goal was to specifically inhibit an enzyme that forms an allylic carbocation, we decided to install a guanidinium functionality in the structure of the inhibitor (Figure 3.2). Besides the fact that a guanidinium provides the desired positive charge, it possesses a resonance structure that delocalizes the positive charge over two nitrogen atoms and therefore should serve as a closer mimic of the allylic carbocation. In addition, the sp^2 hybridization of the nitrogen atoms more closely mimic the planar geometry of an allylic carbocation. The phosphorylated phosphonate portion of inhibitor **19** is included to mimic the pyrophosphate group in the dimethylallyl carbocation/pyrophosphate ion pair. We therefore designed inhibitor **19** that we predicted would

serve as a close mimic of the transition state/ion pair intermediate formed in the 4-DMATS reaction (Figure 3.2).

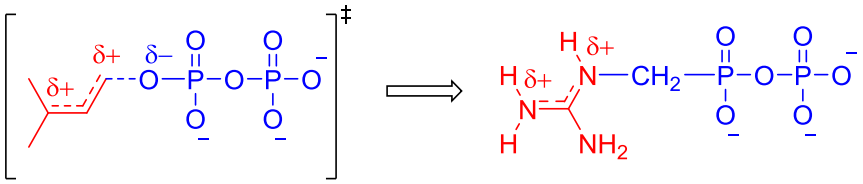

Figure 3.2 Structure of the transition state formed in the reaction catalyzed by 4-DMATS is shown on the left and the structure of the inhibitor 19 is shown on the right. The guanidinium functionality is shown in red.

In this chapter we will describe our strategy towards the design and synthesis of inhibitor **19**. We will then proceed to discuss the complications we encountered with the stability of this compound. Next, we describe the testing of compound **19** with 4-DMATS and report the qualitative kinetic results that we obtained. Finally, we will discuss the future of this project in terms of design and synthesis of potential inhibitors of 4-DMATS, and their potential to inhibit the farnesyl diphosphate synthase enzyme.

3.2 Synthesis of Inhibitor 19

Two different approaches for the synthesis of inhibitor **19** are described here. The synthesis of inhibitor **19** was not completed using the first approach, pathway A, as we encountered difficulties during the synthesis. We therefore modified the synthesis and the new approach, pathway B, was successful and provided us with the desired inhibitor in milligram quantities.

3.2.1 Attempts towards the Synthesis of Inhibitor 19: Pathway A

The first approach towards the synthesis of inhibitor **19** comprises six steps: protection of the amine functional group of the phosphonic acid **47** to give compound **48**, conversion of the phosphonic acid **48** to the corresponding phosphonic diester **49**, removal of the amine protecting group to give compound **50**, introduction of the guanidinium functionality to give **51**, deprotection of the benzyl group by hydrogenolysis to give compound **52**, and the final step which involves installing the pyrophosphate linkage (Figure 3.3).

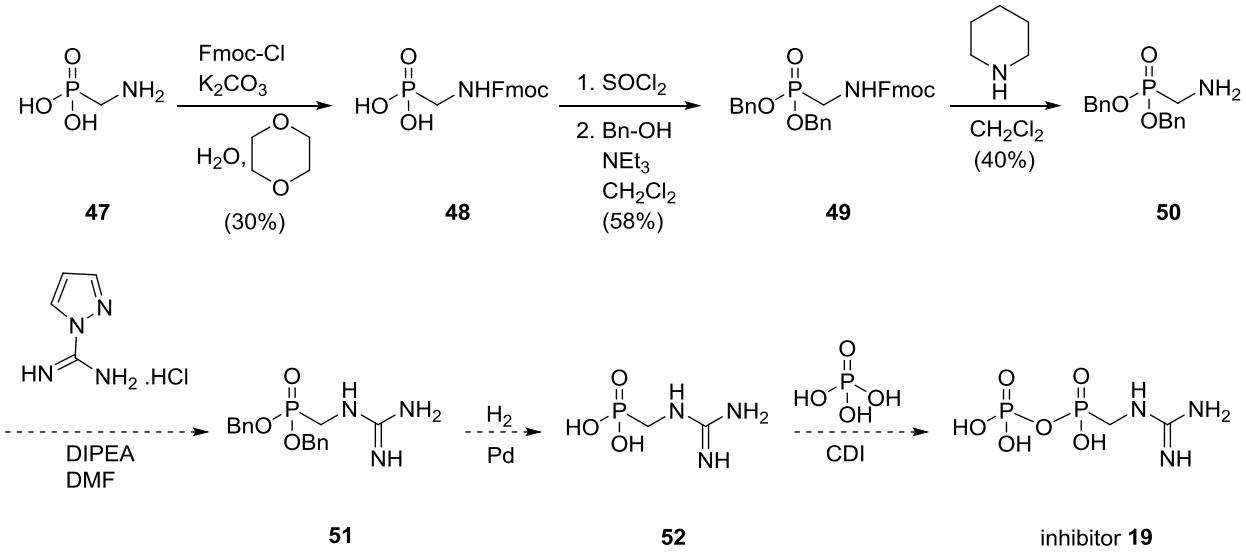

Figure 3.3 Pathway A: first attempted synthetic pathway for inhibitor 19.

Pathway A employs dibenzyl (aminomethyl)phosphonate **50** as the key intermediate for the generation of inhibitor **19** (Figure 3.3). We chose benzyl protecting groups since a benzyl ester is easily prepared and can be removed either by treatment with strong acid or by the milder alternative, hydrogenolysis. To synthesize intermediate **50**, the commercially available amino phosphonic acid **47** was first protected with a 9-fluorenylmethoxycarbonyl (Fmoc) group in a dioxane/water mixture. The Fmoc protected phosphonic acid **48** was then activated as a

phosphonodichloridate by reaction with thionyl chloride. Due to its instability, the crude product was used immediately in the subsequent step without any purification. The benzylation of the activated phosphonic acid was achieved by reaction with benzyl alcohol in the presence of a base to give compound **49**. Synthesis of intermediate **50** was completed by the cleavage of the Fmoc protecting group under mild basic conditions using piperidine. [188]

Due to the relatively high cost of the amino phosphonic acid **47** ($280 per gram) and the low overall yield of the synthesis leading to the formation of intermediate **50** (7% over three steps), the synthesis of inhibitor **19** was not completed through pathway A. We decided to design a new synthesis rather than to spend more time trying increase the yields of this route. We revised the synthesis so that an inexpensive starting material could be employed and higher overall yields could be achieved.

3.2.2 Synthesis of Inhibitor 19: Pathway B

The second pathway towards the synthesis of inhibitor **19** can be divided into four main sections: deprotection of the aminophosphonic diester **53** to give aminophosphonic acid diester **54**, guanidylation of compound **54** with 1*H*-pyrazole-1-carboxamidine hydrochloride **55** to give compound **56**, removal of the ethyl protecting groups to give phosphonic acid **52**, and the introduction of the pyrophosphate linkage to generate inhibitor **19** (Figure 3.4). It is noteworthy that our goal at this stage of the project was to synthesize inhibitor **19** as a pure compound to test for inhibition. If positive inhibition results were observed, we would revisit the synthesis in order to make modifications that would enable us to obtain inhibitor **19** in fewer steps and higher yields.

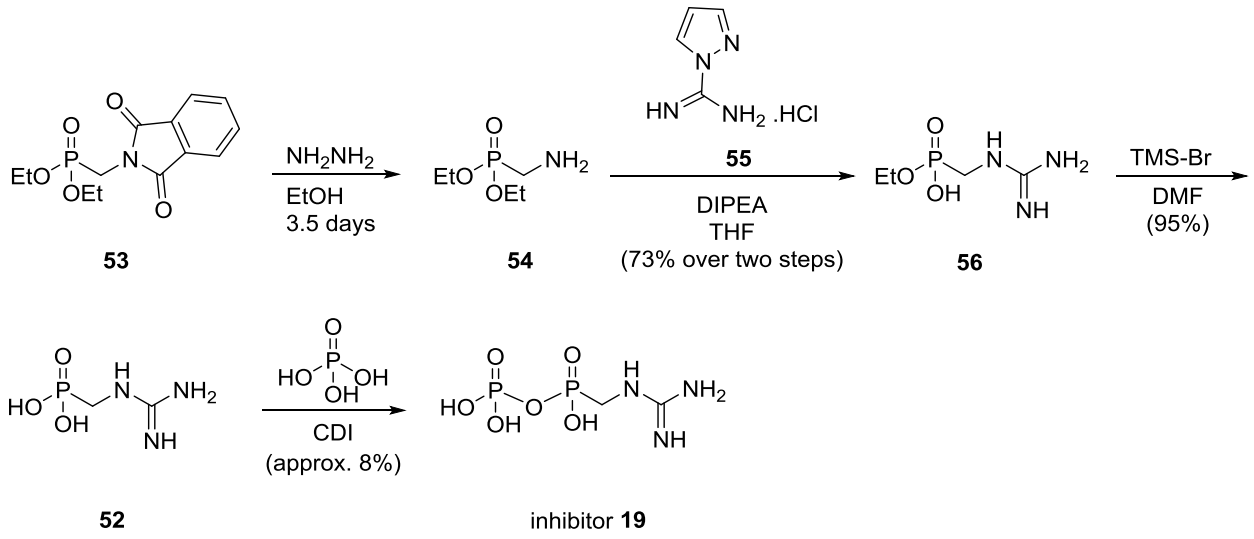

Figure 3.4 Pathway B: synthesis of inhibitor 19.

The alternative starting material that we used in the second synthetic approach was diethyl (phthalimidomethyl)phosphonate **53**. It was commercially available and reasonably priced at $180 per 25 grams. Furthermore, pathway B has fewer steps than pathway A. Compound **53** bears an amine functionality that is masked in the form of a phthalimide group. Phthalimide protecting groups can be conveniently removed by the use of hydrazine in ethanol to give diethyl (aminomethyl)phosphonate **54** and the phthalazine byproduct, which can be conveniently removed by filteration (Figure 3.5). [189]

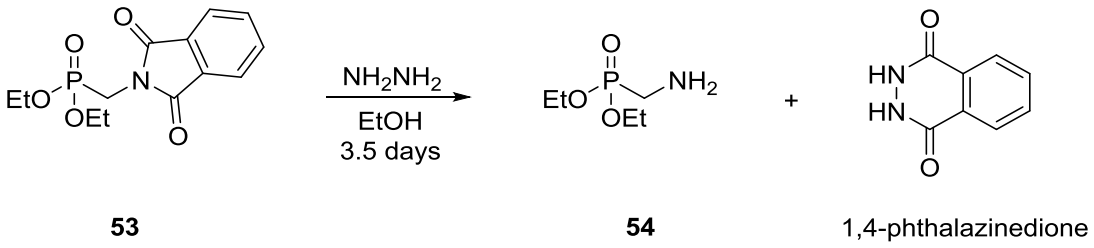

Figure 3.5 Deprotection of the phthalimide group by hydrazine hydrate.

Following the removal of the phthalimide group, our original plan involved the exchange of ethyl protecting groups with benzyl groups. We based our decision on the notion that dibenzyl phosphonates can conveniently undergo deprotection under mild hydrogenolysis conditions later in the synthesis. Removal of the ethyl groups on the other hand, would require harsher deprotection conditions that might potentially cleave off the guanidinium functionality that has been installed in the molecule. Previous studies indicated that phosphonate diesters such as compound **57** can be deprotected by refluxing in strong acids such as HCl (Figure 3.6). [189] Alternatively, trimethylbromosilane has been used to quantitatively convert the alkyl phosphonates into the corresponding trimethylsilylphosphonates **58**. These silylated compounds are then readily transformed into the corresponding phosphonic acids **59** by hydrolysis (Figure 3.6). [190]

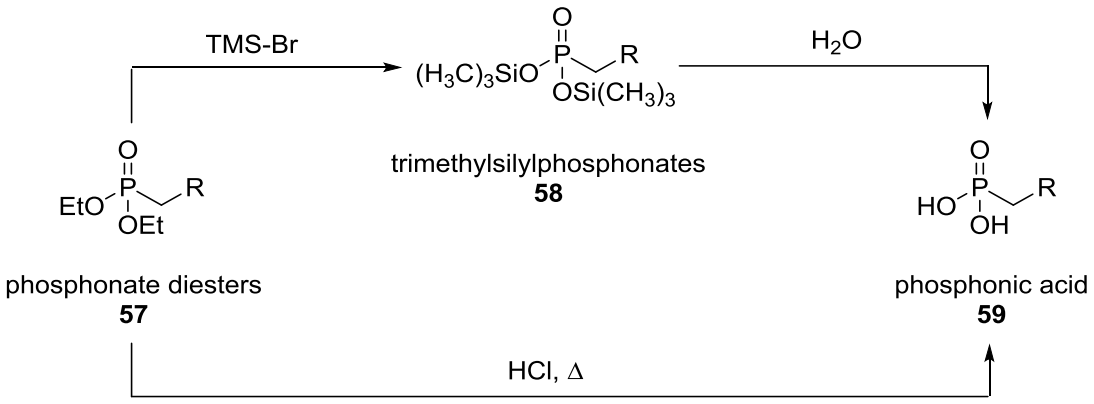

Figure 3.6 Removal of the ethyl protecting groups using either HCl or TMS-Br.

Since converting the diethyl phosphonic acid **54** to the corresponding dibenzylated compound would add two extra steps to the synthesis, it seemed reasonable to examine whether the guanidinium moiety is stable under the ethyl ester deprotection conditions. We therefore chose to install the guanidinium functionality in the molecule and evaluate the outcome of TMS-

Br deprotection before attempting to change the protecting groups. Several methods have been reported in literature for guanidylation of an amine group. A common approach involves the use of 1*H*-pyrazole-1-carboxamidine **55** (Figure 3.7). This reagent can be either purchased at a reasonable price or can be conveniently synthesized by the reaction of pyrazole with cyanamide in a refluxing anhydrous HCl/1,4-dioxane mixture (Figure 3.7). [191,192] Compound **55** is stable at room temperature and is soluble in a variety of water-miscible solvents when neutralized with diisopropylethylamine (DIPEA). Compound **55** has been shown to guanidylate unhindered primary and secondary aliphatic amines under mild conditions.

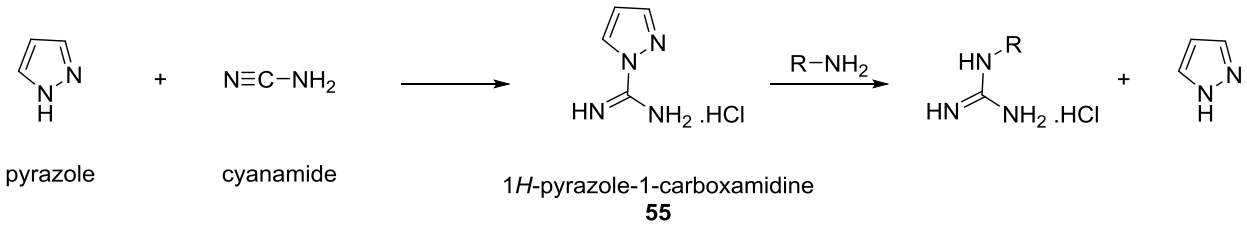

Figure 3.7 Preparation and reaction of 1*H*-pyrazole-1-carboxamidine hydrochloride 55 with a primary amine.

An alternative approach towards the synthesis of guanidinophosphonic acids involves the standard amidination of 1-aminophosphonic acids **60** with *S*-ethylisothiouronium bromide **61** (Figure 3.8). This method affords the desired guanidylated product **62** in good yields. [193]

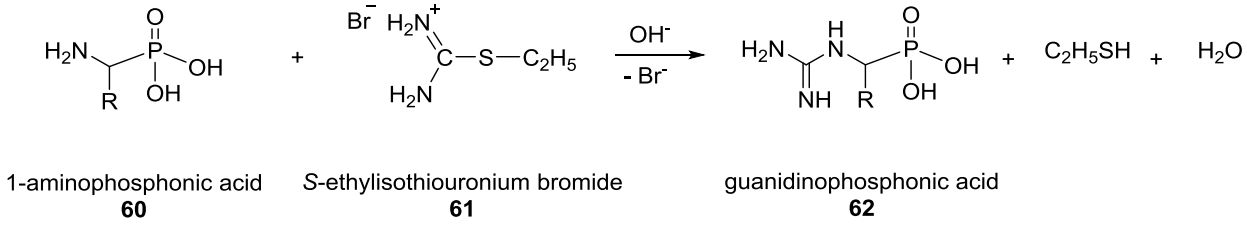

Figure 3.8 Synthesis of guanidinophosphonic acid using *S*-ethylisothiouronium bromide 61.

A shorter second procedure was suggested by Mastalerz *et al.* that eliminates the need to synthesize 1-aminophosphonic acid **60**. The simple substrates thiourea, an aldehyde, and triphenyl phosphite would initially undergo a condensation reaction to give 1-thioureidophosphonate **63** and the diphosphonate **64** (Figure 3.9). [193]

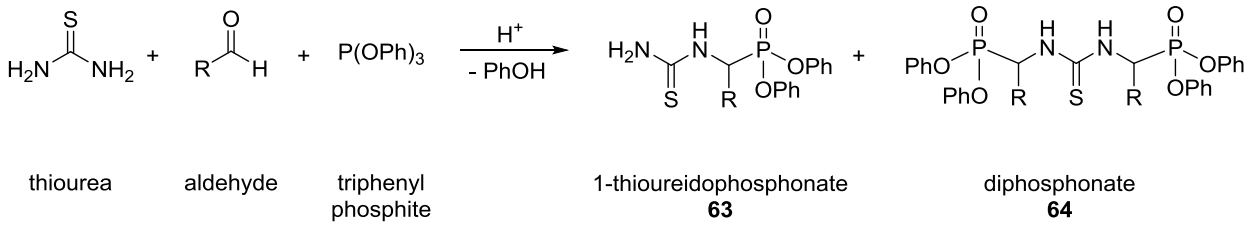

Figure 3.9 Synthesis of guanidylating agent thioureidophosphonate 64 from simple starting materials.

Since the formation of thiourea monophosphonate **63** is accompanied by formation of the diphosphonate **64** even when equimolar quantities of reactants are employed, it is often difficult to isolate pure monophosphonate **63**. However, the monophosphonate **63** undergoes hydrolysis more readily than the diphosphonate **64**, and thus the resulting phosphonic acid **65** can be conveniently isolated. [194] Pure phosphonic acid **65** will then react with methyl iodide to give *S*-methylated intermediate **66**, which will further react with ammonia to give the desired guanidinophosphonic acid **62** (Figure 3.10). [193]

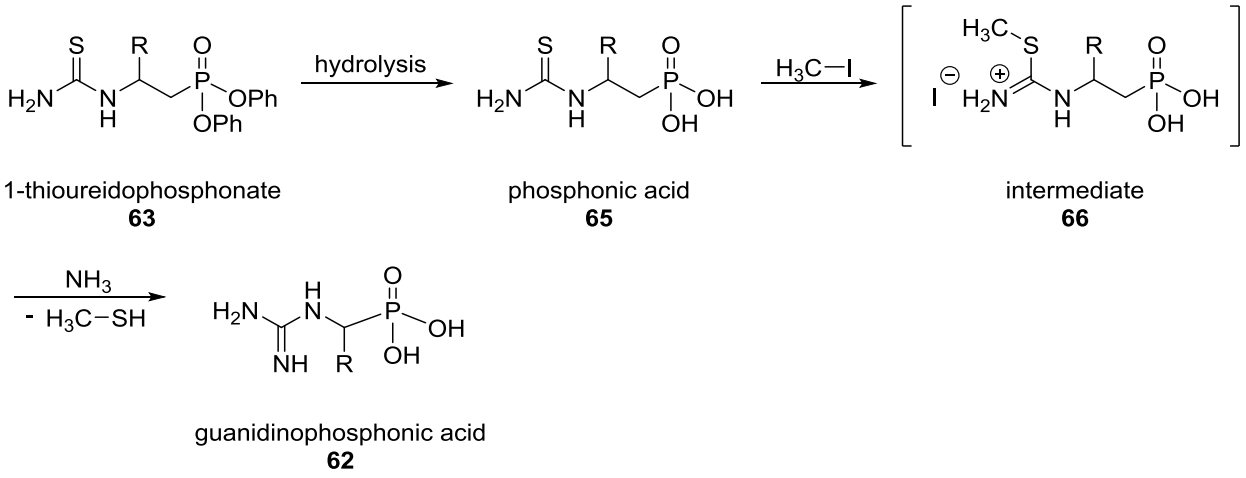

Figure 3.10 Synthesis of guanidinophosphonic acid 62.

Since 1*H*-pyrazole-1-carboxamidine hydrochloride **55** is commercially available at a reasonable price, we chose to use the first method to introduce the guanidinium functionality into compound **54**. Although we opted for the commercially available guanidylating agent **55**, it is important to know that other guanidylating agents bearing alkyl substituents on the amine can be synthesized. The deprotected diethyl (aminomethyl)phosphonate **54** is coupled with 1*H*-pyrazole-1-carboxamidine hydrochloride **55** in refluxing THF under basic conditions to give the zwitterion **56** in which one of the ethyl esters was also cleaved (Figure 3.11). [191]

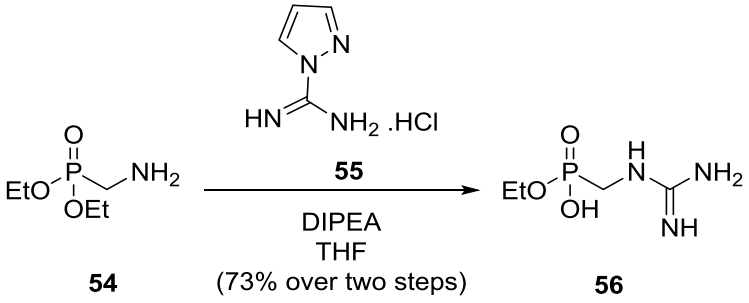

Figure 3.11 Guanidylation reaction of phosphonic acid 54.

This cleavage presumably occurred via nucleophilic attack at the methylene carbon of the ethyl protecting group (Figure 3.12). The original solvent used for guanidylation of compound **54** was anhydrous DMF which facilitates nucleophilic reactions more than THF. We imagined that switching the solvent from DMF to THF will result in the depression of the S_N2 reaction and hence, eliminate the side reaction involving the cleavage of an ethyl group. To our surprise, anhydrous THF gave the same mono-ester product as that of observed with DMF. Since the next step in synthesis involves the removal of the ethyl protecting groups, this unwanted side reaction did not affect the outcome of the overall synthesis.

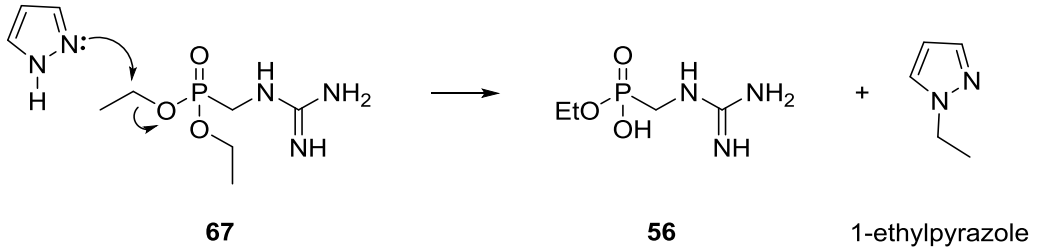

Figure 3.12 Possible side reaction resulting in the cleavage of an ethyl group from phosphonic acid diester 67.

The second ester was cleaved using TMS-Br to give the free phosphonic acid **52** (Figure 3.13). Then the pyrophosphate linkage was introduced via a carbonyl diimidazole coupling with phosphoric acid to give inhibitor **19**. [195] We will discuss the different strategies we employed to make the P-O-P bond in the following section.

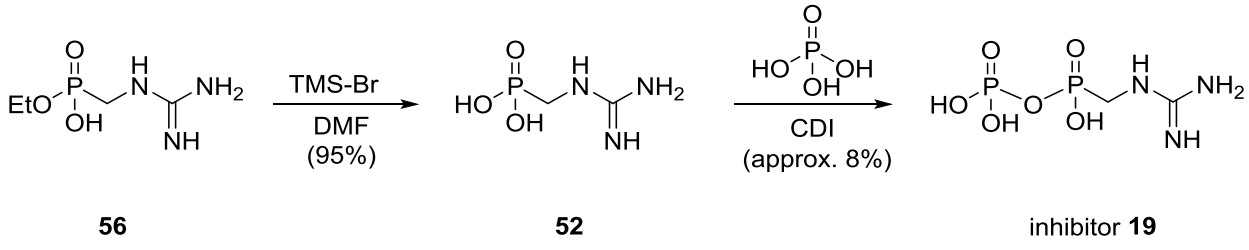

Figure 3.13 Deprotection and introduction of the pyrophosphate linkage.

Different strategies were investigated for performing the final step of the synthesis. Our first attempt at the synthesis of phosphorylated phosphonate **19** involved a modification of Michelson conditions. [196] Phosphonic acid **52** was first converted to its tri-*n*-butylammonium salt to obtain better solubility in organic solvents. It was next activated by reaction with diphenylphosphochloridate **68** to give the phosphorylated phosphonate **69** (Figure 3.14). Displacement of the diphenylphosphate group in **69** was achieved by reaction with tri-*n*-butylammonium salt of phosphoric acid, which was prepared by stirring phosphoric acid with tri-*n*-butylamine in anhydrous methanol. [197]

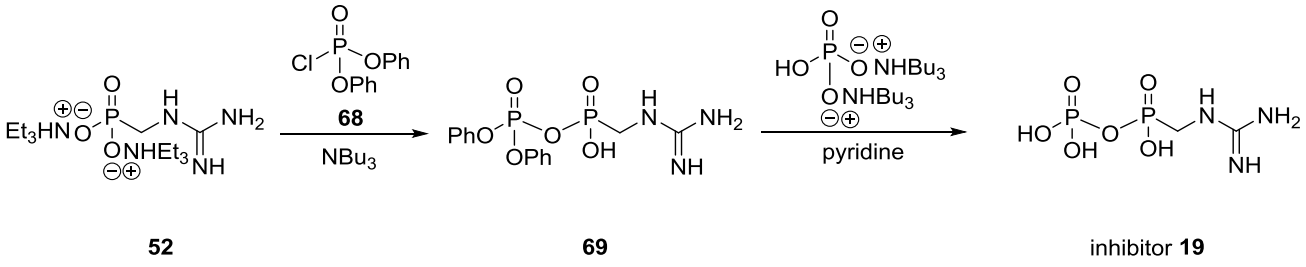

Figure 3.14 Introduction of the pyrophosphate linkage into phosphonic acid 52 using an anion exchange approach.

While the P-O-P bond was successfully formed using this method, it required several preparative steps that made this approach tedious and time consuming. Alternatively, compound **52** can be coupled to phosphoric acid in a CDI mediated reaction to form the inhibitor **19**. *N,N'*-Carbonyldiimidazole (CDI) is a coupling reagent that is typically employed to activate carboxylic acids in amide and ester bond formation reactions. [198] When compared to *N,N'*-dicyclohexylcarbodiimide DCC, the application of CDI is much more efficient as the by-products formed are only CO_2 and imidazole. Imidazole is soluble in a variety of solvents such as water, alcohol, ether, chloroform and pyridine and can be easily removed. The conversion

generally occurs as a one-pot reaction in two stages. First, the phosphonic acid **52** is transformed to its corresponding imidazolide **70** through the reaction with CDI (Figure 3.15). This imidazolide intermediate subsequently reacts with phosphoric acid to give inhibitor **19**. [199] Inhibitor **19** was then purified using anion exchange chromatography.

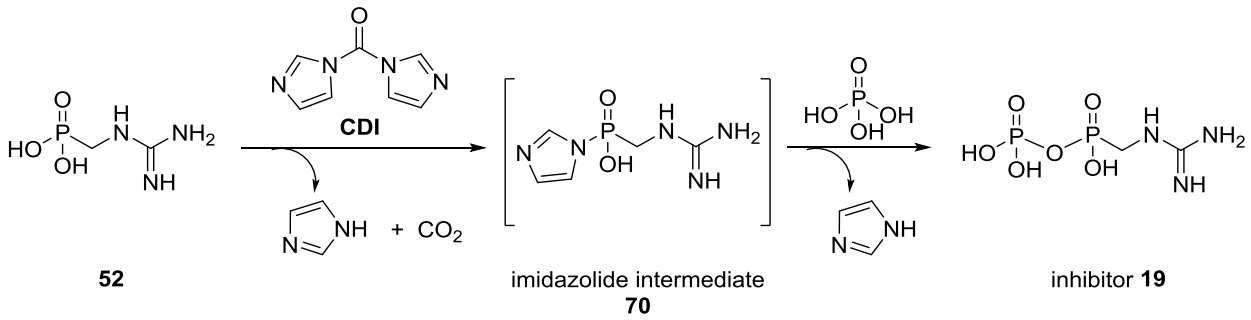

Figure 3.15 CDI mediated coupling reaction to form inhibitor 19.

Our first attempt at purifying inhibitor **19** involved anion exchange chromatrography using AG-1X8 resin. Crude reaction mixture was loaded onto a column of AG-1X8 resin (formate form) and was eluted with various concentrations of formic acid. ^{31}P NMR analysis of the collected fractions did not reveal product as evident by the absence of a doublet of doublet due to the phosphophosphonate linkage. The next method investigated the use of diethylaminoethanol (DEAE) cellulose (DE 52) anion exchange resin. Crude reaction mixture was loaded noto a column of DE 52 and was eluted with various concentrations of freshly prepared triethylammonium bicarbonate buffer (TEAB). All collected fractions were lyophilized and analyzed by ^{31}P NMR spectroscopy. It was shown that inhibitor **19** was purified by anion exchange chromatography using DE 52 resin, but was found to co-elute with phosphate. Column fractions containing the least amount of phosphate were converted to their sodium form and further purified by precipitation from water by the addition of ethanol. In this manner a sample

of inhibitor **19** could be obtained that contained 4 equivalents of phosphate as judged by ^{31}P NMR integration. Traces of compound **52** and pyrophosphate (<10%) also accumulated upon extended handling of the compound, presumably due to phosphate anhydride exchange reactions that occurred during lyophilization (Figure 3.16). This would occur upon heating, or from acidic or basic conditions, and during lyophilization. The amount of phosphate also increased upon handling the compound presumably due to hydrolysis of the phosphophosphonate linkage. As a stability test, a sample of inhibitor **19** was dissolved in D_2O under neutral conditions and monitored using ^{31}P and ^{1}H NMR spectroscopy. No sign of decomposition was observed upon storage for a one-week period at room temperature. However, up to 20% decomposition was observed when solutions of inhibitor **19** were stored in freezer for up to 3 months and thawed for NMR analysis. This is rather unexpected as the pyrophosphate linkage is usually kinetically stable. We believe that the nucleophilic attack on the phosphorous atom of **19** is facilitated by the proximity of the positively charged guanidinium moiety to the negatively charged oxygen atoms in compound **52** and hence; making it a better leaving group.

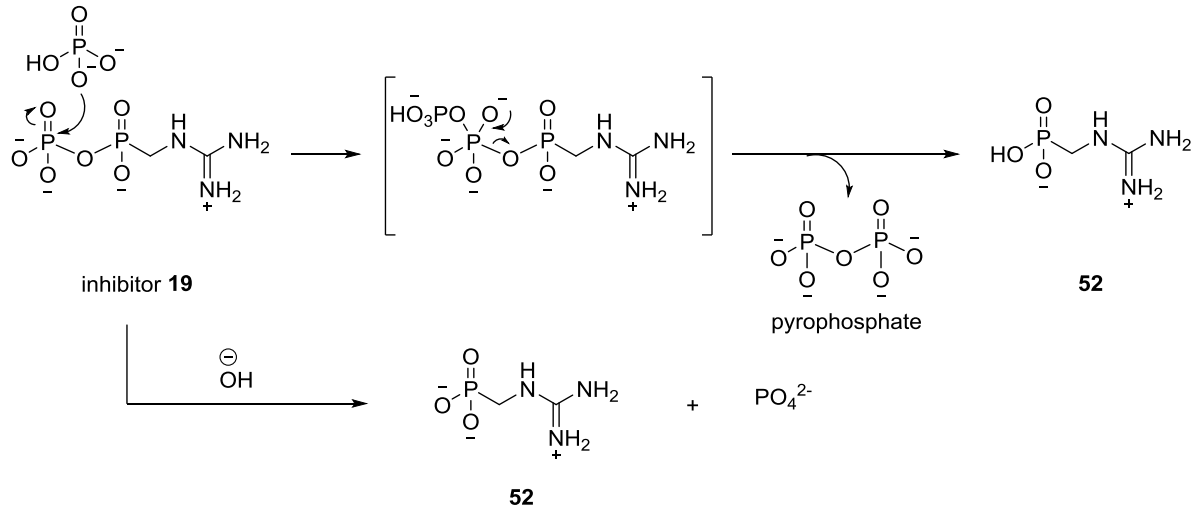

Figure 3.16 Degradation of inhibitor 19 to give compound 52 and either pyrophosphate or phosphate (pH ~ 9).

The yield of the last step of synthesis was determined by the addition of an internal standard of 1,4-dioxane of known concentration. Column fractions containing the least amount of phosphate were pooled and dissolved in 1,4-dioxane (1.0 mM). The yield was estimated using ^{1}H NMR spectroscopy and the integration of the appropriate signals (see section 3.3.1). In this manner a yield of approximately 8% was calculated.

3.2.3 Characterization of Inhibitor 19

Inhibitor **19** was structurally characterized using NMR spectroscopy. The ^{1}H NMR spectrum of inhibitor **19** showed a signal for the methylene protons at 3.51 ppm (Figure 3.17A), which appears as a doublet due to the coupling to the adjacent P atom. The doublet corresponding to the methylene protons of the impurity, compound **52**, appeared at 3.15 ppm. The proton-decoupled ^{31}P NMR spectrum of inhibitor **19** showed a set of two doublets at 1.64 and -9.32 ppm which is characteristic of the phosphophosphonate linkage (Figure 3.17B). The signal corresponding to the phosphate impurity appeared as a singlet at 0 ppm.

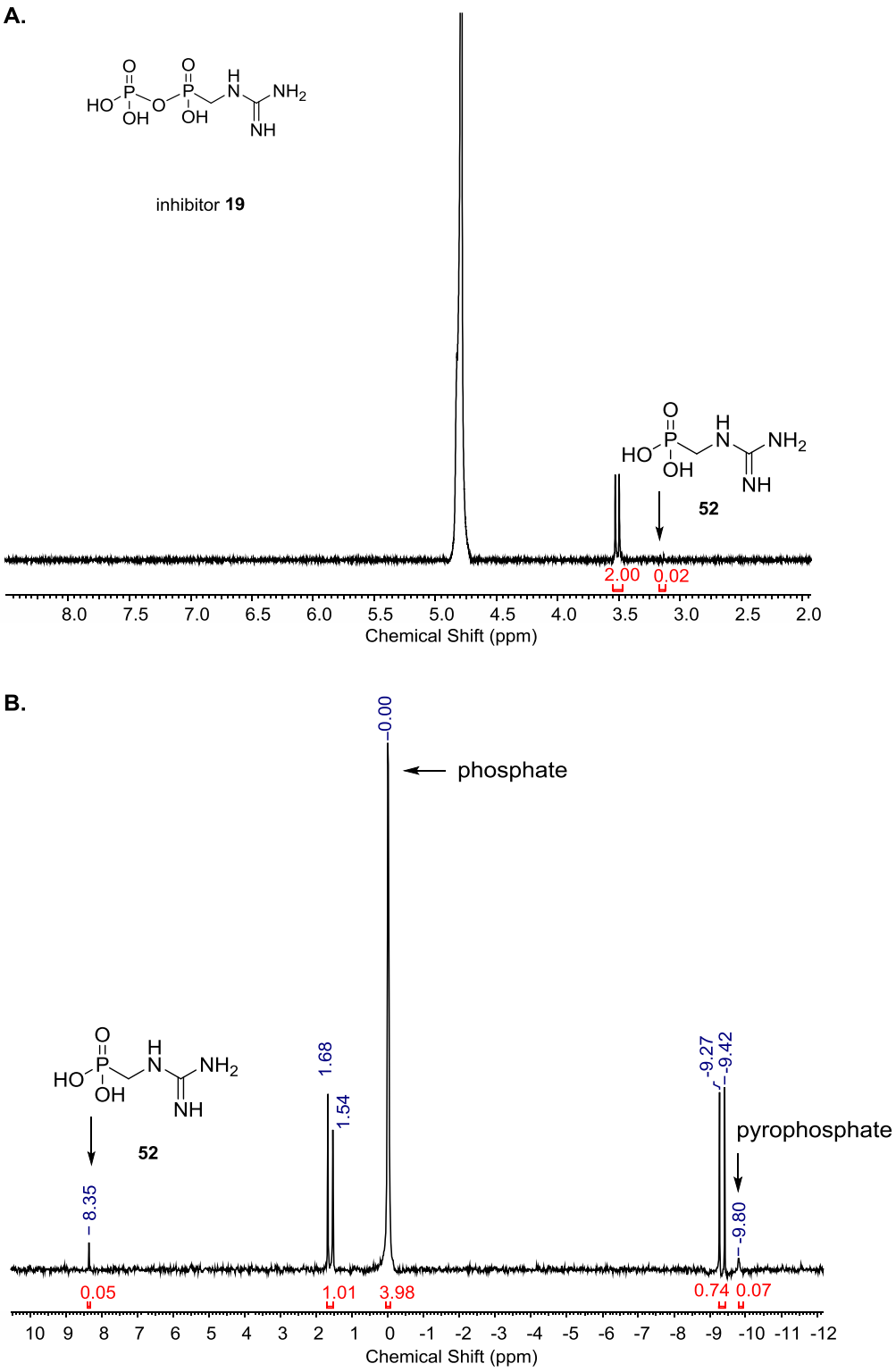

Figure 3.17 Characterization of inhibitor 19 using A) ^{1}H (400 MHz) and B) ^{31}P (162 MHz) NMR spectroscopy (D_2O).

Since only milligram quantities of inhibitor **19** were obtained, the ^{13}C chemical shifts were measured indirectly using 2D NMR spectroscopy. The HSQC spectrum showed a correlation between the signal corresponding to the methylene protons (3.51 ppm) and the carbon signal of the C-1 atom (39.6 ppm), which is coupled to the neighboring P atom and therefore, appeared as a doublet (Figure 3.18A). Moreover, the HMBC spectrum of inhibitor **19** showed a correlation between the signal of the methylene protons (3.51 ppm) and the carbon signal of the C-3 atom of the guanidinium moiety (157.3 ppm) (Figure 3.18B).

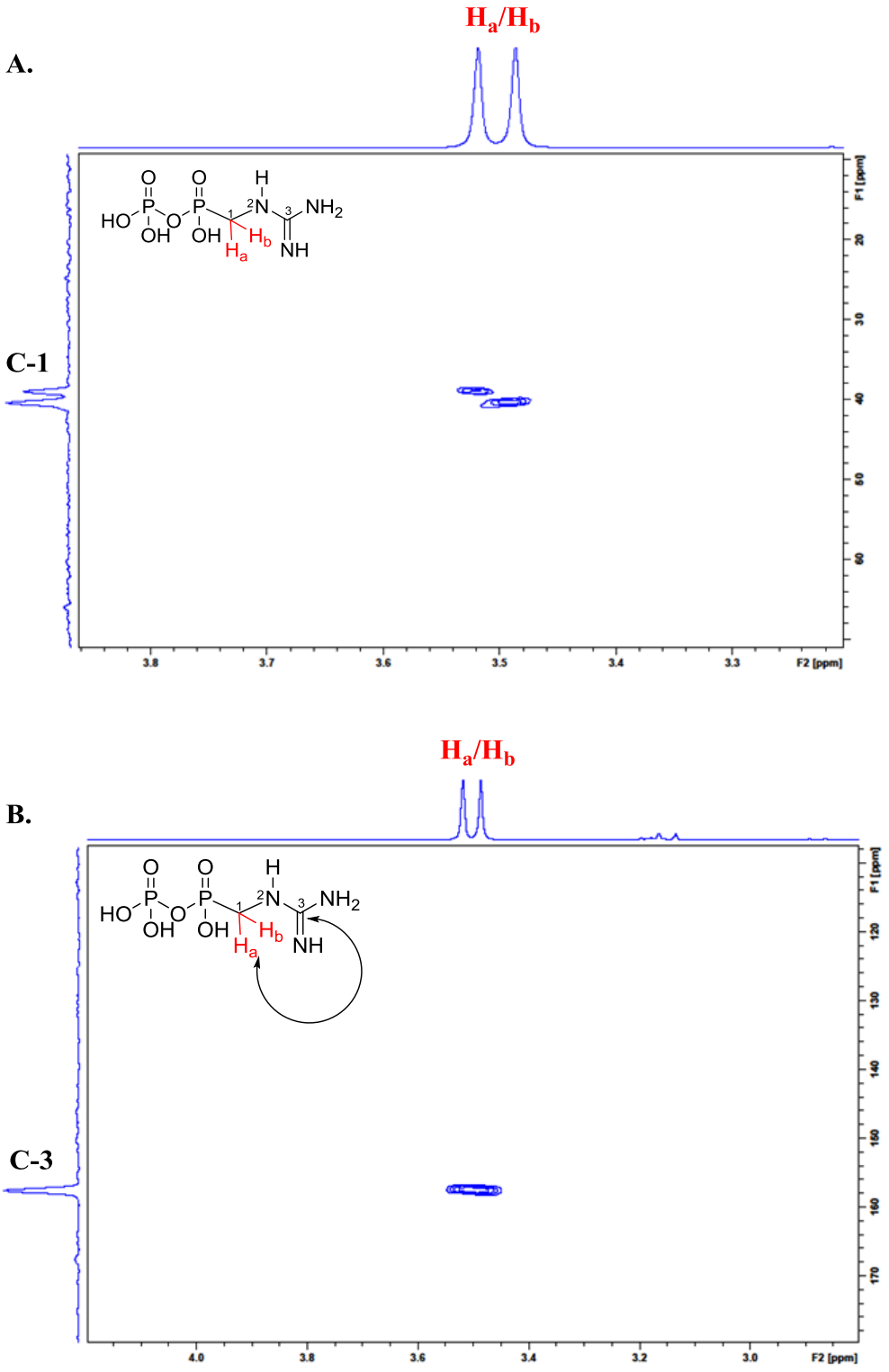

Figure 3.18 The HSQC (A) and HMBC (B) spectra of inhibitor 19 (400 MHz, D_2O).

Following the characterization of inhibitor **19**, we proceeded to the next step which involved the purification of 4-DMATS and the testing of compound **52** as an inhibitor. The following sections will describe our inhibition studies with inhibitor **19**.

3.3 Overexpression and Purification of 4-DMATS

The gene encoding for dimethylallyltryptophan synthase *fgaPT2* from *Aspergillus fumigates* was synthesized by Genscript and cloned into a pET28a plasmid as described previously. [96] The conditions used for overexpression and purification of His-tagged 4-DMATS are identical to those described previously for His-tagged FtmPT1, CdpNPT, and CpaD. [96] Approximately 25 mg of 4-DMATS was purified from 1 litre of cell culture using this method, and was found to be stable when stored at -80 °C for up to six months.

3.3.1 Inhibition Assay of Compound 19

The inhibitory effect of compound **19** towards the activity of 4-dimethylallyltryptophan synthase (4-DMATS) was studied using a continuous coupled assay monitoring the release of free phosphate (Figure 3.19). [96,200] Since the by-product of the 4-DMATS reaction is pyrophosphate, the enzyme pyrophosphatase was added to catalyze its hydrolysis into two equivalents of phosphate. This phosphate then acts as a substrate for another coupling enzyme purine nucleoside phosphorylase (PNP). PNP acts on 2-amino-6-mercapto-7-methylpurine ribonucleoside (MESG) to generate ribose-1-phosphate and 2-amino-6-mercapto-7-methylpurine as products. At a neutral pH, MESG shows a maximum UV absorbance at 330 nm while 2-amino-merapto-7-methylpurine exhibits a maximum UV absorbance at 360 nm (Figure 3.19, curve **A** and **B**, respectively). Therefore, as 4-DMATS catalyzes the prenylation reaction of L-

tryptophan and the enzymatic reaction is followed spectrophotometrically, an increase in absorbance at 360 nm is expected.

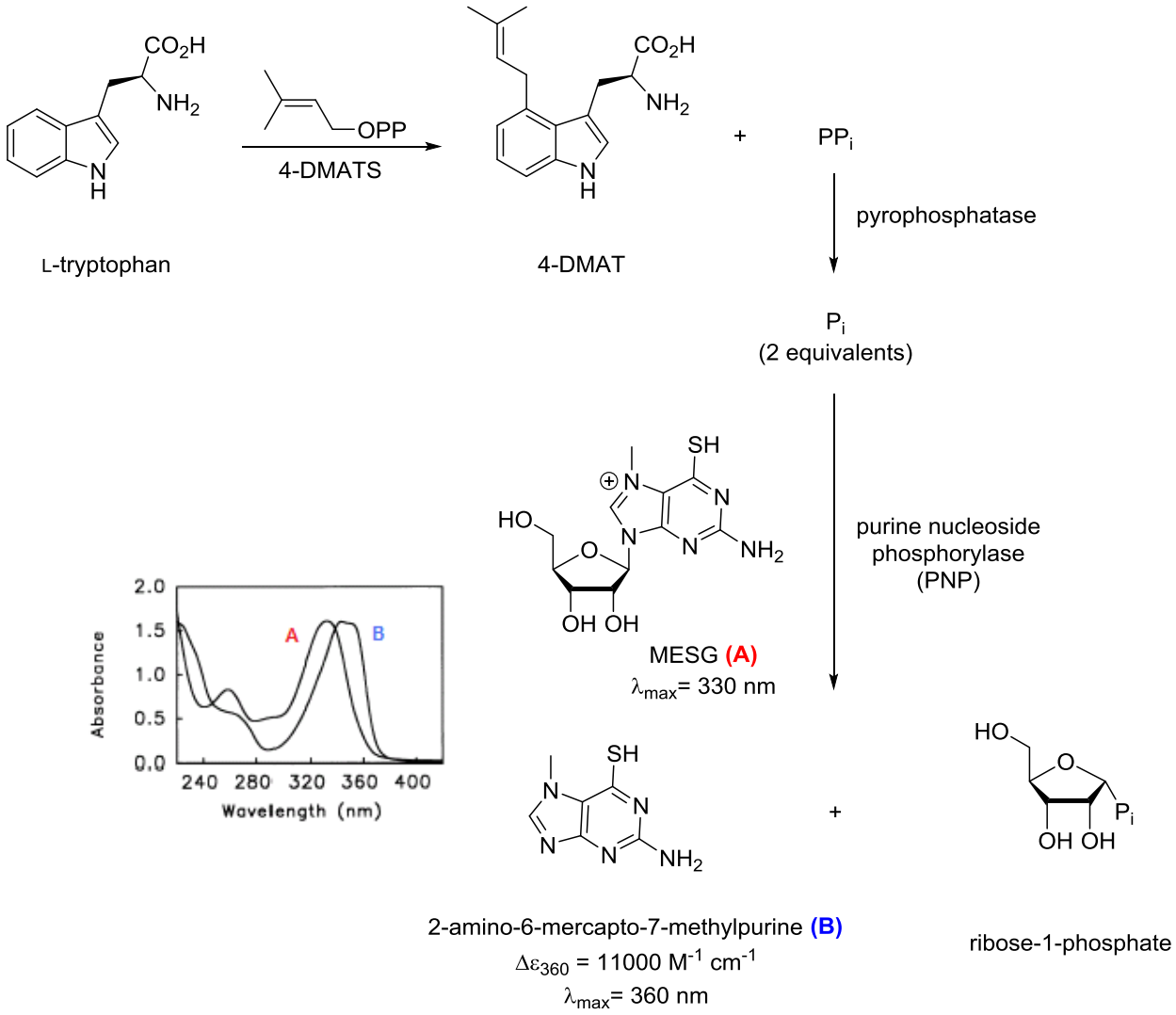

Figure 3.19 A continuous coupled assay for the reaction catalyzed by 4-DMATS. The inset shows the wavelength-dependent absorbance curves of compounds (A), MESG, and (B) 2-amino-6-mercapto-7-methylpurine.

Prior to performing the inhibition studies, the kinetic constants of the reaction catalyzed by 4-DMATS were obtained using the coupled assay described above. The initial velocity of the prenylation reaction was measured at a series of concentrations of DMAPP. By keeping the

concentration of L-tryptophan constant (20 μM) and varying the concentration of DMAPP (0.3 μM - 2.0 μM), a hyperbolic kinetic profile was observed (Figure 3.20). Upon fitting the data to the Michaelis-Menton equation, a K_M value of 1.82 ± 0.02 μM and a k_{cat} value of 0.65 ± 0.06 s^{-1} were obtained.

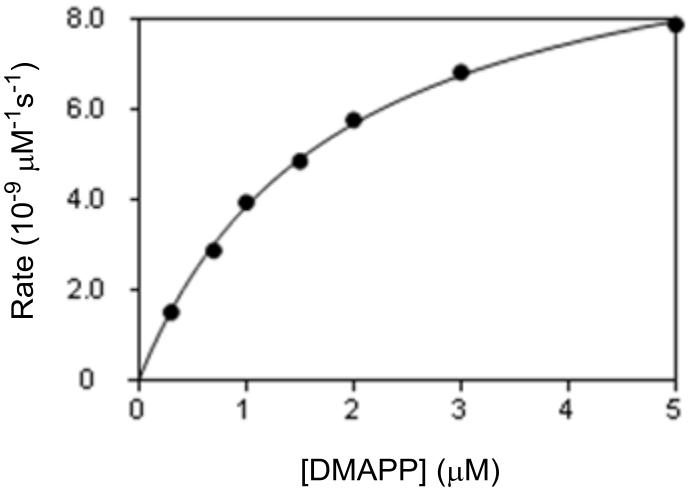

Figure 3.20 A plot of initial velocity vs. DMAPP concentration for the reaction catalyzed by 4-DMATS. The kinetic parameters were determined by fitting the data to the Michaelis-Menten equation and are as follows: k_{cat} = 0.65 ± 0.06 s^{-1} and K_M = 1.82 ± 0.02 μM. Kinetic parameters were determined in Tris-HCl buffer (50 mM, pH 7.5), with [L-Trp] = 20 μM and [4-DMATS] = 7 nM at 35 °C.

Due to the instability of compound **19** and complications associated with its purification, the final sample of **19** was found to be a mixture containing the desired inhibitor **19**, phosphate (4 equiv.), and traces (<10%) of both pyrophosphate and compound **52**. Despite the presence of these impurities, performing the assay in a particular order enabled us to measure the inhibition parameters. First of all, the presence of a phosphate impurity as well as the trace amounts of pyrophosphate did not affect the results of our kinetic studies. Both are immediately consumed during a pre-incubation period prior to initiation with 4-DMATS. We found that a 3 minute pre-

incubation was sufficient to remove all phosphate impurities present in the reaction mixture. Since small quantities of compound **52**(<10%) were also present in the inhibitor **19** mixture, it was necessary to rule out the possibility that compound **52** can act as an inhibitor of 4-DMATS. Independent analysis of the precursor, compound **52**, showed no inhibition at concentrations below 100 μM.

Given that inhibitor **19** had ionic impurities, counter ions, and waters of hydration, it was not practical to measure amounts directly by weight. Therefore, in order to determine the concentrations of stock solutions of inhibitor **19**, an internal standard was added to the samples. A solution of inhibitor **19** was prepared in 1.0 mM dioxane in D_2O and the integration of the appropriate ^1H NMR signals were employed to approximate the concentrations. Besides the doublet at 3.15 ppm that belongs to compound **52**, the ^1H NMR spectrum contains two key signals: a singlet at 3.77 ppm that corresponds to the 8 protons of dioxane and a doublet at 3.52 ppm that represents the methylene protons of the inhibitor **19** (Figure 3.21). The latter two signals were used to approximate the concentration of inhibitor **19** in solution (in the case shown below [inhibitor **19**] = 4.3 mM).

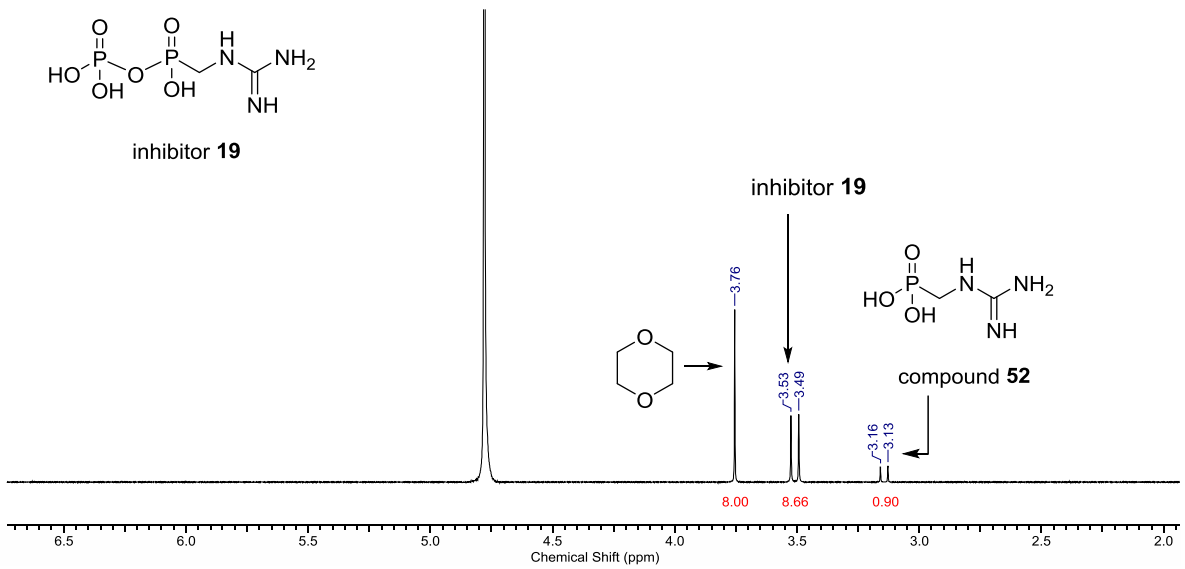

Figure 3.21 ^{1}H NMR spectrum of inhibitor 19 in D_2O with 1,4-dioxane (1.0 mM) as internal standard (D_2O, 400 mHz). Impurities of compound **52** can also be observed.

To test the inhibitory properties of compound **19**, cuvettes containing L-tryptophan and DMAPP were prepared in a buffered solution (pH 7.5). To these cuvettes were added inhibitor **19** and all the reagents and coupling enzymes required to perform the coupled assay. The cuvettes were thermally equilibrated for 5 minutes at 35 °C before the enzymatic reaction was initiated by the addition of 4-DMATS. Initial velocities were obtained with a fixed concentration of L-Trp (20 μM) and variable concentrations of DMAPP (0.3 μM - 2.0 μM) and inhibitor **19** (0 μM – 0.6 μM, approximately). Inhibitor **19** was found to be a potent 4-DMATS inhibitor with a K_i value of approximately 240 nM as evident in the Dixon plot shown in Figure 3.22A. Moreover, the parallel lines in the Cornish-Bowden plot demonstrated that the inhibition was competitive against DMAPP as can be seen in Figure 3.22B. Subsequent NMR analysis of the stock sample of inhibitor **19** that had been stored in the freezer indicated that approximately 20% had decomposed upon storage. Therefore, the reported K_i value perhaps bears as much as 20% error.

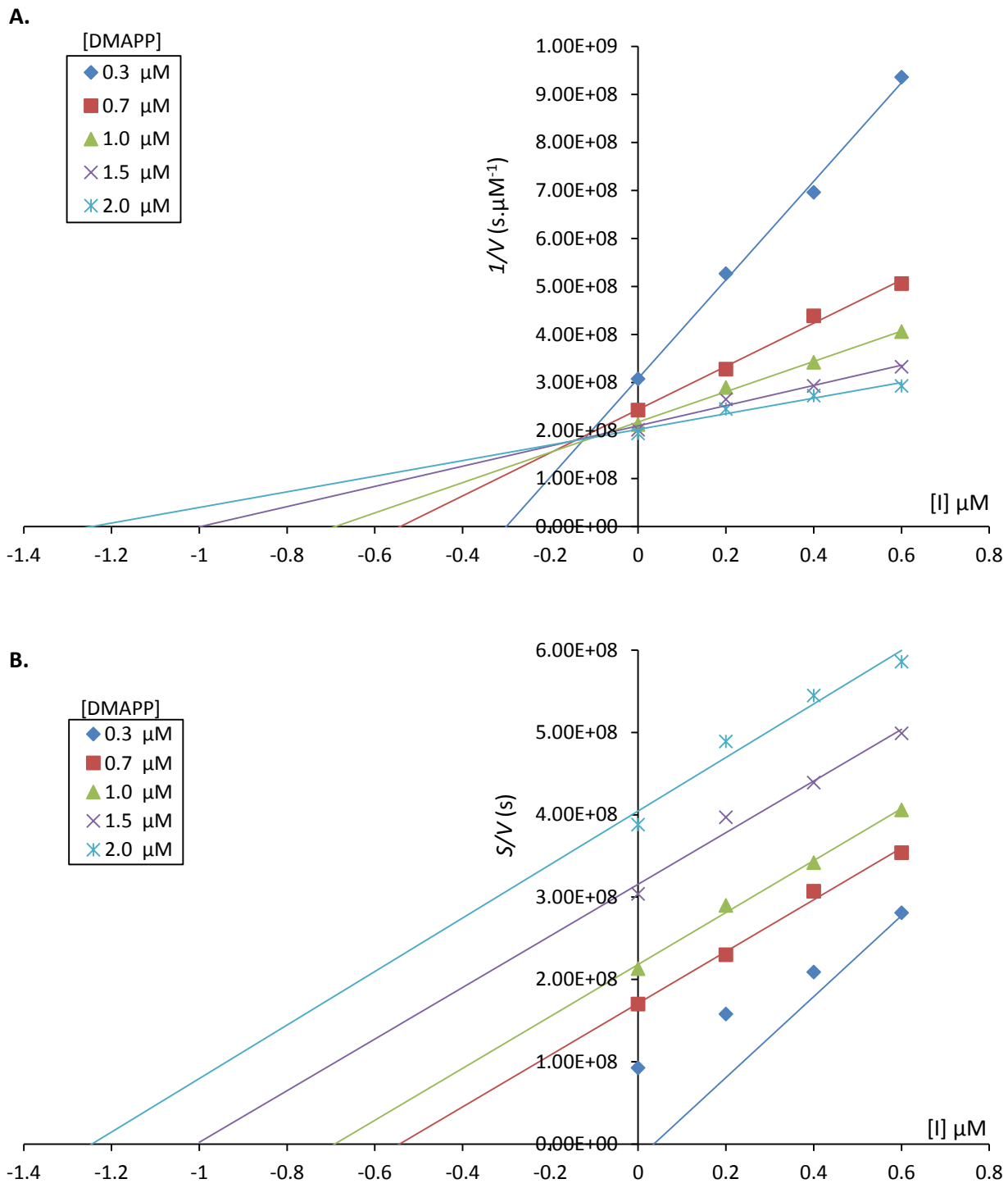

Figure 3.22 Kinetic analysis of the inhibition of the 4-DMATS reaction by inhibitor 19. A) The upper panel shows a Dixon plot with intersecting lines at sub-micromolar concentrations. B) The lower panel shows a Cornish-Bowden plot with parallel lines that are indicative of competitive inhibition.

Our kinetic results show that compound **19** is a competitive inhibitor of 4-DMATS with a sub-micromolar K_i value. The observation that inhibitor **19** binds significantly tighter than DMAPP (K_M = 1.82 μM) strongly suggests that it mimics the properties of the carbocation-pyrophosphate ion pair or the transition state leading to it. Thus, inhibitor **19** represents a promising new strategy for prenyltransferase inhibition, in which a guanidinium group is used to mimic an allylic carbocation. While the partial purification of compound **19** enabled us to conduct preliminary kinetic studies, obtaining a pure sample is essential for future work. Given the presence of a hydrolyzable P-O-P bond that resulted in gradual decomposition of compound **19** over time, further efforts in the Tanner lab will focus on more stable analogs of inhibitor. For the above reasons, the kinetic data presented in this chapter are primarily qualitative in nature and further studies would require addressing the instability and purification issues.

3.4 Conclusion and Summary

In this chapter, we described the design, synthesis, and testing of a water-soluble inhibitor of the prenyltransferase enzyme 4-DMATS. Inhibitor **19** was synthesized in four steps from commercially available starting materials and purified using anion-exchange chromatography. During the last step of synthesis, excess phosphoric acid was used to introduce the P-O-P linkage. The separation of unreacted phosphate from inhibitor **19** proved to be challenging as they co-eluted even under careful gradient elution conditions. Further purification of the fractions containing the mixture of inhibitor **19** and phosphate was achieved through several precipitation steps from ethanol. Upon extended handling of inhibitor **19**, traces of phosphonic acid **52**, pyrophosphate, and increasing amounts of phosphate accumulated in the sample. Since the P-O-P bond in inhibitor **19** is susceptible to both phosphorolysis and hydrolysis, a gradual

increase in the amount of these impurities was observed. These unfavorable side reactions were considered as the main source of error in our kinetic studies. Finally, compound **19** was tested as an inhibitor of 4-DMATS and was found to be a competitive inhibitor of this enzyme (against DMAPP) with a sub-micromolar K_i value. Due to the instability of the inhibitor and the difficulties in purification, the kinetic characterization was not further pursued. Nevertheless, this study provided valuble information indicating that guanidinium-based diphosphates could act as potent prenyltransferase inhibitors.

The promising inhibitory properties of inhibitor **19** suggests that this compound bears remarkable structural resemblance to the dimethylallyl carbocation/pyrophosphate ion pair, or the transition state that leads to its formation. A structural analysis of 4-DMATS in a complex with L-Trp and the non-hydrolyzable version of DMAPP, dimethylallyl *S*-thiolodiphosphate (DMSPP), shows that the prenyl group is sandwiched between the indole of the L-Trp substrate and the phenolic ring of an active site tyrosine residue 345 (Figure 3.23A). [97] Consequently, it has been suggested that the dimethylallyl carbocation is stabilized through π-cation interactions on both faces. One can imagine that the planar geometry of the guanidinium moiety in inhibitor **19** results in a similar binding mode in the active site. Furthermore, binding to the diphosphate moiety is facilitated by electrostatic interactions with five lysine and arginine residues as well as hydrogen bonding with multiple tyrosine residues (Figure 3.23B).

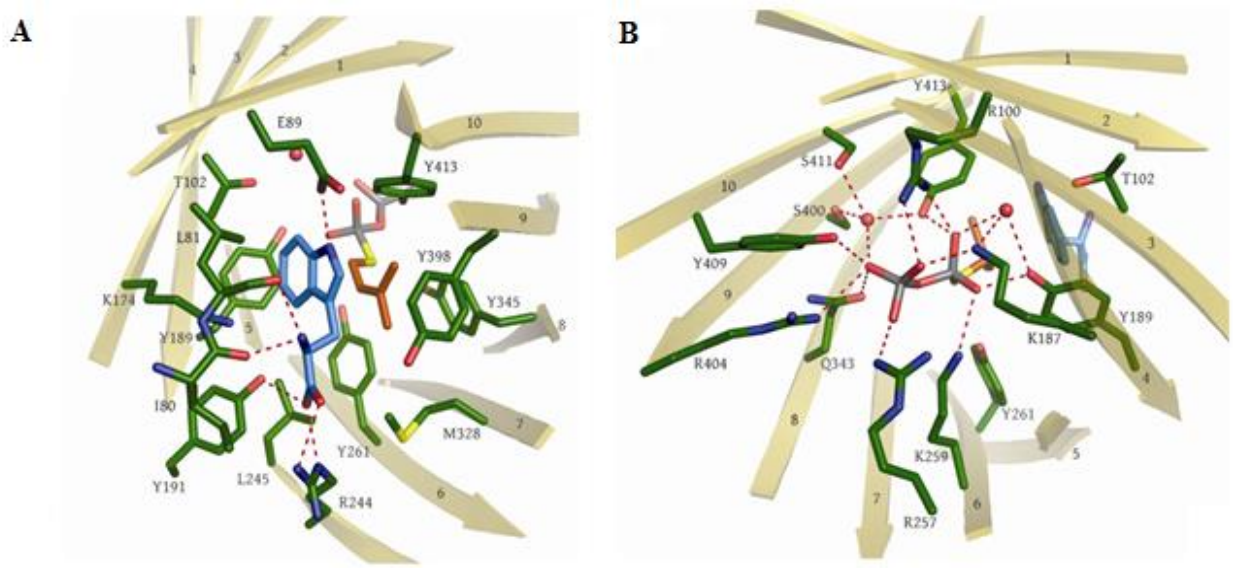

Figure 3.23 Active site structure of 4-DMATS. (A) the binding pocket for L-tryptophan and the dimethylallyl chain of DMSPP are displayed. (B) view of the DMSPP in the active site and the residues binding to the pyrophosphate are shown.[97]

Inhibitor **19** shows strong structural similarities to the widely-used nitrogen containing bisphosphonates including zoledronate and BPH-678 (Figure 3.24). In addition to the usual bisphosphonate linkage, they carry a resonance-delocalized cation that is attached to the P-C-P linkage. These compounds are potent inhibitors of human farnesyl diphosphate synthase with IC_{50} values of 1.2-3.0 nM and 12 nM, respectively. [137,158]

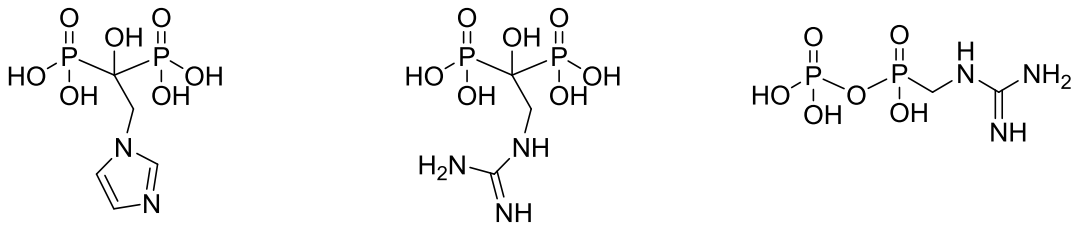

Figure 3.24 Structures of nitrogen-containing bisphosphonates that contain resonance delocalized cations. Structure of inhibitor **19** is shown for comparision.

We believe that it is likely that inhibitor **19** and suitably substituted derivatives will also show potent inhibition of the metal-dependent prenyltransferases, such as farnesyl diphosphate synthase, and that the structural differences between these compounds and the bisphosphonates may give rise to desirable properties. Inhibitor **19** contains a "side-on" linkage between the guanidinium and the pyrophosphate moieties whereas in the literature-known bisphosphonates the positive charge is attached onto the carbon bridging the phosphorus atoms (Figure 3.24). The former situation is a closer mimic of the actual prenyltransferase transition states and may lead to tighter binding in certain cases. In addition, the absence of an alcoholic functionality disrupts the structure of the "bone hook" and should decrease problems associated with binding to bone and rapid clearance. The results of a recent study in our lab performed by a post-doctoral fellow, Dr James Morrison, indicated that zoledronate does not inhibit 4-DMATS at concentrations below 200 μM. This finding implies that inhibitor **19** is selective for metal-independent aromatic prenyltransferases and that much of the bisphosphonate binding energy comes from metal chelation.

3.5 Future Directions

The potent inhibition of 4-DMATS observed with inhibitor **19** has provided incentive for the Tanner lab to pursue the development of a new generation of prenyltransferase inhibitors. As described earlier, the structure of inhibitor **19** comprises a P-O-P linkage that has been shown to be prone to hydrolysis (Figure 3.16). The first logical strategy towards the synthesis of a more stable inhibitor would involve the conversion of the labile P-O-P bridge to a more robust and non-hydrolyzable P-CH_2-P linkage. It is expected that exchanging the oxygen atom for a methylene group will generate a more stable bisphosphonate inhibitor that will be amenable to

purification. The first inhibitor that would satisfy these requirements would be compound **71** where the P-CH_2-P linkage has been installed and the rest of the molecule has been kept intact (Figure 3.25). A PhD student in our group, Walid Abdelmagid, is pursuing this project and has successfully completed the synthesis of compound **71** in 9 steps. Compound **71** was tested as an inhibitor of 4-DMATS using the same coupled assay and a K_i value of 4 μM was measured. This increase in the K_i value could be due to the substitution of the more electronegative bridging oxygen atom with a less electronegative carbon atom. This could subsequently increase the pK_a values of the neighboring phosphonate groups. Since interactions with the negative charges are presumably extremely important for binding, loss of even one charge could dramatically affect the K_i value. One possible strategy to address this issue involves the introduction of electron-withdrawing groups (such as F and OH) onto the bridging carbon (Figure 3.25). While the resulting compounds **72** and **73** maintain the desired non-hydrolyzable P-C-P linkage, the introduction of -F and -OH groups should help to keep the phosphonate groups fully ionized. These new bonds resemble the original P-O-P linkage in inhibitor **19** more closely and thus, an enhancement in the inhibitory properties could be expected.

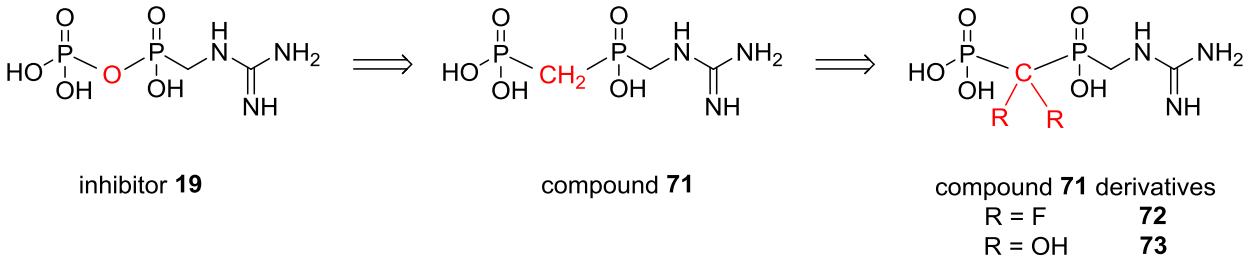

Figure 3.25 Structures of potential competitive inhibitors of 4-DMATS

We propose two other molecules that can act as intermediate/transition-state based inhibitors of 4-DMATS, compound **74** and **75** (Figure 3.26). In the former **74**, the terminal nitrogen of the guanidinium moiety is decorated with two methyl groups. This substitution provides the inhibitor with even more structural similarity to the proposed transition state as it bears methyl groups that mimic those of the dimethylallyl cation (Figure 3.27). Furthermore, one can imagine that the introduction of alkyl groups onto the terminal nitrogen could facilitate the purification step and improve the overall yield. In a similar sense, long alkyl chains could be appended to the terminal nitrogen to make inhibitors against farnesyl and geranyl diphosphate prenyltransferases (not shown here).

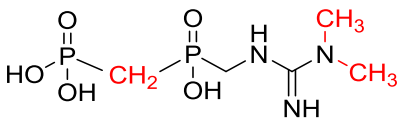

compound **74**

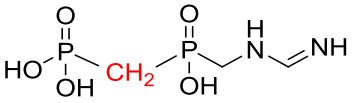

compound **75**

Figure 3.26 Structures of two inhibitors with modification on the guanidinium side of the molecule.

In the latter example, compound **75**, one of the amine groups of the guanidinium functionality is removed to give an amidinium functionallity. This serves to localize the resonance stabilized positive charge onto just two nitrogen atoms, instead of three in the guanidinium-based inhibitors. This will more closely mimic the structure of the dimethylallyl cation intermediate (Figure 3.27). Finally, future endeavors involve testing these potential inhibitors against other prenyltransferase enzymes, such as human farnesyl diphosphate synthase.

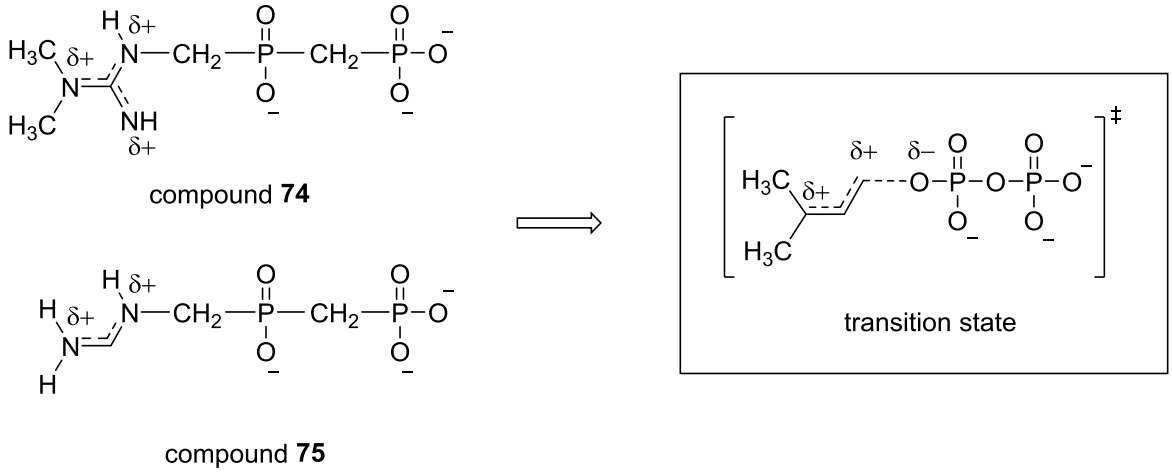

Figure 3.27 Structures of compounds 74 and 75 with the related charges. The inset displays the structure of transition state in the reaction catalyzed by 4-DMATS. This structure is provided for ease of comparison.

3.6 Experimental Procedures

3.6.1 Materials and Methods

All reagents were purchased from Sigma-Aldrich, Fluka, Toronto Research Chemicals Inc. (TRC), or Advanced ChemTech (Louisville, KY) and used without further purification unless otherwise stated. Isopropyl-β-D-galactopyranoside (IPTG) was purchased from Invitrogen. D_2O (99.9%) was purchased from Cambridge Laboratories. Dowex® 50WX8 (H^+ form) resin was purchased from Sigma-Aldrich. Tetrahydrofuran (THF) was distilled from sodium and benzophenone under an atmosphere of Ar. Triethylamine was distilled over CaH_2 under an atmosphere of Ar. Silica gel chromatography was performed using Silica Gel SiliaFlash F60 (230-400 mesh, Silicycle).

^{1}H NMR spectra were recorded on a Bruker AV400 spectrometer at a field strength of 400 MHz. Proton-decoupled ^{31}P NMR spectra were recorded on Bruker AV400 spectrometer at a field strength of 162 MHz. ^{13}C NMR spectra were recorded on Bruker AV400 spectrometer at a field strength of 100 MHz. Mass spectra were obtained on a Waters Micromass LCT mass spectrometer using electrospray ionization (ESI-MS). Neutral compounds were detected as positive ions, and negatively charged compounds were detected as negative ions.

3.6.2 Synthesis of Inhibitor 19

3.6.2.1 Synthesis of Diethyl (Aminomethyl)phosphonate (54)

Compound **54** was prepared following a previously described procedure. [189] To a stirred solution of commercially available diethyl (phthalimidomethyl)phosphonate **53** (5.0 g, 16.8 mmol) in 10 mL ethanol was added hydrazine hydrate (896 mg, 1.52 mL, 17.9 mmol) and the reaction mixture was left stirring at room temperature for 3.5 days. Following the completion of reaction, the white precipitates were filtered and ethanol was evaporated under reduced pressure to give compound **54** as white solids, which were used in the following step without further purification (2.48 g). ^{1}H NMR and ESI-MS data were identical to those reported in the literature. [189]

3.6.2.2 Synthesis of Ethyl (Guanidinomethyl)phosphonate (56)

To a mixture of the crude diethyl (aminomethyl)phosphonate **54** and 1H-pyrazole-1-carboxamidine hydrochloride **55** (2.66 g, 18.2 mmol) in 30 mL anhydrous THF was added diisopropylethylamine (2.35 g, 3.16 mL, 18.2 mmol) under an Ar atmosphere. [191] The reaction

was heated at 60 °C for 18 h. Removal of the solvent under reduced pressure resulted in an oily residue which was stirred in 20 mL CH_2Cl_2. The resulting solids were removed by filtration and rinsed with 10% MeOH in CH_2Cl_2. They were then dissolved in 20 mL water and washed with three portions of 30 mL of EtOAc. Removal of the water under reduced pressure gave 2.12 g of reaction product **56** (73% over two steps). ^{1}H NMR (D_2O, 400 MHz): δ ppm 3.98 (m, 2H), 3.41 (d, 1H, *J* = 11.9 Hz), 1.27 (t, 3H, *J* = 7.2 Hz). ^{31}P NMR (D_2O, 162 MHz): δ ppm 16.77 (s). ^{13}C NMR (D_2O, 100 MHz): δ ppm 157.36 (s), 61.58 S4 (s), 38.22 (d, *J* = 146.0 Hz), 15.91 (s). HRMS (ESI) *m/z* calcd for $[C_4H_{12}N_3O_3PNa]^+$, 204.0514, found 204.0515.

3.6.2.3 Synthesis of (Guanidinomethyl)phosphonic acid (52)

To a suspension of ethyl (guanidinomethyl)phosphonate **56** (2.12 g, 11.7 mmol) in 20 mL anhydrous DMF was added trimethylbromosilane (5.38 g, 4.64 mL, 35.1 mmol) at 0 °C under an Ar atmosphere. [197] The reaction mixture was warmed to rt and stirred for 16 h. The solvent was then removed under reduced pressure, and the resulting residue was dissolved in 20 mL water. The aqueous solution was washed with three 30 mL portions of EtOAc. The aqueous layer was evaporated under reduced pressure, and excess DMF was partially removed by repeated coevaporation of the residue with water to give 1.7 g of compound **52** containing 1.5 equiv. of DMF (95% crude yield). ^{1}H NMR (D_2O, 400 MHz): δ ppm 3.43 (d, 1H, *J* = 11.9 Hz). ^{31}P NMR (D_2O, 162 MHz): δ ppm 18.28 (s, 1P). ^{13}C NMR (D_2O, 100 MHz): δ ppm 157.29 (d, *J* = 5.0 Hz), 38.74 (d, *J* = 149.0 Hz). HRMS (ESI) *m/z* calcd for $[C_2H_9N_3O_3P]^+$, 154.0382, found 154.0382.

3.6.2.4 Synthesis of (Guanidinomethyl)phosphonophosphonate (Inhibitor 19)

To a stirred solution of (guanidinomethyl)phosphonic acid **52** (1.00 g, 6.6 mmol) in 15 mL anhydrous DMF was added carbonyldiimidazole (1.70 g, 10.5 mmol) under Ar atmosphere.[195] The reaction mixture was stirred for 6 h at room temperature before 99.99% phosphoric acid crystals (1.41 g, 14.4 mmol) were added. The mixture was stirred at room temperature for 20 h. Removal of the solvent under reduced pressure resulted in a thick brown syrup which was purified using ion-exchange chromatography. The crude inhibitor **19** was dissolved in 3 mL triethylammonium bicarbonate buffer (20 mM, pH = 7.5) and loaded onto a 15 mL column of DEAE cellulose (DE 52, Whatman® Inc.) and eluted with a stepwise gradient of 20 to 100 mM triethylammonium bicarbonate buffer (pH = 7.5). All fractions were lyophilized to dryness and analyzed using ^{1}H and ^{31}P NMR spectroscopy. Selected fractions containing inhibitor **19** and minimal amounts of phosphate were dissolved in water and treated with Dowex® 50WX8 (H^+ form) resin until the pH reached 2. The acidified solution was neutralized with NaOH (0.1 M) and then lyophilized. To a solution of lyophilized solids in water (600 μL) was added EtOH (200 μL) and the cloudy mixture was centrifuged (10K rpm, 10 min) to yield a pellet. The resulting pellet was subjected to the same precipitation procedure as described above to give inhibitor **19** containing 4 equiv. of Na_2HPO_4. The final product was dissolved in 1.0 mM 1,4-dioxane in D_2O solution and ^{1}H NMR spectroscopy was used to quantify the concentration. A yield of approximately 8% was estimated for this reaction based on ^{1}H NMR integration of selected fractions. ^{1}H NMR (D_2O, 400 MHz): δ ppm 3.51 (d, 1H, *J* = 12.0 Hz), 3.15 (d, 1H, *J* = 12.0 Hz). ^{31}P NMR (D_2O, 162 MHz): δ ppm 1.64 (d, *J* = 24.3 Hz, 1P), 0.0 (s, 1P), -9.32 (d, *J* = 24.3 Hz, 1P). ^{13}C NMR (D_2O, 100 MHz): δ ppm 157.3 (s), 39.6 (d, *J* = 142.0 Hz). HRMS (ESI) *m/z* calcd

for $[C_2H_8N_3O_6P_2]^-$, 231.9888 found 231.9883 (Note: ^{13}C chemical shifts were measured indirectly using HMBC and HSQC spectra which were referenced to MeOH in water).

3.6.3 General Enzyme Methods

Centrifugal filters (4 mL 10 000 MWCO) were purchased from Millipore. Acryl-cuvettes used in enzyme kinetic assays were from Sarstedt. Chelating Sepharose® Fast resin was purchased from Pharmacia Biotech. Protein concentrations were determined by the method of Bradford on a Cary 3E UV-Vis spectrophotometer using bovine serum albumin as standard. [184] All measurements were performed at room temperature. Protein purity was assessed using SDS-PAGE, stained with Coomassie blue according to Laemmli. [185] Molecular weight standards for SDS-PAGE were BSA (66 kDa) and carbonic anhydrase (29 kDa), both purchased from Sigma. The enzyme kinetic assays were carried out on a Cary 300 UV-Vis spectrometer with a Cary temperature controller attached. Protein concentrations were determined by the Bradford assay using a commercial kit (Bio-Rad).

3.6.3.1 Overexpression and Purification of 4-Dimethylallyltryptophane Synthase (4-DMATS)

The gene encoding for *fgaPT2* from *Aspergillus fumigatus* was synthesized by GenScript with codon optimization for overexpression is *E. coli* and was cloned into a pET28a vector (Novagen/EMD Millipore) at BamH1 and HindIII restriction sites. Overproduction of 4-dimethylallyltryptophan synthase (4-DMATS) was achieved following a previously described procedure. [96] Rosetta(DE3) pLysS (Novagen) harboring the recombinant *fgaPT2*/pET28a construct was grown at 37 °C in 1 L of Terrific Broth (TB) medium containing 35 μg/mL

chloramphenicol and 30 μg/mL kanamycin until an OD_{600} of 0.6 was reached. Cells were induced for overexpression by the addition of 119 mg (0.5 mM) of isopropyl-1-thio-*β*-D-galactopyranoside (IPTG). After growing at 24 °C for an additional 24 hours, cells were harvested and lysed with a French press in sodium phosphate buffer (20 mM, pH 8.0) containing dithiothreitol (DTT, 2 mM), aprotinin (1 μgmL^{-1}), and pepstatin A (1 μgmL^{-1}). The lysate was cleared by centrifugation (34 155g, 45 min) and filtering through a 0.22 mm filter. A column containing chelating Sepharose fast flow resin (GE Healthcare, 10 mL) was charged with 100 mM $NiSO_4$ and washed with sodium phosphate buffer (20 mM, pH 8.0) containing NaCl (500 mM) and imidazole (5 mM). The clarified lysate was loaded onto the column and eluted with same buffer but containing imidazole at 5, 100, and 500 mM. Glycerol (7%) was added to the resulting eluent before flash freezing with liquid N_2. Typically, 25 mg of enzyme was purified from 1 L of culture.

3.6.3.2 Measurement of Inhibition Kinetics

Kinetic constants for the inhibition of dimethylallyltryptophan synthase (4-DMATS) by inhibitor **19** were measured by a modification of a previously described continuous coupled assay for phosphate release. A cuvette containing 50 mM Tris-HCl buffer (pH 7.50, final volume 1000 μL), L-tryptophan (20 μM), dimethylallyl diphosphate (DMAPP) (0.3 μM – 2.0 μM), inhibitor **19** (0 μM – 0.6 μM, approximately), 2-amino-6-mercapto-7-methylpurine ribonucleoside (MESG) (100 μM), purine nucleoside phosphorylase (PNPase) (1 unit), and inorganic pyrophosphatase (PPase) (0.5 unit) was thermally equilibrated for 5 min at 35 °C. The enzymatic reaction was initiated by the addition of 4-DMAT synthase (0.4 μg) and the rate was

calculated from the observed increase of absorption at 360 nm (ε = 11000 $M^{-1}.cm^{-1}$). Kinetic parameters were determined from the fit of initial velocities to Michaelis-Menten equation.

Chapter 4: Conclusion

Three different research projects have been discussed in this thesis. The first project focuses on the mechanistic studies of the cyclic dipeptide *N*-prenyltransferase (CdpNPT) that catalyzes the reverse C-3 prenylation of a variety of cyclic dipeptides and benzodiazepinediones (Chapter 2). The second project was comprised of our efforts towards elucidating the mechanism of brevianamide F prenyltransferase (FtmPT1) that catalyzes the C-2 normal prenylation of brevianamide F (Chapter 2). The third project describes the design and synthesis of a potent inhibitor of the indole prenyltransferase 4-DMATS (Chapter 3). The following information was taken from section 2.4 of Chapter two and section 3.4 of Chapter three.

4.1 Chapter 2: Conclusion

In the first part of this chapter, we reinvestigated the CdpNPT-catalyzed reaction between cyclo-L-Trp-L-Trp and DMAPP and correctly identified the product as a C-3 reverse prenylated compound containing a hexahydropyrroloindole structure. This finding enabled us to propose a mechanism for this enzyme that involves an initial reverse prenylation at the C-3 position of the indole ring. We then studied the acid-induced non-enzymatic Cope and aza-Cope rearrangements of this product at 37 °C. Our studies demonstrated that the energy barrier to the aza-Cope rearrangement can be relatively low and that it can readily proceed at room temperature. The C-3 reverse prenylated product of the CdpNPT was found to undergo a rearrangement onto the N-1 position (aza-Cope) rather than onto the C-4 position (Cope). Based on this observation, we concluded that in the absence of other factors, such as an enzyme active site, an aza-Cope rearrangement onto the N-1 position is favored. This has implications for 4-DMATS catalysis as

it means that enzymatic control of the substrate must play a key role if a Cope mechanism is operative.

In the second part of this chapter we have detailed our studies on the mechanism of the brevianamide F prenyltransferase, FtmPT1. When incubated with different substrates, FtmPT1 produced an exceptional variety of products, including C-4 normal, C-3 normal, C-3 reverse, and N-1 normal prenylated compounds (Table 4.1). This observation greatly expands the product scope of this interesting enzyme. Formation of the C-3 reverse prenylated compound **1** from L-tryptophan is consistent with a mechanism involving an initial reverse C-3 prenylation followed by a premature release of the reaction intermediate into the solution. Similarly, the observation of compound **45** from 2-methylbrevianamide F can be explained from an initial C-3 reverse prenylation followed by an aza-Cope rearrangement. Together with previous studies on the Gly115Thr mutant (section 1.5.5) and the alternate substrate **6** (section 1.5.5), a reaction case can be made for initial C-3 reverse prenylation mechanism. We also showed that 5-hydroxybrevianamide F **17** gave exclusively C-4 normal prenylation. This suggests that the active site architecture present in the X-ray structure is significant. Such a positioning provides indirect evidence for a C-3 reverse prenylation mechanism. Since the C-3 position of the indole is in close proximity to the C-3 of the prenyl group, without the highly activating C-5 hydroxyl group, one would expect C-3 prenylation to occur.

Substrate	Enzyme	Prenylation position
brevianamide F	WT	C-2 normal
brevianamide F	Gly115Thr	C-3 reverse
indole butenone **6**	WT	external alkene
cyclo-L-Trp-L-Gly, cyclo-L-Trp-L-Ala, cyclo-L-Trp-L-His and others	WT	C-2 normal and C-3 normal
L-Trp	WT	C-3 reverse
5-hydroxybrevianamide F **17**	WT	C-4 normal
2-methylbrevianamide F **18**	WT	C-3 normal and N-1 normal

Table 4.1 Product scope of FtmPT1.

The observation of the products that were normal prenylated at the C-3 position indicates that such an attack is also possible in the FtmPT1 active site. In this study, we used cyclo-L-Trp-L-Trp and 2-methylbrevianamide F (where the C-2 position is blocked) and found that C-3 normal prenylated compounds were formed as the major product in each case. These findings support a mechanism involving an initial C-3 normal prenylation (Figure 2.39). In order to obtain the C-2 normal prenylated structure observed with tryprostatin B, a subsequent 1,2-alkyl migration, or Wagner Meerwein rearrangement would have to occur (Figure 2.39). Despite the fact that these product studies on their own do not allow one to conclude the mechanism that the enzyme employs for catalysis, they clearly indicate that C-3 prenylation is a feasible first step of catalysis.

4.2 Chapter 3: Conclusion

In this chapter, we described the design, synthesis, and testing of a water-soluble inhibitor of the prenyltransferase enzyme 4-DMATS. Inhibitor **19** was synthesized in four steps from commercially available starting materials and purified using anion-exchange chromatography. During the last step of synthesis, excess phosphoric acid was used to introduce the P-O-P linkage. The separation of unreacted phosphate from inhibitor **19** proved to be challenging as they co-eluted even under careful gradient elution conditions. Further purification of the fractions containing the mixture of inhibitor **19** and phosphate was achieved through several precipitation steps from ethanol. Upon extended handling of inhibitor **19**, traces of phosphonic acid **52**, pyrophosphate, and increasing amounts of phosphate accumulated in the sample. Since the P-O-P bond in inhibitor **19** is susceptible to both phosphorolysis and hydrolysis, a gradual increase in the amount of these impurities was observed. These unfavorable side reactions were considered as the main source of error in our kinetic studies. Finally, compound **19** was tested as an inhibitor of 4-DMATS and was found to be a competitive inhibitor of this enzyme (against DMAPP) with a sub-micromolar K_i value. Due to the instability of the inhibitor and the difficulties in purification, the kinetic characterization was not further pursued. Nevertheless, this study provided valuble information indicating that guanidinium-based diphosphates could act as potent prenyltransferase inhibitors.

The promising inhibitory properties of inhibitor **19** suggests that this compound bears remarkable structural resemblance to the dimethylallyl carbocation/pyrophosphate ion pair, or the transition state that leads to its formation. A structural analysis of 4-DMATS in a complex with L-Trp and the non-hydrolyzable version of DMAPP, dimethylallyl *S*-thiolodiphosphate (DMSPP), shows that the prenyl group is sandwiched between the indole of the L-Trp substrate

and the phenolic ring of an active site tyrosine residue 345. [97] Consequently, it has been suggested that the dimethylallyl carbocation is stabilized through π-cation interactions on both faces. One can imagine that the planar geometry of the guanidinium moiety in inhibitor **19** results in a similar binding mode in the active site. Furthermore, binding to the diphosphate moiety is facilitated by electrostatic interactions with five lysine and arginine residues as well as hydrogen bonding with multiple tyrosine residues.

Inhibitor **19** shows strong structural similarities to the widely-used nitrogen containing bisphosphonates including zoledronate and BPH-678 (Figure 3.24). In addition to the usual bisphosphonate linkage, they carry a resonance-delocalized cation that is attached to the P-C-P linkage. These compounds are potent inhibitors of human farnesyl diphosphate synthase with IC_{50} values of 1.2-3.0 nM and 12 nM, respectively. [137,158]

We believe that it is likely that inhibitor **19** and suitably substituted derivatives will also show potent inhibition of the metal-dependent prenyltransferases, such as farnesyl diphosphate synthase, and that the structural differences between these compounds and the bisphosphonates may give rise to desirable properties. Inhibitor **19** contains a "side-on" linkage between the guanidinium and the pyrophosphate moieties whereas in the literature-known bisphosphonates the positive charge is attached onto the carbon bridging the phosphorus atoms (Figure 3.24). The former situation is a closer mimic of the actual prenyltransferase transition states and may lead to tighter binding in certain cases. In addition, the absence of an alcoholic functionality disrupts the structure of the "bone hook" and should decrease problems associated with binding to bone and rapid clearance. The results of a recent study in our lab performed by a post-doctoral fellow, Dr James Morrison, indicated that zoledronate does not inhibit 4-DMATS at concentrations below 200 μM. This finding implies that inhibitor **19** is selective for metal-independent aromatic

prenyltransferases and that much of the bisphosphonate binding energy comes from metal chelation.

References

1. Greenhagen, B.; Chappell, J. *Proc. Natl. Acad. Sci. U.S.A* **2001,** *98,* 13479-13481.
2. Breitmaier, E. *Terpenes: Flavors, Fragrances, Pharmaca, Phermones;* Wiley-VCH: Weinheim Germany, 2006.
3. Christianson, D. W. *Chem. Rev.* **2006,** *106,* 3412-3442.
4. Connolly, J. D.; Hill, R. A. *Dictionary of Terpenoids;* Chapman and Hall, 1991; Vol. 1.
5. Goodwin, T. W. *Aspects of Terpenoid Chemistry and Biochemistry;* Academic Press: New York, 1971.
6. Templeton, W. *An Introduction to the Chemistry of Terpenoids and Steroids;* Butterworth: London, 1969.
7. Loza-tavera, H. *Adv. Exp. Med. Biol.* **1999,** *464,* 49-62.
8. Kim, J.-K.; Kang, C.-S.; Lee, J.-K.; Kim, Y.-R.; Han, H.-Y.; Yun, H. K. *Entomol. Res.* **2005,** *35,* 117-120.
9. Rajab, M. S.; Cantrell, C. L.; Franzblau, S. G.; Fischer, N. H. *Planta Med.* **1998,** *64,* 2-4.
10. Mills, J. J.; Chari, R. S.; Boyer, I. J.; Gould, M. N.; Jirtle, R. L. *Cancer Res.* **1995,** *55,* 979-983.
11. Burkhart, C. G.; Burkhart, C. N.; Burkhart, K. M. *J. Am. Acad. Derm.* **1998,** *38,* 979-982.
12. Abraham, W. R. *Curr. Med. Chem.* **2001,** *8,* 583-606.
13. Robert, A.; Dechy-Cabaret, O.; Cazelles, J.; Meunier, B. *Accounts Chem. Res.* **2002,** *35,* 167-174.
14. Schinella, G. R.; Giner, R. M.; Recio, M. D.; De Buschiazzo, P. M.; Manez, S. *J. Pharm. Pharmacol.* **1998,** *50,* 1069-1074.
15. Dewick, P. M. The Mevalonate and Deoxyxylulose Phosphate Pathways: Terpenoids and Steroid. In *Medicinal Natural Products,* 2nd ed.; John Wiley & Sons, Ltd., 2002; pp 167-289.
16. McMorris, T. C.; Lira, R.; Gantzel, P. K.; Kelner, M. J.; Dawe, R. *J. Nat. Prod.* **2000,** *63,* 1557-1559.

17. De Clercq, E. *Med. Res. Rev.* **2000,** *20,* 323-349.

18. Ling, T. T.; Xiang, A. X.; Theodorakis, E. A. *Angew. Chem.* **1999,** *38,* 3089-3091.

19. El Sayed, K. A.; Bartyzel, P.; Shen, X. Y.; Perry, T. L.; Kjawiony, J. K.; Hamann, M. T. *Tetrahedron* **2000,** *56,* 949-953.

20. Gogas, H.; Fountzilas, G. *Ann. Oncol.* **2003,** *14,* 667-674.

21. Long, B. H.; Carboni, J. M.; Wasserman, A. J.; Cornell, L. A.; Casazza, A. M.; Jensen, P. R.; Lindel, T.; Fenical, W.; Fairchild, C. R. *Cancer Res.* **1998,** *58,* 1111-1115.

22. Rodriguez, A. D.; Ramirez, C. S. *J. Nat. Prod.* **2001,** *64,* 100-102.

23. Kellog, B. A.; Poulter, C. D. *Curr. Opin. Chem. Biol.* **1997,** *1,* 570-578.

24. Reardon, D.; Farber, G. K. *FASEB J.* **1995,** *9,* 497-503.

25. Rohmer, M. *Nat. Prod. Rep.* **1999,** *16,* 565-574.

26. Bohlmann, J.; Steele, C. L.; Croteau, R. *J. Biol. Chem.* **1997,** *272,* 21784-21792.

27. Davis, E. M.; Croteau, R. *Top. Curr. Chem.* **2000,** *209,* 53-95.

28. Croteau, R. B.; Davis, E. M.; Ringer, K. L.; Wildung, M. R. *Naturwissenschaften* **2005,** *92,* 562-577.

29. O'Neil, M. J.; Smith, A.; Heckelman, P. E. *Merck Index: an Encyclopedia of Chemicals, Drugs, and Biologicals,* 13th ed.; Merck & Co.: Whitehouse Station, NJ, USA, 2001.

30. Vesonder, R. F.; Ciegler, A.; Jensen, A. H.; Rohwedder, W. K.; Weisleder, D. *Appl. Environ. Microbiol.* **1976,** *31,* 280-285.

31. Tanaka, T.; Hasegawa, A.; Yamamoto, S.; Lee, U.-S.; Sugiura, Y.; Ueno, Y. *J. Agric. Food Chem.* **1988,** *79,* 979-983.

32. Rücker, G. *Pharm. Unserer Zeit* **1994,** *23,* 223-225.

33. Wani, M. C.; Taylor, H. L.; Wall, M. E.; Coggon, P.; McPhail, A. T. *J. Am. Chem. Soc.* **1971,** *93,* 2325-2327.

34. Cornforth, J. W. *Chem. Br.* **1968,** *4,* 102-106.

35. Geris, R.; Simpson, T. J. *Nat. Prod. Rep.* **2009,** *26,* 1063-1094.

36. Aniszewski, T. *Alkaloids-Secrets of Life: Alkaloid Chemistry, Biological Significance, Applications and Ecological Role,* 1st ed.; Elsevier: Amsterdam, 2007.

37. Floss, H. G. *Tetrahedron* **1976,** *32,* 873-912.

38. Kutchan, T. M. *Plant Cell* **1995,** *7,* 1059-1070.

39. Facchini, P. J. *J. Annu. Rev. Plant Physiol. Plant Mol. Biol.* **2001,** *52,* 29-66.

40. Ziegler, J.; Facchini, P. *J. Annu. Rev. Plant Biol.* **2008,** *59,* 735-769.

41. Aripov, K. N. *Chem. Nat. Compd.* **1978,** *14,* 624-634.

42. Cherney, E. C.; Baran, P. S. *Isr. J. Chem.* **2011,** *51,* 391-405.

43. Maimone, T. J.; Barab, P. S. *Nat. Chem. Biol.* **2007,** *3,* 396-407.

44. Buckingham, J.; Baggaley, K. H.; Roberts, A. D.; Szabo, L. F. *Dictionary of Alkaloids,* 2nd ed.; CRC Press Inc: London, 2010.

45. Djerassi, C. *Tetrahedron* **1962,** *18,* 183-188.

46. Pfister, J. A.; Gardner, D. R.; Panter, K. E.; Manners, G. D.; Ralphs, M. H.; Stegelmeier, B. L.; Schoch, T. K. *J. Nat. Toxins* **1999,** *8,* 81-94.

47. Ulubelen, A.; Mericli, A. H.; Mericli, F.; Kilincer, N.; Ferizli, A. G.; Emekci, M.; Pelletier, S. W. *Phytother. Res.* **2001,** *15,* 170-171.

48. Aoki, S.; Watanabe, Y.; Sanagawa, M.; Setiawan, A.; Kotoku, N.; Kobayashi, M. *J. Am. Chem. Soc.* **2006,** *128,* 3148-3149.

49. Watanabe, Y.; Aoki, S.; Tanabe, D.; Setiawan, A.; Kobayashi, M. *Tetrahedron* **2007,** *63,* 4074-4079.

50. Aoki, S.; Watanabe, Y.; Tanabe, D.; Setiawan, A.; Arai, M.; Kobayashi, M. *Tet. Lett.* **2007,** *48,* 4485-4488.

51. Pictet, A.; Spengler, T. *Ber. Dtsch. Chem. Ges.* **1911,** *44,* 2030-2036.

52. Cox, E. D.; Cook, J. M. *Chem. Rev.* **1995,** *95,* 1797-1842.

53. Uesato, S. K.; Iida, A.; Inouye, H.; Zenk, M. H. *Phytochemistry* **1986,** *25,* 839-842.

54. Uesato, S.; Matasuda, S.; Inouye, H. *Chem. Pharm. Bull.* **1984,** *32,* 1671-1674.

55. O'Connor, S. E.; Maresh, J. J. *Nat. Prod. Rep.* **2006,** *23,* 532-547.

56. Li, S.-M. *Nat. Prod. Rep.* **2010,** *27,* 57-78.

57. Tanner, M. E. *Nat. Prod. Rep.* **2015,** *32,* 88-101.

58. Lindel, T.; Marsch, N.; Adla, S. K. *Top. Curr. Chem.* **2012,** *309,* 67-130.

59. Williams, R. M.; Stocking, E. M.; Sanz-Cervera, J. F. *Top. Curr. Chem.* **2000,** *209,* 97-173.

60. Cardellina, J. H. I.; Marner, F. J.; Moore, R. E. *Science* **1979,** *204,* 193-195.

61. Aimi, N.; Odaka, H.; Sakai, S.; Fujiki, H.; Suganuma, M.; Moore, R. E.; Patterson, G. M. *J. Nat. Prod.* **1990,** 1593-1596.

62. Tagami, K.; Liu, C.; Minami, A.; Noike, M.; Isaka, T.; Fueki, S.; shichijo, Y.; Toshima, H.; Gomi, K.; Dairi, T.; Oikawa, H. *J. Am. Chem. Soc.* **2013,** *135,* 1260-1263.

63. Tello, M.; Kuzuyama, T.; Heide, L.; Nowl, J. P.; Richard, S. B. *Cell. Mol. Life Sci.* **2008,** *65,* 1459-1463.

64. Liang, P.-H.; Ko, T.-P.; Wang, A. H.-J. *Eur. J. Biochem.* **2002,** *269,* 3339-3354.

65. Poulter, C. D.; Rilling, H. C. *Acc. Chem. Res.* **1978,** *11,* 307-313.

66. Dorsey, J. K.; Dorsey, J. A.; Porter, J. W. *J. Biol. Chem.* **1966,** *241,* 5353-5360.

67. Holloway, P. W.; Popják, G. *Biochem. J.* **1967,** *104,* 57-70.

68. Tarshis, L. C.; Yan, M.; Poulter, C. D.; Sacchettini, J. C. *Biochemistry* **1994,** *33,* 10871-10877.

69. Song, L.; Poulter, C. D. *Proc. Natl. Acad. Sci. U. S. A* **1994,** *91,* 3044-3048.

70. Tarshis, L. C.; Proteau, P. J.; Kellogg, B. A.; Sacchettini, J. C.; Poulter, C. D. *Proc. Natl. Acad. Sci. USA* **1996,** *93,* 15018-15023.

71. Mash, E. A.; Gurria, G. M.; Poulter, C. D. *J. Am. Chem. Soc.* **1981,** *103,* 3927-3929.

72. Gassman, P. G.; Gurria, G. M.; Poulter, C. D. *J. Am. Chem. Soc.* **1970,** *92,* 2549-2551.

73. Harris, C. M.; Poulter, C. D. *Nat. Prod. Rep.* **2000,** *17,* 137-144.

74. Zhang, F. L.; Casey, P. J. *Annu. Rev. Biochem.* **1996,** *65,* 241-269.

75. Cohen, L. H.; Pieterman, E.; van Leeuwen, R. E. W.; Overhand, M.; Burm, B. E.; van der Marel, G. A.; van Boom, J. H. *Biochem. Pharmacol.* **2000,** *60,* 1061-1068.

76. Huang, C.-C.; Hightower, K. E.; Fierke, C. A. *Biochemistry* **2000,** *39,* 2593-2602.

77. Dolence, J. M.; Poulter, C. D. *Proc. Natl. Acad. Sci. USA* **1995,** *92,* 5008-5011.

78. Weller, V. A.; Distefano, M. D. *J. Am. Chem. Soc.* **1998,** *120,* 7975-7976.

79. Hemmi, H.; Shibuya, K.; Takahashi, Y.; Nakayama, T.; Nishino, T. *J. Biol. Chem.* **2004,** *279,* 50197-50203.

80. Yazaki, K.; Kunihisa., M.; Fujisaki, T.; Sato, F. *J. Biol. Chem.* **2002,** *277,* 6240-6246.

81. Schultz, A. W.; Lewis, C. A.; Luzung, M. R.; Baran, P. S.; Moore, B. S. *J. Nat. Prod.* **2010,** *73,* 373-377.

82. Pojer, F.; Wemakor, E.; Kammerer, B.; Chen, H.; Walsh, C. T.; Li, S.-M.; Heide, L. *Proc. Natl. Acad. Sci. USA* **2003,** *100,* 2316-2321.

83. Pojer, F.; Li, S.-M.; Heide, L. *Microbiology* **2002,** *148,* 3901-3911.

84. Kuzuyama, T.; Noel, J. P.; Richard, S. B. *Nature* **2005,** *435,* 983-987.

85. Yang, Y.; Miao, Y.; Wang, B.; Cui, G.; Merz, K. M. J. *Biochemistry* **2012,** *51,* 2606-2618.

86. Steffan, N.; Unsöld, I. A.; Li, S.-M. *ChemBioChem* **2007,** *8,* 1298-1307.

87. Unsöld, I. A.; Li, S.-M. *Microbiology* **2005,** *151,* 1499-1505.

88. Rementeria, A.; López-Molina, N.; Ludwig, A.; Vivanco, A. B.; Bikandi, J.; Pontón, J.; Garaizer, J. *Rev. Iberoam. Micol.* **2005,** *22,* 1-23.

89. Unsöld, I. A.; Li, S.-M. *ChemBioChem* **2005,** *7,* 158-164.

90. Kremer, A.; Westrich, L.; Li, S.-M. *Microbiology* **2007,** *153,* 3409-3416.

91. Shibuya, M.; Chou, H. M.; Fountoulakis, M.; Hassam, S.; Kim, S. U.; Kobayashi, K.; Otsuka, H.; Rogalska, E.; Cassady, J. M.; Floss, H. G. *J. Am. Chem. Soc.* **1990,** *112,* 297-304.

92. Popják, G.; Cornforth, J. W. *Biochem. J.* **1966,** *101,* 553-568.

93. Poulter, C. D.; Satterwhite, D. M.; Rilling, H. C. *J. Am. Chem. Soc.* **1976,** *98,* 3376-3377.

94. Gelber, J. C.; Woodside, A. B.; Poulter, C. D. *J. Am. Chem. Soc.* **1992,** *114,* 7354-7360.

95. Richard, J. P.; Jencks, W. P. *J. Am. Chem. Soc.* **1984,** *106,* 1383-1396.

96. Luk, L. Y. P.; Tanner, M. E. *J. Am. Chem. Soc.* **2009,** *131,* 13932-13933.

97. Metzger, U.; Schall, C.; Zocher, G.; Unsöld, I.; Stec, E.; Li, S.-M.; Heide, L.; Stehle, T. *Proc. Natl. Acad. Sci. USA* **2009,** *106,* 14309-14314.

98. Luk, L. Y. P.; Qian, Q.; Tanner, M. E. *J. Am. Chem. Soc.* **2011,** *133,* 12342-12345.

99. Wenkert, E.; Sliwa, H. *Bioorg. Chem.* **1977,** *6,* 443-452.

100. Lakhdar, S.; Westermaier, M.; Terrier, F.; Goumont, R.; Boubaker, T.; Ofial, A. R.; Mayr, H. *J. Org. Chem.* **2006,** *71,* 9088-9095.

101. Yin, W.-B.; Ruan, H.-L.; Westrich, L.; Grundmann, A.; Li, S.-M. *ChemBioChem* **2007,** *8,* 1154-1161.

102. Schuller, J. M.; Zocher, G.; Liebhold, M.; Xie, X.; Stahl, M.; Li, S.-M.; Stehle, T. *J. Mol. Biol.* **2012,** *422,* 87-99.

103. Koblish, H. K.; Zhao, S.; Franks, C. F.; Donatelli, R. R.; Tominovich, R. M.; LaFrance, L. V. *Mol. Cancer Ther.* **2006,** *5,* 160-169.

104. Grundmann, A.; Li, S. M. *Microbiology* **2005,** *151,* 2199-2207.

105. Yu, X.; Zocher, G.; Xie, X.; Liebhold, M.; Schutz, S.; Stehle, T.; Li, S.-M. *Chem. Biol.* **2013,** *20,* 1492-1501.

106. Yin, W.-B.; Cheng, J.; Li, S.-M. *Org. Biomol. Chem.* **2009,** *7,* 2202-2207.

107. Ruan, H.-L.; Yin, W.-B.; Wu, J.-Z.; Li, S.-M. *ChemBioChem* **2008,** *9,* 1044-1047.

108. Li, S.-M. *J. Antibiot.* **2011,** *64,* 45-49.

109. Zhao, S.; Smith, K. S.; Deveau, A. M.; Dieckhaus, C. M.; Johnson, M. A.; Macdonald, T. L.; Cook, J. M. *J. Med. Chem.* **2002,** *45,* 1559-1562.

110. Jost, M.; Zocher, G.; Tarcz, S.; Matuschek, M.; Xie, X.; Li, S.-M.; Stehle, T. *J. Am. Chem. Soc.* **2010,** *132,* 17849-17858.

111. Chen, J.; Morita, H.; Wakimoto, T.; Mori, T.; Noguchi, H.; Abe, I. *Org. Lett.* **2012,** *14,* 3080-3083.

112. Winchester, B.; Fleet, G. W. J. *Glycobiology* **1992,** *2,* 199-210.

113. Asano, N. *Glycobiology* **2003,** *13,* 93R-104R.

114. Koshland, D. E. J. *Biol. Rev.* **1953,** *28,* 416-436.

115. Vasella, A.; Davies, G. J.; Böhm, M. *Curr. Opin. Chem. Biol.* **2002,** *6,* 619-629.

116. Vocadlo, D. J.; Davies, G. J.; Laine, R.; Withers, S. G. *Nature* **2001,** *412,* 835-838.

117. Leaback, D. H. *Biochem. Biophys. Res. Commun.* **1968,** *32,* 1025-1030.

118. Legler, G. *Adv. Carbohydr. Chem. Biochem.* **1990,** *48,* 319-384.

119. Dale, M. P.; Ensley, H. E.; Kern, K.; Sastry, K. A. R.; Byers, L. D. *Biochemistry* **1985,** *24,* 3530-3539.

120. Asano, N. *Curr. Top. Med. Chem.* **2003,** *3,* 471-484.

121. Inoue, S.; Tsuruoka, T.; Niida, T. *J. Antibiot.* **1966,** *19,* 288-292.

122. Niwa, T.; Inoue, S.; Tsuruoka, T.; Koaze, Y.; Niida, T. *Agric. Biol. Chem.* **1970,** *34,* 966-968.

123. Yagi, M.; Kouno, T.; Aoyagi, Y.; Murai, H. *J. Agric. Chem. Soc. Japan* **1976,** *50,* 571-572.

124. Saul, R.; Ghidoni, J. J.; Molyneux, R. J.; Elbein, A. D. *Proc. Natl. Acad. Sci. USA* **1985,** *82,* 93-97.

125. Butters, T. D.; Dwek, R. A.; Platt, F. M. *Curr. Top. Med. Chem.* **2003,** *3,* 561-574.

126. Heightman, T. D.; Vasella, A. T. *Angew. Chem. Int. Ed.* **1999,** *38,* 750-770.

127. Ermert, P.; Vasella, A.; Weber, M.; Rupitz, K.; Withers, S. G. *Carbohydr. Res.* **1993,** *250,* 113-125.

128. Reardon, J. E.; Abeles, R. H. *J. Am. Chem. Soc.* **1985,** *107,* 4078-4079.

129. Muehlbacher, M.; Poulter, C. D. *J. Am. Chem. Soc.* **1985,** *107,* 8307-8308.

130. Cane, D. E.; Ha, H.; Pargellis, C.; Waldmeier, F.; Swanson, S.; Murthy, P. P. N. *Bioorg. Chem.* **1985,** *13,* 2136- 2139.

131. Grove, J. F. *Nat. Prod. Rep.* **1988,** *5,* 187-209.

132. Cane, D. E.; Yang, G. *J. Org. Chem.* **1992,** *57,* 3454-3462.

133. Pandit, J.; Danley, D. E.; Schulte, G. K.; Mazzalupo, T.; Pauly, T. A.; Hayward, C. M.; Hamanaka, E. S.; Thompson, J. F.; Harwood, H. J. *J. Biol. Chem.* **2000,** *275,* 30610-30617.

134. Sandifer, R. M.; Thompson, M. D.; Gaughan, R. G.; Poulter, C. D. *J. Am. Chem. Soc.* **1982,** *104,* 7376-7378.

135. Sagami, H.; Korenaga, T.; Ogura, K.; Steiger, A.; Pyun, H. J.; Coates, R. M. *Arch. Biochem. Biophys.* **1992,** *297,* 314-320.

136. Steiger, A.; Pyun, H. J.; Coates, R. M. *J. Org. Chem.* **1992,** *57,* 3444-3449.

137. Zhang, Y.; Cao, R.; Yin, F.; Hudock, M. P.; Guo, R.-T.; Krysiak, K.; Mukherjee, S.; Gao, Y.-G.; Robinson, H.; Song, Y.; No, J.-H.; Bergan, K.; Leon, A.; Cass, L.; Goddard, A.; Chang, T.-K.; Lin, F. Y.; Van Beek, E.; Papapoulos, S.; Wang, A. H.-J.; Kubo, T. *J. Am. Chem. Soc.* **2009,** *131,* 5153-5162.

138. Widler, L.; Jaeggi, K. A.; Glatt, M.; Müller, K.; Bachmann, R.; Bisping, M.; Born, A. R.; Cortesi, R.; Guiglia, G.; Jeker, H.; Klein, R.; Ramsier, U.; Schmid, J.; Schreiber, G.; Seltenmeyer, Y.; Green, J. R. *J. Med. Chem.* **2002,** *45,* 3721-3738.

139. Blomen, L. J. M. J. Bisphosphonates on Bones. In *History of the Bisphosphonates: Discovery and History of the Non-medical Uses of Bisphosphonates;* Bijvoet, O. L., Fleisch, H. A., Canfield, R. E., Russel, R. G., Eds.; Elsevier: Amsterdam, 1995; pp 111-124.

140. Delmas, P. D. *Lancet* **2002,** *359,* 2018-2026.

141. Langston, A. L.; Ralston, S. H. *Rheumatology* **2004,** *43,* 955-959.

142. Berenson, J. R. *Semin. Oncol.* **2002,** *29,* 12-18.

143. Fleisch, H.; Russel, R. G. G.; Straumann, F. *Nature* **1966,** *212,* 901-903.

144. Francis, M. D.; Russel, R. G.; Fleisch, H. *Science* **1969,** *165,* 1264-1266.

145. Kašpárek, F. *Monatsh. Chem.* **1968,** *99,* 2016-2023.

146. Strates, B. S.; Firschein, H. E.; Urist, M. R. *Biochim. Biophys. Acta* **1971,** *244,* 121-124.

147. Coutkell, A. J.; Markham, A. *Drugs Aging* **1998,** *12,* 149-168.

148. Ebetino, F. H.; Francis, M. D.; Rogers, M. J.; Russell, R. G. G. *Rev. Contemp. Pharmacother.* **1998,** *9,* 233-243.

149. Rodan, G. A.; Fleisch, H. A. *J. Clin. Invest.* **1996,** *97,* 2692-2696.

150. Fisher, J. E.; Rogers, M. J.; Halasy, J. M.; Luckman, S. P.; Hughes, D. E.; Masarachia, P. J.; Wesolowski, G.; Russell, R. G. G.; Rodan, G. A.; Reszka, A. A. *Proc. Natl. Acad. Sci. USA* **1999,** *96,* 133-138.

151. Beek, E. V.; Pieterman, E.; Cohen, L.; Löwik, C.; Papapoulos, S. *Biochem. Biophys. Res. Commun.* **1999,** *264,* 108-111.

152. Dunford, J. E. *Curr. Pharm. Des.* **2010,** *16,* 2961-2969.

153. Heymann, D. *Curr. Pharm. Des.* **2010,** *16,* 2948-2949.

154. Sun, S.; McKenna, C. E. *Expert Opin. Ther. Patents* **2011,** *21,* 1433-1451.

155. Oldfield, E. *Acc. Chem. Res.* **2010,** *43,* 1216-1226.

156. Bergstrom, J. D.; Bostedor, R. G.; Masarachia, P. J.; Reszka, A. A.; Rodan, G. *Arch. Biochem. Biophys.* **2000,** *373,* 231-241.

157. Dunford, J. E.; Thompson, K.; Coxon, F. P.; Luckman, S. P.; Hahn, F. M.; Poulter, C. D.; Ebetino, F. H.; Rogers, M. J. *J. Pharmacol. Exp. Ther.* **2001,** *296,* 235-242.

158. De Schutter, J. W.; Park, J.; Leung, C. Y.; Gormley, P.; Lin, Y.-S.; Hu, Z.; Berghuis, A. M.; Poirier, J.; Tsantrizos, Y. S. *J. Med. Chem.* **2014,** *57,* 5764-5776.

159. Mukherjee, S.; Song, Y.; Oldfield, E. *J. Am. Chem. Soc.* **2008,** *130,* 1264-1273.

160. Mukherjee, S.; Huang, C.; Guerra, F.; Wang, K.; Oldfield, E. *J. Am. Chem. Soc.* **2009,** *131,* 8374-8375.

161. No, J.-H.; Dossin, F. D.; Zhang, Y.; Liu, Y.-L.; Zhu, W.; Feng, X.; Yoo, J. A.; Lee, E.; Wang, K.; Hui, R.; Freitas-Junior, L. H.; Oldfield, E. *Proc. Natl. Acad. Sci. USA* **2012,** *109,* 4058-4063.

162. Qian, Q.; Schultz, A. W.; Moore, B. S.; Tanner, M. E. *Biochemistry* **2012,** *51,* 7733-7739.

163. pET System Manual. Novagen: Madison, WI, 2002.

164. Bonitz, T.; Alva, V.; Saleh, O.; Lupas, A. N.; Heide, L. *PLoS One* **2011,** *6,* e27336.

165. Rudolf, J. D.; Wang, H.; Poulter, C. D. *J. Am. Chem. Soc.* **2013,** *135,* 1895-1902.

166. Sun, T.; Li, Z. -L.; Tian, H.; Wang, S. -C.; Cai, J. *Molecules* **2009,** *14,* 5339-5348.

167. Sanz-Cervera, J. F.; Stocking, E. M.; Usui, T.; Osada, H.; Williams, R. M. *Bioorg. Med. Chem.* **2000,** *8,* 2407-2415.

168. Liu, X.; Walsh, C. T. *Biochemistry* **2009,** *48,* 11032-11044.

169. Voûte, N.; Philip, D.; Slawin, A. M. Z.; Westwood, N. J. *Org. Biomol. Chem.* **2010,** *8,* 442-450.

170. Jung, M. E.; Piizzi, G. *Chem. Rev.* **2005,** *105,* 1735–1766.

171. Cardoso, A. S. P.; Marques, M. M. B.; Srinivasan, N.; Prabhakar, S.; Lobo, A. M.; Rzepa, H. S. *Org. Biomol. Chem.* **2006,** *4,* 3966-3972.

172. Caballero, E.; Avendaño, C.; Menéndez, J. C. *J. Org. Chem.* **2003,** *68,* 6944-6951.

173. Zou, H.; Zheng, X.; Li, S.-M. *J. Nat. Prod.* **2009,** *72,* 44-52.

174. Depew, K. M.; Marsden, S. P.; Zatorska, D.; Zatorski, A.; Bornmann, W. G.; Danishefsky, S. J. *J. Am. Chem. Soc.* **1999,** *121,* 11953-11963.

175. Loh, C. C. J.; Raabe, G.; Enders, D. *Chem. Eur. J.* **2012,** *18,* 13250-13254.

176. Kanaoka, Y.; Miyashita, K.; Yonemitsu, O. *J. Chem. Soc.* **1969,** 1365a.

177. Nakazaki, M.; Yamamoto, K.; Yamagami, K. *Bull. Chem. Soc. Jpn.* **1960,** *33,* 466-472.

178. Wollinsky, B.; Ludwig, L.; Xie, X.; Li, S.-M. *Org. Biomol. Chem.* **2012,** *10,* 9262-9270.

179. McIntosh, J. A.; Donia, M. S.; Nair, S. K.; Schmidt, E. W. *J. Am. Chem. Soc.* **2011,** *133,* 13698-13705.

180. Goss, R. J. M.; Newill, P. L. A. *Chem. Commun.* **2006,** 4924-4925.

181. Strand, R. B.; Helgerud, T.; Solvang, T.; Sperger, C. A.; Fiksdahl, A. *Tetrahedron : Asymmetry* **2011,** *22,* 1994-2006.

182. Trotter, N. S.; Brimble, M. A.; Harris, P. W. R.; Callis, D. J.; Sieg, F. *Bioorg. Med. Chem.* **2005,** *13,* 501-517.

183. Crosignani, S.; Gonzalez, J.; Swinnen, D. *Org. Lett.* **2004,** *6,* 4579-4582.

184. Bradford, M. M. *Anal. Biochem.* **1976,** *72,* 248-254.

185. Ausubel, F. M.; Brent, R.; Kingston, R. E.; Moore, D. D.; Seidman, J. G.; Smith, J. A.; Struhl, K. *Short Protocols in Molecular Biology;* John Wiley: New York, N.Y, 1992.

186. Ayral-Kaloustian, S.; Salaski, E. J. *Curr. Med. Chem.* **2002,** *10,* 1003-10032.

187. Sousa, S. F.; Fernandes, P. A.; Ramos, M. J. *Curr. Med. Chem.* **2008,** *15,* 1478-1492.

188. Ishibashi, Y.; Kitamura, M. *Chem. Commun.* **2009,** 6985-6987.

189. Hirschmann, R.; Yager, K. M.; Taylor, C. M.; Witherington, J.; Sprengler, P. A.; Phillips, B. W.; Moore, W.; Smith, A. B. *J. Am. Chem. Soc.* **1997,** *119,* 8177-8190.

190. McKenna, C. E.; Schmidhauser, J. *J. Chem. Soc. Chem. Commun.* **1979,** 739.

191. Bernatowicz, M. S.; Wu, Y.; Matsueda, G. R. *J. Org. Chem* **1992,** *57,* 2497-2502.

192. Bernatowicz, M. S.; Wu, Y.; Matsueda, G. R. *Tet. Lett.* **1993,** *34,* 3389-3392.

193. Oleksyszyn, J.; Tyka, R.; Mastalerz, P. *Communications* **1977,** 571-572.

194. Birum, G. H. *J. Org. Chem.* **1974,** *39,* 209-213.

195. DeGraw, A. J.; Zhao, Z.; Strickland, C. L.; Taban, A. H.; Hsieh, J.; Jeffries, M.; Xie, W.; Shintani, D. K.; McMahan, C. M.; Cornish, K.; Distefano, M. D. *J. Org. Chem.* **2007,** *72,* 4587-4595.

196. Michelson, A. M. *Biochem. Biophys. Acta* **1964,** *91,* 1-13.

197. Zgani, I.; Menut, C.; Seman, M.; Gallois, V.; Laffont, V.; Liautard, J.; Liautard, J.-P.; Criton, M.; Montero, J.-L. *J. Med. Chem.* **2004,** *47,* 4600-4612.

198. Paul, R.; Anderson, G. W. *J. Am. Chem. Soc.* **1960,** *82,* 4596-4600.

199. Heinze, T.; Liebert, T.; Koschella, A. Esterification of Polysaccharides. Springer, 2006; pp 86-103.

200. Webb, M. R. *Proc. Natl. Acad. Sci. USA* **1992,** *89,* 4884-4887.

Appendix: NMR of Selected Compounds

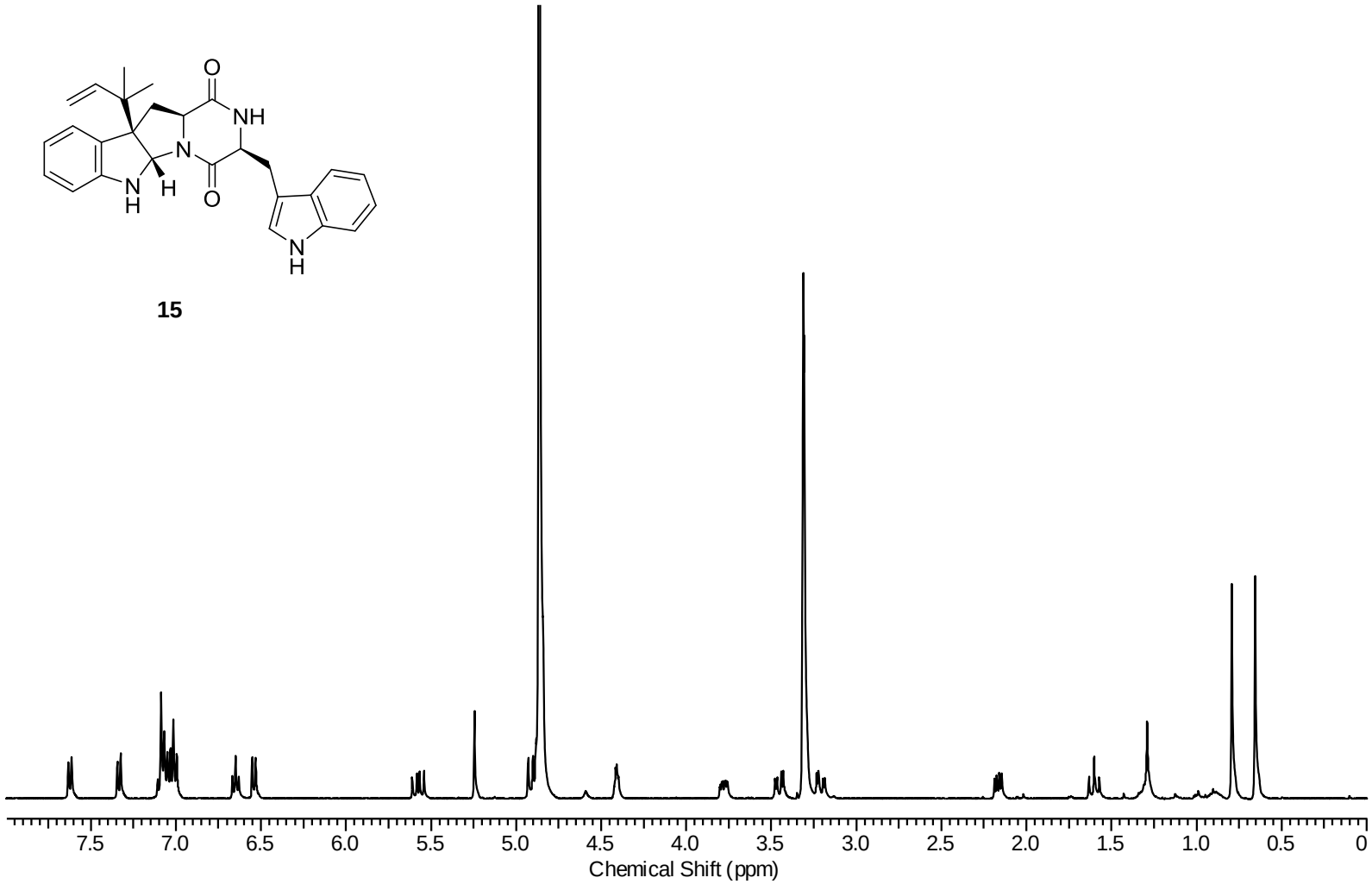

Figure A. 1 ^{1}H NMR spectrum of compound 15 (CD_3OD, 400 MHz).

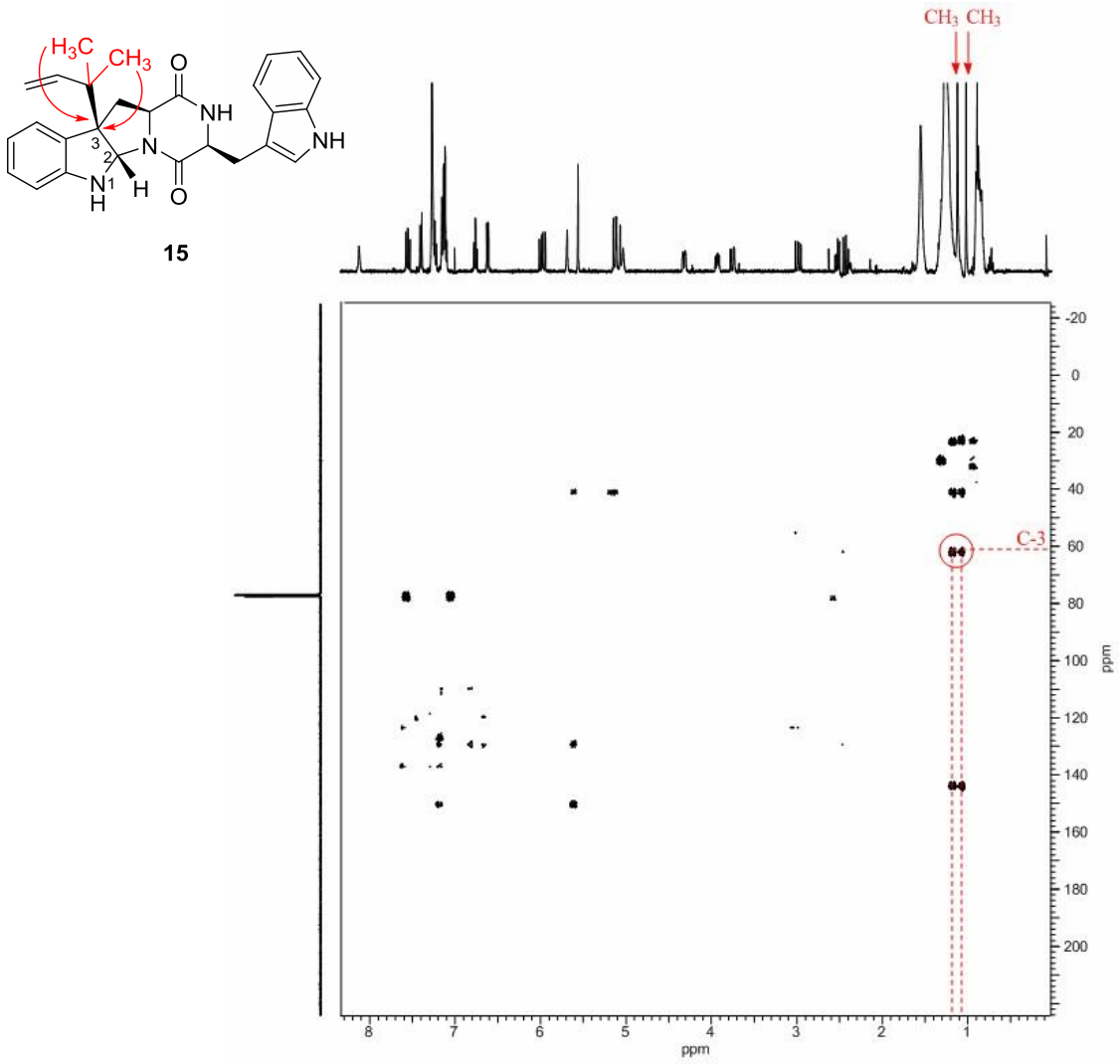

Figure A. 2 HMBC spectrum of compound 15 ($CDCl_3$, 400 MHz).

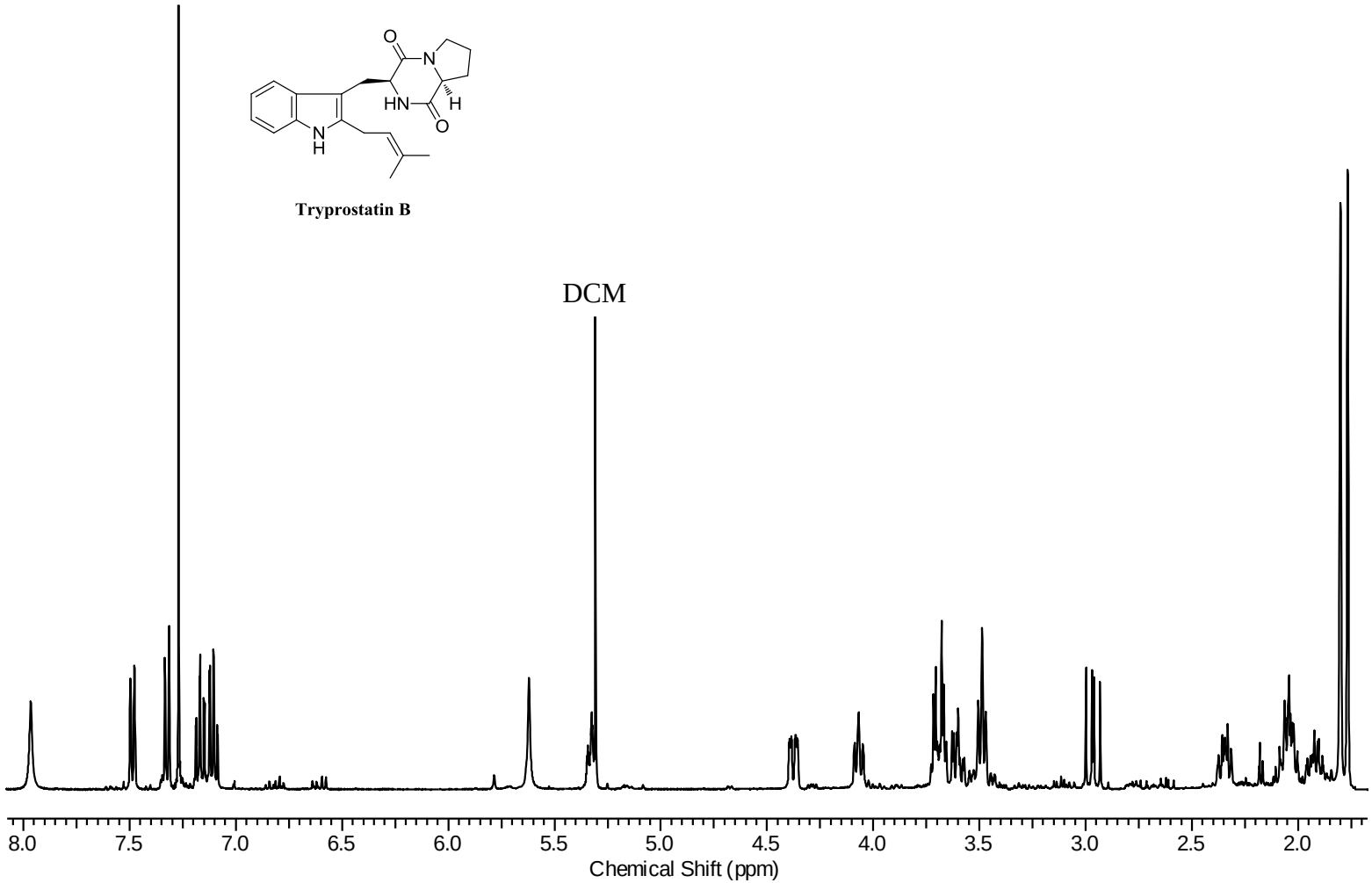

Figure A. 3 ^{1}H NMR spectrum of tryprostatin B (CDCl3, 400 MHz).

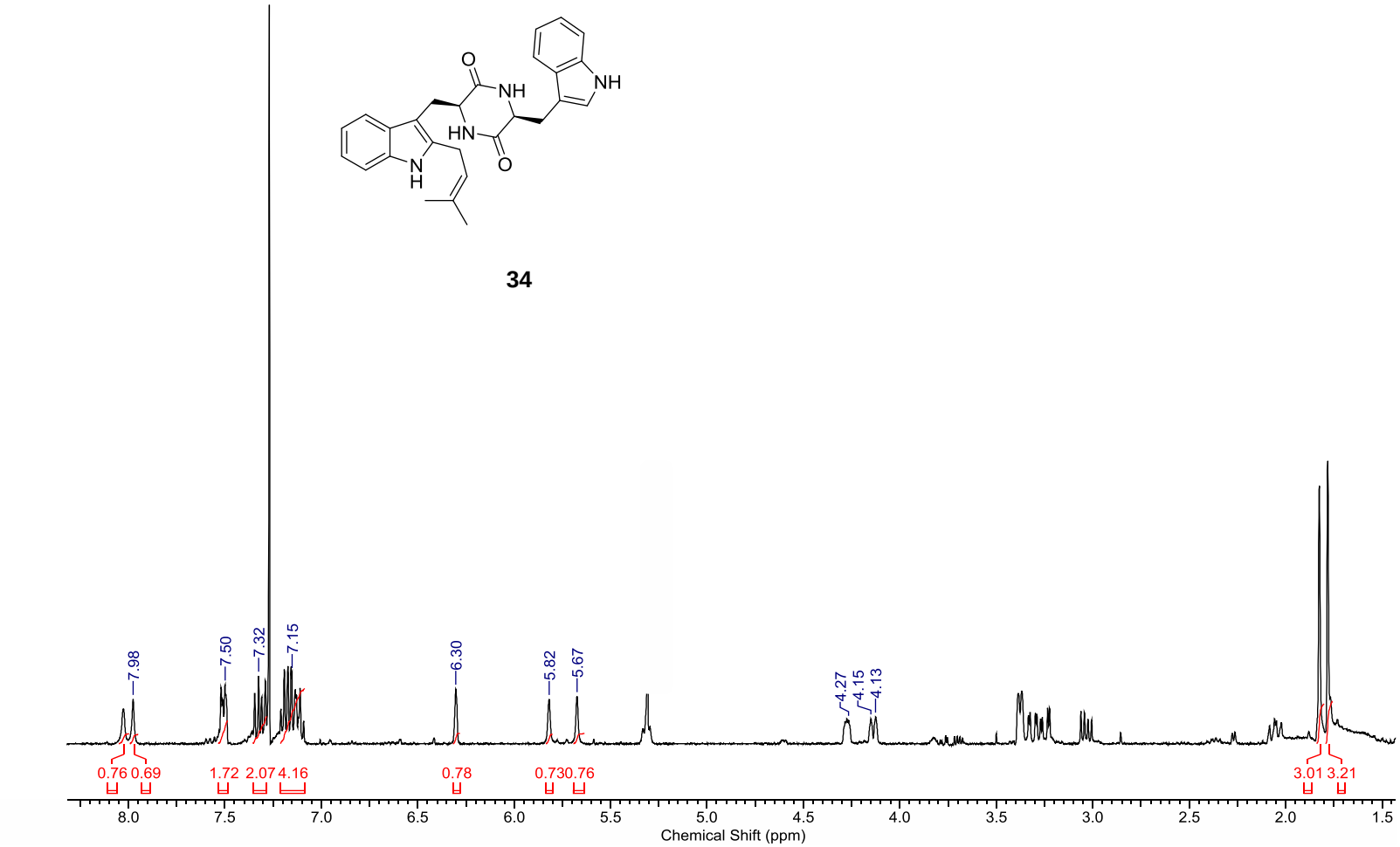

Figure A. 4 ^{1}H NMR spectrum of compound 34 ($CDCl_3$, 400 MHz).

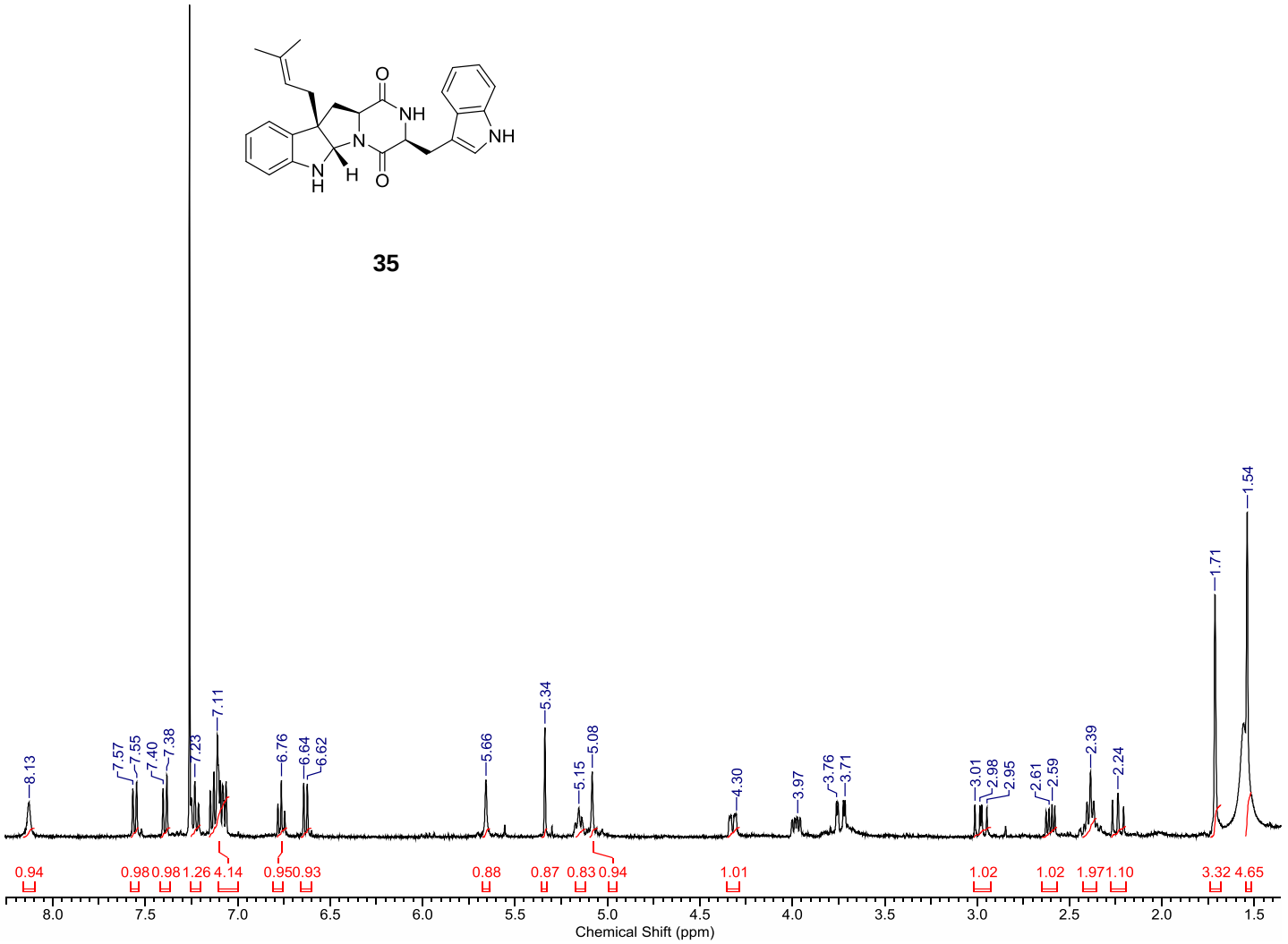

Figure A. 5 ^{1}H NMR spectrum of compound 35 ($CDCl_3$, 400 MHz).

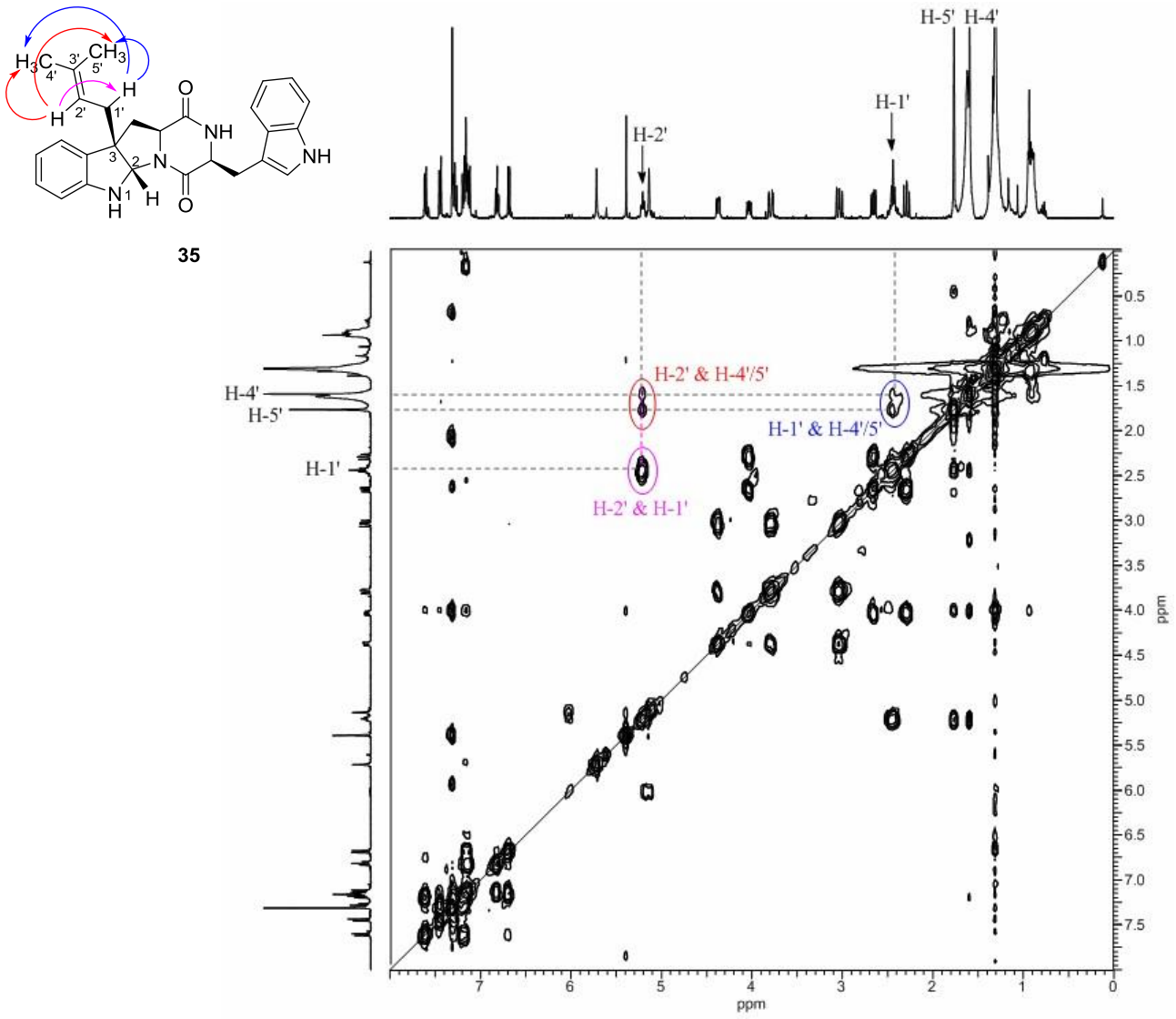

Figure A. 6 COSY spectrum of compound 35 ($CDCl_3$, 400 MHz).

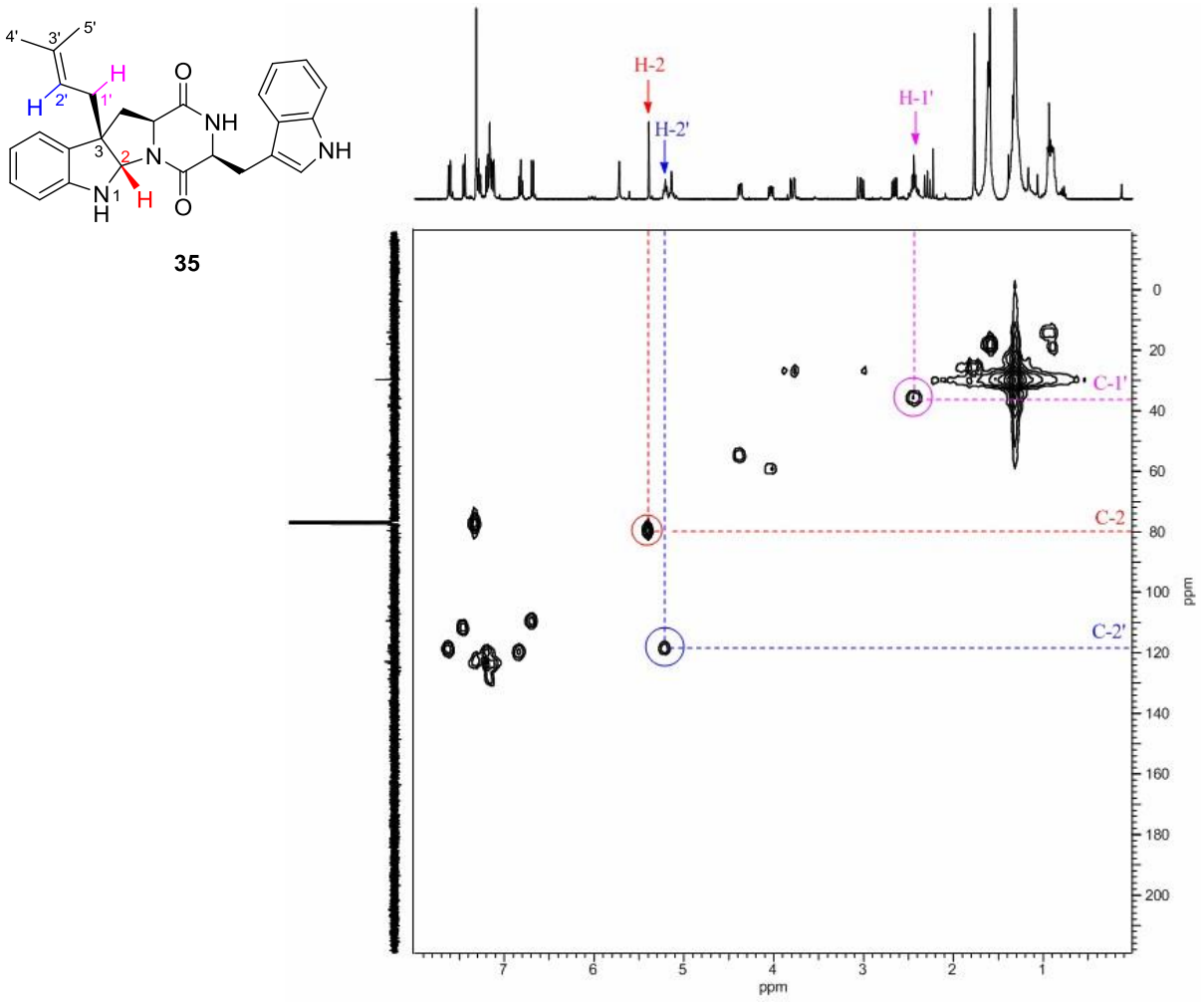

Figure A. 7 HSQC spectrum of compound 35 ($CDCl_3$, 400 MHz).

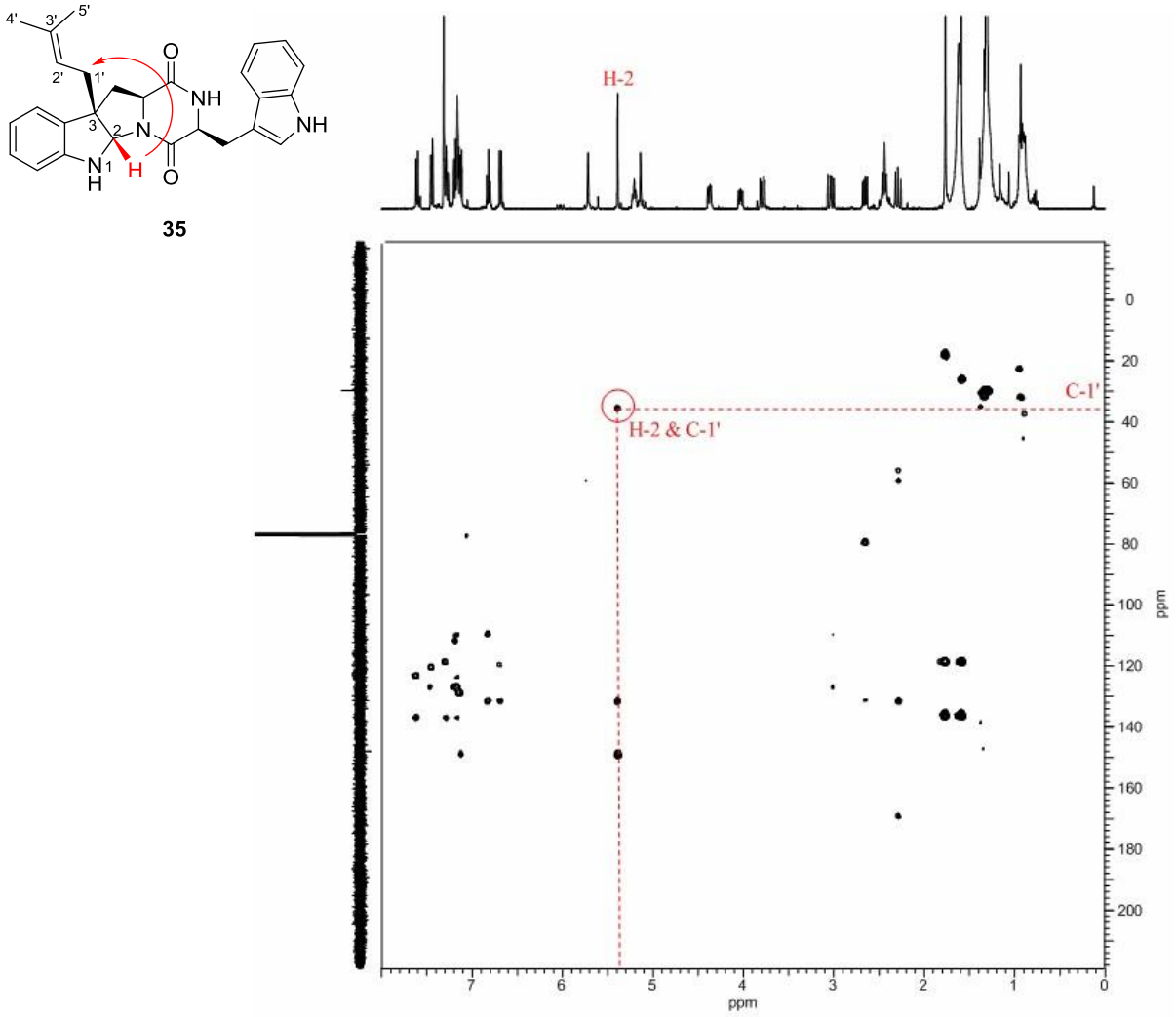

Figure A. 8 HMBC spectrum of compound 35 ($CDCl_3$, 400 MHz).

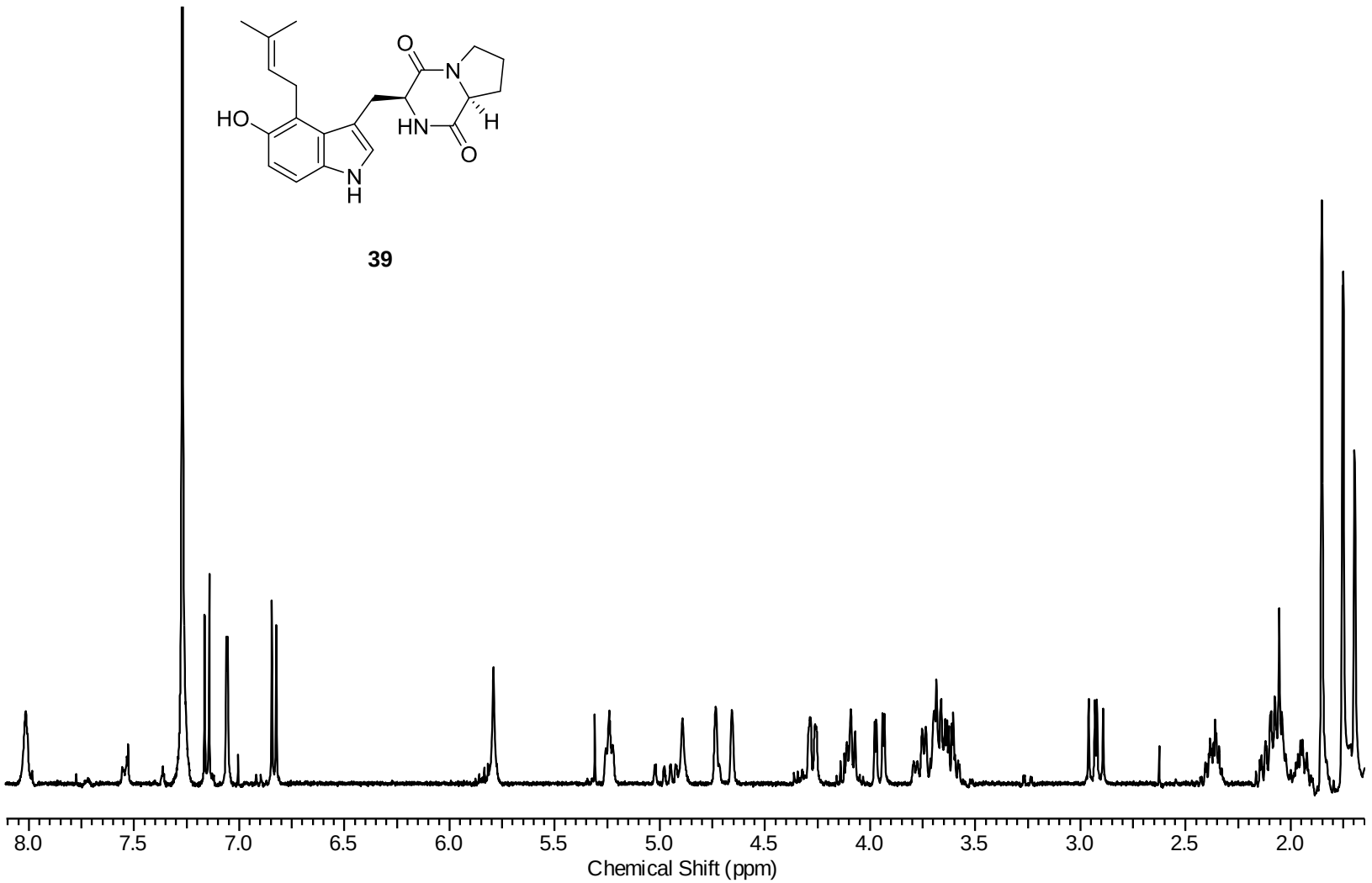

Figure A. 9 ^{1}H NMR spectrum of compound 39 ($CDCl_3$, 400 MHz).

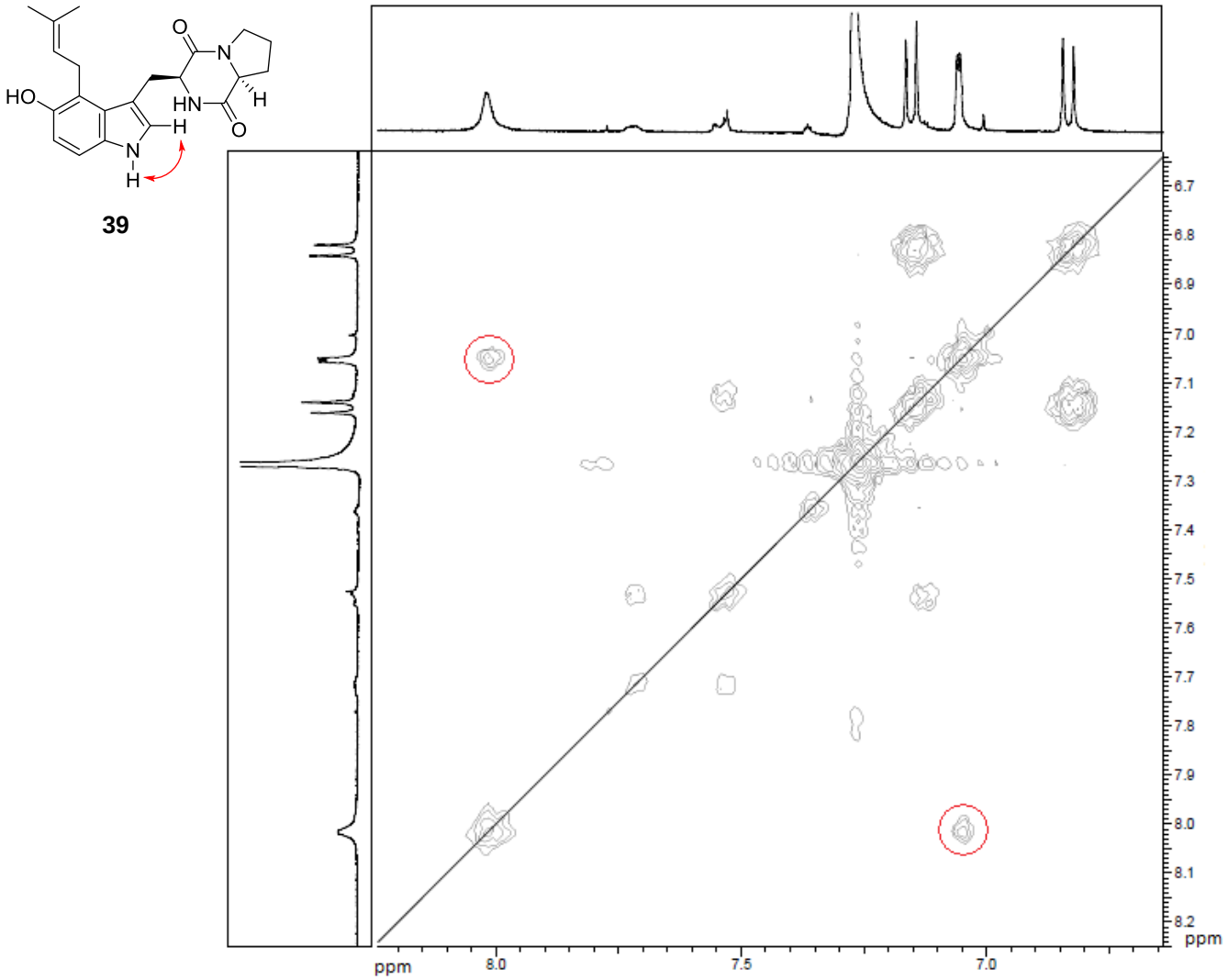

Figure A. 10 COSY spectrum of compound 39 ($CDCl_3$, 400 MHz).

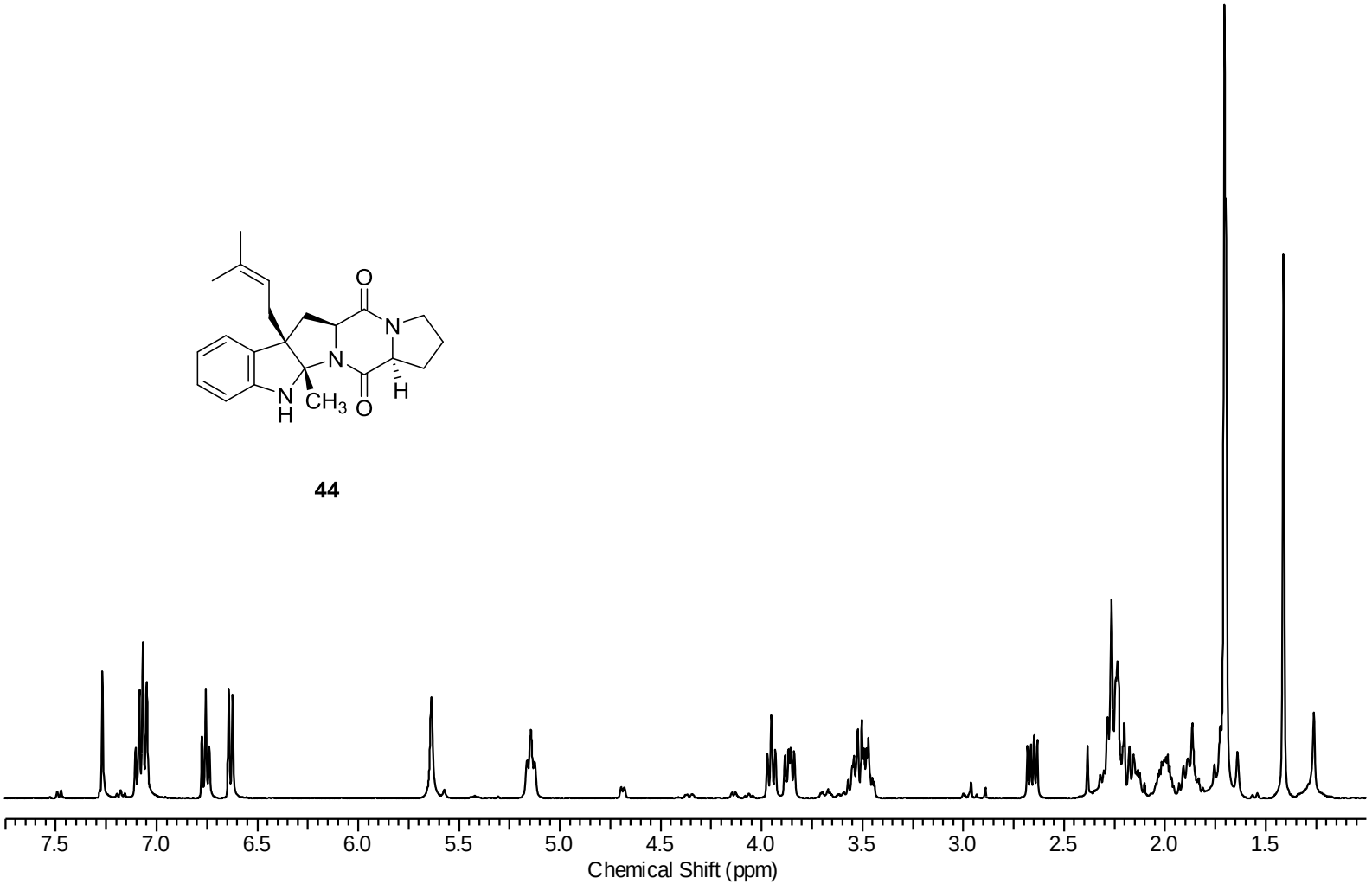

44

Figure A. 11 ^{1}H NMR spectrum of compound 44 ($CDCl_3$, 400 MHz).

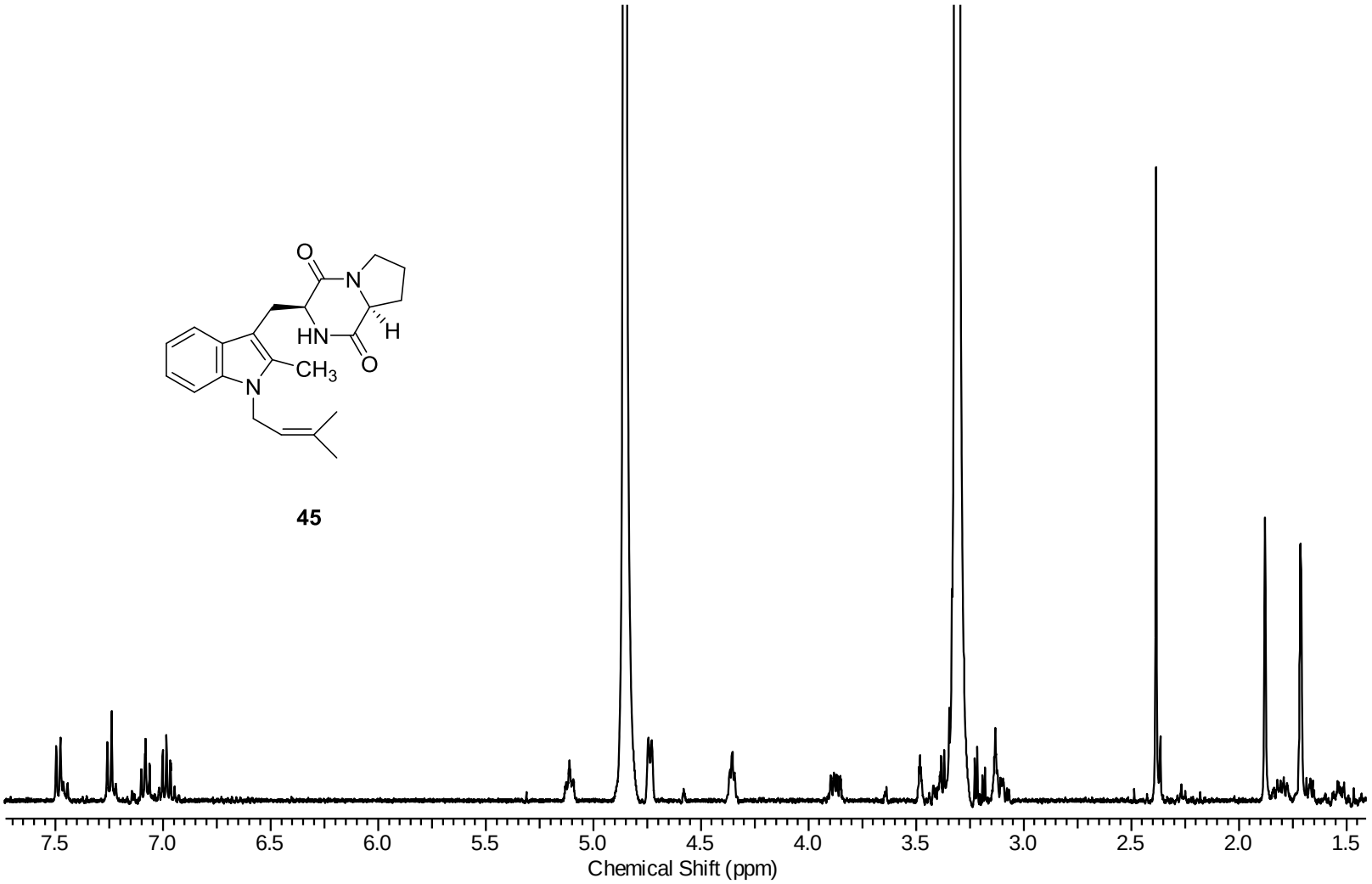

Figure A. 12 ^{1}H NMR spectrum of compound 45 (CD_3OD, 400 MHz).

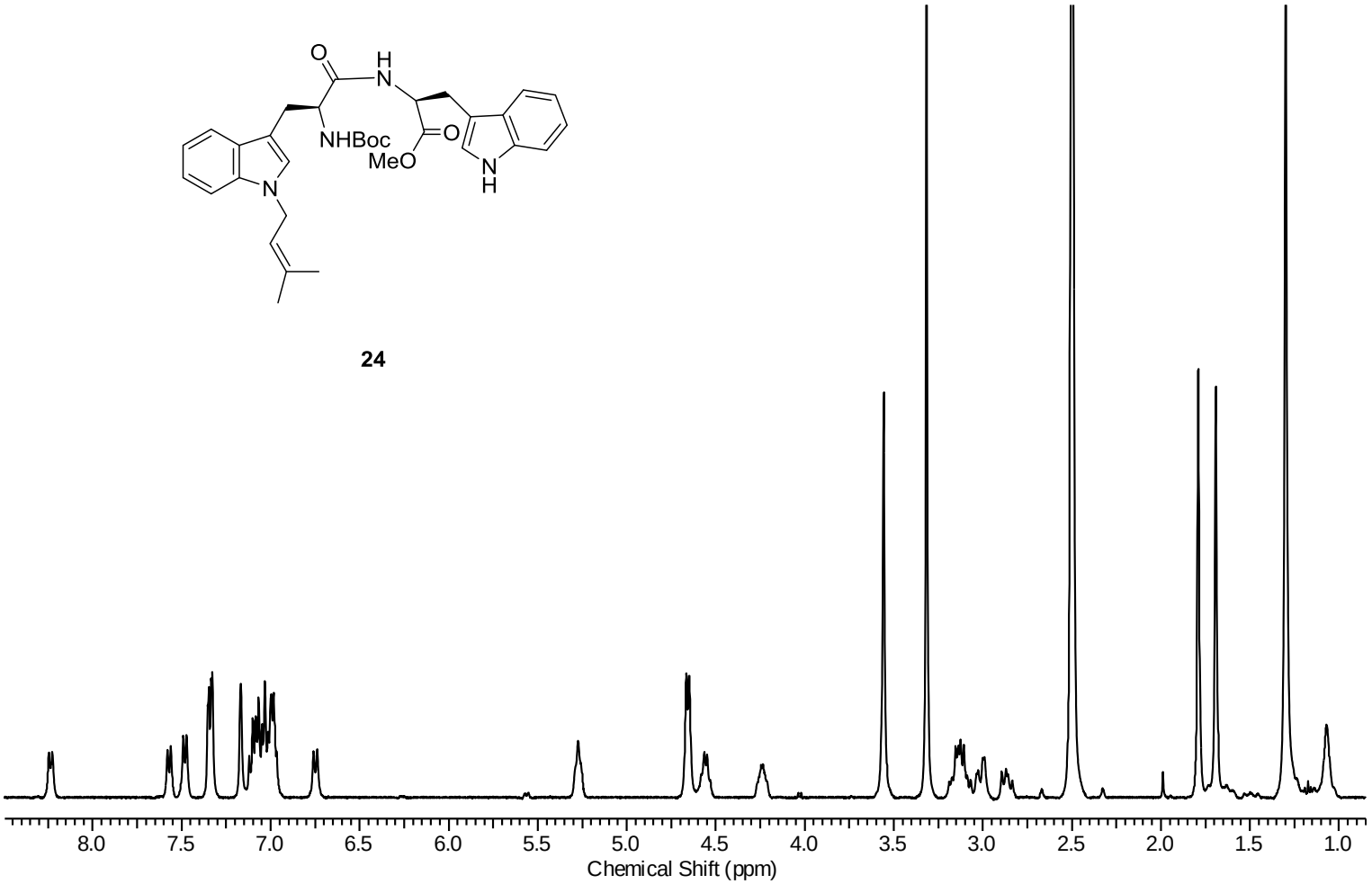

Figure A. 13 ^{1}H NMR spectrum of compound 24 (DMSO-d_6, 400 MHz).

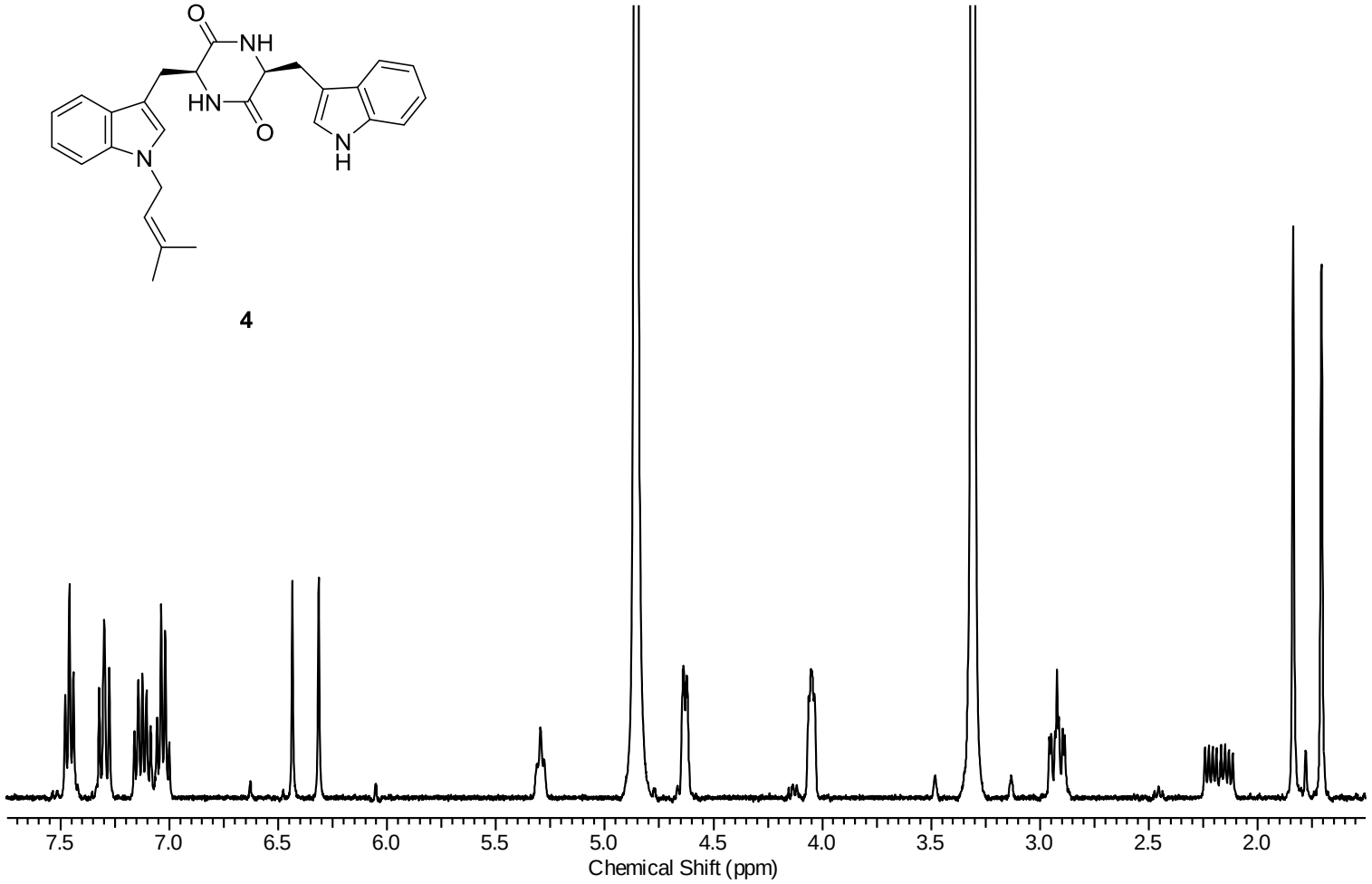

Figure A. 14 ^{1}H NMR spectrum of compound 4 (CD_3OD, 400 MHz).

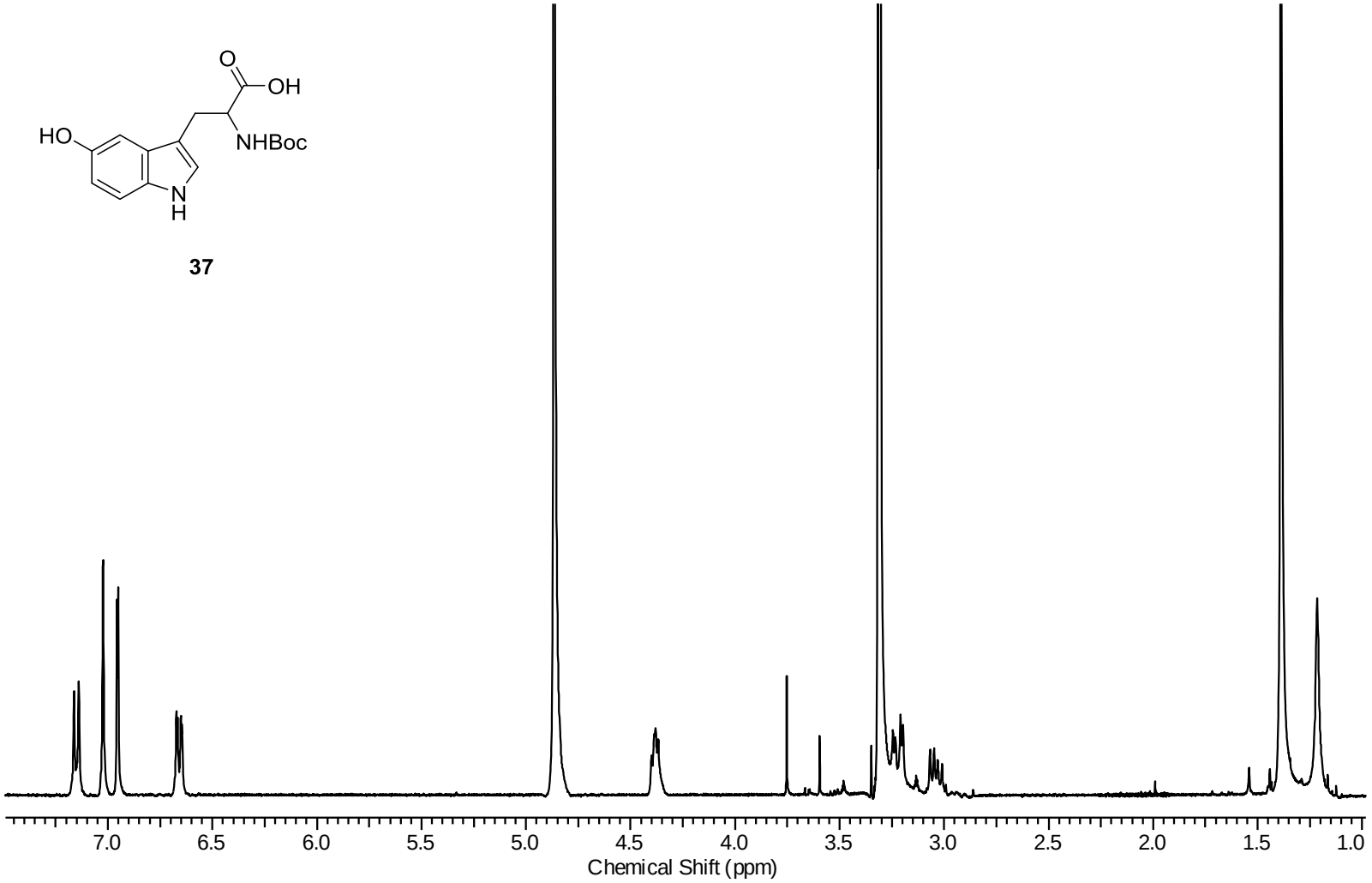

Figure A. 15 ^{1}H NMR spectrum of compound 37 (CD_3OD, 400 MHz).

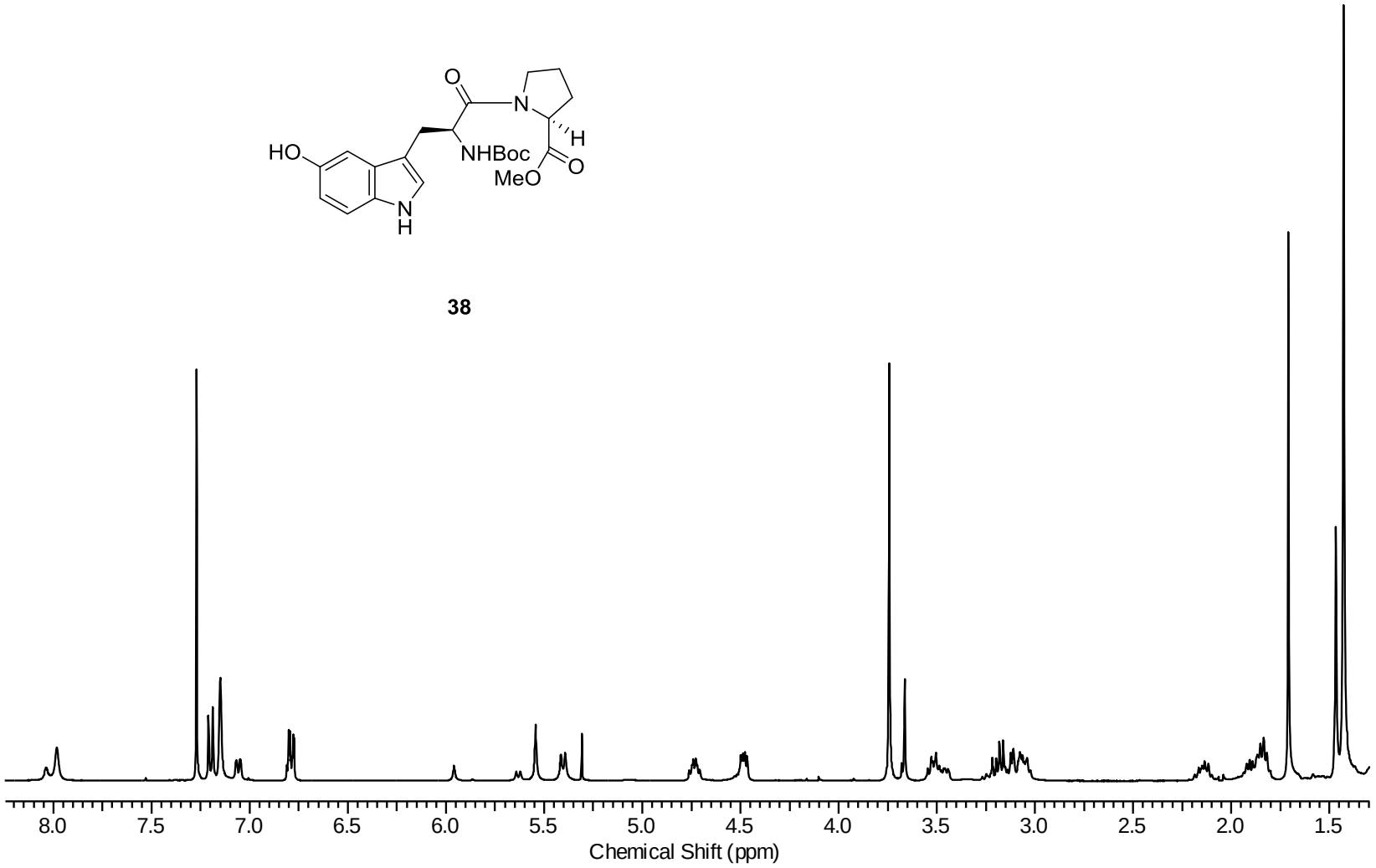

Figure A. 16 ^{1}H NMR spectrum of compound 38 ($CDCl_3$, 400 MHz).

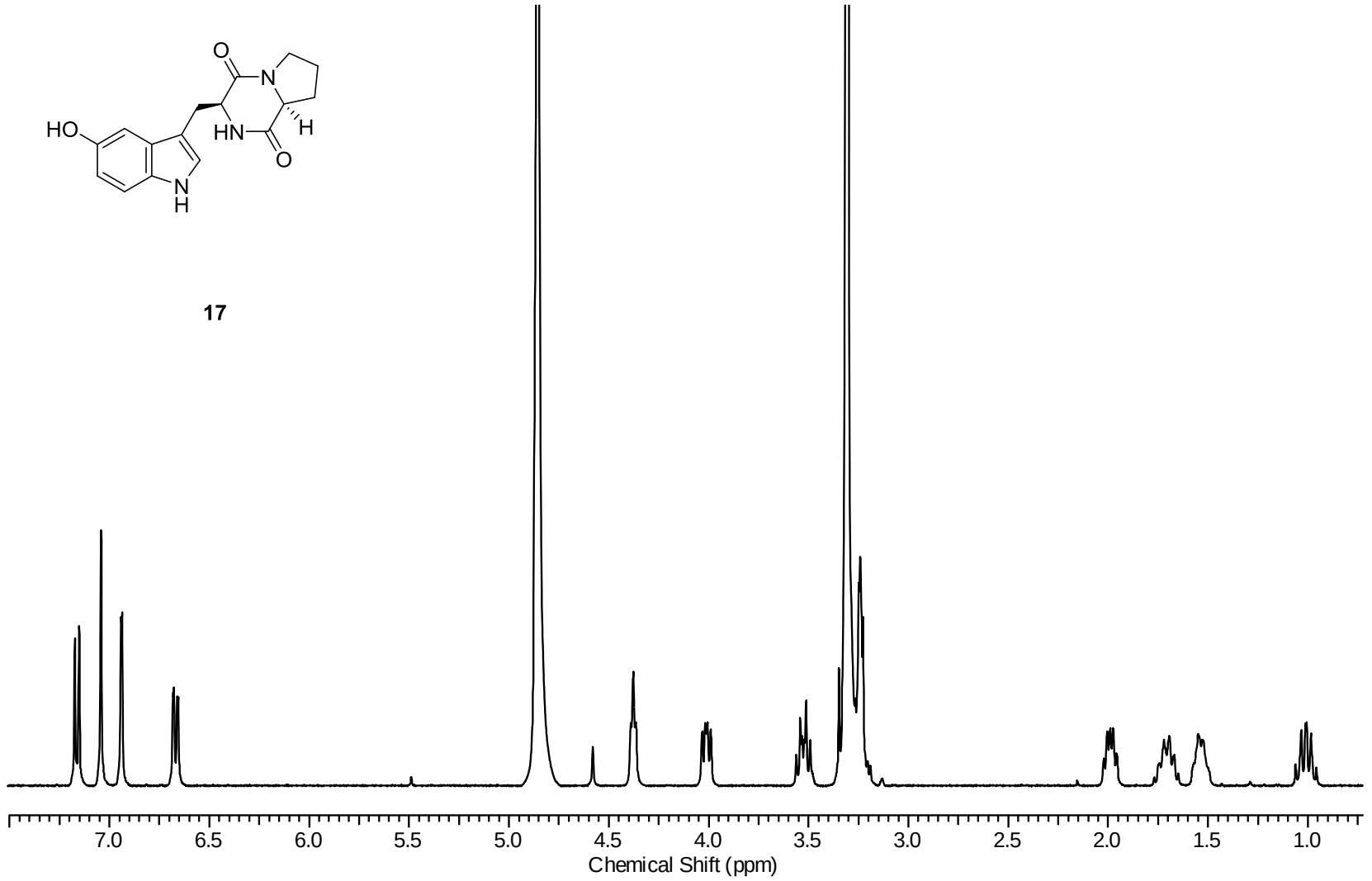

Figure A. 17 ^{1}H NMR spectrum of compound 17 (CD_3OD, 400 MHz).

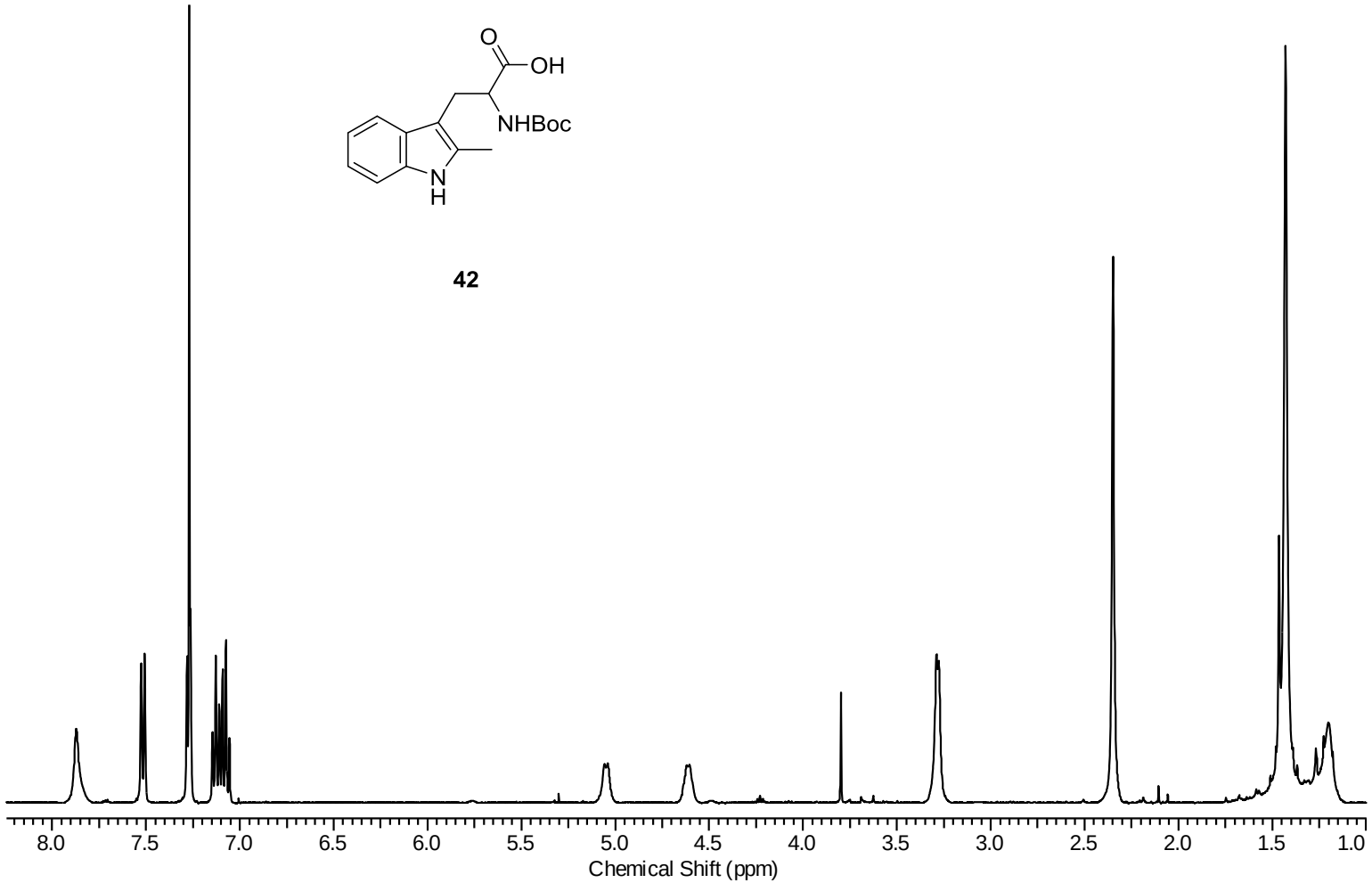

Figure A. 18 ^{1}H NMR spectrum of compound 42 ($CDCl_3$, 400 MHz).

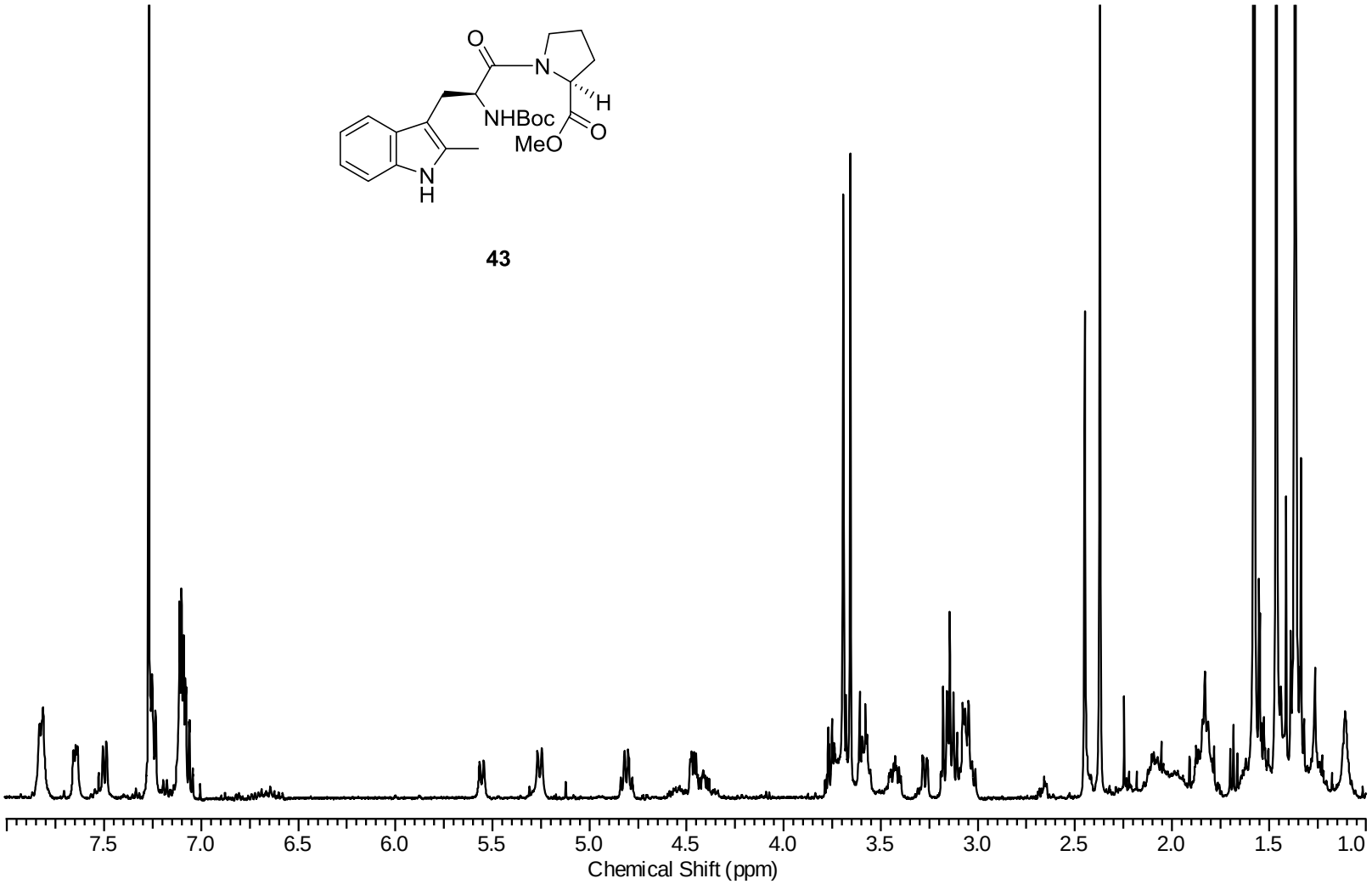

Figure A. 19 ^{1}H NMR spectrum of compound 43 ($CDCl_3$, 400 MHz). Impurities due to dicyclohexylurea are present in this spectrum.

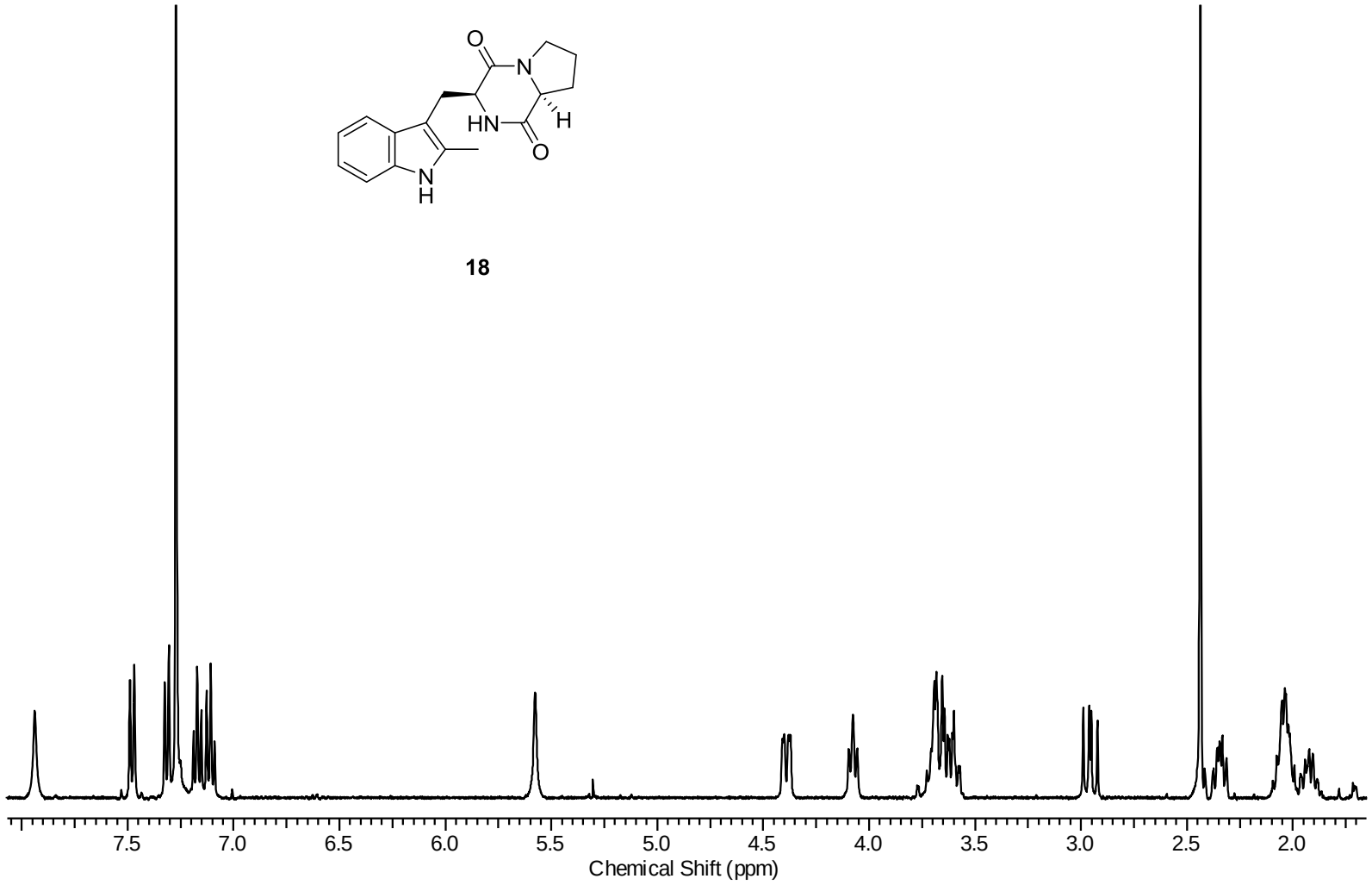

Figure A. 20 ^{1}H NMR spectrum of compound 18 ($CDCl_3$, 400 MHz).

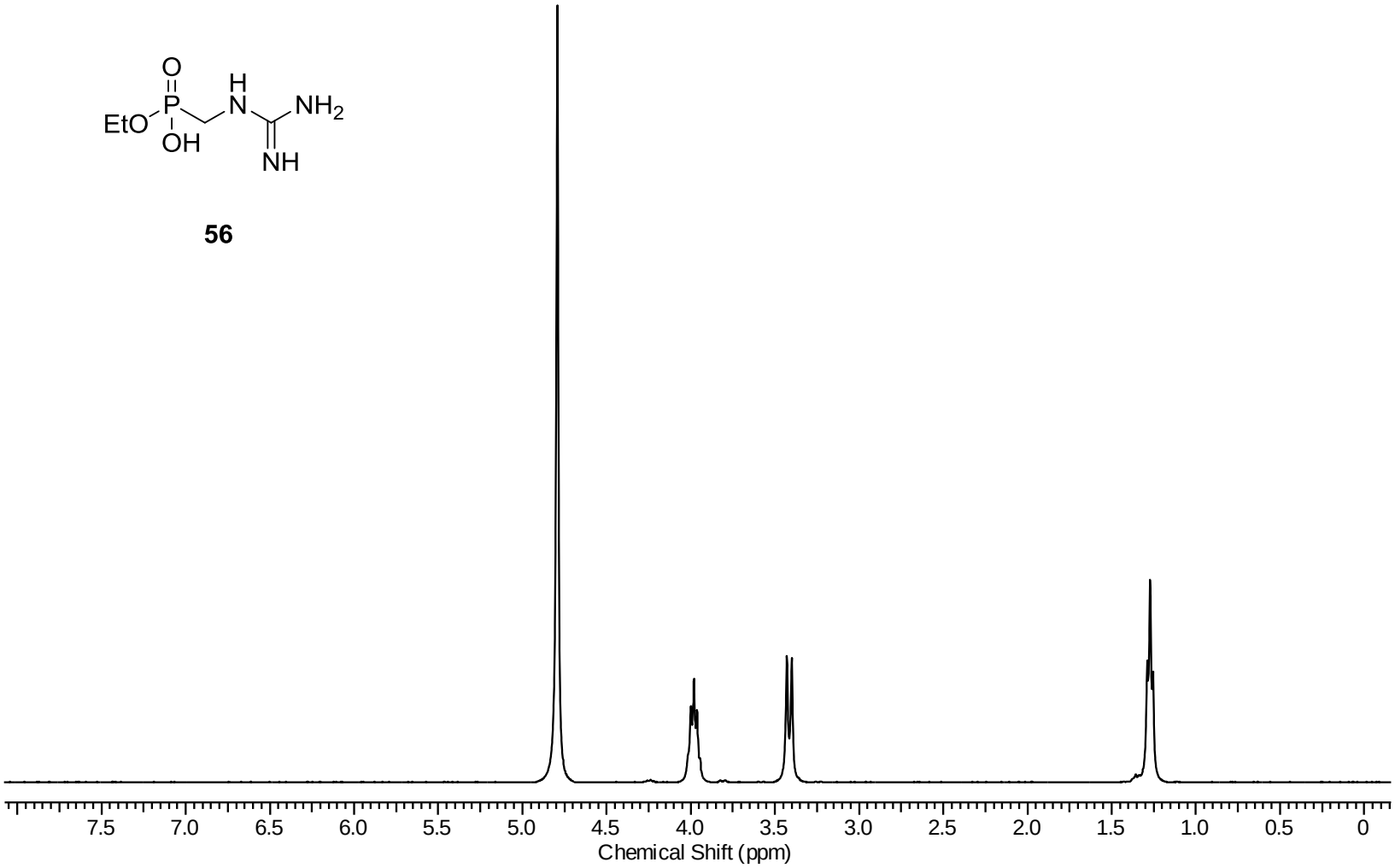

56

Figure A. 21 ^{1}H NMR spectrum of compound 56 (D_2O, 400 MHz).

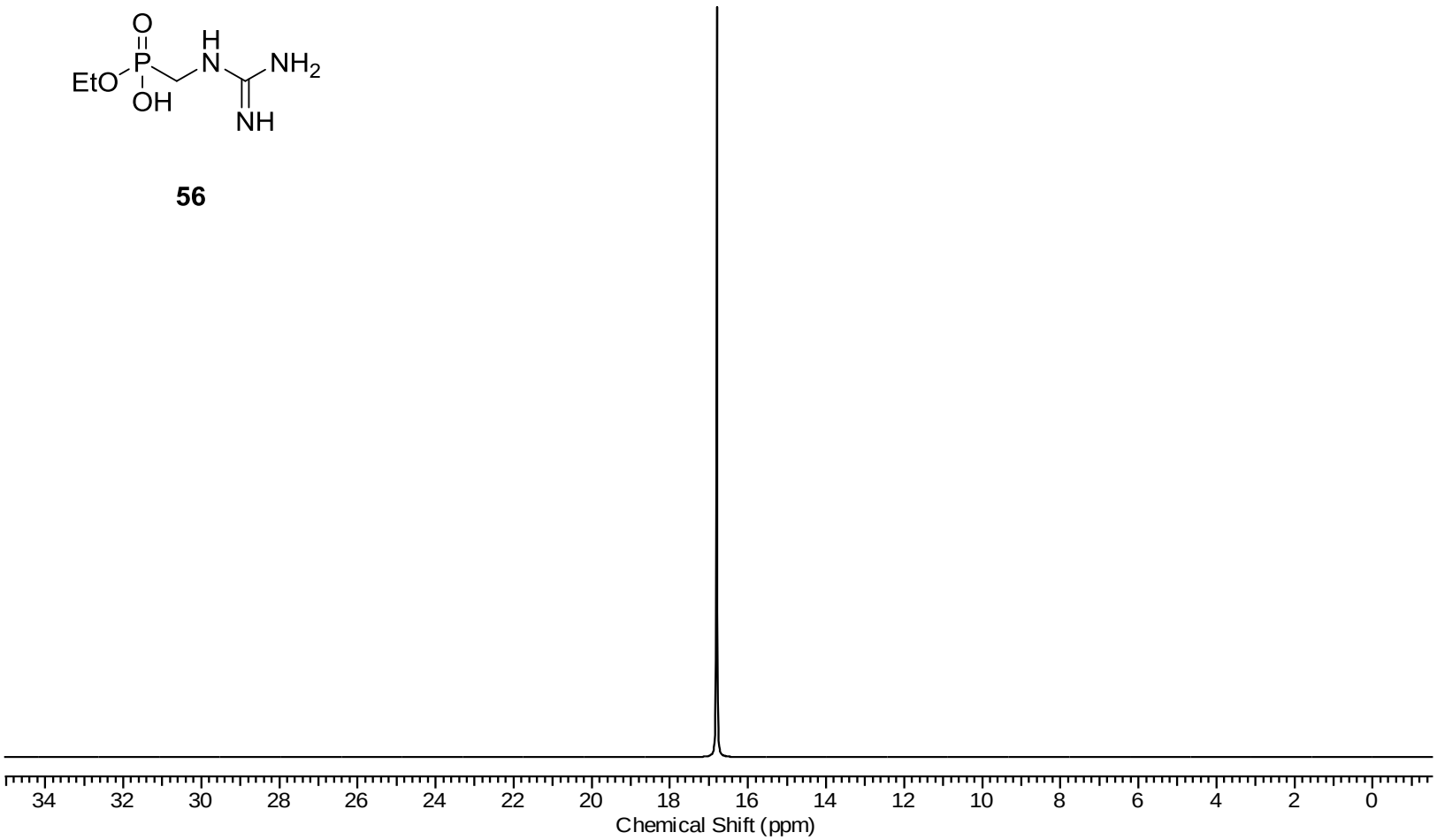

Figure A. 22 ^{31}P NMR spectrum of compound 56 (D_2O, 162 MHz).

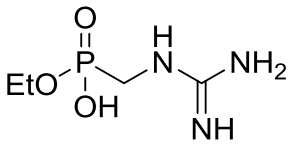

56

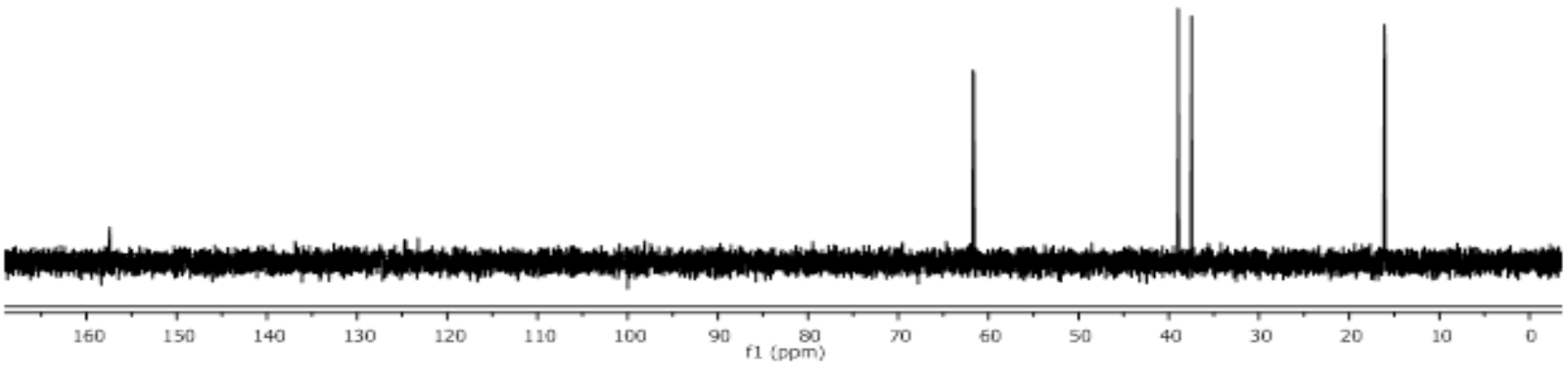

Figure A. 23 ^{13}C NMR spectrum of compound 56 (D_2O, 100 MHz).

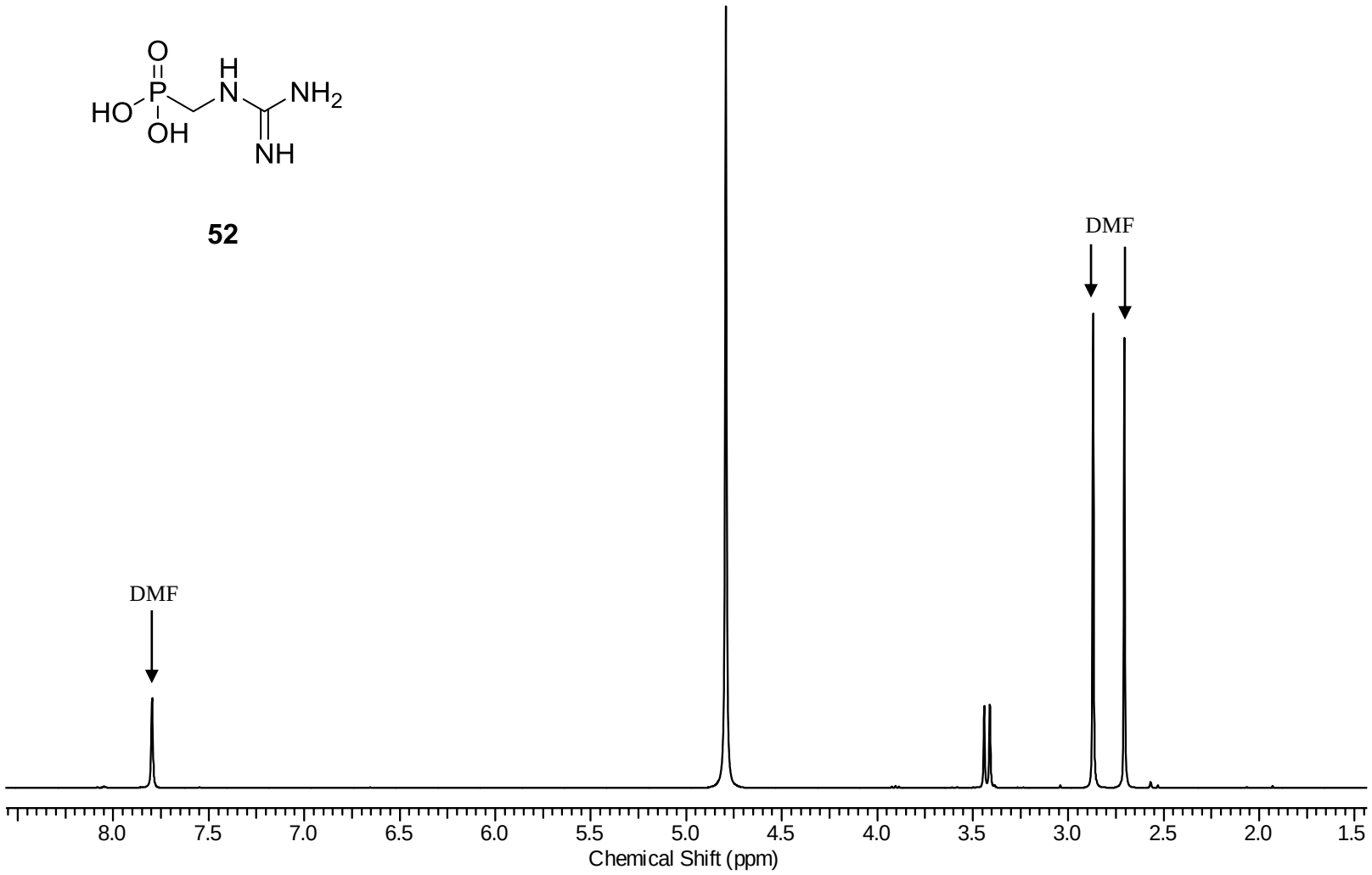

Figure A. 24 ^{1}H NMR spectrum of compound 52 (D_2O, 400 MHz).

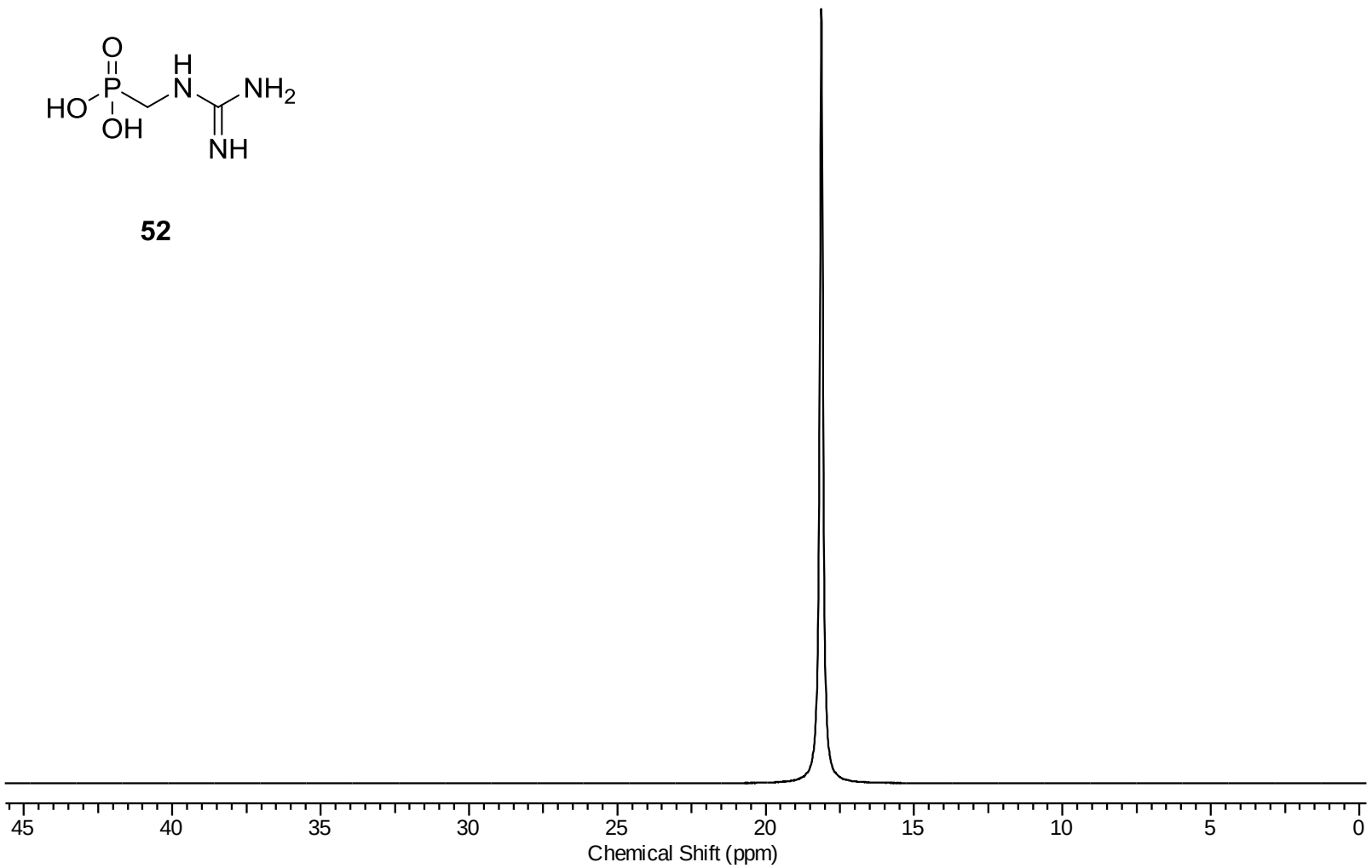

Figure A. 25 ^{31}P NMR spectrum of compound 52 (D_2O, 162 MHz).

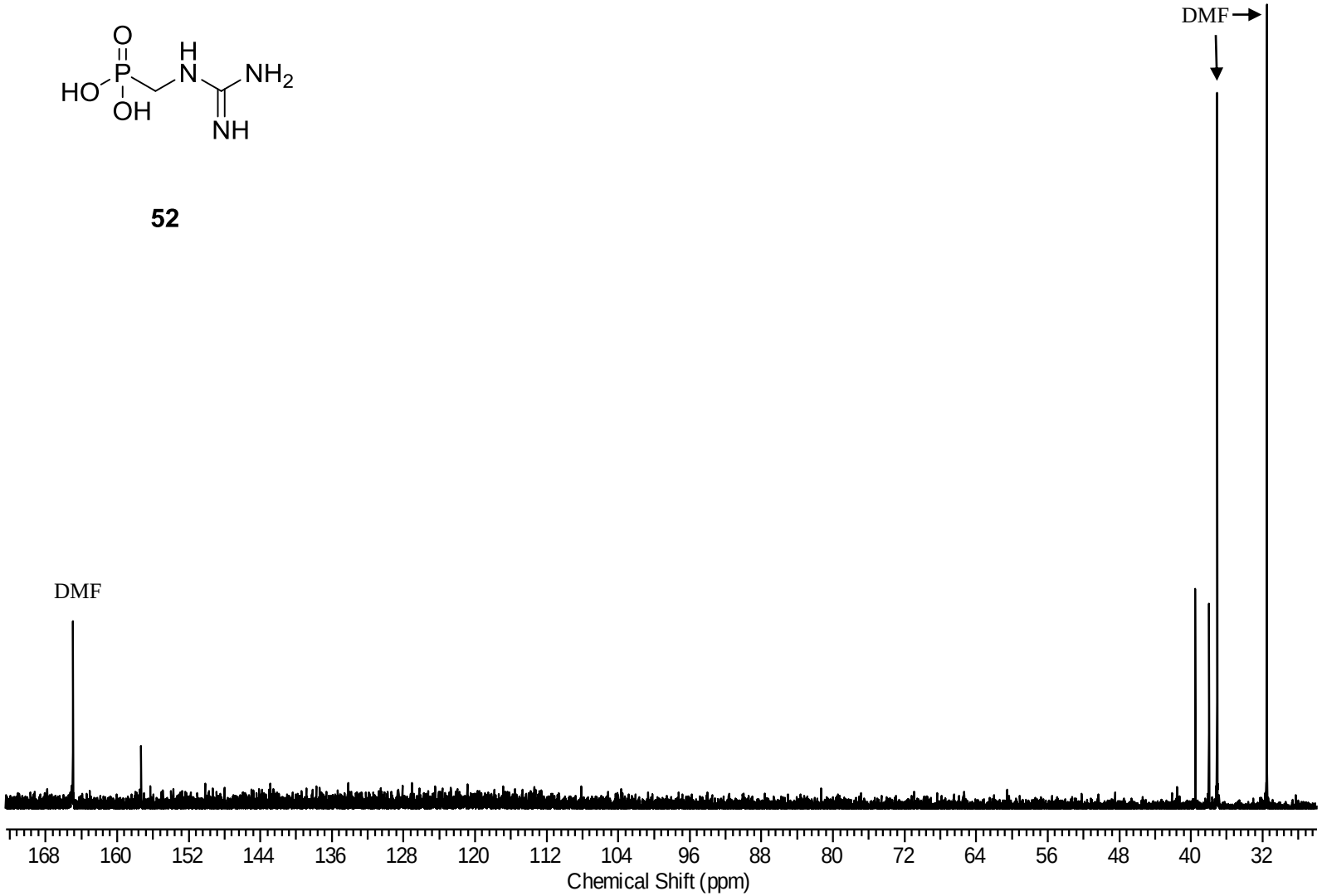

Figure A. 26 ^{13}C NMR spectrum of compound 52 (D_2O, 100 MHz).

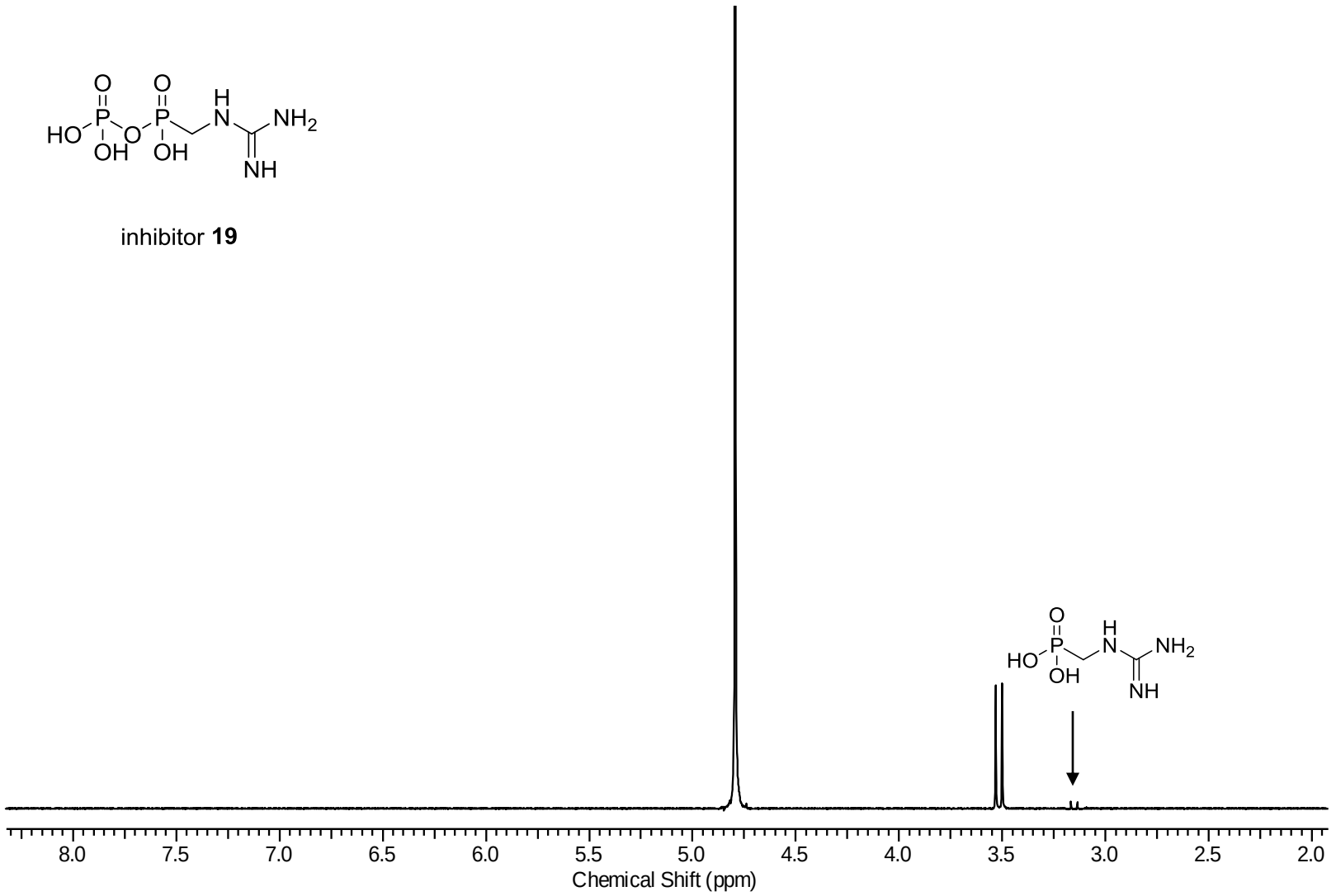

Figure A. 27 ^{1}H NMR spectrum of inhibitor 19 (D_2O, 400 MHz).

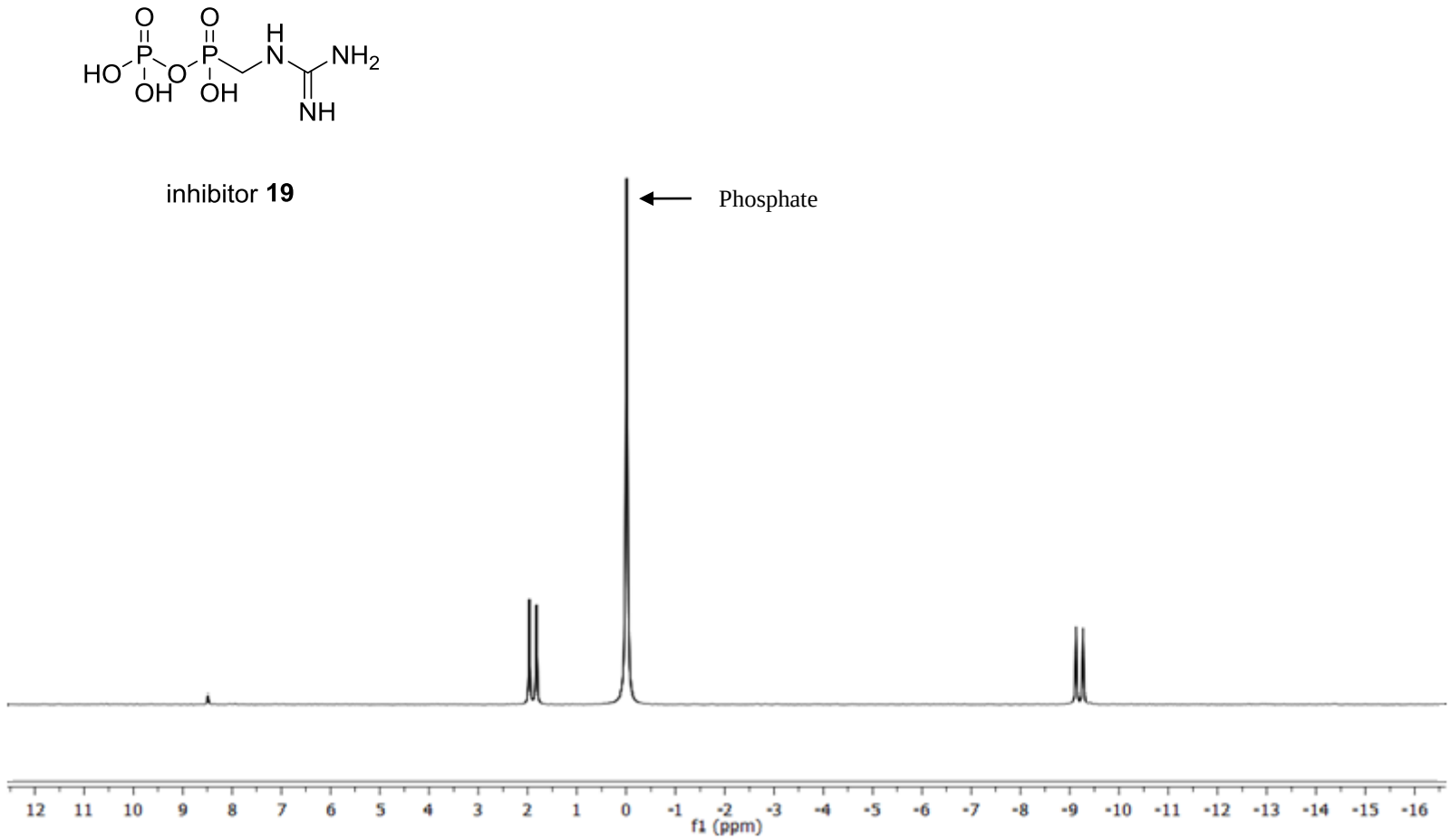

Figure A. 28 ^{31}P NMR spectrum of inhibitor 19 (D_2O, 162 MHz).

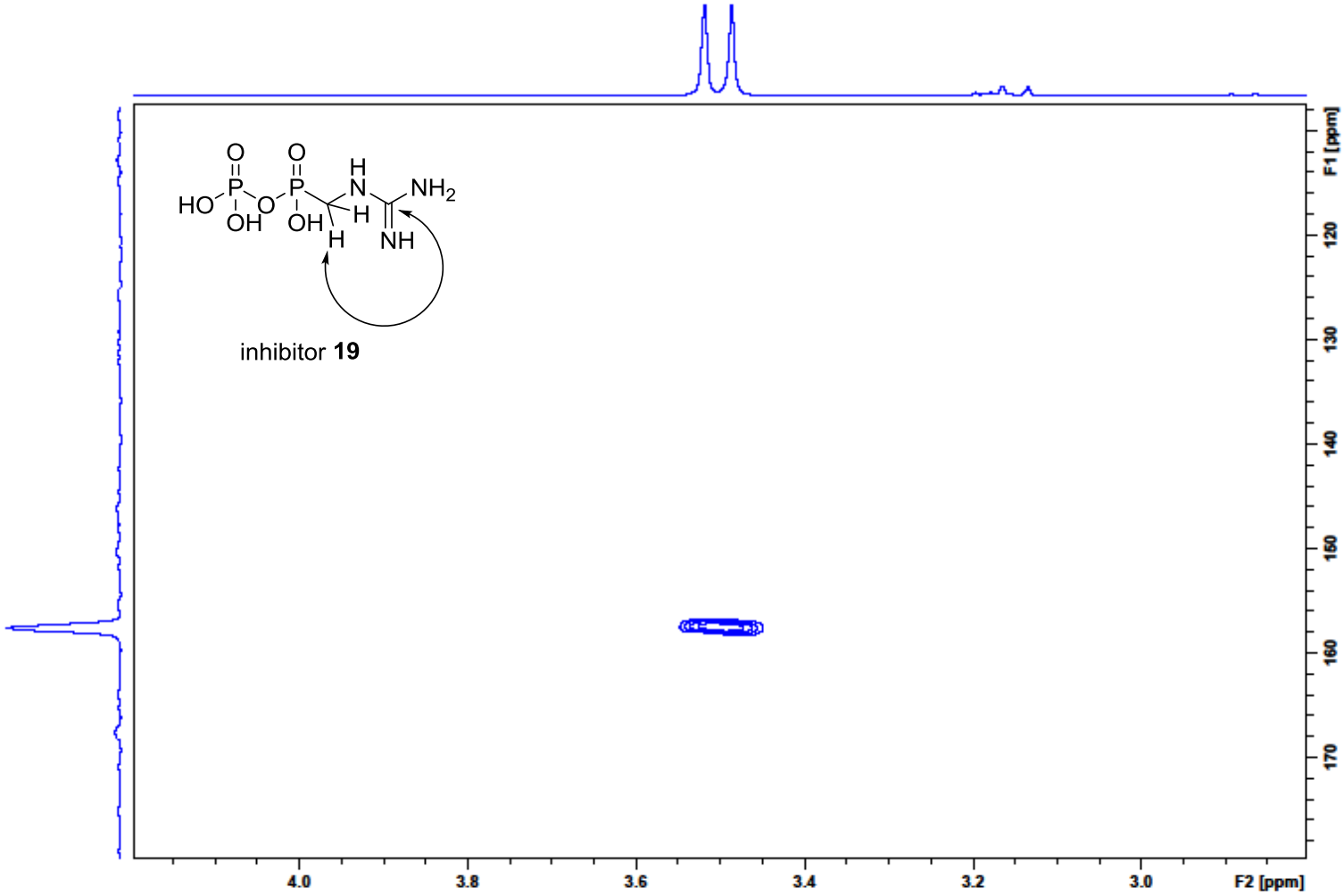

Figure A. 29 HMBC NMR spectrum of inhibitor 19 (D_2O, 400 MHz).

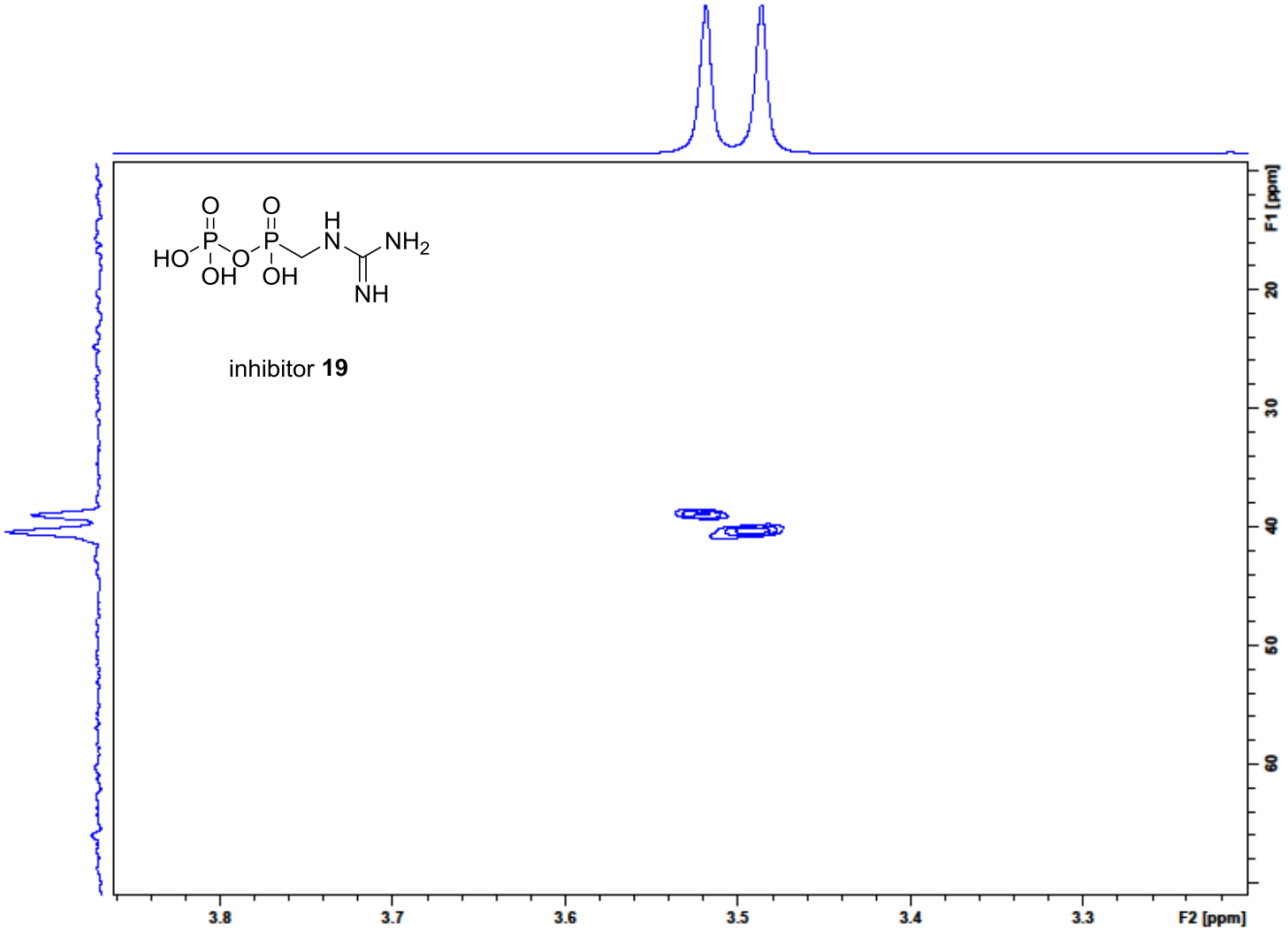

Figure A. 30 HSQC NMR spectrum of inhibitor 19 (D_2O, 400 MHz).